KATHOLIEKE UNIVERSITEIT
LEUVEN

Arenberg Doctoraatsschool Wetenschap & Technologie
Faculteit Ingenieurswetenschappen
Departement Werktuigkunde

Development of a Tactile Feedback System for Robot Assisted Minimally Invasive Surgery

Pauwel Goethals

Proefschrift voorgedragen
tot het behalen van de
graad van Doctor in de
Ingenieurswetenschappen

Januari 2011

Development of a Tactile Feedback System for Robot Assisted Minimally Invasive Surgery

Pauwel Goethals

Jury:
Prof. Dr. Ir. Adhemar Bultheel, voorzitter
Prof. Dr. Ir. Hendrik Van Brussel, promotor
Prof. Dr. Ir. Dominiek Reynaerts, promotor
Prof. Dr. Ir. Jos Vander Sloten, assessor
Prof. Dr. Ir. Robert Puers, assessor
Prof. Dr. Ir. Vincent Hayward
(ISIR, UPMC, Paris)
Dr. Ir. Jan Peirs

Proefschrift voorgedragen
tot het behalen van de
graad van Doctor in de
Ingenieurswetenschappen

Januari 2011

Wettelijk depot D/2011/7515/1
ISBN 978-94-6018-294-5

Voorwoord

De tekst is geschreven, het einde in zicht.
Uw hulp hier bezingen, dat is nu mijn plicht.

Een ster uit revue, Adhemar Bultheel,
geachte heer voorzitter, d'eer was mij teveel.
Een betere promotor dan Hendrik Van Brussel had ik niet kunnen dromen;
voor steun en advies kon ik steeds bij hem komen.
Ook Dominiek Reynaerts, die stond steeds paraat,
met opbouwende feedback en praktische raad.
Jan Peirs en Bob Puers en Jos Vander Sloten,
Van onze discussies heb ik eerlijk genoten.
Vincent Hayward, il vient de Paris,
pour toutes nos discussions, je vous dis: merci.

Het administratief en technisch personeel,
hebben ook vaak geholpen, het was nooit teveel.
Bedankt dus aan Karin, aan An en Regine,
voor d'administratie, aan Lieve en Carine.
Ook bij productie ben ik vaak bijgestaan,
door Eddy en Franske en Dirk Bastiaan.
Voor al het elektrisch en elektronisch advies,
dankjewel Bertram, ook van kaarten niet vies.

Dank aan de mensen van de mechatronics systems group.
Op collega's van de MPE deed ik vaak beroep.
Ook aan de RAS groep, heb ik veel gehad,
chirurgische robots, en nog meer van dat.
Speciale dank ook aan Paul Vanherck,
vele discussies, die maakten licht werk.

Maar werktuigkunde was meer dan werken alleen.
SET activiteiten, daar ging ik graag heen.
Karten, wafels en moddervoetbal,
zijn van die dingen die ik missen zal.
En elke middag was er vertier,
bedankt aan de kaarters, pico met vier [294].

Thierry heeft jaren op mijn kop moeten zien,
op bureau nul één punt nul zeventien.
Mauro was always there with his Italian panache,
Gorka from Spain, or was it Gorki, Orka or Gorache?
Hsiao-Wei Tang and Tjahjowidodo Tegoeh.
Discussiëren met Bert, dat werd ik nooit moe.
Mohamed is the nicest person I ever met.
En Manu heeft er eventjes een bureau bij gezet.
Als laatste toegekomen, de Kroaat Gabrijel;
aan al mijn bureaugenoten, een gemeend dankjewel.

For those of you who still don't know Dutch,
thanks for the wonderful, colourful time.
Al the interesting cultures matched like a rime.
Just know I appreciate you at least as much.

Aan al de collega's wiens naam in dit rijmschema niet past:
het advies en de babbel verlichtten de last.

En dan, clichématig, maar even gemeend,
de tekst nagelezen, van taalfouten gespeend,
zonder wie dit allemaal niet mogelijk was geweest,
bedankt aan mijn ouders, zonder hen nu geen feest.

Het is tijd voor de climax, bedankt aan mijn vrouw,
voor al het geduld, Eve, ik hou zoveel van jou.

Abstract

Minimally Invasive Surgery (MIS) continues to grow in importance and to gradually change and improve the medical practice. This technique comes with great advantages, such as lower risk, fast patient recovery and a reduced hospital stay, but requires an increased dexterity and concentration on the part of the surgeon. To solve those problems, robots were introduced that mimic the movements of the surgeons, allowing them to focus solely on the medical procedure. Currently, there is only visual feedback from the patient to the surgeon. The lack of haptic feedback is one of the most important drawbacks of minimally invasive surgery.

To restore the tactile information channel, a tactile feedback systems has to be developed. Such a feedback system consists of two main parts. A tactile sensor to register the tactile information inside the patient, and a tactile display to reflect the tactile information to the skin of the surgeon. The requirements for such a tactile feedback system are derived from the properties of the human sense of touch in the application of soft tissue palpation.

The first part of a tactile feedback system is the tactile sensor. After studying different sensor principles, elastoresistance is chosen for its simplicity and robustness, and examined more closely. Elastoresistance is found to be often poorly understood and its physical principle misconceived. Simple experiments show that only the contact resistance plays a role in an elastoresistive tactile sensor. The design of a new tactile sensor is discussed, together with improved readout electronics. These electronics are optimised for high speed and low interference with the sensor signal. They can easily be adapted for different sensitivity and resistance ranges, and only use very low voltages, which is relevant in the context of MIS. The prototype tactile sensor is simple, flexible, cheap, thin and adjusted for the desired pressure range, but still suffers from large hysteresis and drift.

The second part of a tactile feedback system is the tactile display. After going through some general design guidelines, an overview is given on existing tactile displays with a slight focus on small scale shape displays. Several prototypes are built in an attempt to meet the challenging requirements. These include the first appearances of hydraulics applied in tactile displays. The first is a closed hydraulic

system, profiting from the incompressibility of water to transfer the actuation over a distance. The second uses an open hydraulic system with a piezoelectric proportional valve to actuate the individual pins of the tactile display. A final prototype uses pneumatics and needs a pneumatic proportional valve to control the force of the pins. Existing commercial valves are too large to fit into an already crowded operating room, and make too much noise. Therefore a small and noiseless proportional valve is designed and built, which allows for easy integration into a compact array to operate the necessary large amount of pins. The pressure range which this valve can produce, however, is too small for a tactile display, and the design needs considerably more research before it can be employed.
To realise an integrated, functional tactile feedback system a tactile display 'lite' is built with commercial pneumatic valves. The aim of the system is to serve as a proof of concept rather than to fulfil all the requirements. It does stand out among other tactile displays found in literature. While there are displays with a larger bandwidth, a higher resolution or a higher force, none of them combines those in a single display. On top of that, the display is very compact and has an almost negligible weight. An experiment to evaluate the combined system shows that it allows to perform a relatively complex discrimination task, even though it is too difficult to distinguish a hard ball in soft tissue.

Samenvatting

Minimaal invasieve chirurgie blijft aan belang winnen en geleidelijk verandert en verbetert ze de gezondheidszorg. Deze techniek heeft enerzijds enorme voordelen, zoals een verlaagd risico, een snellere genezing en een korter verblijf in het ziekenhuis, maar anderzijds vereist ze extra concentratie en behendigheid van de chirurg. Om dit probleem aan te pakken, werden robots ontwikkeld die de bewegingen van de chirurg nabootsen, waardoor die laatste zich uitsluitend op de medische procedure kan concentreren. Momenteel is enkel visuele terugkoppeling beschikbaar van de patiënt naar de chirurg. Het gebrek aan tactiele terugkoppeling is één van de belangrijkste nadelen van minimaal invasieve chirurgie.
Om de tastzin terug te bezorgen aan de chirurg, moet een tactiel terugkoppelingssysteem worden ontwikkeld. Een dergelijk systeem bestaat voornamelijk uit twee delen. Een tactiele sensor registreert de tactiele informatie binnenin de patiënt, terwijl een tactiele display die tactiele informatie weergeeft op de huid van de chirurg. De vereisten voor een tactiel terugkoppelingssysteem zijn afgeleid van de eigenschappen van de menselijke tastzin.
Het eerste deel is de tactiele sensor. Na het bestuderen van verschillende meetprincipes, is er gekozen voor elastoresistiviteit omwille van de betrekkelijke eenvoud en de robuustheid. Dit principe is meer in detail bestudeerd, en het bleek vaak misbegrepen te zijn. Eenvoudige experimenten tonen dat het enkel de contactweerstand is die een rol speelt in een elastoresistieve tactiele sensor. Vervolgens wordt het ontwerp van een nieuwe tactiele sensor en verbeterde elektronica besproken. Die elektronica is geoptimaliseerd voor een hoge snelheid en een minimale invloed op het tactiele signaal. Ze kan eenvoudig worden aangepast voor verschillende gevoeligheden of weerstanden en gebruikt slechts lage elektrische spanningen, wat zeer relevant is in de context van minimaal invasieve chirurgie. Het sensor prototype is eenvoudig, flexibel, goedkoop, dun en aangepast voor het gewenste drukbereik. Het lijdt evenwel nog van een grote hysteresis en veel drift.
Het tweede deel is de tactiele display. Na enkele algemene ontwerprichtlijnen, wordt een overzicht gegeven van bestaande tactiele displays met een lichte nadruk op displays die kleine vormen weergeven. Verschillende prototypes zijn gebouwd in een poging tegemoet te komen aan de uitdagende vereisten. Om te beginnen wordt

voor de eerste keer hydraulica toegepast in een tactiele display. De eerste is een gesloten hydraulisch systeem dat gebruik maakt van de onsamendrukbaarheid van water om de beweging over een afstand te transporteren. De tweede in een open hydraulisch systeem met een piezo-elektrische proportionele klep om de individuele pinnen van de tactiele display aan te sturen. Het laatste prototype maakt gebruik van pneumatica, en heeft dus een pneumatische proportionele klep nodig om de kracht op de pinnen te regelen. Bestaande commerciële kleppen, die ook in reeds bestaande tactiele displays worden gebruikt, zijn te groot om in een al overvolle operatiekamer te passen en maken teveel lawaai. Daarom is een kleine en geruisloze proportionele klep gebouwd. Die klep kan gemakkelijk in grote aantallen geïntegreerd worden in één compact geheel om een tactiele display met een grote hoeveelheid pinnen te kunnen aansturen. Het drukbereik van deze klep is echter onvoldoende voor een goed werkende tactiele display. Er is dus meer onderzoek nodig voor ze kan gebruikt worden.
Uiteindelijk is een vereenvoudigde tactiele display met commerciële pneumatische kleppen gebouwd om te integreren in een werkend tactiel terugkoppelingssysteem. Dat systeem heeft als doel het concept aan te tonen, en niet om te voldoen aan alle vooropgestelde criteria. Het neemt wel een unieke plaats in tussen de tactiele displays die in de literatuur te vinden zijn. Hoewel er andere displays bestaan met een groter frequentiebereik, een fijnere resolutie of een groter krachtbereik, integreert geen enkele al deze eigenschappen in een enkele display. Daarenboven is de display erg compact en weegt ze bijna niets. Een experiment om dit te evalueren toont dat het systeem het mogelijk maakt om een niet voor de hand liggend onderscheid te maken tussen objecten. Het is echter niet mogelijk om een harde bal in zacht weefsel te onderscheiden zonder meer geavanceerde technieken te gebruiken.

Nomenclature

Introduction

CPB	Cardiopulmonary bypass
CPU	Central processing unit
CT	Computed tomography
FAI	Fast adapting mechanoreceptor type I (usually associated with Meissner's corpuscles)
FAII	Fast adapting mechanoreceptor type II (usually associated with Pacinian corpuscles)
IOUS	Intraoperative ultrasound
ISO	International Organization for Standardization
MIS	Minimally invasive surgery
MRI	Magnetic resonance imaging
OR	Operating Room
SAI	Slowly adapting mechanoreceptor type I (usually associated with Merkel disks)
SAII	Slowly adapting mechanoreceptor type II (usually associated with Ruffini endings)
US	Ultrasound

Tactile sensor

AC	Alternating current
CCD	Charge-coupled device
DC	Direct current
DRAM	Dynamic random access memory
ERG	Electrorheological gel
IC	Integrated circuit
IR	Infrared
LED	Light emitting diode
LVDT	Linear variable differential transformer
PCB	Printed circuit board
PDMS	Polydimethylsiloxane
PTFE	polytetrafluoroethylene
PVDF	Polyvinylidene fluoride
PVF2	Polyvinylidene fluoride
PZT	Lead zirconate titanate
A	area
C	capacitance
d	distance
e	2.7182818...; Euler's number
F	force
L	inductance
p	volume percent (V%)
p_c	percolation threshold
R	electrical resistance
R_0	nominal resistance
R_g	bridge resistance in voltage divider
t	time
V	voltage
V_in	input voltage
V_out	output voltage
ϵ	strain
ε_0	$8.85\ 10^{-12}\,\mathrm{F/m}$; permittivity of vacuum
ε_r	relative permittivity or dielectric constant
μ	conductivity exponent
τ	time constant

Tactile display

CAD	Computer aided design
C-SMA	Coil-type shape memory alloy
DC	Direct current
EDM	Electric discharge machining
ERF	Electrorheological fluid
MRF	Magnetorheological fluid
PET	Polyethylene terephthalate
SMA	Shape memory alloy
a	distance
A	area or cross section
A_{eff}	effective area
b	width or thickness
B	magnetic induction, magnetic flux density
d	distance or width
d_{p}	piezoelectric coefficient
D	diameter
D_{i}	inner diameter
D_{o}	outer diameter
e	eccentricity
E	electric field
	Young's modulus
E_{e}	electrical energy
E_{m}	magnetic energy
E_{Y}	Young's modulus
F_{em}	generalised electromagnetic force
F_{es}	electrostatic force
F_{ext}	external force
F_{m}	magnetic reluctance force
F_{s}	spring force
G	shear modulus
h	height
H	magnetic field strength
I	electric current
	second moment of inertia
I_{p}	polar moment of inertia
k	stiffness
l	length
Δl	displacement
L	length of conduit

$\dot{m}$	mass flow
M	Mach number
M_m	magnetic reluctance moment
M_v	moment caused by foil spring
n	number of springs
N	number of turns of a coil
P	pressure
P_0	atmospheric pressure
P_high	high pressure
P_low	low pressure
P_supply	supply pressure
ΔP	pressure drop
Q	volume flow
r	radius
r_C	0.5283; critical pressure ratio for air
R	hydraulic resistance
	$287.058\,\mathrm{J/kg\,K}$; specific gas constant for dry air
R_e	Reynolds number
$\Re_\mathrm{m}$	magnetic reluctance
S	area
t	time
T	temperature
U	applied voltage
v	speed
V	volume
ΔV	volume change
w	energy density
W	mechanical work
x	position or displacement
y	position or displacement
$\dot{y}$	derivative of the position
α	angle
β	angle
γ	twisting angle
ε_0	$8.85\ 10^{-12}\,\mathrm{F/m}$; permittivity of vacuum
ε_r	relative permittivity or dielectric constant
Θ	angle of rotation
κ	ratio of specific heats
μ	magnetic permeability
	dynamic viscosity
μ_0	$4\pi \cdot 10^{-7}\,\mathrm{Vs/Am}$; magnetic permeability of vacuum

π	3.14159265...; mathematical constant
ρ	density
σ	mechanical stress
Φ	magnetic flux
Ψ	flow factor
Ψ_{C}	critical flow factor

Magnetic modelling

PM	Permanent magnet
B	magnetic induction, magnetic flux density
F_{m}	reluctance force
H	magnetic field strength
I	electric current
l	length
M	magnetisation
N	number of turns of a coil
$\Re_{\mathrm{m}}$	magnetic reluctance
S	area
x	displacement
Θ	magnetomotive force
μ_0	$4\pi \cdot 10^{-7}$ Vs/Am; magnetic permeability of vacuum
Φ	magnetic flux

Contents

Contents xiii

List of Figures xvii

List of Tables xxiii

1 Introduction 1

1.1 Minimally Invasive Surgery 3

1.1.1 Importance of Touch 6

1.2 Psychophysics of Touch 7

1.2.1 Mechanoreceptors in the Skin 9

1.2.2 Limits of Human Perception 13

1.2.3 Vibration and Simulation of Sensation 14

1.3 Requirements of Tactile Feedback in Surgery 15

1.3.1 Spatial Resolution 16

1.3.2 Frequency Range 17

1.3.3 Sensitivity, Force and Stroke 18

1.3.4 Miscellaneous Requirements 18

2 Tactile Sensor 21

2.1 Overview of Tactile Sensors 21

2.1.1 General Design Issues 22
2.1.2 Applications of Tactile Sensors 26
2.1.3 Tactile Sensors in Literature 27
2.1.4 Comparison of Tactile Sensors 38
2.2 Elastoresistive Tactile Sensor Design 42
2.2.1 Elastoresistance 42
2.2.2 Structure and Examples from Literature 51
2.2.3 Readout Electronics for an Elastoresistive Tactile Sensor . . 53
2.2.4 Rubber Tests 57
2.2.5 Conclusion 61
2.3 Results and Discussion 61
2.3.1 Prototype Tactile Sensor 61
2.3.2 Single Taxel Response 63
2.3.3 Crosstalk 65
2.3.4 Phantom Tests 67
2.3.5 Discussion 68
2.4 General Conclusion on Tactile Sensors 70

3 Tactile Display 71

3.1 Overview 71
3.1.1 General Design Issues 72
3.1.2 Tactile Displays in Literature 74
3.1.3 Braille Displays 85
3.1.4 Comparison of Tactile Displays 86
3.2 Closed Hydraulic System 88
3.2.1 Results and Discussion 93
3.2.2 Conclusion on the Closed Circuit Hydraulic Tactile Display 94
3.3 Hydraulic Piezo Valve 94

3.3.1 Experiments and Results 97
3.3.2 Conclusion on the Hydraulic Valve 99
3.4 Pneumatic Solenoid Valve 100
3.4.1 Principle of Operation 100
3.4.2 Prototypes and Results 123
3.4.3 Single Taxel Display 129
3.4.4 Conclusion on the Pneumatic Valve 130
3.5 Conclusion 131

4 Integrated System **133**
4.1 Proof of Concept 134
4.1.1 The Display 135
4.1.2 Discussion 137
4.2 Evaluation Experiment 140
4.2.1 Experiment Description 140
4.2.2 Results and Discussion 141
4.3 Conclusion 142

5 General Conclusion **145**
5.1 Contributions 146
5.2 Future Work 147

A Magnetic Modelling **151**

Bibliography **157**

List of Publications **187**

List of Figures

1.1 Schematic overview of a telesurgical system with tactile feedback . 4

1.2 Nerve endings usually associated with mechanical triggers in the human glabrous skin 10

1.3 Response of mechanoreceptors to rising and dropping stimuli . . . 11

2.1 Schematic principle of a reflection based optical sensor 33

2.2 Schematic principle of two types of optical tactile sensors 34

2.3 Schematic principle of an ultrasonic tactile sensor 37

2.4 Test setup to measure the respective influence of contact and bulk resistance on the elastoresistive effect 43

2.5 Variation of the contact resistance with applied force 44

2.6 Variation of the bulk resistance with applied force 44

2.7 Principle of percolation as applied to elastoresistance 45

2.8 Piezoresistive effect around the percolation threshold 46

2.9 The force-resistance curve of conductive rubber with considerable hysteresis 49

2.10 Double sided contact electrodes on conductive rubber 50

2.11 Single sided contact electrodes on conductive rubber 50

2.12 Reduction of the number of wires in an elastoresistive sensor . . . 51

2.13 Row and column structure of an elastoresistive tactile sensor . . . 51

2.14 Compact configuration of the electrodes of an elastoresistive tactile sensor 53
2.15 Leak current paths in an elastoresistive sensor 54
2.16 Schematics of the sensor electronics 55
2.17 Setup to test the elastoresistive behaviour of conductive rubbers . 56
2.18 Example of signal degradation in a conductive rubber 57
2.19 On–off behaviour of some conductive rubbers 58
2.20 Frequency dependency of some conductive rubbers 58
2.21 Comparison between force-resistance curve and several fitted models 59
2.22 Decent repeatability of the selected rubber between measurements at different frequencies 60
2.23 Flat and finger shaped prototypes of the tactile sensor 62
2.24 Matrix structure and working principle of sensor electrodes on the PCB-layout 62
2.25 Single taxel repeatability 63
2.26 Output curves of different taxels 64
2.27 Comparison between the sensor output while stimulating with a double or a single indenter 65
2.28 Hysteresis of the tactile sensor 66
2.29 Step response of the tactile sensor 66
2.30 Viscoelastic behaviour of rubber during a step in the position . . . 66
2.31 Mechanical crosstalk 67
2.32 Output of the sensor on a phantom with a simulated tumour . . . 68
2.33 Output of the sensor on a phantom with a simulated tumour . . . 69
2.34 Output of the sensor on a phantom with a simulated tumour . . . 69

3.1 One-pin prototype of an SMA based tactile display 78
3.2 Frequency response of an SMA pin with forced air cooling 79
3.3 Frequency response of an SMA pin with still water cooling 80

3.4 Schematic representation of the closed hydraulic system 88
3.5 CAD model of the display 89
3.6 Hydraulic circuit 91
3.7 Influence of an external force on the transmission ratio 91
3.8 Prototype of the closed hydraulic system 93
3.9 Proportional valve with a pressure divider 95
3.10 Lightweight hydraulic tactile display 96
3.11 Proportional valve based on a piezo bimorph 96
3.12 Characteristics of a tactile display controlled by a piezo bimorph based proportional valve 97
3.13 Models of the tactile display characteristics with increasing complexity 98
3.14 Schematic drawing of the proportional valve 101
3.15 Characteristics of a pressure divider with only slit B varying 104
3.16 Characteristics of a pressure divider with only slit A varying . . . 105
3.17 Characteristics of a pressure divider with both slits varying. 105
3.18 Valve slit produced to test the manufacturing technology 106
3.19 Comparison of the valve characteristics with rectangular slits or with round slits 107
3.20 Schematic representation of the magnetic circuit with the definition of the variables 108
3.21 Comparison between reluctance force and spring force to find the equilibrium position of the piston 111
3.22 Intersection points of the spring force with the reluctance force at several currents 112
3.23 Position-current characteristic of the reluctance actuator 113
3.24 Concertina spring 114
3.25 Schematic concept of a valve with a foil spring 115
3.26 Bending mode and stretching mode of foil spring 116
3.27 Comparison between reluctance force and foil spring force to find the equilibrium position of the piston 117

3.28 Intersection points of the foil spring force with the reluctance force at several currents 118
3.29 Current-position characteristic of the piston with a foil spring . . . 119
3.30 Influence of piston weight and foil pretension on the current-position characteristic 120
3.31 Influence of the air bearing on the valve 122
3.32 Piston of the valve 123
3.33 Concertina spring 123
3.34 The central parts of the valve 123
3.35 The different parts of the display before assembly 124
3.36 The assembled valve prototype 125
3.37 Characteristic of the reluctance actuator with magnetic hysteresis . 125
3.38 Comparison of the actuator performance with the theoretical model 126
3.39 Characteristics of the valve 127
3.40 The force on the taxel in function of the current through the valve 129

4.1 Valve assembly of 32 valves of the proof of concept tactile display . 134
4.2 Characteristic of a taxel in a bronze display 135
4.3 Characteristic of a taxel in an Ertalyte TX display 136
4.4 The 8×4 proof of concept tactile display 137
4.5 A 3D view of how 100 valves can be built into an array of limited dimensions 138
4.6 Cross section of a schematic principle of an array of valves 138
4.7 Experimental setup to evaluate the integrated system 139
4.8 The signal of the tactile sensor sent to the display while manipulating cylinders of different diameters 143

5.1 Improved layout of the flexible PCB 148

A.1 Axisymmetrical model of a magnetic circuit with a coil and a permanent magnet 152

A.2 Comparison between analytical and numerical models with only a coil 153

A.3 Comparison between analytical and numerical models with only a permanent magnet 154

A.4 Comparison between analytical and numerical models with a coil and a permanent magnet 155

List of Tables

1.1 Characteristics of the mechanoreceptors in the skin of the human fingertip 10

1.2 Summary of the quantitative requirements for a tactile feedback system 16

2.1 Comparison of tactile sensors (continued in Table 2.2) 40

2.2 Comparison of tactile sensors (continuation of Table 2.1) 41

2.3 Estimation of the size of a hard ball in a simulated liver 69

2.4 Comparison of the characteristics of the elastoresistive tactile sensor with the requirements 70

3.1 Comparison of tactile displays 87

3.2 Comparison of the characteristics of the different prototypes with the requirements 130

4.1 Results of the cylinder diameter discrimination task per couple . . 142

5.1 Comparison of the characteristics of the tactile sensor and the different tactile displays with the requirements 146

Chapter 1

Introduction

Minimally Invasive Surgery (MIS) continues to grow in importance and to gradually change and improve the medical practice. This technique comes with great advantages, such as lower risk, fast patient recovery and a reduced hospital stay, but requires an increased dexterity and concentration on the part of the surgeon. To solve those problems, robots were introduced that mimic the movements of the surgeons, allowing them to focus solely on the medical procedure. In conventional operations, the surgeon often uses his fingers to palpate tissue and underlying structures. This palpation is necessary to determine for example the location and thickness of hidden arteries —the pulsatile pressure variation can be detected— or nerves [41] [112]. Tactile feedback can furthermore be useful for the localisation of lesions [47] and tumours [112] [257] [349], which often appear as hard lumps embedded in soft tissue, such as the lungs and the liver. Currently, there is only visual feedback from the patient to the surgeon. The lack of haptic feedback is one of the most important drawbacks of minimally invasive surgery.

To restore the tactile information channel, a lot of research has already been performed to develop tactile feedback systems. Surgery was already mentioned as a possible, but difficult, application for tactile sensors long before there was actual research in this area [96], and attempts to make a tactile sensor for minimally invasive surgery date from before 1994 [242]. Such a feedback system consists of two main parts. A tactile sensor to register the tactile information inside the patient, and a tactile display to reflect the tactile information to the skin of the surgeon. A central processing unit to controls and monitors the system, but is not the focus of this dissertation.

Section 1.1 elaborates more on MIS and the application of tactile feedback in MIS. To get some insight in tactile sensing before designing an artificial tactile sensor, Section 1.2 studies the human sense of touch, with its mechanisms, properties and capabilities. Based on this, Section 1.3 derives the specific requirements for a

tactile feedback system for MIS. This is an evaluation of the requirements posed in literature, comparing them with sensible values based on the properties of the human skin and of soft tissue palpation.

Chapter 2 discusses the tactile sensor, the first part of the tactile feedback system. After studying different sensor principles, elastoresistance is chosen for its simplicity and robustness, and examined more closely. Elastoresistance is found to be often poorly understood and its physical principle misconceived. Simple experiments show that only the contact resistance plays a role in an elastoresistive tactile sensor. The importance of different contact properties such as surface roughness or adhesion are not specifically studied in this dissertation. The design of a new tactile sensor is discussed, together with improved readout electronics. These electronics are optimised for high speed and low interference with the sensor signal. They can easily be adapted for different sensitivity and resistance ranges, and only use very low voltages, which is relevant in the context of MIS. The prototype tactile sensor is simple, flexible, cheap, thin and adjusted for the desired pressure range, but still suffers from large hysteresis and drift.
Chapter 3 discusses the second part of the tactile feedback system, the tactile display. After going through some general design guidelines, an overview is given on existing tactile displays with a slight focus on small scale shape displays. Several prototypes are built in an attempt to reach the challenging requirements. These include the first two appearances of hydraulics applied in tactile displays. The first is a closed hydraulic system, profiting from the incompressibility of water to transfer the actuation over a distance. The second uses an open hydraulic system with a piezoelectric proportional valve to actuate the individual pins of the tactile display. A final prototype uses pneumatics and thus needs a pneumatic proportional valve. Existing commercial valves are too large to fit into an already crowded operating room, and make too much noise. Therefore a small and noiseless proportional valve is designed and built, which allows for easy integration into a compact array to operate the necessary large amount of pins. The pressure range which this valve can produce, however, is too small for a tactile display, and the design needs considerably more research before it can be employed.
Chapter 4 integrates the knowledge and results of the previous chapters in a functional tactile feedback system. The aim of the system is to serve as a proof of concept rather than to fulfil all the requirements. Still, it occupies a specific spot among other tactile displays found in literature. While there are displays with a larger bandwidth, a higher resolution or a higher force, none of them combine those in a single display. On top of that, the display is very compact and has an almost negligible weight. An experiment to evaluate the combined system shows that it allows to perform a relatively complex discrimination task, even though it is too difficult to distinguish a hard ball in soft tissue without advanced signal processing techniques.
Finally, Chapter 5 offers a conclusion and makes suggestions for improvements and future research.

1.1 Minimally Invasive Surgery

In minimally invasive surgery or medical endoscopy the patient is operated on via only a few small incisions, through which a camera (endoscope) and instruments are inserted. In laparoscopy or abdominal surgery the abdomen is inflated with CO_2 to create a cavity. Other types of MIS include thoracoscopy or chest surgery and arthroscopy or orthopaedic surgery. Many experts believe that minimally invasive techniques may eventually be used in as many as 75% of abdominal and thoracic operations [271]. It is for example often used for cholecystectomy (gall bladder removal) or colectomy (resection of the colon). By the early nineties, laparoscopic cholecystectomies in the USA already outnumbered open surgery by a ratio of 65 to 35 [2].
The success and popularity of laparoscopic cholecystectomy led the way to the development of the endoscopic resection of various intra-abdominal and intrathoracic tumours [290]. There have been many reports of laparoscopic colectomy for large bowel cancer. Many cases of video-assisted thoracic surgery for lung cancers have also been carried out. Small numbers of laparoscopic hepatectomy (resection of the liver) and pancreatectomy (resection of the pancreas) have also been reported. This is obviously an ideal method for the removal of early cancers. There is a large and increasing variety of minimally invasive interventions, because the performed procedures can be more effective than in open surgery [2]. Procedures such as radiosurgery, radiofrequency ablation, and video-assisted endoscopic resections can achieve cancer control with minimised risk and morbidity. However, concerns were raised when reports of laparoscopic port-site recurrence of cancer appeared. There has also been doubt whether lymph node dissection can be carried out laparoscopically as adequately as in open surgery.
The main advantages to minimally invasive surgery as compared to conventional surgery are lower risk and pain, shorter postoperative stay and thus an overall reduction of health-care costs, resulting in a speedy return to daily activities. The trauma to surrounding tissue is minimised, followed up with better cosmetics [2] [229] [269] [271].
One of the main obstacles to the general and widespread adoption of these techniques is the difficulty of teaching them [2]. In the future, students will likely have to carry out simulated training before turning their hand to real operations, thus cutting down the number of surgical errors. The likely benefits of surgical simulation teaching are a shorter time and an increased safety for surgical operations. For this purpose, GMV, among others, developed a virtual medical trainer with two PHANTOM® Omni joysticks to provide haptic feedback [2].

Conventional MIS has some issues, such as an unstable camera platform, limited motion of the straight laparoscopic instruments, two-dimensional imaging, poor ergonomics for the surgeon, and the ‘fulcrum’ effect. This last effect denotes the fact that the laparoscopic instruments pivot around a fixed entry point into the

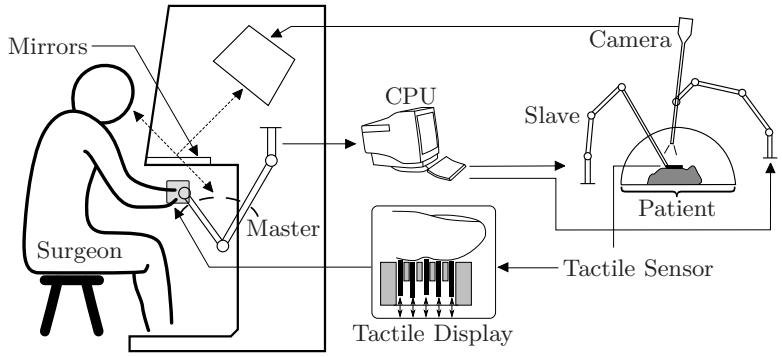

Figure 1.1: *Schematic overview of a telesurgical system with tactile feedback. The surgeon manipulates a 'joystick' at the master side and the robotic 'slave' arms move the instruments inside the body. One of these instruments could be a tactile sensor to gather tactile information, which is then sent to the tactile display at finger of the surgeon.*

body, which means the surgeon has to move his hands in the reversed direction. To overcome these problems, robot assisted surgical systems where developed [12] [167]. These systems are teleoperated with the surgeon at a console, controlling a 'joystick' —the 'master' side— and the instruments manipulated by robotic arms inside the patient —the 'slave' side (Figure 1.1). Rassweiler et al. [255] and Boehm et al. [34] discuss the development, advantages and disadvantages of telesurgery.
There are some advantages to robotic telemanipulation [269]. First, limited dexterity is restored and the fulcrum effect is eliminated, so the surgeon no longer has to move the instruments in reverse direction. Additionally, a foot pedal can be used to freeze the instruments, which allows repositioning the controllers and forearms to an ergonomically favourable position. Coupled with the fact that the surgeon can sit in a comfortable position makes robotic telemanipulation more ergonomic. Visualisation is improved, and can even be three-dimensional, with two different images displayed for each eye, which is demonstrated to improve performance [212]. Other key advantages are tremor eradication and scaling opportunities [63]. All these factors result in a significantly improved dexterity for the surgeon [205]. In robot assisted surgery, the surgeon can focus more on the medical aspect, without worrying about the technical skills required. As a result, robots facilitate surgeries which previously were technically impossible or unfeasible with conventional treatment, such as totally endoscopic coronary artery grafting [167].
Examples of surgical robots include the 'da Vinci'–system produced by Intuitive Surgical and the ZEUS robot by Computer Motion. Computer Motion and Intuitive Surgical merged in 2003 and the ZEUS is no longer supported. Although the da Vinci robot is the only commercially available system for abdominal and

thoracic surgery, there are plenty of experimental setups or systems for other types of surgery. One promising surgical robot is the Vesalius robot, recently developed at the Katholieke Universiteit Leuven. Despite all the advantages, the benefit for the patient is not always readily apparent because of the difficulty and cost involved in large scale randomised tests [167] [193].

Because a robot assisted system is teleoperated, the surgeon can even be in a distant location. Faster intervention for astronauts in space, miners, fire fighters, and others working in hazardous environments is facilitated. The military has been the driving force behind robotic surgery in general and the da Vinci system in particular, even though it has not yet seen application on an actual battlefield [167]. Medical vehicles equipped with such remote-controlled robots could get surgical care to soldiers much faster than it would be to evacuate them to the nearest base or hospital [271]. Robotic telesurgery is in this context possible with an unmanned aircraft circling over the scene for communication [267]. There is a time delay of 20 ms for manipulation and 200 ms for video. The robot design should be as small as possible. The maximum time delay to successfully perform teleoperation or telesurgery is 200 ms. If tactile feedback is available, this increases to 400 ms [55].
In 2001, Jacques Marescaux, a surgeon at the University of Strasbourg, in France, worked with Computer Motion to modify its system and perform the first remote surgery on a human patient: a gallbladder removal procedure called laparoscopic cholecystectomy [192]. Using a dedicated high-speed connection, Marescaux controlled the robot from New York City while the patient was lying in an operating room in Strasbourg.

Robot assisted surgery has some disadvantages as well. Because of the setup time, the time in the OR (Operating Room) is still longer than for conventional laparoscopic interventions, even if effective dissection time is shorter [269]. However, this only results in a slight increase of the total operation time [193]. The criticism in the case of heart surgery is that the duration is substantially longer and the patient spends significantly longer on a heart pump than in open surgery [80]. Despite the improvement of the vision to 3D, the operation times for robotic coronary surgery are still longer than with conventional techniques [260]. Several studies do show that totally endoscopic coronary artery bypass is feasible off-pump using an endoscopic stabiliser [167]. In the future the need of cardiopulmonary bypass (CPB) can also be avoided with virtual stabilising systems, which will have automatic safety margins.
The surgeons have to be convinced that MIS has an overall benefit for the patient. A lot of them consider robotic cardiac surgery as too daunting, too futuristic, or simply ‘overkill’ [51], time-consuming and prohibitively expensive, without proven medical benefits [167] [266]. The same results can often be obtained with manual

MIS. Rather than a practical tool, a surgical robot is often a marketing tool and a must have for a centre that wants to be known for its excellence in MIS [167].

Lack of haptic feedback, both kinaesthetic and tactile, is one of the main limitations inherent to all surgical robotic systems [112] [167] [208] [269] [271]. In open surgery the surgeon controls his actions by visual and tactile feedback. Even in conventional endoscopy feedback of forces is reduced by friction. Hayward and MacLean [100] [186] give a good tutorial and overview about haptic feedback. A lot of research is done in the field of kinaesthetic feedback [63] [352]. Peirs et al. [244] built a special force sensor for this purpose. The forces measured during an operation on a rat stayed below 2.5 N. Puangmali et al. [249] give an overview of sensing in MIS. Tissue properties can also be estimated with active excitation of the instrument [202], but the possible effects of this on the tissue are unsure. Force feedback allows discrimination between tissues of different stiffness. Enhanced sensitivity makes it even possible to discriminate between smaller differences than would be possible with direct manual manipulation [64].
The usefulness of force feedback has been illustrated repeatedly. Performance increases significantly in a task where tubes have to be sorted by compliance with or without force feedback [185]. Another study shows that both surgeons and non surgeons exert lower forces during blunt dissection with force feedback [343]. This would result in lower tissue damage. Force feedback also helps to guide the instrument to the softest tissue. Okamura [226] discusses the necessity of haptic feedback in robot assisted surgery and gives an overview. Forces and the variance of those forces decrease when force feedback is added in suturing tasks. Force feedback can also be substituted successfully with visual or auditory signals. In a suturing task, a colour bar on the screen indicating the force level improves performance [151]. In a task to insert one tube into another, force feedback also decreased the applied force [341]. Part of the effect might be due to the fact that only 2D vision, and thus limited spatial information, was available. Westebring – van der Putten et al. [350] give a general application driven overview of research in the field of haptic feedback for MIS.

1.1.1 Importance of Touch

Touch is very important in a lot of operations. As discussed previously, the absence of tactile feedback is one of the main drawbacks of minimally invasive surgery. This is especially true for procedures demanding higher technical skills [269]. In laparoscopic colectomy, the absence of palpation is a major limitation, because it greatly limits the surgeon's ability to stage the disease adequately [229]. When tactile sensation is regained, laparoscopic-assisted colectomy is safer and faster [18]. Palpation is also a standard screening procedure for the detection of breast, thyroid, prostate, and liver abnormalities. The pathological state of soft tissues is often correlated with changes in stiffness, which yields a qualitative

estimation of the Young modulus of the tissue [152]. Bholat et al. [25] investigate the importance of tactile feedback in surgery. They found that, in comparison with conventional and laparoscopic (not robot assisted) instruments, palpation is clearly faster and more accurate to detect shape or consistency in absence of visual feedback. Several prospective studies compare palpation to other visualisation techniques like intraoperative ultrasound (IOUS) and computed tomographic (CT) scans. Ravikumar et al. [257] found that palpation is able to find more lessions than a CT scan, but less than IOUS, while Nies et al. [222] showed that palpation of the liver had the highest sensitivity (83%) and specificity (100%) compared to CT scans, and percutaneous and operative US. In another study, palpation allowed to detect most (>90%) liver metastases with perfect specificity [47]. Palpation is less sensitive with respect to small and deeply located lesions.

The above mentioned examples and studies show that a highly developed sense of touch is one of the most important tools of a surgeon. This is true despite the fact that the surgeon wears a glove, or often even two, which reduces tactile sensitivity somewhat. The lack of tactile feedback can cause problems when visual feedback is not adequate. Surgeons can accidentally cut a blood vessel hidden underneath a layer of fat [208]. They rely on sensations from the finger tips to guide manipulation and to perceive a wide variety of anatomical structures and pathologies. The surgeon uses his perception of small-scale shape to find hidden anatomical features and to locate tumours [112], but he also relies on force reflection [111].

The lack of tactile feedback during laparoscopic surgery can be overcome by the adoption of a 'hand-port', through which the surgeon inserts one hand into the operative field to aid dissection [290]. This necessitates a large cut, which makes the operation a lot less 'minimally invasive'. In video assisted thoracoscopic surgery, tumours found in peripheral lung zones are difficult to locate [201]. Accurate localisation of the embedded tumour is critical to ensure that the entire nodule is removed and minimises the amount of healthy lung tissue resected. The tumours are often not visible from the lung surface. A frequently used method is sliding against the lung surface with a long metal rod inserted through the chest wall, to 'feel' the hard inclusion. This is difficult and time consuming. Miller et al. [201] propose a capacitive tactile sensor probe from Pressure Profile Systems, Inc. with 12×3 elements. With this probe, it is easier to locate inclusions. The location of the instrument is determined with image processing and the tactile image is overlaid on the screen.

1.2 Psychophysics of Touch

In order to design a tactile feedback system that can produce a realistic feeling it is important to understand the psychophysics of touch. This section discusses the function of the different mechanoreceptors in the skin, the sensitivity of the human tactile sense and the reaction on different inputs like vibration or electricity.

Lederman [171] gives a good overview of the psychology and the psychophysics of touch. McGlone and Reilly [197] give a broad overview of the human cutaneous sense, including touch, temperature, pain and pleasure.
Perception of our environment through the sense of touch is described by haptics. Haptics has been an active field of research for about two decades, but progress has been hampered by its interdisciplinary nature [262]. It requires the cooperation of experts in such diverse areas as neurology, applied psychology, robotics, human-computer interaction, control systems engineering, and communications. The origin of the term haptics if found in the Greek word "haptesthai" which means the sense of touch with both tactile and kinaesthetic components [42]. Similar Greek words are "haptomai" ($\dot{\alpha}\pi\tau o\mu\alpha\iota$), which means to touch and "haptikos" for to grasp, to touch. Haptics is usually subdivided in two modalities: the kinaesthetic and the tactile sense. This is also the terminology proposed in recently established ISO norms on the subject [329]. Some more specific, less used terms are somesthesia (sense of the skin), statesthesia (sense of posture), kinaesthesia (sense of movement), and stereognosis (ability to determine shape and weight of an object) [68].
Kinaesthetic sensing or proprioception refers to the perception of the internal state of the limb through parameters such as joint angle and muscle effort, which allows us to feel large scale contour, shape, inertia and weight of objects. Tactile or cutaneous sensing refers to the distributed sensation in the skin [112] [181], which relates to sensations like textures, vibrations, and small scale shape, but tactile sensing can also provide information about compliance, friction and mass [109]. Kinaesthesia is an unconscious sense: the sensory input from inside the muscles and between the muscles and the tendons arrives in the unconscious part of the brain. Humans are not consciously aware of these stimuli so they can move around and use the information about where their limbs are without having to worry about it [174]. Other proprioceptors are located in the joints and ligaments or the sense of gravity in the ear. Kinaesthetic information is insufficient where transmission dynamics (friction, backlash, compliance and inertia) tend to mask the desired signal [109].
People become clumsy when deprived of reliable tactile information through numbness of anaesthetised or cold fingers [126]. When our arm is sleeping we can still move it, but cannot use it effectively because of the lack of sensory feedback. This shows that tactile sensation is essential for many exploration and manipulation tasks not only in a real environment but also in a virtual environment [163]. Mott and Sherrington [207] suggest that the kinaesthetic sense is less important in performing tasks than the tactile sense. They severed sensory roots in the spinal nerves of monkeys. When the upper limb was rendered insensible, with the exception of most of the tactile sense in the hand, they used their arm as normal; when the skin of the hand was rendered insensitive, they did not use their arm at all, even under strong incentive. They also note that when only the tactile sense of the thumb and part of the index finger is retained, movement is only slightly impaired. This is supported by an experiment conducted by Srinivasan and LaMotte [301]

which studies the importance of both tactile and kinaesthetic information in softness discrimination. When the objects had a deformable surface, the tactile sense is necessary and sufficient. When the surface is not deformable, both senses are needed. Bicchi et al. [27] have similar results. Stiffness or compliance of an object, while relating closely to kinaesthesia, is measured mainly in the skin by using information about the deformation of the surface. Force and displacement cues do also influence the judgement, especially for soft materials [22]. Similarly, kinaesthetic feedback can be substituted by tactile stimulation. A normal stress on the fingertip alone is nearly indistinguishable from a joystick with force feedback [248].

Moreover, a sense is never on its own. There is an interaction between different senses, called multimodality [7]. We move our hand, see what our fingers are feeling and feel the tactile input at the same time. For a tactile feedback system, it is important that the surgeon intuitively connects the sensation he feels on his finger with the movement he makes with his hand and with what he sees on the screen. Sight is the most important aid in manipulation and recognition tasks [353]. Kammermeier et al. [135] elaborately discuss multimodality in the context of telepresence systems and propose a mathematical model of human perception for this application. The performance of a simple task such as pushing a virtual button improves with simple tactile feedback [144]. This suggests that the improvement would be even larger in more complicated tasks.

An example of the strong information capabilities of touch is Tadoma. That is a technique for which one places a hand on the face and neck of a talker and monitors a variety of actions associated with speech. This way trained deaf and (almost) blind people can understand what is said [311] and even learn how to speak [259].

The pain threshold on the fingertip is 3.2 N at a pin diameter of 1.75 mm which corresponds to a pressure of 1.3 MPa [41]. That is about 1 N for a pin diameter of 1 mm. The stiffness of the fingertip is nonlinear; soft for small deformations and more rigid for larger deformations, as is typical for human tissue [79]. The stiffness increases when the fingertip is tilted. For an applied total force of 7 N of the entire fingertip against a flat surface, the deformation is between 2 mm and 3 mm [95].

1.2.1 Mechanoreceptors in the Skin

Mechanoreceptors convert the mechanical deformations caused by indentation, vibration or slip of the skin into electrical nerve impulses. Apart from mechanoreceptors, the human skin also has thermoreceptors to sense temperature and nociceptors for pain. The human perception is the interpretation of these signals in the brain [208]. The four most important types of mechanoreceptors in the glabrous skin can be categorised according to their temporal frequency response and the

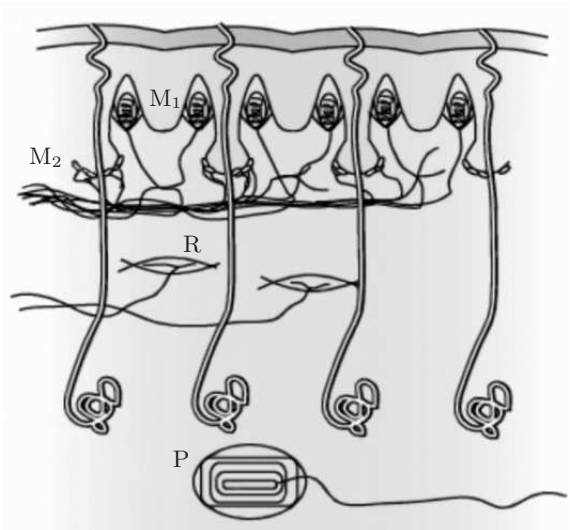

Figure 1.2: *Nerve endings usually associated with mechanical triggers in the human glabrous skin; M_1: Meissner's corpuscle; M_2: Merkel cell; R: Ruffini corpuscle; P: Pacinian corpuscle (adapted from [133])*

receptor type	FAI (Meissner)	SAI (Merkel)	FAII (Pacinian)	SAII (Ruffini)
field diameter	3–4 mm	3–4 mm	> 20 mm	> 10 mm
mean receptive area	12.6 mm^2	11 mm^2	101 mm^2	59 mm^2
spatial resolution	fair	good	very poor	poor
frequency range	8–200 Hz	DC–200 Hz	50–1000 Hz	DC–200 Hz
most easily excited frequency range	8–64 Hz	2–32 Hz	> 64 Hz	< 8 Hz
relative amount	43%	25%	13%	19%
postulated sensed parameter	skin stretch	compressive stress (curvature)	vibration	directional skin stretch
density	70–140 /cm^2	70–140 /cm^2	20 /cm^2	50 /cm^2

Table 1.1: *Characteristics of the mechanoreceptors in the skin of the human fingertip (compiled from [109] [123] [208] [246] [285] [324])*

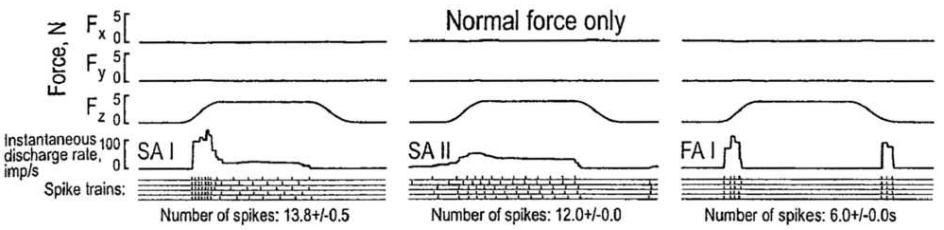

Figure 1.3: *Response of mechanoreceptors to rising and dropping stimuli [31]. While an orthogonal force F_z is applied to the fingerpad, the nerve signals of single mechanoreceptors of different types are measured. A large discharge rate in the nerve signal suggests a strong sensation. SAI and SAII receptors are not stimulated by a dropping force, and FAI receptors only when contact is broken.*

size of their receptive fields [112] [125]. The hairy skin also has touch sensitive hair follicles. Figure 1.2 shows how they are located in the skin and Table 1.1 gives their properties. All receptors show large hysteretic behaviour, reacting strongly to an increase of pressure, and nearly not to a decrease. Fast adapting receptors are stimulated by a decrease, but mostly at the actual moment of release and very little before that [30] [31] [324] (Figure 1.3). For weak stimuli, only the nerve endings in the touching skin are involved, while for everyday manipulations, also nerve endings in the side or the end of the fingertip are triggered [30].

Cutaneous mechanoreceptors are described as slowly adapting (SA) or fast adapting (FA or RA: rapidly adapting) according to their frequency response, particularly to static stimuli. The other criterion is receptive field size: Type I units have small receptive areas and well defined boundaries, while Type II units have large receptive areas with poorly defined boundaries. Type I receptors (both SA and FA) are located close to the surface of the skin where the deformations and induced stresses are more pronounced. The nerve endings commonly associated with the mechanoreceptors are Merkel disks for SAI receptors, Meissner's corpuscles for FAI, Ruffini endings for SAII and Pacinian corpuscles for FAII [109] [208]. Merkel disks (SAI) and Ruffini corpuscles (SAII) react to static pressure, Meissner's corpuscles (FAI) —and to a lesser degree Merkel disks— measure speed of skin indentation and Pacini corpuscles (FAII) respond to higher frequencies [273]. There is an apparent trade-off between spatial and temporal resolving power [171]. SAI units are better than FAI at resolving the finest spatial details. FAI are somewhat better at resolving vibrotactile patterns, and are also important to detect contact. The FAII units are sensitive to the highest portion of the frequency spectrum, but can hardly code any spatial details at all. They have onion-like sheets, which effectively function as a mechanical high-pass filter to the indentation signal [273].
Neurophysiological studies suggest that SAI mechanoreceptors are most important

in small-scale shape perception [7] [166], which suggests that a relatively low bandwidth display may suffice in many applications [112]. The ability to separately perceive two pointed indenters on the finger tip requires that the points be separated by 1–2 mm, and humans perceive a surface as textured rather than perceiving each small surface feature individually if the features are less than about 1 mm in extent. Texture perception is mediated primarily by spatial encoding for coarse textures and by vibrotactile encoding for fine textures [106]. Displacing a finger over the explored surface generates the perceived vibration [19].

There are about 17000 mechanoreceptors in the grasping surfaces of the human hand. Their spacing ranges from about 0.7 mm in finger tip to 2 mm in the palm [324]. Both FAI and SAI elements are much more prevalent in the fingertip than in the palm, while FAII and SAII are almost evenly distributed. Density at the finger tip is estimated to be about 241 units/cm^2, while in the palm it is only 58 units/cm^2 [124].

Sensitivity to the direction of stretch is often attributed to Ruffini endings. Recently, these Ruffini endings have come under discussion. Paré et. al [234] suggest almost no Ruffini endings can be found in the human glabrous skin. The SAII signal and directional sensitivity found in electrophysiological studies may not originate from Ruffini endings after all.
Birznieks et al. [30] show that SAI, SAII and FAI afferents all have a preferred direction of force, and they are distributed in all directions for each type, but not uniformly. SAI is biased in the distal direction, SAII in the proximal direction, and FAI in proximal and radial directions.
There are indications that different receptors influence each other in a mechanism called lateral inhibition, which helps e.g. in edge detection. It is also a possible explanation for the fishbone illusion, in which the sides of the finger are stimulated by moving over a rough or sticky surface, and the middle of the finger feels like it is going over a gap [218]. In a personal discussion with Johansson, he gives three mechanisms for lateral inhibition. The first, and most important, is mechanical. When a square object is pressed on the skin, the stress level in the skin is highest under the edges of the object. On a lower level, different endings of a single tactile unit might interfere with one another. An activated ending dominates the nerve and even backfires to the other endings. It is not clear whether this is important. At an even lower level, the nerves interfere with each other where they meet, which could result in lateral inhibition.

1.2.2 Limits of Human Perception

Humans are very good at recognising common objects by touch, within 1–2 s [171]. The skin is very sensitive to light pressure. Studies have determined that the perceived intensity of stimulation is affected by both depth of penetration and by rate of skin indentation [171]. Actual intensity judgements are more closely correlated with stimulus force than with indentation. Under ideal condition a displacement of the skin less than 0.001 mm can be perceived as a stimulation of touch, although the amount of stimuli needed to achieve such a sensation differs between body parts [272]. The absolute threshold for touch force perceived on the fingertip is 0.8 mN [284]. The minimum perceivable height of a static raised feature on a smooth surface is 0.85 μm. Small dots with 40 μm in diameter and 8 μm in height can be detected 75% of the time with active scanning [122]. 75% gap detection and grating detection thresholds are 0.87 mm and 0.5 mm [127] [325]. Johnson and Phillips [127] have shown that humans can reliably distinguish between two points that are separated by as little as 0.9 mm [349], while Sherrick and Craig [284] found this value to be 2.5 mm and Loomis [180] found 2.8 mm. This is often called the two point discrimination threshold and depends on the frequency of the applied input. For the design of a tactile display, it determines whether an array is felt as separate pins, or as a smooth surface. There is an increased sensitivity between 1–3 Hz and between 25–40 Hz, which are the frequency ranges of SAI and FAI receptors [162]. There is an important difference between discrimination of spatial misalignment, spatial interval discrimination, point localisation and spatial resolution [180]. Hyperacuity was discovered, where perceptual thresholds can be much finer than the spatial resolution. Vernier acuity (two parallel lines, of which one is slightly displaced to left or right) was found between 0.37 mm and 0.70 mm. Point localisation (excitation left or right from reference) was 0.17 mm. While position localisation is within about 1 mm, a shift of 0.1 mm can be detected [171]. The spatial discriminative capacities of the skin are strongly task-dependent. The just noticeable difference of pressure amplitude is 14% for static pressure and 20% at 160 Hz [170].

The maximum frequency of perceptible vibrations is about 1000 Hz [312] with a maximum in sensitivity at 250 Hz [131], which corresponds to the FAII receptors. Bolanowski et al. [35] show a maximum sensitivity at 300 Hz, at which frequency a vibration with an amplitude of 0.1 μm can be detected. According to Sherrick and Cholewiak [283], this threshold is between 0.2 μm and 0.5 μm at 200 Hz to 400 Hz. At 30 Hz, amplitudes of 5 μm to 20 μm can still be detected. Another study also shows a lower threshold at 320 Hz than at 40 Hz [308]. Van Doren et al. [328] confirmed these findings and combined spatial and temporal components. At frequencies above 64 Hz they did not find any influence of the spatial components on the threshold; below this frequency, they found that a higher spatial frequency corresponds to a lower threshold.

1.2.3 Vibration and Simulation of Sensation

Humans have a limit in how much information they can process. That limit can be dispersed between different perceptual systems. The use of more sensory channels can augment the coding of information without overloading any of the perceptual systems used [7]. Humans can have difficulty detecting change between vibrotactile patterns [86]. Tactons are structured, abstract, tactile messages [39]. These tactons can e.g. be used to replace visual progress bars [37]. MacLean and Enriquez [311] investigate the possibility to use haptic icons, represented by vibrations at different frequencies, waveforms and amplitudes, as a haptic language. The Weber factors to discriminate time duration of vibrational stimuli or to discriminate sweeping velocity of vibrational stimuli are about 0.2–0.4 [108]. Pasquero [235] gives an overview of the efforts made to create tactile languages.
Geldard and Sherrick [87] describe the effect of 'sensory saltation' or 'cutaneous rabbit'. For this sensation three stimulators are evenly spaced in a line and vibrating pulses are delivered in the following sequence: three pulses on the first stimulator, three on the second and one on a last. The observer feels the pulses seemingly distributed with more or less uniform spacing from the first stimulator to the last. The sensation is characteristically discrete as if a tiny rabbit was hopping up the arm. Similar effects are experienced with an array of vibrotactile stimulators on the back or anywhere on the body. Hayward [98] gives other examples of haptic illusions.

Apart from providing information, vibration also contains information about the touched objects. Vibration can enhance certain telemanipulation tasks, which are more difficult when vibration is absent [153]. Humans also perceive texture information from high frequency input or vibration [153] [163]. Combined with the speed of the finger, the temporal frequency is related to the perceived roughness. Konyo et al. [155] assume that the perceived roughness becomes larger when the frequency decreases. Lederman [171] on the other hand found that temporal frequency of vibrations set up in the skin by the relative motion between skin and surface is not used to perceive roughness, and friction nor groove-ridge ratio influences this perceived roughness. Without lateral motion between skin and surface, it is impossible to perform fine texture discriminations, but the velocity is not important, and neither is the distinction between active and passive touch in this case. 2% to 5% of variation in the spatial period of patterns such as dots can be discriminated.
Vibrations are sometimes unwanted, because the sensitivity can decrease after exposure of the skin to vibrations [21] [183]. This adaptation is also noticed during experiments with an electromagnetic tactile display [305] which can provide small stimuli up to 2.5 mN. The perception of sinusoidal waves often decreases in time, and more so for waves of 100 Hz and 250 Hz than for 10 Hz. When the wave is interrupted with a rest time, the signal remained perceivable much longer.

Electrodes on the skin can stimulate different mechanoreceptors [130] [256]. Experiments in single-nerve stimulation showed that Merkel cells generate a pressure sensation, while Meissner's corpuscles produce a vibratory sensation [323]. It is difficult to confine the general sensation to a small area. The relationship between the amount of current and the generated sensation is unclear and unstable. Sudden pain causes an invasive impression, or even fear [134]. Electrocutaneous stimulation can result in an electric shock because there is no relation with contact force. Use of a force sensor can reduce this problem [134]. The sensation can be slightly improved by compensating for the variable impedance of the human skin [132]. Despite these efforts, the display feels uncomfortable and unnatural.
Alternatively, an electrostatic attraction can be created between the skin and an electrode surface. This results in a 'sticky' or 'buzzing' sensation [15].

Levesque and Hayward [175] found that tactile sensations can be elicited with lateral skin stretch only. They investigate lateral skin strain patterns when passing over simple geometrical features to use this as an input for a tactile display. In movement on a glass flat surface, a central region of the finger skin stays stationary and the surrounding skin moves, resulting in compression or expansion of the intermediate skin. When moving over a bump or a hole, compression is detected on the rising part and expansion on the dropping part. The idea is put into practice for a Virtual Braille Display [233]. At small scale the resulting sensations seem to be indifferent to the details of skin stretch/shear orientation [236]. Drewing et al. [70] investigated with which resolution humans can discriminate the direction of skin stretch and found large individual differences between 21° and 78°. Results achieved by Peeters et al. [240] suggest that a relatively large stretch is required to simulate the same sensation as an orthogonal indentation.
Webster et al. [213] [346] did research on slip. Subjects can notice a difference between moving angle and slip angle of 20° and detect a sinusoidal slip speed difference of 30% of nominal slip speed. For both values, 50% of the test subjects could notice the difference.

1.3 Requirements of Tactile Feedback in Surgery

The aim of this research is to develop a system with a tactile sensor to enter the body through a small incision, and a tactile display to convey a realistic sensation to the surgeon. The technology has to be intuitive and support the knowledge and skill of the surgeon as much as possible so he can focus completely on the medical aspect of the operation. The system has to be optimised in cooperation with the surgeons. The quantitative requirements regarding spatial resolution, frequency range, and sensitivity of the sensor are derived from the psychophysical properties of the human sensory system, as discussed above. Since small-scale

Spatial resolution	1 mm
# taxels	10×16
Frequency range	DC to 20–30 Hz
Stroke	2–3 mm
Force range	0.5 N
Sensitivity	5–10 kPa
Accuracy	10%

Table 1.2: *Summary of the quantitative requirements for a tactile feedback system as derived from the psychophysical properties of the human sense of touch*

shape perception depends mainly on SAI receptors (Merkel disks), their properties are determining. The quantitative requirements used as a goal for this dissertation are summarised in Table 1.2. The origin of these requirements is discussed below, together with some miscellaneous or application specific requirements.
In literature, not always the same requirements are given, and they can even be contradictory. This reflects the fact that currently no tactile display is capable of verifying them, so they are based on well informed guesses. The requirements listed are meant to be a realistic trade-off between technological feasibility and usefulness of the resulting system. Both tactile sensor and display have the same requirements, since the aim is a direct link between the two and any 'excess' performance at one end would be lost at the other.
Little can be said about requirements of tactile sensors in general, since those vary widely between applications. Especially in industry, binary sensors in small, compact arrays can already suffice [96]. However, systems that combine a tactile display and a tactile sensor to sense remote objects, teletaction systems, have similar requirements. For an ideal or transparent teletaction system, the patterns felt by the user would be indistinguishable from direct contact with the environment [208].
There is no real naming convention for the separate tactile elements; tactels (tactile element) [208] [231], taxels (tactile pixel) [19], texels [347] or tactors (tactile actuator) [112] [270] are used. Taxel is the most frequently used and is adopted here.

1.3.1 Spatial Resolution

To get a realistic feel, the spatial resolution should be close to the spatial resolution of the mechanoreceptors in the human skin. A spatial resolution of 1 mm in both directions is necessary [8] [208] [209] [342]. Wellman et al. [349] state that a resolution of 0.9 mm is required to experience shape instead of separate pins. If the

problem is approached as spatial frequency, a resolution of 1 mm corresponds to a two point discrimination threshold of 2 mm or, according to the Nyquist–Shannon sampling theorem, a signal with a frequency of $0.5\,\mathrm{mm}^{-1}$. Often an elastic layer is used as a low-pass filter to make the separate pins impossible to detect [208]. Care should be taken that the spatial resolution is not reduced by crosstalk [353], or by this elastic cover (Section 2.1.1). Crosstalk is mainly an issue of the sensor and usually less of the display.
Another approach is to state that the resolution should match the size of the receptive field of the relevant mechanoreceptors. For SAI receptors that leads to a resolution of 2–4 mm [238] [277]. The taxels must cover the entire fingerpad area, which is typically between $1\,\mathrm{cm}^2$ and $2\,\mathrm{cm}^2$ [238].

Since a realistic feeling is an important goal, the distance between the taxels should be about 1 mm. For a fingerpad area of approximately $10\times16\,\mathrm{mm}^2$, this means that the tactile feedback system should have 160 taxels.

1.3.2 Frequency Range

The sensitive frequency range of the skin with its different receptors is very high, about 1000 Hz [238]. Pasquero and Hayward [236] suggest this high rate should be matched. This, however, depends on the desired perception. For coarse textures and shapes, the perception is mediated primarily by spatial encoding and for fine textures by vibrotactile encoding [106]. If the perception of texture is desired, a frequency range from 1 Hz to more than 500 Hz should be available [163].
However, not all receptors in the skin are equally important for specific applications. The frequency range or temporal resolution is connected to the spatial resolution. Peine et al. [243] found that the average palpation speed of a surgeon is 120 mm/s. A spatial resolution of 2 mm leads with this speed to 30 Hz, a spatial resolution of 1 mm leads to 60 Hz required bandwidth. According to Howe et al. [112] a low bandwidth display may suffice in many applications. The SAI receptors are mainly sensitive to frequencies below 32 Hz. However, in literature 50 Hz is often cited as required [208] [209] [342]. Experiments show that in a search task, the average time to find dots in one dimension halves when the bandwidth is increased from 5 Hz to 30 Hz [349]. This shows that a frequency higher than 5 Hz is certainly desired.

Based on this information, a frequency range from DC up to 20–30 Hz should suffice for small scale shape perception during surgical palpation.

1.3.3 Sensitivity, Force and Stroke

The display has to be strong enough to support the force applied by the surgeon while maintaining the desired shape [112]. 1 N of force per taxel [112] [208] [209] or a maximum pressure of 0.5 MPa [342] are mentioned. This 1 N of force on a sharp wedge is needed for 1 mm skin indentation [163] [300]. The maximum pressures during grasping and manipulation are typically less than 50 kPa [238]. In soft tissue palpation a pressure of 10–40 kPa is used [188]. To avoid pain, a pressure of 1.3 MPa should not be exceeded [41].
The given desired stroke is not consistent between references. 2 mm [208] [210], 3 mm [112] and 4 mm [209] [342] are mentioned. Since the maximum deformation of the skin at the fingertip is limited, 2–3 mm should certainly be sufficient as a requirement. As mentioned above, the just noticeable difference of pressures on the fingertip at low frequencies is 14% [170]. Therefore, an accuracy of about 10% on force or stroke should do.
Peine and Howe [241] show that in soft tissue palpation —detecting a hard ball in soft tissue— the absolute pressure hardly plays a role. More important is the indentation, caused by pressure differences. This means that the pressure distribution is useful, but the offset pressure is not. They also suggest that the tactile sensor needs a sensitivity of 0.5 kPa and the tactile display needs a displacement resolution of 0.05 mm. The sensitivity, sometimes referred to as the pressure resolution, denotes the smallest relative difference that is measurable, while the accuracy relates to the absolute measurement.

This last requirement is significantly more stringent and harder to meet than above. 5–10 kPa is chosen as a more realistic requirement for an initial tactile feedback system.

1.3.4 Miscellaneous Requirements

In general a low hysteresis and linear behaviour are desirable for sensors, but if limited or compensated for, those are not hard requirements. Because the purpose of the sensor is to enter the body through a small incision, some miscellaneous requirements have to be taken into account. First of all, the sensor should be flexible to be shaped like a finger and compact enough to fit on a surgical instrument. A round shape is important because a flat sensor would create stress concentrations near the edges, and increase the required total force to palpate. That could be circumvented by embedding a smaller flat sensor in an instrument with rounded sides, but this would reduce the useful area.
The sensor also needs to be biocompatible, resistant to body fluids, sterilisable, robust, reliable and inherently safe [353]. Klein et al. [152] elaborate on the safety requirements. Some important aspects are toxicity, risk of injury by e.g.

electrical hazard or electromagnetic interference. The price can also be an issue, since surgical instruments are often thrown away after a few uses. Because electro ablation is frequently used in MIS, care should be taken that this does not interfere with electrical signals of the sensor. For this reason, it might be more difficult to get approval for a tactile sensor that relies on those.

The tactile display has to be light enough to avoid limiting responsiveness and inertial forces while moving the hand and small enough to fit on the finger [112]. These requirements also apply for displays to be built into other devices of which the movement should not be restricted, such as a mouse or a steering wheel [236]. In applications in virtual reality and texture perception a combination of kinaesthetic and tactile feedback is needed. A 'passive' feeling on the skin, without the assorted exploratory movement of the arm, is less intuitive.
Of course the display has to be safe as well, but not as stringent as the sensor, because it does not have to enter the body. It does however need to be able to resist prolonged exposure to skin abrasion and be impervious to skin secretions [236].
Care should be taken that the power input per taxel is not too high, since it is multiplied by the number of taxels. An excess of dissipated power should not heat the taxels either. The price of the display is less of an issue than of the sensor, since the former probably need not be disposable.

According to Schuenemann and Widmann [277] and Kyung et al. [163] there is a need for reversible lateral movement of the display regions for the skin slip/stretch, from 0 cm/s to more than 5 cm/s. Since mainly SAII receptors detect directional skin stretch the requirements are based on their receptive properties: a resolution of 7–10 mm, a frequency range of 10–100 Hz and a force of 10 N. This can be separate from a distributed pressure display for small-scale shape. Lateral forces must be known to asses the coefficient of friction. Moreover, sensitivity to microscopic surface irregularities also appears to involve, or be mediated by, shear forces [171].

Chapter 2

Tactile Sensor

The first part of a tactile feedback system is a tactile sensor to acquire the desired tactile information. Throughout the past decades, a myriad of touch sensors have been developed for all sorts of different applications. Section 2.1 gives an overview of the different approaches and the physical principles employed to sense touch, starting with a few more general design issues, and finishing with a summarising table. Section 2.2 goes deeper into the principle of elastoresistance, elaborating on its origin, existing designs, the required readout electronics and, finally, some tests performed on elastoresistive rubbers. Afterwards, Section 2.3 applies this knowledge to an actual prototype and discusses the performance and properties of an elastoresistive tactile sensor. Finally, Section 2.4 offers a conclusion.

2.1 Overview of Tactile Sensors

The term 'tactile sensor' is used for a wide variety of sensors which rely on physical contact. Tactile sensors are used to measure force, force direction and/or contact location, thermal properties, texture, material stiffness, or simply to detect whether there is contact or not. This dissertation focusses specifically on pressure distribution sensors. This corresponds most with the human sense of touch, located near the surface of the skin. This means a tactile sensor measures the force, pressure or deformation in a distributed array of separate elements.
Throughout the last decades, a lot of tactile sensors for different applications and with different working principles were designed. Several overviews on tactile sensing have already appeared. Wolffenbuttel [353] presented an elaborate overview of tactile sensing technologies in 1994. Lee and Nicholls [173] gave an overview in 1999 for mechatronic applications. Eltaib and Hewit [75] discuss tactile sensing

technology for MIS, while Tegin and Wikander [318] give a more recent overview (2005) for robotic manipulation. De Rossi et al. [65] give an overview of smart skin in general with a section about tactile sensing. Schostek et al. [276] give a good application-driven overview of all aspects of tactile feedback systems for MIS, but have little focus on technology. Dahiya et al. [57] give a very broad overview on the sense of touch and its application in robotic tactile sensors, but has little focus on the actual technologies involved.

First, some general design guidelines are given in Section 2.1.1, with a special focus on the impact of a compliant layer on the sensor and some general remarks concerning the readout electronics. Because tactile sensors have a lot of different applications, Section 2.1.2 discusses some of those. Section 2.1.3 gives an overview of all the different sensor principles and their application in tactile sensors. Section 2.1.4 concludes with a brief comparison between the different techniques and a summarising table.

2.1.1 General Design Issues

Designing a tactile sensor for robot assisted minimally invasive surgery is not as straightforward as it may seem. While there are plenty of tactile sensors described in literature or commercially available, most of them do not match the resolution and sensitivity of the human skin, without sacrificing compactness or flexibility. The readout electronics should also be taken into account, as well as the connection to the multitude of flexible elements through the slender shaft of a surgical instrument. This section discusses different sensor principles and their application in tactile sensors.
While selecting a suitable sensor principle, a choice has to be made to sense either strain or stress [208]. Studies have determined that the perceived intensity of stimulation is affected by both depth of penetration and by rate of skin indentation. Actually, intensity judgements are more closely correlated with stimulus force than with indentation [171].
Another important issue is the difference between static and dynamic sensing. A static sensor can feel constant pressure and shape, while a dynamic sensor is better at feeling very small features and textures by moving over them and detecting change [110]. Dynamic tactile sensors respond to changes, in analogy with FA (Fast Adapting) mechanoreceptors. They measure vibrations or changes in stress [109]. Since palpation in surgery is a relatively slow process, a purely dynamic sensor is less suited. See Section 1.3.2 for the desired frequency range. If both high and low frequencies are desired which cannot be realised with a single sensor, it is possible to combine static and dynamic sensors [61] [273]. In a tactile feedback system, a low spatial resolution generally suffices for the dynamic sensor (Section 1.2.1).
The relationship between the surface profile and the observed image is ill-conditioned [43]. The reason for this could be that depends on the uncertain

contact condition between two surfaces. One method to improve the signal is to combine several sets of data from different perspectives using spatial filtering to suppress the effect of the noise. This approach appears to be used by human touch, which relies heavily on motion for collecting tactile data. The analysis reveals that motion is not only beneficial to touch, but essential in amassing sufficient data to extract accurate surface information.

Silicon IC (Integrated Circuit) technology suits itself very well for the production of arrays of elements with a high spatial density, and thus for tactile sensors. These sensors can be of nearly all varieties described below. Performance of silicon sensor structures is better than rubber based structures with respect to fabrication and sensing characteristics. Thanks to the possibility to integrate the sensor with a readout circuit on site, it is possible to reduce the noise level.
The biggest disadvantage of Silicon IC technology is that the material is rigid, and it is very difficult to produce a flexible tactile sensor. For this reason, this overview does not focus on this technology. While several examples are mentioned, a lot of research is done on fabrication technology, processing, integration and packaging which is not studied here.
Printed circuit board technology is also widely used [232], with the additional advantage that the circuits can be printed on flexible or even stretchable substrates [46].

Elastomer layer The cover of the sensor is sometimes an overlooked topic in tactile sensor development [261]. A frequently adopted sensor concept is that of the elastomer-based tactile sensors [353]. This broad category of tactile sensors utilises a layer of elastic material which constitutes the essential transduction element. The elastic layer transduces pressure loads into an indentation distribution, or vice versa, and a variety of physical principles, such as the resistive, inductive, capacitive, optical, magnetic, piezoelectric or acoustic sensitivity of the elastomer to an applied load have been explored. The properties of the covering material can severely influence the measurement properties of the underlying sensor [288].
Shimoga and Goldenberg [286] present an interesting study on soft materials for robotic fingers. They claim that the human skin has three useful features in terms of grasping properties: it reduces impact forces, conforms to uneven surfaces and dissipates repetitive strains. The materials that appear to be good candidates for robotic fingers can be classified into three categories: solids, elastomers and rheological materials. Shimoga and Goldenberg performed experiments comparing six materials chosen as representatives of these three categories. The criteria for the experiments were the above mentioned properties of the human skin. The results show that elastomer foam is the most suitable and hard plastic is the least suitable covering for robotic fingers. For practical reasons, however, a gel is a good compromise over the foam. Cabibihan et al. [286] conclude that the fingertip's conformity can be best approximated by a silicone inner layer, and

a polyurethane or Technogel® outer layer. The material for a soft robot finger has to be carefully chosen. According to Cutkosky [56], the ideal properties of a robotic skin are durability, compliance to conform to rough surfaces, texture to reduce lubricating effects of liquids and a moderate but uniform and reliable coefficient of friction. The right choice is also application dependent. To feel hard objects, a thicker, softer material is better. Although it blurs the image, it allows to discern the object shape [101] [359]. Compliant skin also improves grasp stability, because it provides damping and can absorb small position errors [268]. For a soft environment, however, a stiffer material can compress it more homogeneously. Peine et al. [242] suggest that a rigid sensor is preferable in surgical applications, since it will most effectively compress the artery and surrounding tissue, thus increasing the perceived pressure from blood pulses. However, some compliance in the sensor surface is useful as it permits the sensor to conform to geometric and elastic irregularities in the sensed region.

An important function of an elastic layer is that of a spatial low-pass filter [287]. Consider the spatial impulse response of the teletaction system, i.e. the response to a pin prick. Without some superficial layer, it is impossible to localise the pin to better than one taxel, no matter how dense the sensors, and the pin may be between sensors and not sensed at all [208] [160]. As a downside, the fact that an elastomer acts as a low-pass filter also results in unwanted mechanical crosstalk. As a result, an optimal choice of the thickness has to result in the right spatial cutoff frequency.

Elastomers inherently introduce other undesired behaviour into tactile sensors, like creep and hysteresis [353]. This is not necessarily a huge problem for a tactile feedback system because the human fingertip reacts similarly. The aim is to connect the system with the human fingertip and the human might not even be able to feel slow and/or small changes caused by creep or hysteresis. Whether or not this affects the performance of a surgeon is a possible subject for further research.

Like the human skin however, tactile sensors must not only serve as a source of information regarding physical contact with the external world, they must also serve as the frontline barrier against chemical and mechanical contact [76]. Howe and Cutkosky [110] solve this problem with a thin outer skin of relatively tough rubber to be less fragile and less easily damaged, and an inner layer of rubber foam to improve grasp stability and to control contact forces. The challenge of designing and building a successful tactile sensor is thus a difficult balancing act. Strength and durability are traded against sensitivity and repeatability [76].

A last reason to use an elastomer layer is that traditional microfabricated tactile sensors are typically based on silicon, which is usually a rigid and fragile material from a mechanical point of view. Exposing the sensors presents problems if silicon is used, because silicon easily fractures upon mechanical impact and over-loading. An elastomer layer can spread the mechanical forces and protect a more fragile underlying structure.

Something else to keep in mind is the surface quality. An extremely smooth surface

(local roughness less than about 1 μm) can produce a very large coefficient of friction. A mat finish (local roughness of a few tens of μm) has a substantially lower coefficient of friction and can slide evenly over smooth surfaces [110]. Cutkosky et al. [56] found that a high coefficient of friction is not necessarily the hallmark of an excellent skin material. A high coefficient of friction is found to be very sensitive to outside contamination. From this point of view 'fingerprints' are very important because they improve the consistency of the coefficient of friction under moist conditions.

The geometry of an elastic cover can be used to enhance tactile signals [338] or change the contact conditions. Nature does it in the form of fingerprints. Pyramid structures can concentrate the pressure on the sensitive element [211]. Hemispherical bumps are also interesting, because they are not as direction selective as ridges [199] [338] [339]. Positioning a silicone rubber hemisphere over four taxels decreases the number of taxels by four, but allows to measure 3D pressure instead of only 1D pressure. Both concerning the compression of the bump as the measurement of the stress below, there is no crosstalk between X and Z components of stress.
A similar strategy is used by Holweg [107] [359]. Instead of hemispheres, the rubber is shaped in blocks, each covering four taxels. A block that is not completely covered will, however, result in a wrong measurement. Thicker rubber results in higher sensitivity to shear forces.

Readout circuitry and processing Because of the large amount of sensitive elements, attention should be paid to the design of the readout circuitry. This circuit has to take all the properties of the sensor into account and minimise the noise. If not carefully designed, the electronics circuit can be a limiting factor for the bandwidth and sensitivity of the sensor. Especially for sensors with a large amount of taxels, the readout time of a single taxel has to be very short in order to reach an acceptable frame rate for the entire tactile sensor. To avoid this trade-off between resolution and speed, a variable resolution technique can be implemented. By shunting different rows or columns, the resolution can be reduced to decrease the processing time for applications where speed is more important than a detailed tactile image [299].
Another possible function of the readout circuit is to reduce the number of wires coming from the sensor. One way to do this is to make an array of tactile elements and select a taxel by selecting a row and a column. This reduces the number of wires from a quadratic to linear dependence on the size of the sensor.
An alternative for wires to connect the different sensor elements is using a different communication technology. An example of this is based on two-dimensional signal transmission technology. In such a system, a high frequency 2.4 GHz microwave is transmitted through conductive fabric. The sensor elements are capacitively coupled with the fabric. The miniaturisation of the elements, down to 6 mm by

6 mm, is limited by the wavelength of the waves [50]. Because of the absence of individual wires, the sensor is flexible and stretchable. A third method is to insert the sensor elements in a ring-type sensor network [225].
Image processing techniques can also be applied on a tactile image [353]. This can be useful for shape identification. Neural networks can be used to classify tactile contacts [121] or derive force vectors from a tactile image [295]. Lacour et al. [164] describe a skin-like, stretchable transistor circuit, to be used in e.g. a robot skin. Another example is a super resolution algorithm to improve the resolution. This was implemented on a tactile sensor composed of 5×5 cheap commercial pressure sensors, with a spatial resolution of only 10 mm [327]. Combining 25 different tactile images provides more detail, but excludes the possibility of dynamic sensing. In a similar way, Hellard et al. [101] augmented a 4×4 array to a 7×7 signal.

2.1.2 Applications of Tactile Sensors

Apart from robotic surgery, robotic manipulation is the main application for tactile sensors, and has been since one of its earliest uses in an automatic robotic grasper in 1962 [78]. A first application is telemanipulation, where a human operator controls the robot from a distance, and gets sensory feedback from the robot. This feedback is usually limited to visual or audiovisual information. Robot assisted MIS is one example of this. Telemanipulation can also prove useful when objects have to be manipulated in hazardous environments [78], such as in space or underwater [40] [200] [208], on the battlefield [271] or in the remains of an exploded chemical or nuclear plant. Humans can quickly perceive complex shapes and textures while touching or feeling the surface of an object with their fingers [163] [353]. If they can do the same during telemanipulation, their actions will be much faster.
Tactile sensors can also give a greater autonomy to robots, e.g. in assembly tasks [96]. Compared to computer vision, in tactile sensing less data is required, the measurements are direct, location and recognition are combined with a grasping function and some of the disadvantages of vision like occlusion or the influence of lighting are absent. Not only does a tactile sense allow to detect contact, but also the magnitude and distribution of contact forces can be determined [299]. A tactile sensory system facilitates automatic grasping, edge tracking and rolling manipulation [109] [261]. Tactile or force feedback is also necessary to prevent a robot from crushing a fragile or compliant object [4] [13] [137] [326] or to avoid letting it slip [73] [107] [353]. Several other possibilities include detection of surface roughness and burs, object localisation, orientation and weight detection, material and object recognition [107] [154] [263], predicting frictional behaviour and rolling motions [154], or detecting curvature [109].
Distributed pressure sensors are also applicable in a robotic skin [225] which covers the body and limbs of the robot. If robots have to interact with humans it is important that they can immediately detect contact or collision and respond to it. Tactile sensors can also serve as a sensitive skin for an arm prosthesis [237] or to

measure the ground reaction force on the soles of a walking robot [74].

There is a large variety of other applications that use tactile sensors. For most, however, the requirements are not as demanding as for teleoperation. The sensor can be used in all applications where pressure distribution is important, such as mouse pads, ergonomic tests in the design of wheelchairs and saddles [353], lip pressure before facial plastic surgery [322], and breast lump detection [10] [348].
In other medical and ergonomic applications larger area tactile sensors can be very useful to measure pressure maps of the foot [24], the back or the buttocks. For the design of prostheses and wheelchairs, it can be utilised for reducing the discomfort and to assist in the patient's movements. For limb disabled patients, load cells can measure the force changes, assess the functions, and assist in the rehabilitation of the patient's limbs [14].
Tactile sensors are also used in intelligent robotic toys like Pleo of UGOBE, which react to their environment [304], the seal robot Paro [340], or in service robots in general to detect contact all over the body [211]. Other applications include crash tests, pressure control between big rolls, grip comfort tests and tire profile measurements.

2.1.3 Tactile Sensors in Literature

Piezoresistance

Piezoresistance is the general term to describe the change of electrical resistance when pressure is applied. If the resistivity of the material itself changes, it is called piezoresistivity. In general, the piezoresistive effect in metals is due to the change in geometry, as is the case in strain gauges. In semiconductors, the effect can be several orders of magnitude larger [293]. In some sources 'piezoresistance' only refers to these effects, but in this text, any force or pressure induced resistance change is included.
A lot of piezoresistive tactile sensors utilise the effect that the contact resistance between two surfaces changes according to the applied load [347]. This was first discovered by the French electrical engineer Theodore du Moncel in the late 19th century. He discovered that an electrical current flowing between a sooted metal plate and a nail can be modulated by acoustic waves. Based on this observation, he invented the carbon microphone which revolutionised telephony [71].
Elastoresistance refers to piezoresistance where the active material is a conductive elastomer or foam of which the bulk resistance, or the contact resistance with electrodes, changes. A conductive elastomer is most often a composite of a rubber filled with some sort of conductive particles. Elastoresistance is discussed in detail in Section 2.2.
In general, the construction and readout electronics of piezoresistive tactile sensors

can be relatively simple and very fast, as it only requires the measurement of the electrical resistance.

Rigid piezoresistance Very small strain gauge elements can be fabricated with semiconductor techniques. A typical semiconductor pressure sensor consists of a beam or membrane of semiconductor material over a cavity. The membrane deflects as pressure is applied to the sensor. Several piezoresistive elements are formed on the top side of the membrane [62] [295]. These pressure sensitive elements can be made very small and easily put into a large array to form a tactile sensor.
The response of this kind of silicon tactile sensor is very linear, and exhibits low hysteresis and creep. Another advantage is that signal-conditioning electronics could be built into the same piece of silicon, although different processes are required for this. The planar nature of silicon integrated circuits presents a problem when curved sensors are required, since the silicon material is mechanically brittle and rigid [76]. This problem can be avoided by producing small individual chips, but assembling them in an array is not as straightforward.

Vásárhelyi et al. [339] present a tactile sensor using this principle. The sensor consists of a silicon membrane, 300 µm by 300 µm, with four perpendicular piezoresistive bridges connected in the middle, and a cavity underneath. In the centre of the membrane, where the bridges meet, there is a hole in which a vertical lever can be placed to increase lateral sensitivity. The sensitivity is very high and can be adapted by applying a silicone rubber layer on top of the membrane and inside the cavity. The resolution is 0.5 mm. Four of these sensors can be combined to determine the orientation of torque and force [149] [150].
A similar sensor is produced by Sugiyama et al. [137]. It comprises of full bridges of polysilicon piezoresistors, and has 32×32 elements, a resolution of 0.25 mm. An access time of 16 µs to a single element leads to 60 Hz readout for the entire sensor.
To increase the sensitivity of silicon piezoresistors, a porous silicon membrane of 63% porosity can be used [247]. Increasing the porosity further decreases the sensitivity, possibly because of the percolation threshold at 66%. The element has a mostly linear region between 10 kPa and 60 kPa or 0.01–0.06 N/mm^2, with a sensitivity that is about three times higher than conventional silicon piezoresistors.

Flexible tactile sensors can be made with micromachined thin-film metal strain gauges, positioned on the edges of or into polyimide or polydimethylsiloxane (PDMS) substrates. Because doped silicon is not readily compatible with polymer substrates, the geometrical piezoresistive effect has to be used, which is smaller. The result is a flexible, robust, monolithic, polymer-based sensor with embedded thin-film metal sensors and interconnects [76]. The gauge factor of 1.3 is lower than silicon, but the use of a thicker polymer film can counteract this slightly. The resolution is sub-mm. Engel et al. [77] use Dupont Kapton as the base for

a multimodal sensor measuring hardness, temperature and thermal conductivity. Two structures with different stiffness, located more than 1 mm from each other are responsible for the hardness measurements [76]. This, however, does not work on irregular surfaces. The sensing elements are 5 mm apart, and need 10 wires each.
Hwang et al. [113] developed a tactile sensor with four strain gauges in each element and a polymer bump on top to be able to measure shear forces. The spatial resolution is about 2 mm. The load range is 0–4 N and the sensor is protected from overload. Mukai [211] designed an 8×8 flexible tactile sensor by embedding silicon pressure sensitive elements in a flexible sheet, with a distance of 10 mm between them. The threshold is about 1.5 kPa with a range up to 437 kPa.

Other types of piezoresistance Piezoresistive tactile sensors can also be realised with conductive fibres, inks, fluids or carbon nanotubes. Both conductive fibres and inks depend on a change in contact resistance. Carbon fibres of 7–30 μm diameter can be pressed to form carbon felt, which is sandwiched between metal electrodes [169].
Pressure sensitive paint, or 'Pressistor', is made by mixing piezoresistive semiconductor powders with an organic material. The combination produces a liquid that can be painted onto electrode arrays or used to impregnate porous foam to produce a tactile sensor. For a similar sensor, a conductive polymer film or ink is deposited with a screening technique, which allows for patterned features. Rows on one flexible substrate and columns on another can form a tactile sensor with a reduced number of wires. Feeding the output voltage back to the other columns avoids crosstalk by eliminating stray current flows. The advantage of having a patterned conductive layer with respect to a continuous layer is that it avoids in-plane conduction between rows.
Helsel et al. [102] built a one-dimensional tactile sensor with a conductive fluid under a membrane and an array of electrodes on the bottom. An AC voltage is applied over the liquid and the voltage between each electrode is measured and thus the resistance, which is dependent on the indentation of the membrane between the concerning electrodes. This is an example of purely geometrical piezoresistance. The resolution is less than 1 mm. Russel [268] built a 10×8 sensor according to this principle with a resolution of 2.5 mm. As upper electrodes, he used strips of conductive rubber.
A block of pure carbon nanotubes also exhibits piezoresistive behaviour [182] [251] [356] [358]. The tubes buckle, resulting in a larger interconnectivity and a decreased resistance. Some advantages are supercompressibility, resilience, and large elastic modulus of carbon nanotubes. These kind of multiwalled carbon nanotube brushes can also be embedded in a polymer like PDMS [128] [182] [356]. This results in a flexible skin with a pattern of aligned nanotubes. The resistance of these patterns is very sensitive to pressure and the skin can be used as a pressure sensor.

Piezocapacitance

Piezocapacitance denotes a change in capacitance as a result of a pressure change. Usually, capacitive sensors measure small displacements very accurately. This is not different for capacitive tactile sensors, where the pressure alters the distance between two metal plates, which in turn changes their capacitance. They are static strain sensors, although high bandwidths are possible. The capacitance between two plates with a surface A and a distance d between them is

$$C = \varepsilon_{\mathrm{r}} \varepsilon_0 \frac{A}{d}, \tag{2.1}$$

with $\varepsilon_0 = 8.8510^{-12}\,\mathrm{F/m}$ the permittivity of vacuum and $\varepsilon_{\mathrm{r}} \approx 1$–$8$ the relative permittivity or dielectric constant. In most capacitive tactile sensors, the transduction from pressure to displacement is accomplished with an elastomer layer, yielding a very simple and cheap sensor. As a result, the properties of the sensor are governed by the deformable elastic material between the capacitor plates [291]. A simple way to make an array is to put a layer of metal strips on either side of the elastomer, perpendicular to each other. One of the layers consists of the drive lines and the other consists of the sense lines. At any moment in time only one drive and one sense line is active to read out a single element. To reduce crosstalk, the unused rows and columns can be put on ground potential [81] [238] [292]. Besides being easy to produce, capacitive sensors can easily be adapted to cylindrical and hemispherical configurations [208] [291]. Siegel et al. [291] [292] analyse the performance of an elastomer based sensor with 8×8 taxels and a spatial resolution of 1.9 mm. Hysteresis is limited and mainly caused by the relaxation of the rubber material.

The changes in capacitance are in the range of femtofarads which is very difficult to detect [347]. Therefore, a capacitive sensor requires a good design of the readout electronics. Miniaturising the sensor decreases the capacitance, and changes thereof, quadratically with the size of a taxel. As an example, the capacitance between two plates of $1\,\mathrm{mm}^2$ with a rubber layer of 0.1 mm is considerably smaller than $10^{-12}\,\mathrm{F}$. Stray capacitance, such as between the wires, can reach the same order of magnitude as the measured capacitance [273].

Due to the required high sensitivity of the electronics, capacitive sensor systems in general are very susceptible to electromagnetic interferences [96]. An additional conductive layer on top of the sensor can shield the capacitive cells [292]. A technique that integrates a capacitive tactile matrix into a single chip with the signal conditioning, greatly improves the interference robustness [347]. Bracke et al. [36] and Dimitropoulos et al. [69] describe electronics for the measurement of capacitance with high accuracy and low power consumption. It is possible to increase both the range and the sensitivity by making the bottom electrode curved instead of flat [198].

Compared to piezoresistive sensors, capacitive sensors have in general a higher pressure sensitivity and are less influenced by temperature. Piezoresistive sensors

are better suited for miniaturisation and need a less complex readout circuit.

Fearing [81] gives an elaborate discussion about how to make capacitive tactile sensors and has even made a construction guide available. The sensor has 8×12 elements around a 25.4 mm diameter cylinder with 3.3 mm spacing. With a 3.2 mm thick elastomer layer of elastomer on top of the capacitive sensor, the impulse localisation is only 0.2 taxel. For more complicated signals this layer acts as a low-pass filter and decreases the gain. Because of the stiffness of the copper wires used, the resolution around the circumference is reduced. The nominal capacitance is about 1 pF for a dielectric constant of about 4, and the sensitivity is 5 mN/element or about 500 Pa with an accuracy of 20%. The scanning frequency is 7 Hz. This design with crossed copper strips separated by strips of silicone rubber is followed by Howe et al. [112] [154] [242] to be used for MIS. Their sensor is thin and compliant and has 8×8 force sensitive elements with 2 mm spacing. The readout time for the entire sensor is 5 ms. The force range is over 2 N/element with a noise level of 0.001 N. A thin rubber layer is used over the sensor, because a thick layer makes it difficult to interpret the signal.
Another capacitive tactile sensor, based on Fearing's design is produced to examine the human tactile sense. It has 8×8 elements [238]. The spatial resolution is 2 mm. The sensor is covered with a 2 mm layer of elastomer, and shielded from outside influences with a rigid back plane and a thin gold layer embedded in the elastomer. A 200 kHz sine wave on the column scans the sensor. The noise level is 0.5 kPa (1.2 g per element), and the crosstalk less than 8%. Moy [208] designed a sensor with 4×8 elements, of which 4×6 are used. The spacing is 2.7 mm, the frequency range 100 Hz and the force range 1.1 N/sensor element.
Silicon IC technology is also suited for the fabrication of capacitive tactile sensors. An air gap functions as dielectric, while the force-displacement transduction is done by a spring structure. This was used by Wolffenbuttel [353] for a sensor with a spatial resolution of 0.5–0.7 mm which can detect a surface profile down to 1 μm. Forces between 0.1–0.5 mN are detected with 6 bit resolution. The capacitance varies from 2 pF to 4 pF. While an elastomer layer is often included to protect the silicon and act as a spatial low-pass filter, it is not directly responsible for the change in capacitance. Gray and Fearing [91] describe such a microtactile capacitive sensor with 8×8 elements and a spatial resolution of 0.1 mm. An unexplained large hysteresis and drift were a problem. Another potential problem with capacitive air gap sensors is pull-in under DC bias, where the electrostatic force pulling together the plates is larger than the restoring forces. With micromachined polysilicon plates, this is particularly detrimental since irreparable stiction or welding of the plates may result [91]. Printed circuit board (PCB) technology can also be used to produce capacitive sensors [232].

Chen et al. [48] produced a tactile element with superelastic carbon microcoils. The tactile element has a size of 80×80×80 μm^3 with a sensitivity of 1 Pa, and a response time of 1 ms. The capacitance changes logarithmically with the load.

Finally, Voyles et al. [335] describe an electrorheological sensor and dual 'inside-out' display. The sensor is a combined intrinsic and extrinsic sensor. The intrinsic sensor is a strain gauge sensor to measure force/torque [26] [336]. The extrinsic sensor uses an electrorheological gel (ERG) as a dielectric for capacitive sensing. A problem with this approach is that it is hard to derive force from displacement since it is not a Newtonian but a Bingham fluid. Under excitation, the gel can move, but does not return to any known state. It also tends to sag in the gravity field. Another option is to measure the pressure with pressure sensors, because an ERG does not have a uniform pressure, but the exact behaviour is difficult to model. Both compressive and shear pressures could be measured.

Piezoelectricity

Some materials, like quartz or polarised ceramics produce an electric charge when a force is applied. They are generally brittle and are hard to give the desired shape. Piezoelectric polymers like Polyvinylidene Fluoride (PVDF/PVF2) are often used in tactile sensors that are small, flexible, sensitive and have a large electrical output [58] [59]. PVDF shows a relatively strong piezoelectric effect, is inexpensive, commercially available in thin flexible sheets, durable and rugged. It is also used in medical ultrasonic imaging systems.
Piezoelectric sensors are inherently dynamic stress sensors because the stress induced voltage will disappear over time. The lack of DC measurement is an important limitation. The electric signal typically decays in milliseconds [59] [96] [273] [353], although a cutoff bandwidth of at least 0.1 Hz has been reported [61]. Another disadvantage is the sensitivity to temperature or pyroelectricity. Inside the human body this might not be a big problem because the temperature is more or less constant.

The piezoelectric tactile sensor array of Dargahi [58] has a high force sensitivity, a large bandwidth and good linearity. It is 15 mm long, has four elements, with 3 mm spacing, and a linear response from 0.1–2.0 N. The sensor is mounted on a laparoscopic grasper. Ramezanifard et al. [254] use seven elements with a 2 mm spatial resolution to compress tissue with hard lumps embedded. They derive position and size from this small amount of data.
Krishna and Rajanna [160] developed a 15×15 element sensor with about 1 mm spacing. Electrode strips are applied perpendicular to both sides of a PZT disk. The elements consist of the intersection of these electrode strips and the PZT material in between. Applying pressure on the material changes the resonance frequency, and this change can be measured. This sensor has a lot of hysteresis and crosstalk and the sensitivity is limited.
Dario et al. [61] built a 16×8 tactile sensor with a spatial resolution of 3 mm and a threshold force of less than 0.01 N. Later, they described a sensor containing two force sensing layers and has the additional capacity of sensing thermal properties

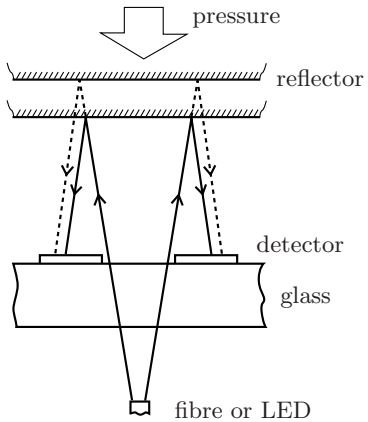

Figure 2.1: *Schematic principle of a reflection based optical sensor (adapted from [224]). The amount of light caught by the detectors depends on the position of the reflector, resulting in a relation between pressure on the sensor and the light intensity on the detectors.*

[59]. The sensor structure comprises a deep sensing layer, a relatively thick, intermediate compliant layer, and a superficial thin sensing layer. The dermal sensor consists of a 5×7 array of sensor elements spaced 5 mm apart and the epidermal layer contains seven elements arranged in a hexagon. A last PVDF tactile sensor has 3×3 sensitive elements on one membrane, which means it is not capable of detecting more than a single feature [252]. It is mounted on a grasper for MIS.

Optics

This section includes a wide variety of optical tactile sensors employing different approaches, all of them using light as information carrier. The advantage of approaches that use fibres to connect readout and sensor is that they are insensitive against corrosion and electromagnetic disturbances [347]. Approaches using a charge-coupled device (CCD) do not have that advantage and are rigid. Three main principles will be discussed first.

The first approach employs an elastic layer with a reflective surface [274] (Figure 2.1). Light is directed through a bundle of glass fibres. A contact force deflects the elastic layer and changes the distance between the reflective surface and the fibres, and thus the intensity of the reflected light. Instead of a reflective surface, a white silicone rubber layer is used by Dario and De Rossi [60]. Their sensor has 330 sensitive spots per cm^2, but large optical fibres make it heavy and bulky.

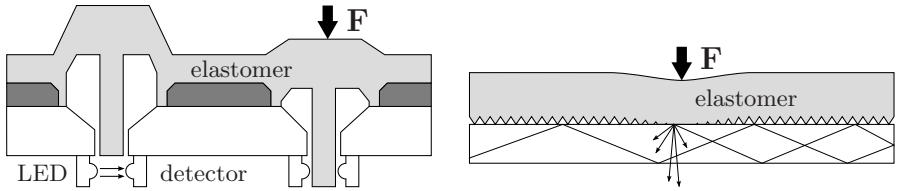

Figure 2.2: *Schematic principle of two types of optical tactile sensors (adapted from [258] [353]). On the left, a force on a sensor element pushes a pin down to block the light between a light source and a photodetector. On the right, a force results in a loss of internal reflection, instead scattering the light towards a photodetector.*

Nomura et al. [224] describe a 15×15 element array with 2 mm spatial resolution without fibres. LEDs and photo detectors are arranged on different transparent layers, one for each taxel. The top layer is again reflective. The accuracy is 5% of the maximum 50 kPa. It takes 100 ms to scan one frame. In a variant of this approach, the tactile sensing element consists of a photo-reflector covered by urethane foam [225]. Fibre-optic cables are used to irradiate the foam. The light is scattered by the urethane foam and concentrated upon deformation. The photo-reflector used has a size of $3.2\times1.7\times1.1\,\text{mm}^3$. It is a large-area conformable sensor. The output is nonlinear with high hysteresis. Hellard at al. [101] did the same with 4×4 infrared (IR) emitters and detectors. Another variant is to measure the displacement through self-mixing interferometry in a vertical cavity surface emitting laser [330]. These elements are small, have a high sensitivity and can be embedded in thin optical foils. Ayyildiz et al. [10] use infrared emitters and detectors for a 10×10 element sensor. It is calibrated for 0–5 N per element and the theoretical scan rate is 91.7 Hz.

The second type of optical tactile sensors use obstruction of light. In such a configuration, a load on a touch-sensitive surface is transduced into a displacement of an elongated pin, which extends from the lower surface of the elastic structure [104] [258] (Figure 2.2; left). The pin blocks the beam of light between a LED and a phototransistor. This structure is used by the Lord LTS-100 tactile sensor, which has 8×8 elements with a spatial resolution of 7.6 mm. In another sensor a fibre array is used and on each point a pin under pressure can block the light of one fibre [216]. The application is sound detection, which requires the switching time to be very fast because it has to be above the sampling frequency of audible sound. The spatial resolution is very coarse: 100 mm. A similar design is described by Allen [6] where the fibres are separated and pressing a metal pin causes misalignment of the fibre endings. This misalignment results in a measurable intensity decrease. The sensor has 16×16 elements, 2.54 mm resolution and a force range of 1–100 g per taxel or 0.16–16 kPa.

A third optical principle that can be used is changing the internal reflection (Figure 2.2; right). Light can be transmitted trough the side of a glass plate. The light remains inside because of total internal reflection [206]. An elastomer is separated from the glass with an air gap. When forces apply on the elastomer, it makes contact with the glass plate and the high refractive index of the elastomer results in a scattering of rays instead of internal reflection. The scattered light can be captured on the other side of the glass. Hysteresis is caused by the rubber layer sticking to the glass after contact. The sensor has a thickness of 10 mm. Beedie [16] uses a clear acrylic plate instead of glass. The scattered light is captured on a CCD with 64×64 elements. Begej [17] proposes a 32×32 element tactile sensor to be mounted on a parallel-jaw gripper and a sensor with the size and shape of a human fingertip for a dexterous robotic hand with 256 taxels. The same principle is used, but this time the light is conveyed to a CCD camera with optical fibres. Maekawa et al. [187] use the same principle in a finger shaped sensor to detect the contact location and the direction of the normal of the contact surface. A hemispherical shell of glass is the optical waveguide. The light stays in the glass due to total internal reflection. An elastic shell around it can be pressed against the waveguide and disturb the total internal reflection. Light is shattered and can be detected on a CCD camera. Since the shape of the sensor is known and the object is rigid, the normal of the object depends only on the contact location. A fibre optic plate guides the image from the waveguide to the detector. The diameter of the sensor is 32 mm, the length 60 mm. The position accuracy is 1–2 mm. Osumi et al. [228] achieve the same by pressing 15×27 silicone cones with a resolution of 1 mm into an acrylic plate and capturing the image with a CCD. The maximum pressure is 200 kPa. Finally, Umemori et al. [322] use pyramids instead of cones. The spatial resolution is 1 mm and the force range is 100 Pa to 100 kPa. The purpose is preoperative planning of facial surgery by measuring the lip pressure. Since only a static image is desired, the light is captured with single use light sensitive film.

Some other sensors are based on the influence of bending on optical fibres. This is an internal effect, so these sensors have the advantage to be less sensitive to contamination or misalignment. Jenstrom and Chen [120] place four layers of fibres perpendicular on top of each other, so that under pressure the fibres in the second and third layers are bent between two layers. There are 6×5 elements with 2 mm spacing and the force range is 0–1000 kPa with an uncertainty of 12 kPa and a resolution 0.5 kPa. Toal et al. [320] use a fibre loop. There is a loss of light when the loop is bent upon contact. It is, however, hard to miniaturise and put in an array. Calibration is difficult as well.

Another technique is the use of fibre Bragg gratings [103]. A grating in the fibre (±250 μm) reflects a narrow band of the spectrum. By detecting the shift in the reflected wavelengths, bending or stretching of the fibre can be detected. Different gratings reflect different wavelengths and can thus be applied to the same fibre. This results in a large reduction of fibres needed. The sensor is flexible and has 3×3 elements with 5 mm spacing. The force resolution is 0.001 N and the accuracy

99.9%. Because gratings are very sensitive to temperature changes, appropriate measures have to be taken to compensate for this [220].
The sensor array by Schoenwald et al. [275] is based on a matrix of optical fibres in perpendicular rows and columns, separated by an elastomeric pad. The magnitude of the force applied is measured by a change in transmitted light coupling across the elastomer between the fibres. The same concept can be applied between crossing optical waveguides with a thin layer of silicone in between [203]. Eghtedari and Morgan [73] use a photoelastic layer in a binary sensor with 256×128 elements. The layer changes the polarity of the polarised light when put under pressure and causes a phase shift. The outgoing light goes again through a polariser and is captured by DRAM. Cameron et al. [43] use a similar principle.

Electromagnetic induction

Inductive sensors are large and more suited for force/torque sensors [273]. A tactile sensor based on magnetic induction detects either changes in the magnitude or in the orientation of a magnetic field [353]. One example is a rather bulky magnetic sensor that detects the change in orientation of magnetic flux under applied load. The spatial resolution is 2–3 mm and thickness is typically 8 mm [184]. Coiffet [53] describes several needle based tactile sensors, where an array of rods slide through a guide. The position of those rods is then measured in several ways, e.g. LVDTs. Takenawa [309] designed a rather large inductive tactile sensor element with four coils under one permanent magnet embedded in silicone, which can measure the force in three dimensions. Because the magnet only induces a voltage in the coils when it changes position, it is an inherently dynamic sensor.

Magnetoresistance

Vranish [337] uses the sensitivity of permalloy resistors to detect changes in the magnitude of magnetic fields under an applied load. Copper strips provide the magnetic field, which increases at the permalloy resistors when the copper strips are pressed down. The tactile sensor has 8×8 elements with 2.5 mm spacing. Another sensor using this technique is a single point sensor sensitive to lateral displacement [4]. Because a DC magnetic field causes hysteresis, an AC magnetic field is used. The waveform is still polluted, but the amplitude is not affected.
Magnetic dipoles (vicalloy: Co, V, Fe; chromidur: Cr, Fe, Co) can be embedded in an elastic layer [332]. Under this layer, magnetoresistive sensors transduce the change in the magnetic field into a change in electrical resistance. The magnetic layer suffers from interference from external fields. The tactile sensor has 7×7 elements, a small force range, a brittle layer, small hysteresis, low cost, and is easy to fabricate. The sensitivity is 2.5 g and the resolution 1–2 mm. Nelson

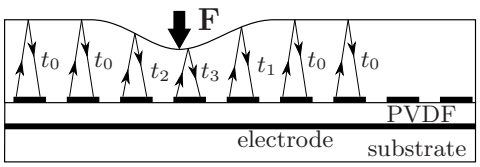

Figure 2.3: *Schematic principle of an ultrasonic tactile sensor (adapted from [353]). Each sensor element emits an ultrasound signal into an elastomer layer. The signal is reflected at the boundary. The time between the moment the signal is sent and the moment it is received is a measure for the deformation of the elastomer.*

et al. [221] use this principle to build a 2×2 element prototype of a shear-sensitive tactile sensor.

Ultrasound

There are different ways of using ultrasound to measure tactile stimuli. The first is the only one really measuring the surface, while the others measure deeper into the tissue. In general PVDF is used for both transmitters and receivers of ultrasound. Such a sensor consists mainly of an elastomer layer that is deformed under a load. The local thickness of this layer is evaluated from the time span of an ultrasonic pulse that is needed to cross the elastomer layer and to return to the transmitter [89] [90] (Figure 2.3).

Böse et al. [40] propose ultrasonic elastography as a means to get tactile information. Instead of direct tactile information, the stiffness information of the tissue is measured and translated into tactile information for the display. Elastography is an imaging technique based on strain estimation in soft tissues under quasi-static compression. The stress is usually created by a compression plate, and the target is imaged by an ultrasonic linear array. This configuration is used for breast elastography. Phenomena such as strain decay with tissue depth and strain concentrations have been reported. In vivo elastography in the rectal cavity is also possible with inflated balloons [298]. From the strain image a model of the Young modulus can iteratively be built [279] [280]. Sette et al. [281] give a comprehensive overview of this method.

Electro-optics

In the tactile sensor described by Maheshwari and Saraf [188], a dielectric barrier separates conductive nanolayers. By pressing the layers together, electrons can

tunnel through the barrier and this current causes localised electroluminescent light. This light is then captured on a CCD. The resolution is about 20–40 µm and the sensitivity about 10 kPa. No load above 90 kPa is mentioned. The described sensor is flat and rigid, but the authors suggest complex shapes are possible because of its ease of fabrication.

2.1.4 Comparison of Tactile Sensors

Tables 2.1 and 2.2 summarise the properties of different tactile sensors found in literature. The tables also indicate which sensors were specifically designed for surgery, and whether those are applied as a separate, finger shaped tool or inside the jaws of a grasper. Often some of the information is missing. Comparing some of the characteristics that are given can be difficult as well. Sensitivity values are nigh impossible to compare, because of the different employed definitions of sensitivity and the relative ease with which it is adapted to an application. It depends highly on the elastomer cover, the packaging, the tuning of the readout electronics, the spatial resolution and even the size and shape of the probe used to test it. A silicon membrane, e.g. would be sensitive to the slightest touch, but would break just as easily. Protecting it and increasing the range with an elastomer layer also decreases the sensitivity. Increasing the thickness of the rubber layer from 220 µm to 500 µm can reduce the sensitivity 30 times [339]. Sensitivity is sometimes given in other units, such as V/Pa or Ω/Pa, which is hard to judge if noise levels, amplification or output range is not given. In some sensors there can be a difference between pressing a single taxel or several at the same time, since the sensitive area of each taxel can be smaller or larger than the spatial resolution. A better measure would be the dynamic range, but it is rarely given, and even then does not always take the actual resolution into account.
Likewise, other properties such as number of elements, resolution and bandwidth are not straightforward measures for comparison. These requirements are bound by trade-off conditions. The bandwidth depends largely, but not completely, on the number of elements, the number of elements can often be chosen more or less arbitrarily and the spatial resolution is often limited to limit the number of elements. This is especially true for prototypes, which are not built to full potential of the technology but only as a proof of concept. Moreover, the figures given often reflect the properties of the acquisition system rather than of the sensor itself.

Different applications call for different sensor principles, and the choice depends on the requirements. Piezoresistive and elastoresistive sensors can be very cheap, easy and fast to build if the assorted nonlinearities are acceptable. Capacitive sensors have slightly more complex readout electronics to make them less sensitive to noise, and are more difficult to miniaturise to the smallest spatial resolutions, but in general suffer less from the viscoelastic behaviour of the rubber. Piezoelectric sensors naturally facilitate high bandwidths, but are not suited for static sensing.

It is also less straightforward to make them flexible. Optical tactile sensors include a wide assortment of sensors, but are in general rather bulky and rigid if they include optical elements on site. If the signals are guided through optical fibres, there is no electricity necessary in the tactile sensor itself, which is certainly a bonus for surgical applications.
In truth, most of the discussed technologies are able to meet the requirements for a tactile sensor posed in Section 1.3, with the proper modifications.

reference	principle	# elements	spatial resolution	bandwidth (frame rate)	sensitivity	range	flexible?	MIS?
[76]	Piezoresistive	10×10	< 1 mm				yes	
[113]	Piezoresistive	8×8	∼2 mm			0–4 N	no	
[137]	Piezoresistive	32×32	0.25 mm	60 Hz			no	
[149]	Piezoresistive	2×2	0.5 mm				no	
[211]	Piezoresistive	8×8	10 mm		1.5 kPa	437 kPa	yes	
[268]	Piezoresistive	10×8	2.5 mm				no	
[339]	Piezoresistive	1		up to 100 Hz			no	
[48]	Piezocapacitive	1	0.08 mm	1000 Hz	1 Pa		no	
[81]	Piezocapacitive	8×12	3.3 mm	7 Hz	0.5 kPa		yes	
[91]	Piezocapacitive	8×8	0.1 mm		2.3 kPa		no	catheter
[112]	Piezocapacitive	8×8	2 mm	200 Hz	0.25 kPa	>500 kPa	yes	tool
[208]	Piezocapacitive	4×8	2.7 mm	100 Hz		1.1 N	yes	tool
[232]	Piezocapacitive	5×3					no	
[238]	Piezocapacitive	8×8	2 mm		0.5 kPa		yes	
[291]	Piezocapacitive	8×8	1.9 mm			0–2 MPa	yes	
[353]	Piezocapacitive		0.5–0.7 mm			0.1–0.5 mN	no	
[58]	Piezoelectric	1×4	3 mm		0.1 N	0.1–2.0 N	no	grasper
[61]	Piezoelectric	16×8	3 mm	0.1 Hz and up	1 kPa		no	
[160]	Piezoelectric	15×15	1 mm				no	
[252]	Piezoelectric	3×3			10 mN	3 N	no	grasper
[254]	Piezoelectric	1×7	2 mm				no	grasper
[221]	Magnetoresistive	2×2					no	
[337]	Magnetoresistive	8×8	2.5 mm				no	

Table 2.1: *Comparison of tactile sensors (continued in Table 2.2)*

reference	principle	# elements	spatial resolution	bandwidth (frame rate)	sensitivity	range	flexible?	MIS?
[6]	Optical	16×16	2.54 mm	3 kHz	0.16 kPa	16 kPa	no	
[10]	Optical	10×10	2 mm	91.7 Hz		5 N	no	
[16]	Optical	64×64					no	
[17]	Optical	32×32					no	
[73]	Optical	256×128					no	
[101]	Optical	7×7					no	
[103]	Optical	3×3	5 mm		0.001 N		yes	
[120]	Optical	6×5	2 mm	250 Hz	0.5 kPa	1000 kPa	no	
[216]	Optical	8×8	100 mm	20 kHz			no	
[224]	Optical	15×15	2 mm	10 Hz	2.5 kPa	50 kPa	no	
[225]	Optical	∼8×16	20 mm	∼160 Hz			yes	
[228]	Optical	15×27	1 mm			200 kPa	no	
[258]	Optical	8×8	7.6 mm				no	
[322]	Optical		1 mm	0 Hz	100 Pa	100 kPa	no	
[188]	Electro-optical		20–40 µm		10 kPa		no	
[309]	Induction	1					no	
[107]	Elastoresistive	16×16	∼1.4 mm	∼250 Hz			no	
[138]	Elastoresistive	16×16	6 mm	40 Hz		120 kPa	yes	
[177]	Elastoresistive	8×8	3 mm	∼15 Hz			no	
[288]	Elastoresistive	64×64	1 mm	∼500 Hz			no	
[297]	Elastoresistive	32×32	2.54 mm	2 Hz		0–30 kPa	yes	
[326]	Elastoresistive	16×16	1.2 mm	∼13 Hz	8 bit	500 kPa	no	

Table 2.2: *Comparison of tactile sensors (continuation of Table 2.1)*

2.2 Elastoresistive Tactile Sensor Design

When elastomers show piezoresistance, it is called elastoresistance. Elastoresistance facilitates the construction of a simple, cheap, flexible and robust tactile sensor. It is a relatively old technology, governing some of the earliest tactile sensors to be built. It depends on the measurement of a resistance, which is just as easy for small or large elements, as long as the resistance does not become excessively large or small. This means that a spatial resolution of 1 mm or below is straightforward to achieve, while more complex technologies, such as most optical sensors, are more difficult to miniaturise. Capacitive sensors, which have a similar simple structure, do not scale down as well because of the rapidly decreasing capacitance, which becomes more difficult to measure and more sensitive to noise. Elastoresistance also allows for both static measurements and very high frequencies, where e.g. piezoelectric sensors lack the capacity to measure DC pressures.

This section discusses the design of such an elastoresistive tactile sensor, based on a previous design [326]. First, Section 2.2.1 discusses the properties and the physical origin of elastoresistance and how it behaves in a tactile sensor. Section 2.2.2 gives an overview and discussion of different sensor structures found in literature. Section 2.2.3 discusses the design of the readout electronics specifically for this elastoresistive tactile sensor. Finally, Section 2.2.4 describes the selection procedure for a suitable conductive rubber before Section 2.2.5 offers a conclusion.

2.2.1 Elastoresistance

Conductive elastomers

Conductive composites consist of a nonconductive matrix material with conductive particles or fibres. Electrically conductive polymer matrix composites have unique electrical and mechanical properties as well as many excellent properties of polymeric materials, such as light weight, low cost, ease of processing and corrosion resistance. Conductive composites have been widely used in the areas of electromagnetic interference shielding, electrostatic discharge protection and conductive adhesives for die attachment in electronic packaging applications [314] [315].
The most interesting composites have a nonconductive elastomer matrix, hence the term *elasto*resistance. The most common particles are graphite, carbon black and small metal particles. Other semiconductive particles such as molybdenum, antimony, ferrous sulfide or carborundum are also used [347]. Most, if not all, conductive rubbers show at least some elastoresistive behaviour.
Some of the conductive rubbers are sold as material in pressure sensitive switches and show a binary behaviour with a sudden change from a very high to a

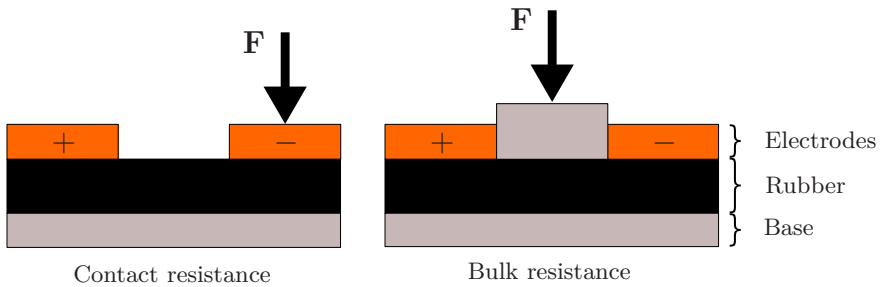

Figure 2.4: *Test setup to measure the respective influence of contact and bulk resistance on the elastoresistive effect. On the left, the positive electrode is clamped firmly to establish good contact, while an external force is applied on the negative electrode to affect its contact resistance. On the right, both electrodes are firmly clamped, and the force is applied on the rubber itself, in order to affect its bulk resistance.*

very low resistance. Others are produced with the purpose of electric connection between parts to prevent static electricity buildup, or as conformable electrodes in connection with the human body. This means most conductive rubbers are not designed to have the right properties for a proportional elastoresistive sensor, and a careful selection is necessary. To manufacture an adequate sensor material, an experimental, iterative process would be required, mixing different loadings of particles and measuring the properties. Moreover, mixing particles homogeneously through rubber can be difficult.

An exception is the CSA rubber produced by PCR Technical [3], which is specifically designed to be used in sensors. The base material is polysiloxane (silicone rubber), and the electrically conductive particles are artificial graphite. The additives red ochre (Fe_2O_3) and amorphous silica (SiO_2) are also present in a small amounts. The material is stabilised chemically, and contains neither the residual substances of antioxidants and plasticisers, nor curing agents. Moreover, volatile poly-siloxane components, which can cause poor contact with the electrodes, are carefully removed.

Weiß and Wörn [347] studied ethyl vinyl acetate foam, silicone rubber and PTFE (polytetrafluoroethylene) for their application in elastoresistive tactile sensors, and concluded that different applications benefit from different materials, but the silicone rubber is preferred for miniaturised sensors.

Hard filler particles have the additional effect of making the composite stiffer. The stiffness increases up to 30 V%. Beyond that, it decreases, possibly due to an increased porosity caused by an increased viscosity and thus more difficult mixing.

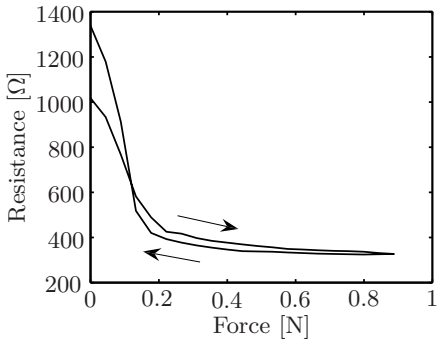

Figure 2.5: *Variation of the contact resistance with applied force. The variation is large and the contact resistance clearly plays an important role. The used rubber is produced by Wandy Rubber Industrial Co., Ltd., and is 1 mm thick.*

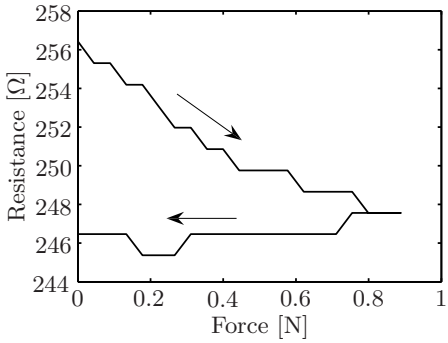

Figure 2.6: *Variation of the bulk resistance with applied force. There is barely any variation. The used rubber is produced by Wandy Rubber Industrial Co., Ltd., and is 1 mm thick.*

The origin of elastoresistance

Both the bulk resistance of the rubber and the contact resistance between rubber and electrodes might change under the influence of pressure. The change in bulk resistance would be caused by the fact that the conductive particles come closer together, which results in more electric paths and thus a lower resistance (see the paragraph about Percolation theory below). The change in contact resistance is the result of a better contact. The relative influence of both on the elastoresistive effect has long been uncertain. It was already known that the surface resistance is important to achieve low sensitivity [96], and Zee et al. [359] assume, without verification, that the contact resistance dominates.

The first experimental proof is acquired by gluing the sensor material to the electrodes with a conductive adhesive, which eliminates the contact resistance [347]. The measurement of the load-resistance curve of this situation reveals no significant load dependency of the electrical resistance. This leads to the assumption that the contacting area, which changes under pressure, is the important factor of the working principle. A mathematical model of the contacting process of two nominally flat surfaces [92] allows to derive a relationship between the applied load and the surface resistance [347]. The theorem uses statistical methods to describe the contact, based on the distribution of the roughness.

Another experiment was designed in the framework of this dissertation to confirm

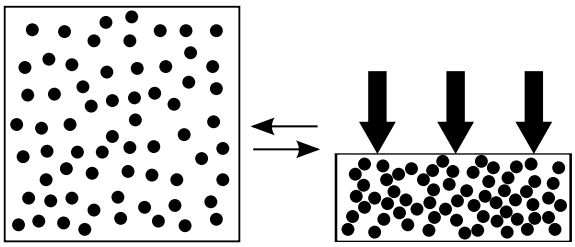

a) high resistance b) low resistance

Figure 2.7: *Principle of percolation as applied to elastoresistance. a) In the uncompressed elastomer, there is a large distance between conductive particles: the conductivity is low. b) In the compressed elastomer, the conductive particles come closer together: the conductivity increases.*

the result. Figure 2.4 shows the test setups. Both have a non-conductive base. In the first experiment, a varying force pushes on one electrode to measure the change in contact resistance. The other electrode is clamped against the rubber for good contact. In the second experiment, both electrodes are clamped and a force is applied via a non-conductive block that covers the entire surface between the electrodes. This way, the contact resistance remains constant and any change is due to a change in bulk resistance. While the test setups are not perfect and a small change in either bulk or contact resistance is possible when the other is measured, this effect is small and does not affect the conclusion.
The results (Figures 2.5 and 2.6) demonstrate very clearly that the influence of the bulk resistance is almost negligible compared to the contact resistance. The change in bulk resistance is barely measurable. Three different conductive rubbers all yield similar results, reinforcing the conclusion.
A first consequence is that the sensitivity of the sensor depends on the material and roughness of the electrodes, which was already known [359]. A second consequence is that most of the unwanted behaviour, such as hysteresis, originates from the contact between the electrode and the rubber. The cause of the hysteresis is probably the fact that the rubber tends to stick to the electrodes, increasing the contact area when the pressure diminishes.

Percolation theory The start of percolation theory is associated with a 1957 publication of Broadbent and Hammersley which introduced the name [38] [94]. The term originally denotes the slow movement of a liquid through a porous substance or small holes, such as hot water through a coffee filter. A more general interpretation is the connectivity of statistically spread entities in a medium. Some examples of percolation theory include the gelation of polymers, the boiling of an egg, forest fires, the connectivity between oil patches, the diffusion in

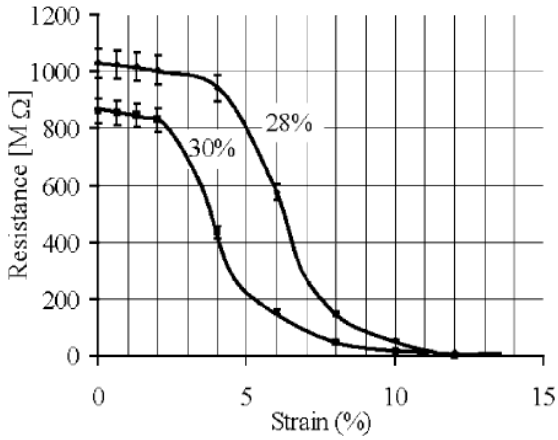

Figure 2.8: *The change of resistivity of a conductive rubber with an applied compressive strain. The materials are composites of silicone elastomer with graphite powder with a volume fraction of 28 V% and 30 V%, which is close to the percolation threshold of 31 V%. The samples are disc-shaped, 18 mm in diameter and 2 mm thick [23].*

porous material, the spread of a disease in an orchard, resistance networks or the spontaneous magnetisation above a critical concentration in a dilute ferromagnet [302].

Percolation theory is relevant to the elastoresistive behaviour of conductive rubbers, as a certain percentage of the volume of these rubbers is conductive and the rest is not. A conductive rubber is in fact a resistance network, which changes under pressure (Figure 2.7). Percolation theory describes which volume of particles is needed to have a conductivity path. This volume fraction is the percolation threshold. Below the threshold, there is no conductivity. Above the threshold, conductivity rises as the number of paths increases and the resistivity network becomes denser. The theoretical value for the percolation threshold in a homogeneous three-dimensional continuum is a volume percent of 16±2 V% [354].

For infinite networks the conductivity is zero below the percolation threshold, and proportional to $(p - p_c)^{\mu}$ above the percolation threshold [140] [302], where μ is the conductivity exponent, p the volume percent, and p_c is the percolation threshold. At high loading of conductive solid, the increasing number of conducting paths forms a three-dimensional network. In this range, the resistivity is low and less sensitive to small changes in volume fraction of conductive solids. Close to the percolation threshold, the resistivity can change drastically by several orders of magnitude for small variations of conductive solid content. In that range a conductive composite exhibits piezoresistivity [278].

The elastoresistive effect, however, is not necessarily due to a change in the volume fraction. It barely changes, since rubber has a Poisson's ratio close to 0.5. The change in configuration might result in a change in resistance. Some conductive elastomer materials are very porous or even foams, and the air gaps that separate the particles can be closed under pressure, in which case the change in volume fraction does play a role. The conductivity of a compressed sample is still lower than of an uncompressed sample with the same effective V% [168]. The reason is that the nonconductive matrix material between the conductive particles stays between those particles even upon compression. Possibly, electron tunnelling also plays a role in elastoresistance.

For a carbon black/polyethylene composite, the percolation threshold was found to be between 17 and 17.5% [199], with $\mu = 2.9$. As temperature rises, conductivity decreases, and the volume fraction can even drops below the percolation threshold. A possible explanation is that the carbon black has a smaller thermal expansion coefficient than polyethylene. Lanotte et al. [168] experimentally found a percolation threshold of 18% for nickel particles in silicone.

Beruto et al. [23] use graphite powder of micrometre size in a silicone matrix. They measured the properties of the rubber in a micrometer with a load cell and a multimeter connected to both sides of the elastomer. The percolation threshold was about 31 V%. The electrical resistance R of the composite, charged a little beyond the percolation threshold, is also strain dependent, according to

$$R = R_0 e^{\beta\epsilon}, \tag{2.2}$$

where ϵ is the strain and R_0 is the resistance at zero strain. β was found to be 51.5. This value corresponds to a very high electric sensitivity of the material to an applied strain and makes it a candidate for application as a logarithmic strain transducer. Figure 2.8 shows the strain-resistance characteristic for two different mixtures.

In conclusion, percolation theory can offer an explanation of why elastoresistance finds its origin in the surface resistance, rather than the bulk resistance. Below a certain threshold of the concentration of conductive particles, the percolation threshold, the material is not conductive. If the concentration is too high, the material is no longer piezoresistive. This is probably the case in most conductive rubbers, since good conductivity is usually desired. Above, but close to this threshold, the material exhibits strong piezoresistive behaviour [278], but this is not necessarily easy to capture.

Influence of particle shape It is difficult to determine the connectivity of the conductive particles as they generally have neither a fixed shape nor a fixed size. This makes it hard, if not impossible, to predict the percolation threshold. Even if the shape and size is controlled, too much variation can have a very large influence. Round particles need a high V%, and the piezoresistance is probably less. Very long particles require only a very small V% to form conductive paths. In

nanotubes/polymer composites the percolation threshold occurs at 0.055 weight % (0.029 V%), with $\mu = 1.36$ [140]. The higher the aspect ratio of the conductive particles, the lower p_c.
The expansion or movement of one phase with respect to the other is not equivalent to changing the volume fraction by varying the volume ratio of the two phases. If there is already nonconductive material between two conductive particles, that is not necessarily going to change. Taya et al. [314] [315] show that an initially electrically conductive short fibre composite can also become less conductive as straining increases, and even non-conductive above a critical strain. This is mainly due to the reorientation of the conductive fibres upon straining. Sett et al. [278] also tested composites with conductive fibres and a percolation threshold of 2.8%. They discovered that for compressive stress, the resistivity at first drops a little bit and than increases strongly. For tensile stress, the resistivity just increased. The piezoresistive sensitivity of the composite depends on the elastic properties of the matrix material and on whether the applied loading is hydrostatic or uniaxial [278]. In any case is the volume fraction important: too high and there is always a high conductivity, too low and the resistance remains high.

Piezocapacitive effect AC-current through a composite with conductive particles exposes a combination of resistance and capacitance between the particles [194] [195]. In low weight percentage materials, there is no DC conductance but there is conductance in AC, depending on the frequency and the gap between the particles. Simple experiments performed in the framework of this research, show that in general, the capacitance decreases under increasing load, but the exact behaviour varies for different rubbers.
Carbon microcoils in a silicone rubber matrix have a percolation threshold of 3 weight % [136], where the impedance stops being frequency dependant. Below the percolation threshold, the composite behaves as pure silicone rubber, with capacitance dominating, above, resistance dominates. The inductance of the microcoils is negligible. These rubbers enable tactile sensing, due to changing R, C or L under an applied load. An increase in conductivity can also be measured in nanotubes/polymer composites when the frequency rises [140].

Behaviour of elastoresistance in a tactile sensor

Elastoresistance is well suited for pressure distribution sensors, because it allows a very simple and robust structure that is easy to miniaturise. The sensor itself only needs a thin sheet of conductive rubber and an array of electrodes. Since only a resistance has to be measured, the readout electronics can be simple as well. This measurement principle can thus offer low cost tactile sensors, which are thin, flexible, sensitive and robust.
The main disadvantages originate from the elastomer and include creep, relaxation,

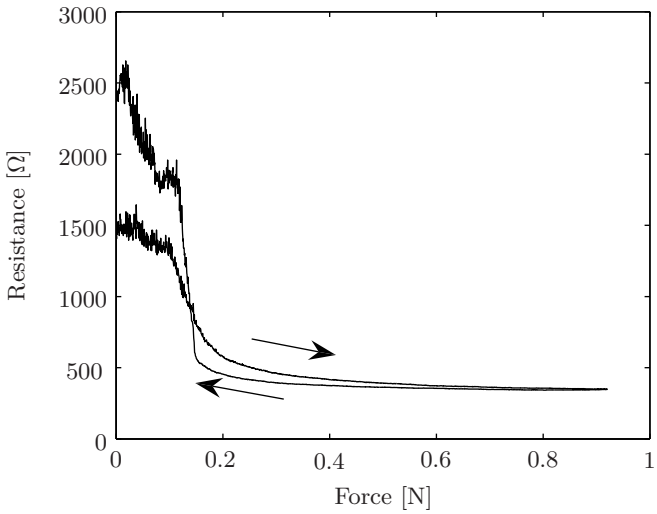

Figure 2.9: *The force-resistance curve of conductive rubber with considerable hysteresis. The rising force curve contains more information than the dropping force curve. The rubber used is produced by Wandy Rubber Industrial Co., Ltd., and is 1 mm thick. The test setup built to measure the contact resistance is used. The leftmost, noisy part of the graph is before good contact is established.*

hysteresis, and nonlinear response. Some additional problems include a large, nonlinear temperature dependence [77] [138], fatigue, low sensitivity and contact noise [109]. Due to this behaviour, elastoresistance cannot provide accurate absolute force measurements. It is suited, however, for force distribution measurements, and relatively fast changes compared to the relaxation behaviour of the rubber, because this distribution is not affected by the nonlinearities [107] [359].
Figure 2.9 shows the force-resistance hysteresis. The part of the curve which represents the rising force, holds the most information. This is very important, because the human tactile sense behaves similarly. The mechanoreceptors in the skin show a very high trigger rate with increasing indentation. When the indentation decreases again, there is almost no nerve activity [30] [324]. When the tactile information is reflected back to the surgeon any additional information about the dropping force would be lost anyway. The nonlinear behaviour can even be an advantage e.g. in collision detection, since for light contact, the sensor is typically more sensitive than at high loads, so the measurement range is expanded [347].

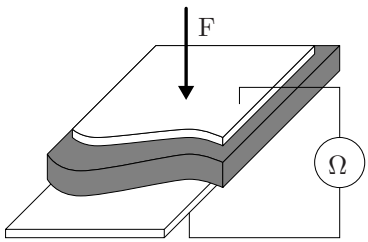

Figure 2.10: *Double sided contact electrodes on conductive rubber (adapted from [347]). In an array, the top electrode will influence the behaviour of the sensor and increase mechanical crosstalk between elements.*

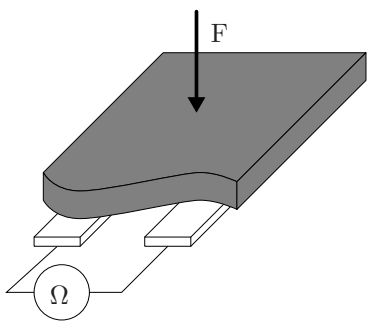

Figure 2.11: *Single sided contact electrodes on conductive rubber (adapted from [347]). In this configuration, there are no electrodes at the outside of the sensor, improving its behaviour and robustness.*

Model The nonlinearities can be difficult to model, especially the time variant effects. Several empirical characteristic curves have been proposed to describe the effect. Lim and Chong [177] suggest an empirical logarithmic characteristic curve of resistance versus force

$$R = C_2 e^{-C_1 F}, \tag{2.3}$$

with R the resistance, F the applied force, and C_1 and C_2 positive constants. Holweg [107] [359] compares the inverse of the force-resistance characteristic with an arctangent function. Weiß and Wörn [347] show a hyperbolic characteristic. None of these are entirely satisfactory for every rubber. Wörn et al. [355] discuss a model of the viscoelastic behaviour of the contact between rubber and electrode which they use very effectively to compensate for the drift of an elastoresistive tactile sensor.

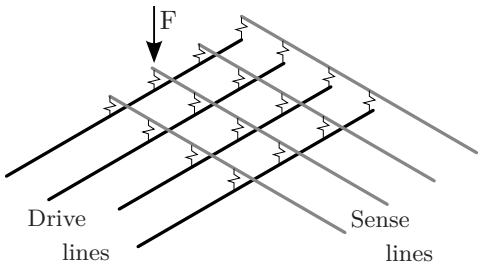

Figure 2.12: *Reduction of the number of wires in an elastoresistive sensor. A single taxel is selected by measuring the resistance between a single drive line and a single sense line.*

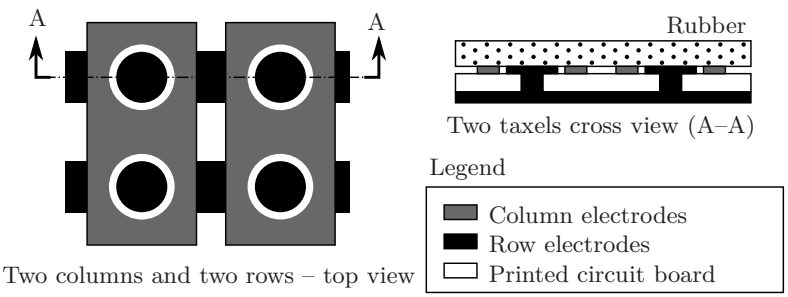

Figure 2.13: *Row and column structure of an elastoresistive tactile sensor (adapted from [107]). The column electrodes surround the row electrodes, eliminating crosstalk.*

2.2.2 Structure and Examples from Literature

There are several possible configurations for elastoresistive tactile sensors [253] [265] [353]. All elastoresistive sensors require an interface between a conducting elastomer and electrodes. As mentioned before, material and surface quality of electrodes require some attention. In order to prevent oxidation, plating of the electrodes with gold is recommended. A layer thickness of about 0.1 µm is enough [3]. The electrodes can also be deposited immediately on the rubber. It is important to put an isolating layer on top of the rubber, to prevent leak currents through the measured object.

In a first configuration, the conducting rubber covers the electrodes, without touching them. If pressure is applied, the contact area increases with the force, and the resistance decreases [105]. This sensor has 16×16 elements in 100 mm^2. D-shaped conductive rubber cords have also been used [250]. They are pressed against electrodes to increase contact surface. Instead of rubber, conductive foam can be used [190]. As explained in Section 2.2.1, the change in contact area on a

microscopic level also governs most of the sensors discussed below.
A common way to construct an elastoresistive tactile sensor is to mount the electrodes on both sides of the sensor material (Figure 2.10). While contacting the sensor material from both sides, the load has to be applied over the upper electrode. This is unfavourable, since the sensor material is usually flexible, whereby the upper electrode is exposed to a bending stress, which reduces the lifetime of the sensor [347]. The stiffer electrode will also cause an increase in crosstalk, because it will compress a larger area underneath it.
It is better to put the electrodes on the same side (Figure 2.11). This is more robust because there are no electrodes at the outside of the sensor.
A common way to reduce the number of wires in elastoresistive sensors is to work with a row and column configuration (Figure 2.12). A specific taxel is selected electronically by connecting the corresponding row and the corresponding column. This reduces the number of wires from a quadratic to a linear dependence on the size of the sensor. This configuration, however, introduces a considerable amount of crosstalk, since leak currents can flow between unselected rows and columns. There are several techniques to prevent this electronically, which will be discussed in Section 2.2.3. Shimojo et al. [288] give an overview.
A way to prevent crosstalk completely is surrounding one electrode completely by the other [93] [359] (Figure 2.13). Holweg [107] [359] employed this structure to produce a sensor with 16×16 taxels, 1.375 mm apart. The force range is 0–20 N and scanning time is 4 ms. The rows are connected rings on top of the PCB (Printed Circuit Board) and the columns are connected on the bottom side with electrodes in the middle of the rings so the elements are electrically isolated. Göger et al. [93] use a similar tactic on a flexible PCB based sensor to cover a service robot, based on earlier work [138]. They measure the resistance between square electrodes and one common electrode which surrounds each square completely, eliminating crosstalk. To reduce the number of wires, they mount the multiplexer circuit directly underneath the sensor. Sampling rate is 12.5 kHz divided by the number of elements. The spatial resolution is 9 mm on the robot arm, 10 mm on its shoulders and 3 mm on the finger.
Shimojo et al. [288] designed a sensor with 64×64 elements with the electrodes on flexible PCBs on both sides of the rubber with 1 mm spatial resolution. The total thickness is 0.7 mm. In another sensor [289], instead of putting the rubber on an array of electrodes, they stitched the electrodes (beryllium copper wires, coated with gold) in a woven structure through the rubber. This sensor should be more wear resistant. The resolution is 3 mm. The tension in the wires causes a preload on the rubber. They report limited hysteresis and drift, and a time response of 1 ms. The pressure range in the experiments is 0.6 MPa.
Another inherent way to avoid crosstalk is to separate the elements completely. The downside is that this makes miniaturisation harder. A tactile sensor by Lim and Chong [177] has 8×8 taxels, with 3 mm resolution, and a zero-force resistance of 0.3 kΩ. The sensor elements are cubes or cylinders of conductive silicone rubber, glued to electrodes with conductive glue. The transient time is 60 ms and the force

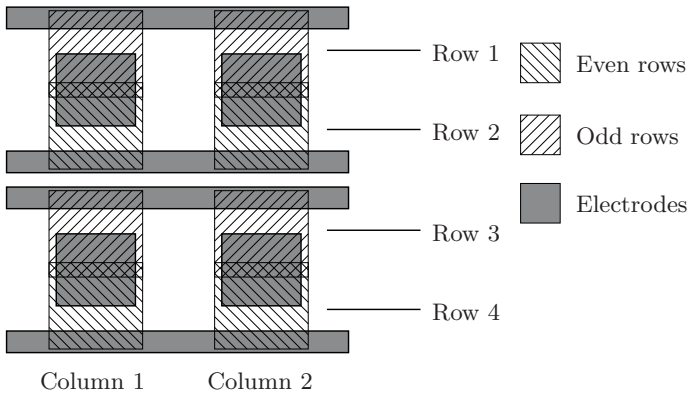

Figure 2.14: *Compact configuration of the electrodes of an elastoresistive tactile sensor. The square column electrodes are connected through the PCB with a copper line on the backside of the PCB. A conductive rubber placed on top of this PCB connects the electrodes. By measuring the resistance between the electrodes, the pressure on the rubber layer can be deduced. The exact location of the taxels is not defined. They reside somewhere in the hashed squares.*

range 0.5–9 N. Someya [296] built a conformable, flexible, stretchable, large-area network of pressure and thermal sensors. The skin is bendable down to a 2 mm radius. Thanks to a net-shaped structure, the E-skin (electronic artificial skin) can be extended by 25%. They use organic field-effect transistors. The resolution is 4 mm, while every element has a width of 0.3–0.5 mm. There is no influence of temperature between 30 and 80 °C. Pressure sensors are combined with thermal sensors. The pressure range is 0–3 N/cm^2 but there is a fairly large variation of the performance of individual transistors. They also present a sensor with 32×32 elements and 2.54 mm resolution. An important downside is the long readout time of 480 ms for a 16×16 sensor [297]. Based on this design, they developed an array of sensors with the same resolution that can be cut and pasted to form smaller or larger arrays, up to 512×512 sensor elements [307]. The elements are piezoresistive, with a very slow access time of 23 ms per element, which results in a frame rate of 0.5 Hz for the standard 16×16 elements.

2.2.3 Readout Electronics for an Elastoresistive Tactile Sensor

The readout electronics are an important part of the sensor. The circuit has to read out a large amount of sensitive elements, and take the properties of the sensor into account. The electronics reduce the number of wires to the sensor and minimise the noise level, crosstalk and response time. An important measure to reduce the noise is to limit the length of the wires or to shield them. There are several ways

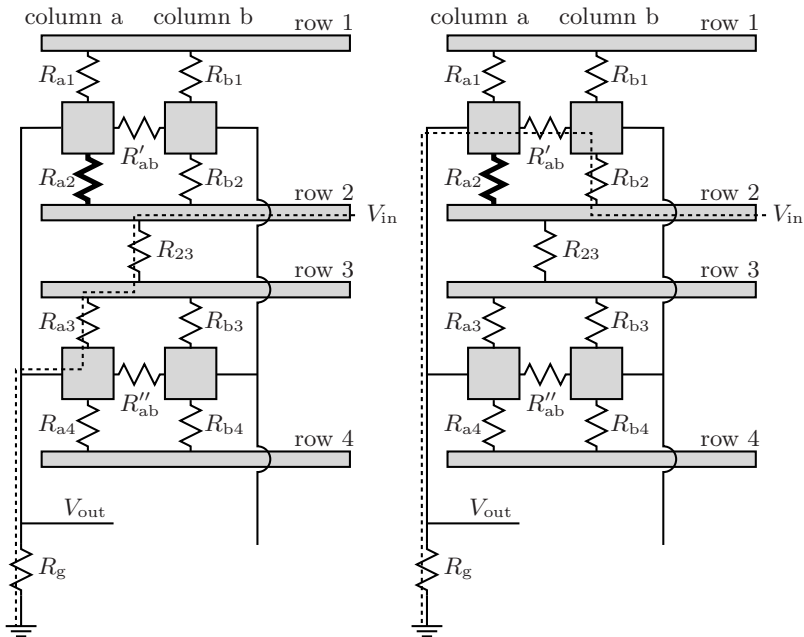

Figure 2.15: *Leak current paths in an elastoresistive sensor [326]. While measuring the resistance R_{a2}, a leak current flows from row 2, via resistance R_{23}, the electrode of row 3, and R_{a3}. The resistances R_{23} and R_{a3} can be the same order of magnitude, or even smaller, than R_{a2}. Putting row 3 on the same voltage as column a can prevent this leakage. A similar current flow can occur via R_{b2} and R'_{ab}, which can be similarly prevented by a feedback of the voltage from column a to column b.*

to measure the electrical resistance, such as by putting a voltage over the sensitive element and measuring the current [107] [359], or by using a constant current and measuring the voltage [76]. The latter method has the disadvantage that the slew rate of the constant current source can limit the sample rate. The most straightforward method, however, is to integrate the resistance in a resistor bridge. This has the additional advantage of somewhat linearising the very nonlinear force-resistance characteristics.

Besides isolating the electrodes in a structural way (Section 2.2.2), which requires more space, the problem of crosstalk can be dealt with electronically. Putting all unused rows and columns to zero is one way [288]. Another is to put them on the output voltage, which will be discussed in the example circuit below.

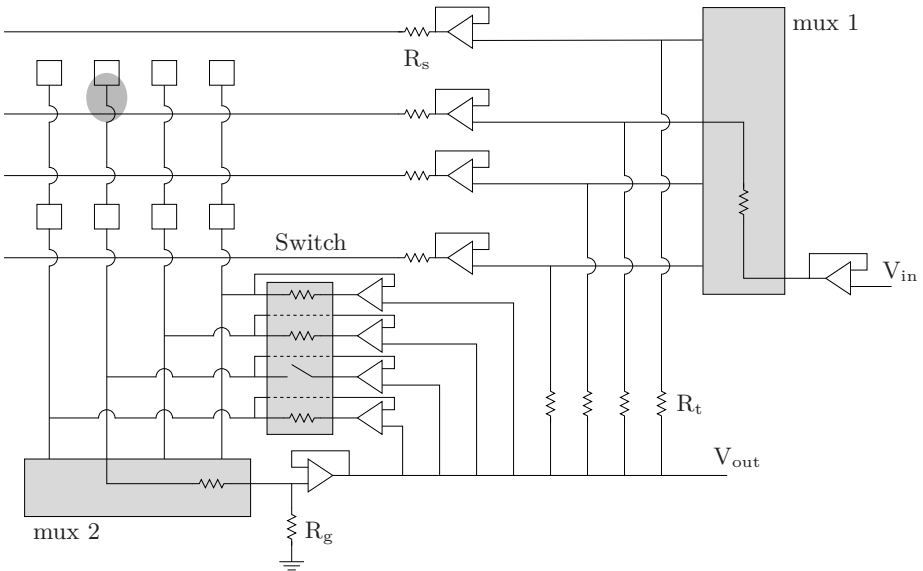

Figure 2.16: *Schematics of the sensor electronics. The multiplexer at the top right selects the row, the multiplexer at the bottom left selects the column. Together with bridge resistance R_g, the taxel resistance forms a resistor bridge. With the aid of a switch and feedback resistances R_t, the output voltage is fed back to the other rows and columns to avoid electrical crosstalk.*

Design of the readout circuit

This section discusses the design issues of the readout circuit designed for the elastoresistive tactile sensor. Figure 2.14 shows a very compact configuration for the electrodes, which can be printed on a flexible PCB. The square column electrodes are connected through the PCB with a copper line on the backside of the PCB, thus employing the principle of Figure 2.11. While the structure depicted in Figure 2.13 inherently reduces electrical crosstalk, the required area for each element is several times larger.

Without proper countermeasures, undesired leak currents flow between electrodes. The reason is that currents can flow in all directions through the conductive rubber. This results in a serious crosstalk problem [326] (Figure 2.15). Namely, if pressure is applied on neighbouring taxels, a current can flow between different rows and columns and result in a parallel circuit with lower resistances than the resistance that should be measured. This is e.g. visible when a circular indentation results in a square on the tactile image.
Figure 2.16 shows a simplified electronic scheme based on previous work [326]. To

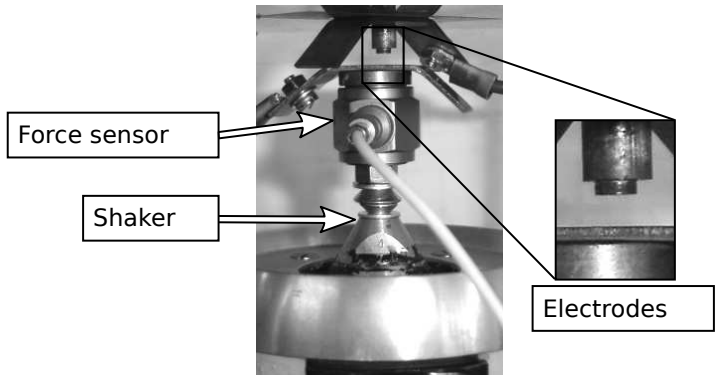

Figure 2.17: *Setup to test the elastoresistive behaviour of conductive rubbers. The rubber samples (not shown) are placed between the two electrodes. The height of the upper electrode is manually adjusted to ensure that the force minimum is as low as possible, while the electrodes do not break contact with the rubber. The shaker provides a sinusoidal force signal. The piezoelectric force sensor does not measure a DC signal.*

reduce the number of wires, one multiplexer (mux 1) connects a specific row with the input voltage V_{in} and another (mux 2) connects a specific column with the fixed resistance R_{g} of the resistance bridge.
To accommodate the problem of crosstalk, the output voltage V_{out} has to be fed back to all rows and columns. To the columns, the output voltage is fed back directly. A switch separates the selected column from the feedback. A voltage follower eliminates the influence of the on-resistance of the switch. To the rows, the output voltage is fed back through a large resistance R_{t}, which is large enough to separate V_{in} from V_{out} on the selected row, but not too large to avoid influencing the feedback to the other rows. A last safety measure is a safety resistance R_{s} after the voltage followers on each row. When an entire row is pushed hard, the resistance between two neighbouring rows can become very small. An R_{s} of $20\,\Omega$ prevents an overload of the components, but does not significantly influence the signal during normal operation of the sensor.
A possible limitation on the readout speed is an RC-circuit consisting of the resistance of the bridge resistance R_{g} and the output capacitance of the multiplexer. Upon changing columns, it will take some time for this capacitance to decharge over the resistance and the output signal will not be accurate. In the designed electronics, the time constant $\tau = RC$ of the RC-circuit is only 50 ns. The practical limit of the frequency range is determined by the data acquisition. The taxels are sampled at a frequency of 20 kHz, which corresponds to a scanning rate of 78 Hz.
There are some issues to keep in mind while selecting the electronic components. The on-resistance of the multiplexers should be sufficiently lower than the taxel

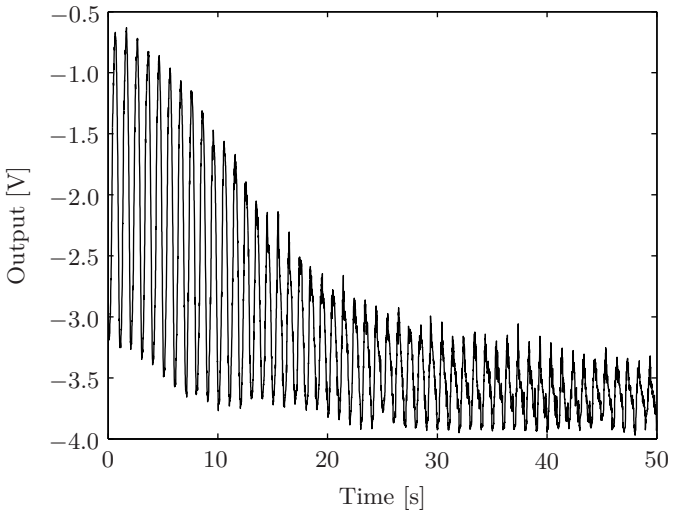

Figure 2.18: *Example of signal degradation in a conductive rubber. The sinusoidal excitation has a constant amplitude of 0.5 N and a frequency of 1 Hz. The rubber sample is Elastosil LR 3162, produced by Wacker Chemie AG, and is 2 mm thick. The bridge resistance is 220 Ω.*

resistance, otherwise the sensitivity can decrease dramatically. The capacitance should also be as low as possible to limit the settling time. The feedback resistance R_t should be as large as possible, but still lower than the input impedance of the opamps. Because there will still flow unwanted currents through the rubber, even though they do not influence the output, those currents have to be absorbed by the opamps. To do this, the opamps need rail-to-rail functionality and be able to sink sufficiently high currents.

2.2.4 Rubber Tests

Because the behaviour of the sensor depends largely on the rubber, the selection of the rubber is one of the most important steps in designing an elastoresistive tactile sensor. There is a large variety in the response of the different rubbers. Some switch very fast from a very high to a very low resistance, making them useless for proportional measurements. Others have a resistance of less than 0.5 Ω, which causes higher currents, and problems for accurate measurements. To this end, five samples of conductive rubber from different companies where tested for their force-resistance characteristics. For comparison, the same tests were performed on old samples that were previously used in tactile sensors [326]. Knowledge about the

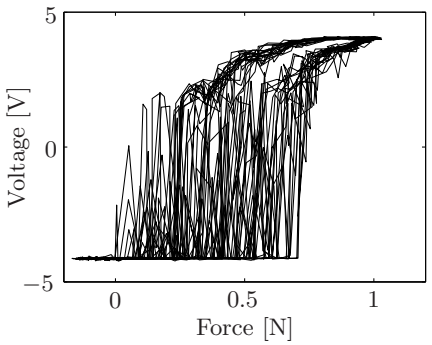

Figure 2.19: *On–off behaviour of some conductive rubbers. This makes them unsuited for a proportional sensor. The sinusoidal excitation has a constant amplitude of 0.5 N and a frequency of 2 Hz. The rubber sample is Zoflex ZL45, produced by XILOR Research LLC, and is 1 mm thick. It is sold as material for binary switches and contains metal spherules with a diameter of 10–30 µm. The bridge resistance is 1000 Ω.*

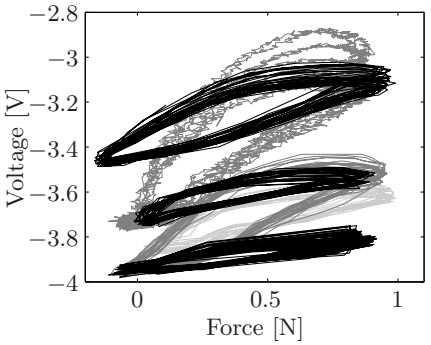

Figure 2.20: *Frequency dependency of some conductive rubbers. Six measurements where performed at 1 Hz (black, bottom), 1.5 Hz (black, middle), 2 Hz (light grey), 3 Hz (black, top), 5 Hz (dark grey, bottom), 10 Hz (dark grey, top). The amplitude of the sinusoidal excitation was each time 0.5 N. The rubber sample is an antistatic rubber produced by Hercorub, and is 2 mm thick. The bridge resistance is 220 Ω.*

dynamic behaviour of the rubber is useful to select the best rubber and predict the behaviour of the tactile sensor. The resistance of the rubber has to change proportionally and repeatably in the desired pressure range.

Test setup Because of the nonlinear time variant behaviour of the rubber, the test setup has to be able to exert a clean sinusoidal force with a certain amplitude and frequency. Large drift makes it more difficult to compare static measurements. The test setup consists of a shaker, a force sensor and two electrodes to make electrical contact with the rubber sample (Figure 2.17). The shaker pushes the rubber against a fixed plate which can be manually adjusted in height. A sine generator with adaptable frequency and amplitude controls the shaker. The rubber is included in a Wheatstone bridge followed by a simple differential amplifier circuit. The output voltage is saved on a computer with a dSpace acquisition system, together with the signal of the force sensor. For these tests, the amplitude of the frequency generator is adjusted at each frequency to have a peak-to-peak force of

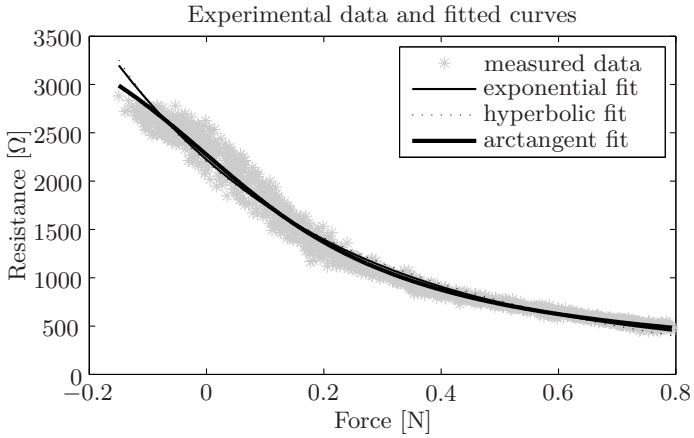

Figure 2.21: *Comparison between force-resistance curve and several fitted models. The rubber used is produced by Wandy Rubber Industrial Co., Ltd., and is 1 mm thick. The sinusoidal excitation has an amplitude of 0.5 N and a frequency of 1 Hz. Only the part of the curve where the force is increasing is shown and used for the fitting. The bridge resistance is 470 Ω. Since a dynamic force cell is used, there is no reference for the abscissa.*

1 N and the horizontal plate is manually adjusted to make the force start as close as possible to 0 N without losing contact.

Results A very common problem is the degradation of the signal (Figure 2.18), which might depend on the stickiness or the viscoelasticity of the rubber. All rubbers suffer from this to a certain degree. Doing the same experiment twice consecutively can yield different results, while waiting a day could give the original results again. Interrupting the signal by making the rubber lose contact with the electrodes reduces this problem somewhat. As mentioned in Section 1.2.3, the human tactile sense shows similar behaviour. Another problem typical for rubbers used in switches is a very binary on–off behaviour, which makes them useless for a proportional sensor (Figure 2.19). A last problem that was encountered was a large frequency dependency, which hurts repeatability (Figure 2.20).

The best performing rubber is from Wandy Rubber Industrial Co Ltd, Taiwan. It is a conductive silicone rubber used for electrodes to make contact with the skin in biomedical applications. The company did not want to share any information about the composition. Compared to the other tested rubbers, the behaviour of the Wandy rubbers is much more repeatable. With the appropriate bridge resistance, it also has a decent linear range in the relation between pressure and output voltage.

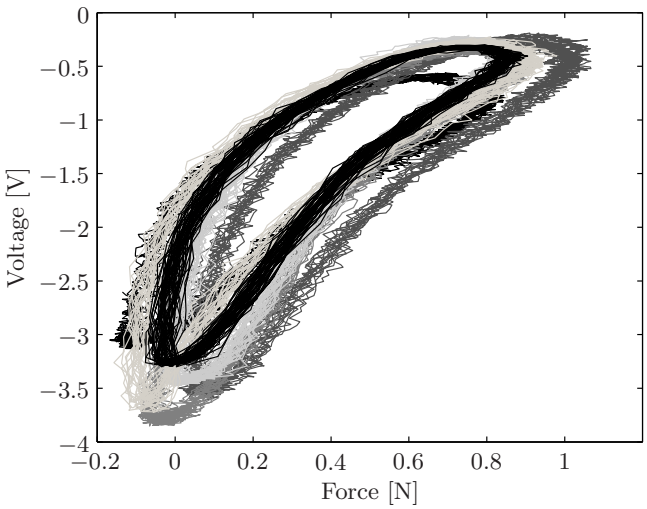

Figure 2.22: *Decent repeatability of the selected rubber between measurements at different frequencies, ranging 1–10 Hz. The rubber used is produced by Wandy Rubber Industrial Co., Ltd., and is 1 mm thick. The sinusoidal excitation has an amplitude of 0.5 N. The bridge resistance is 470 Ω. Since a dynamic force cell is used, there is no reference for the abscissa and the the curves have been moved horizontally.*

Note that the resistance always also depends on the size of the electrodes and the distance travelled through the bulk of the rubber. An exponential, an arctangential and a hyperbolic function are fitted through the measurements of only the parts of the curves where the force is rising (Figure 2.21).

$$R = 2018e^{(-2.64F)} + 205 \tag{2.4}$$

$$R = \frac{1895}{(F + 0.599)} - 958 \tag{2.5}$$

$$R = 1451 \arctan(-3.6F) + 2273 \tag{2.6}$$

Figure 2.22 demonstrates that the repeatability is good, within one curve, but also between measurements. The force offset between the curves is caused by a DC offset of the dynamic force cell. The rubber shows very little degradation, only after long periods of time or at very small amplitudes. The hysteresis is very large, but this is true for all tested rubber samples, and the human tactile sense suffers from it too, so mainly the rising force curve is important.

2.2.5 Conclusion

At first sight, elastoresistance is a very straightforward technology to apply in a tactile sensor. Upon taking a closer look, however, there is still a lot that could be learned. There are very strong indications that the bulk resistance of a conductive rubber stays constant, while the contact resistance changes. Theoretically, however, a carefully designed conductive rubber with a conductive content close to the percolation threshold could have different properties. Since it would not depend on the contact area, hysteresis originating from rubber sticking to the electrodes could potentially be avoided. At present, hysteresis and drift are important issues in an elastoresistive sensor.
The tactile sensor design uses electrodes on one side of a flexible PCB. This means the sensor can be flexible and that there are no electrodes on top of the sensor which cause unnecessary mechanical crosstalk. The electronics are carefully designed to avoid crosstalk, while having the flexibility to set the sensitivity in the desired range. By choosing the right components, very high frequencies can be reached.

2.3 Results and Discussion

The goal is to build a finger shaped tactile sensor for minimally invasive surgery. Because characterising a round sensor in a reliable way is less straightforward, a flat prototype is built for that purpose (Figure 2.23). The structure and the readout electronics are discussed in the previous sections. This prototype is then characterised to determine its sensitivity and range (Section 2.3.2), the level of crosstalk (Section 2.3.3) and its performance in a task to find a hard ball in soft tissue (Section 2.3.4). Finally, Section 2.3.5 offers a conclusion.

2.3.1 Prototype Tactile Sensor

The best performing rubber is produced by Wandy Rubber Industrial Co., Ltd. It is 1 mm thick and sold as medical electrodes in contact with the skin. This means that some attention is given to biocompatibility. Although the rubber is not selected for that reason, it is an advantage for medical applications. Several suggested empirical equations, including an exponential [177], an arctangent [359], and a hyperbolic function, were fitted on the force-resistance curve of this rubber (Figure 2.21). Of the tested rubber samples, it displays the least amount of degradation, and a the highest repeatability. Although there is still a significant hysteresis, the rising force curve is 'less nonlinear' than is the case for the other tested rubbers. In this context 'less nonlinear' denotes a lower C_1 in the exponential fit $R = R_0 e^{C_1 F}$, which results in a more linear output when using a voltage divider in the readout circuit.
For a flexible sensor, the electrodes have to be flexible as well. The electrode

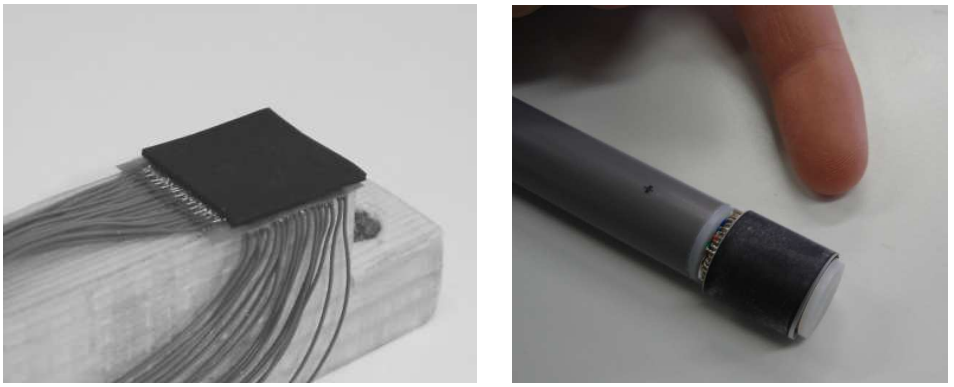

Figure 2.23: *Flat and finger shaped prototypes of the tactile sensor. The flat prototype on the left is produced specifically for testing. All tests were performed on this prototype. The finger shaped sensor on the right serves as a demonstrator.*

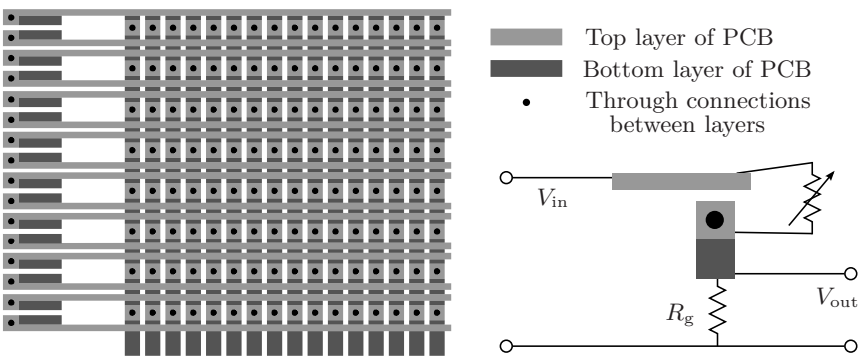

Figure 2.24: *Matrix structure and working principle of sensor electrodes on the PCB-layout. A taxel is located between a line (row) and a square (column). The taxel resistance is measured by putting the row on a voltage V_{in} and connecting the column to the ground via a bridge resistance R_{g}. The output voltage V_{out}, measured between the taxel resistance and the bridge resistance, varies in function of the variable taxel resistance.*

configuration shown in Figure 2.24 was printed on a 0.15 mm thin sheet of Kapton. It is like an ordinary PCB, but flexible and without a solder mask, which would insulate the electrodes. It is possible to make it smaller, but less than 0.2 mm between the lines would require a more expensive process, and more taxels are not required for this application. Note that in this configuration the exact location of each taxel is not defined (Figure 2.14).

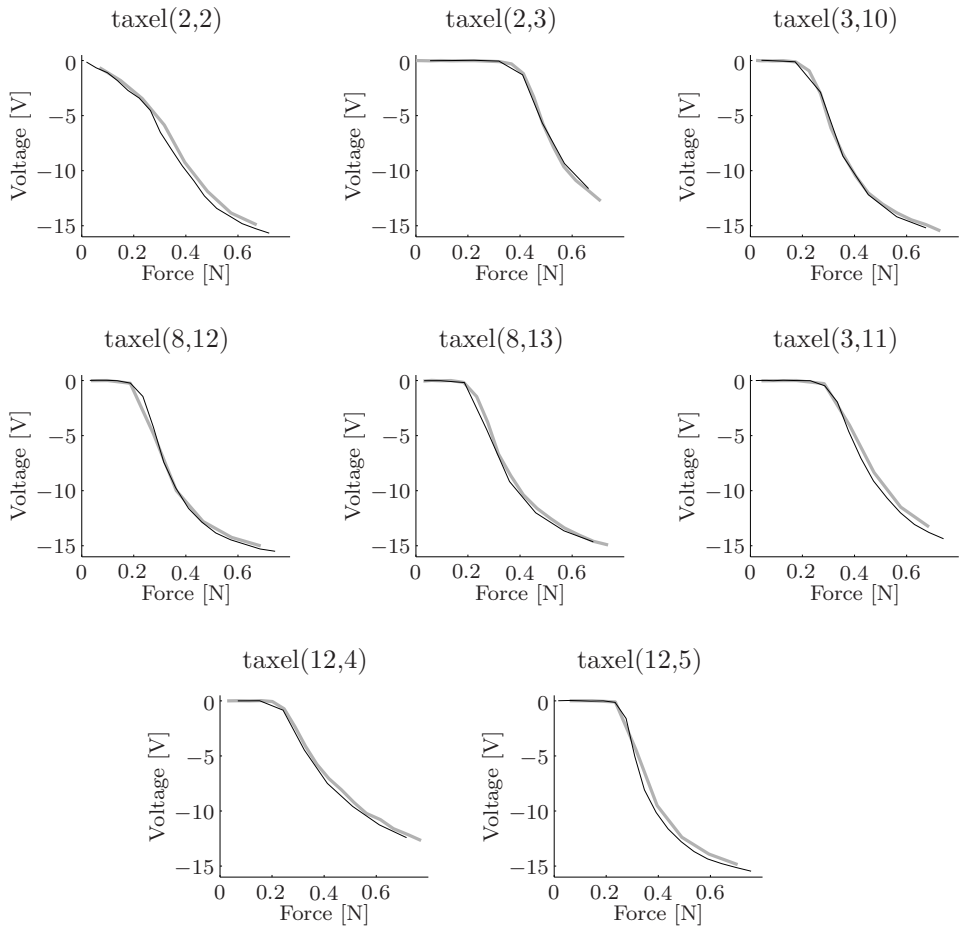

Figure 2.25: *Single taxel repeatability. For all taxels, two different runs were performed to determine its characteristic. It is clear that for each taxel, both runs yield the same behaviour. To compose the curves, a 1 mm by 1 mm square probe was pressed on the taxel with different forces. For each force, the value was sampled exactly one second after the start of the indentation, to circumvent drift.*

2.3.2 Single Taxel Response

Some tests are performed to show the characteristics of the sensor. The test setup consists of a 1 mm by 1 mm square probe attached to a set of leaf springs. By accurately moving the base of the spring up and down and measuring its deflection, an accurate force is applied on a single taxel. The exerted forces were 0.05–0.9 N. The tests were performed on the flat prototype.

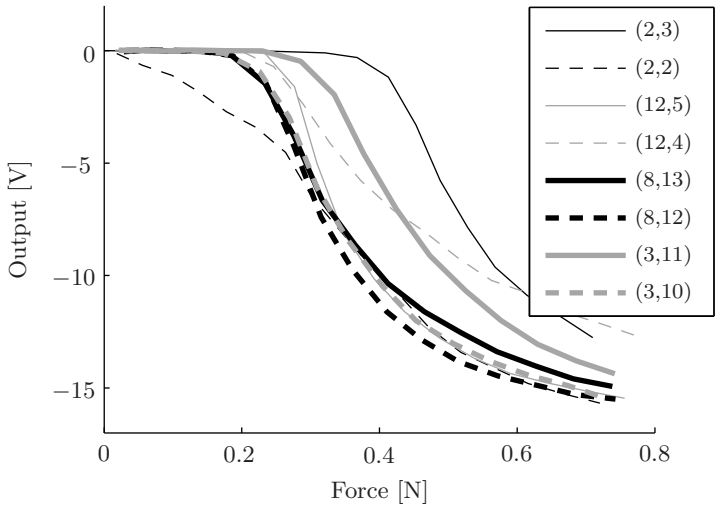

Figure 2.26: *Output curves of different taxels. The legend specifies the taxel locations. Except for taxel (2,2), the characteristics only differ in an offset force and a scaling factor. To compose the curves, a 1 mm by 1 mm square probe was pressed on the taxel with different forces. For each force, the value was sampled exactly one second after the start of the indentation, to circumvent drift.*

To test the pressure resolution of the sensor, the probe is moved down and up at a constant speed. The resolution of the force measurements is 4 mN. In this interval, the output changes 0.3 V, which easily exceeds the noise level. The resolution of the tactile sensor is thus better than 4 kPa, which is equivalent to a dynamic range of more than 250 or 8 bit.

To test the sensitivity and produce a force-output curve, several taxels were indented with intervals of about 0.05 N on one run and intervals of about 0.1 N on a second run. On each taxel, both runs produced nearly identical curves, which demonstrates a high degree of repeatability (Figure 2.25). To compensate for the drift, the output is each time sampled exactly 1 s after the start of the indentation. Figure 2.26 compares some of these force-output curves between different taxels. They have a very similar behaviour (except for taxel (2,2) in the graph); the characteristics only differ in an offset force and a scaling factor. The difference in offset force is a problem of the probe, which is an unnatural trigger. When several taxels are pressed simultaneously, the offset force is distributed, and is no longer an issue (Figure 2.27). When the offset force is neglected and the taxels are equilibrated, all the curves fall within 10% of each other. This is comparable with commercial sensors.

Inevitable in elastomer-based sensors are hysteresis (Figure 2.28) and drift

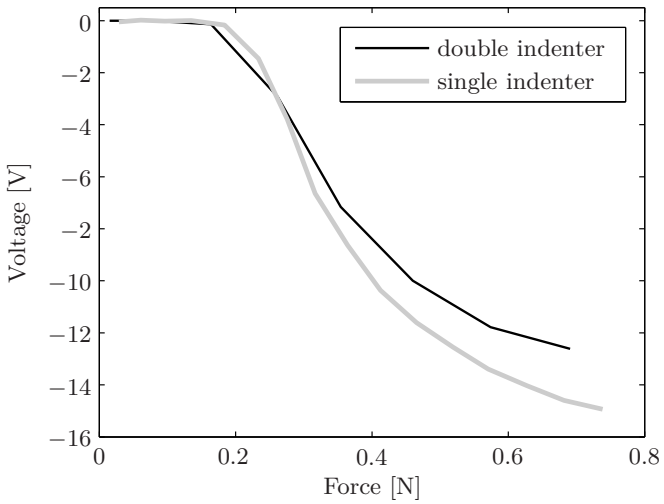

Figure 2.27: *Comparison between the sensor output while stimulating with a double or a single indenter. The single indenter is 1 mm by 1 mm, the double indenter 1 mm by 2 mm. The surface pressure for the double indenter is thus half that of the single indenter, while the offset force remains the same. If the force is divided over the two taxels under the double indenter, the offset force halves. To compose the curves, the probes were pressed on the taxel with different forces. For each force, the value was sampled exactly one second after the start of the indentation, to circumvent drift.*

(Figure 2.29). The viscoelastic behaviour is also visible as a relaxation in the step response of the force output (Figure 2.30). There is also an additional significant memory effect because the rubber sticks to the surface after pressure is applied. This memory effect is even worse for the curved sensor, which has some pretension to keep the rubber in place. This makes it very hard to measure absolute pressures. The sensor, however, is well suited for relative pressure measurements, both in time and in space and that is what is important in surgical tasks. It is possible to measure a useful pressure distribution.

2.3.3 Crosstalk

With the same test setup, the amount of crosstalk is examined by scanning an area around a single taxel with the probe. The same taxel is read out, while the probe presses down in different positions. Figure 2.31 shows that the influence is felt up to 2 mm from the indentation point. This is mainly mechanical crosstalk

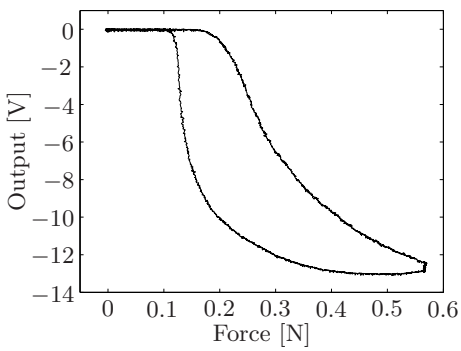

Figure 2.28: *Hysteresis of the tactile sensor. A 1 mm by 1 mm square probe, attached to a leaf spring was pressed against the tactile sensor at constant speed, stopped, and released again at constant speed.*

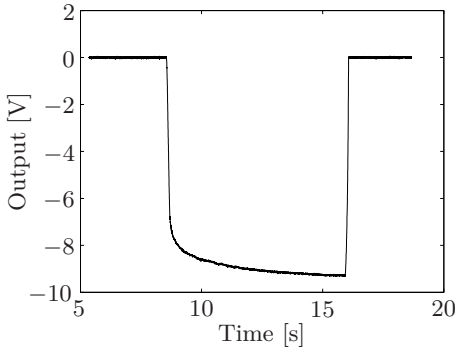

Figure 2.29: *Step response of the tactile sensor. A 1 mm by 1 mm square probe, attached to a leaf spring, was pressed against the sensor and held at constant displacement for a couple of seconds before it was removed again. There is a significant amount of drift.*

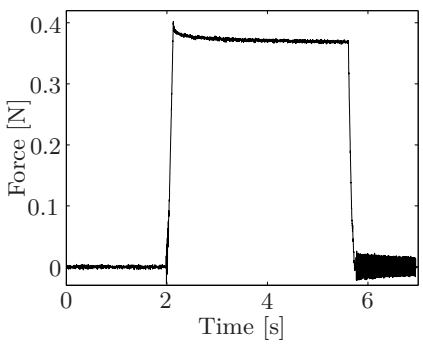

Figure 2.30: *Viscoelastic behaviour of rubber during a step in the position. The machine on which the tests were performed only allows control of the displacement. A 1 mm by 1 mm square probe, attached to a leaf spring, was pressed against the sensor and held at constant displacement for a couple of seconds before it was removed again. The force is derived from the deformation of the leaf spring.*

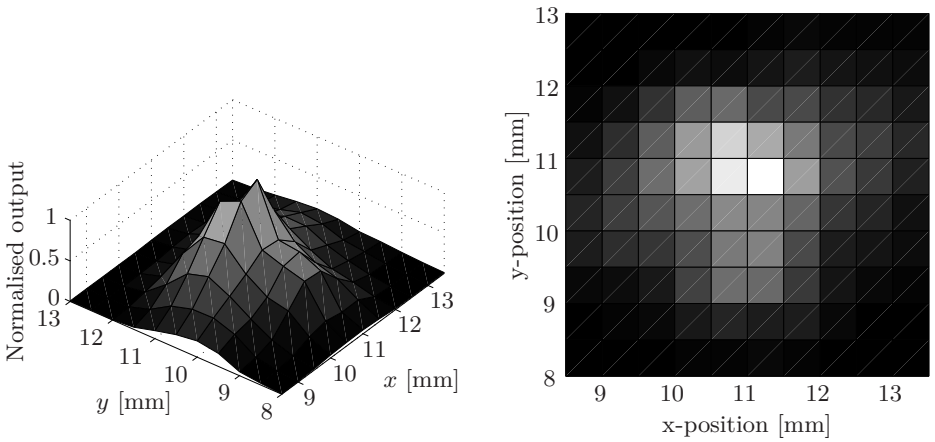

Figure 2.31: *Mechanical crosstalk. While the same taxel is read out, a square 1 mm by 1 mm probe presses down on the sensor at different locations. The influence is felt up to 2 mm from the indentation point. The output is normalised.*

due to the pressure distribution in the 1 mm thick layer of rubber. For this sensor with a spatial resolution of only 1 mm, this is more than necessary to smoothen out the signal, and if a thinner rubber would be available, that would yield better results.
Apart from the mechanical crosstalk, there is also some electronic crosstalk when large areas of the sensor are stimulated with a relatively high pressure. In that case the combined resistance of the different leaking channels can get too small which results in a higher current than the electronic circuit can compensate for.

2.3.4 Phantom Tests

To demonstrate the relevance of the tactile sensor in surgery, the sensor is used to find a simulated tumour. The task is to find a hard ball inside a soft tissue phantom. The phantom consists of silicone and measures 12 cm by 8 cm by 3 cm. The silicone has a Young modulus of about 27 kPa and a Poisson's ratio of 0.42. A hard ball simulates a tumour and resides 5 mm below the surface of the phantom. The tactile sensor is manually pressed on the phantom. As shown in Figures 2.32, 2.33 and 2.34, the tactile sensor has no problem in showing the location of the ball. A convolution filter is applied to the tactile image to reduce the noise level. Table 2.3 shows that a rough differentiation between different ball sizes is possible from the image by counting the number of taxels above a threshold level of $0.1\,\mathrm{N/mm^2}$ above the median pressure level of the tactile image.

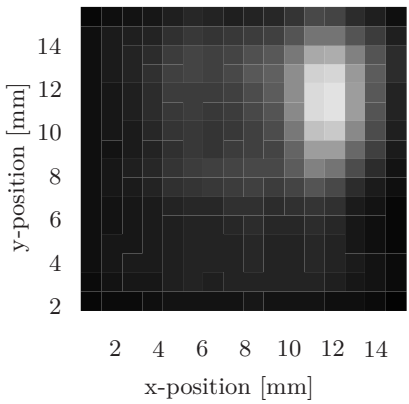

Figure 2.32: *Output of the sensor on a phantom with a simulated tumour. The tactile sensor shows the location of a hard ball with a diameter of 21 mm, 5 mm below the surface of a silicone phantom. The sensor is pressed manually on the phantom. A convolution filter is applied to remove the noise from the tactile image.*

2.3.5 Discussion

The developed tactile sensor has a spatial resolution of 1 mm, as required, although the mechanical crosstalk should preferably be a bit smaller by using a thinner rubber layer. The sensor displays a good force resolution of better than 0.004 N/taxel or 4 kPa, which just ducks under the required 5 kPa, and decent repeatability. It also shows a large hysteresis and nonlinear behaviour. The human tactile sense, however, shows very similar behaviour. Only the 'rising force'–part of the hysteresis is used in practice, and for the tactile sensor too, this part contains the most information. While the sensor is not capable of providing an accurate absolute measurement, it is well suited for pressure distribution sensing, or relative measurements in time. It is this information that the surgeon needs during an operation. A tumour finding task is performed to prove the usefulness of the sensor. The limiting factor for the speed is the data acquisition system. Because of the careful design of the readout electronics, the settling time after switching from one taxel to the next is at most 5 µs. This would allow for a speed of 200 kHz. The acquisition system only samples at a rate of 20 kHz, which corresponds to a scanning rate of 78 Hz for 16×16 taxels. This is almost four times the required frequency range.

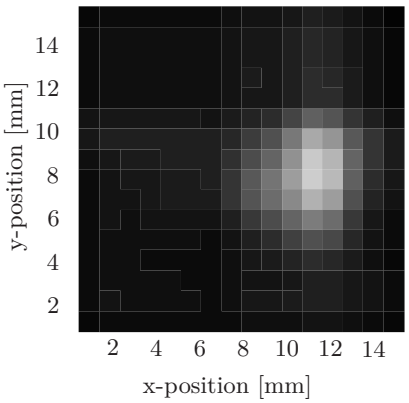

Figure 2.33: *Output of the sensor on a phantom with a simulated tumour. The tactile sensor shows the location of a hard ball with a diameter of 16 mm, 5 mm below the surface of a silicone phantom. The sensor is pressed manually on the phantom. A convolution filter is applied to remove the noise from the tactile image.*

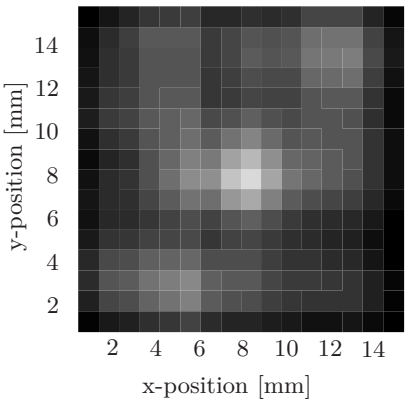

Figure 2.34: *Output of the sensor on a phantom with a simulated tumour. The tactile sensor shows the location of a hard ball with a diameter of 8.1 mm, 5 mm below the surface of a silicone phantom. The sensor is pressed manually on the phantom. A convolution filter is applied to remove the noise from the tactile image.*

Ball size (mm)	6	6	8.1	21	21
# taxels	33	40	54	79	80

Table 2.3: *Estimation of the size of a hard ball in a simulated liver. The size can be roughly derived from the number of taxels above a threshold level of 0.1 N/mm^2 above the median pressure level of the tactile image.*

	Requirement	Sensor
Spatial resolution	1 mm	1 mm
# taxels	10×16	16×16
Frequency range	20–30 Hz	78 Hz
Force range	0.5 N	∼1 N
Sensitivity	5–10 kPa	<4 kPa
Accuracy	10%	∼10%

Table 2.4: *Comparison of the characteristics of the elastoresistive tactile sensor with the requirements*

2.4 General Conclusion on Tactile Sensors

Elastoresistance is a good measurement principle for tactile sensors. Contact resistance is found to be the origin of the elastoresistive effect. The resulting tactile sensor is sensitive and robust, and its simplicity makes it very easy to miniaturise and reach very fine resolutions. The frequency range is mainly limited by the sample rate of the readout electronics. Table 2.4 compares the results with the requirements proposed in Section 1.3. All requirements are met or exceeded, except perhaps the absolute accuracy, which is on the limit. It should also be noted that one source found a required sensitivity of 0.5 kPa [241], which is significantly lower than achieved. It is unclear how important such a high sensitivity is, since it is possible to localise a hard ball in soft tissue by the visualisation of the tactile image, and even determine the size to some extent.
There are still some problems that need to be solved before an actual surgical instrument can be equipped with this tactile sensor. An important design flaw is the proximity of the soldering patches to the actual sensor surface. This introduces undesired deformation of the edges, heat influences caused by the soldering, and a fragile connection. A closer study of the interaction between rubber and electrode material and the influence of their respective roughnesses could help improve undesired effects such as drift and hysteresis. Requirements specific to surgery, such as sterilisability, were not studied at this stage.

Chapter 3

Tactile Display

To present the information acquired by the tactile sensor to the fingertip and complete the tactile feedback system, a tactile display is required. The most direct way of doing this is by deforming the skin of the finger with a dense array of pins. Other methods of stimulation are also possible, but in general they are not yet capable of giving the same intuitive or natural feeling.
While there are already plenty of tactile sensors, even commercially available, that fulfil most or all the requirements, the design of a tactile display is less straightforward. The reason for this is that most actuators loose power quickly when they are scaled down. Because of the amazing sensitivity and versatility of the human tactile sense, it is very difficult to present a natural feeling without loosing a lot of the potential of touch. A display with a lower performance only allows the most basic sensations, with little discriminatory value.
Section 3.1 starts with several design guidelines concerning tactile displays and gives an overview of the state of the art, sorted by actuation principle. The following sections discuss the design and performance of several realised prototypes. Firstly, Section 3.2 describes a display based on a closed hydraulic circuit. Secondly, Section 3.3 discusses a display with on open hydraulic circuit controlled by a proportional piezoelectric valve. Thirdly, Section 3.4 elaborates on the design of a proportional pneumatic valve with a reluctance actuator for a pneumatic display. Finally, Section 3.5 compares these prototypes and offers a conclusion.

3.1 Overview

To tackle the problem of building a powerful and compact tactile display, nearly all possible actuator principles have been explored, with hydraulics as a noteworthy

exception. Stacking powerful actuators in a dense array to form a realistic tactile image is less than straightforward. Eltaib and Hewit [75] give an overview of the technology available before the year 2000. The existing displays were then large, expensive, not user-friendly and not sufficiently accurate. Monkman et al. [204] give an overview of technologies, viable for commercialisation in 2003. More recent overviews are given by Benali Khoudja et al. [20] and Pasquero [235]. The following conclusions are reached: electromagnetic actuation is frequently used, but bulky; shape memory alloys are also widely used, but have a low bandwidth and poor performance; because of high bandwidth and forces, piezoelectricity is used in most commercial displays; other solutions are rare and mostly not far enough in the development cycle.
First, some important design issues are discussed in Section 3.1.1. Section 3.1.2 gives an overview of different displays, arranged according to their actuator principle and a short discussion of the properties of those principles. Section 3.1.3 briefly touches the related subject of Braille displays before Section 3.1.4 concludes with a summarising table and a short comparison of the different actuation principles.

3.1.1 General Design Issues

The design of a tactile display for robot assisted surgery is a big challenge. Different requirements are hard to meet simultaneously. Conflicting requirements include resolution, frequency, force and actuator size [208]. A lot of physical principles have been used in the past in attempts to answer to these conflicting requirements, but none have really led to success. Most existing systems are cumbersome, bulky, expensive, and often focussed on the optimisation of one single feature [236].
Tactile displays can be divided into broadly two categories according to their purpose: direct sensory substitution as opposed to symbolic sensory substitution [135]. The former aims at a realistic feeling of touch, while the latter gives a symbolic input that can be understood when trained to interpret the information. A blind person for example, is trained to interpret the information given by a Braille display. The aim of these displays is to give an extra source of information, but not to give tactile information. This also applies to tactile displays in steering wheels of cars, in military clothing... Even in robot manipulation or virtual reality, the aim is often to add a general information channel rather than a realistic touch. In that context, a vibrotactile display can give a lot of tactile information, without the need for an array. It can convey e.g. the moment of touching a hard object. In a lot of inspection tasks, like searching for loose parts or texture inspection, one point of vibrational information may suffice [153]. The reason for this is that the high frequency receptors, the Pacinian corpuscles, have a very poor spatial resolution. If high frequency information is important, a uniform vibration of the entire display can very easily be added to a shape display.
In the case of surgical systems in particular, the necessity to interpret information

should be avoided, as the surgeon is already working under a high mental load. The surgeon has to be able to do the same as in open surgery, without having to worry about interpreting information. If the system feels natural, the surgeon will more easily trust it and be able to fully concentrate on the medical aspects of the operation. For the same reason it is not necessarily advisable to scale the tactile image, even though this may provide a better spatial and/or force resolution [277]. An important observation is that the passive sensation of pins pressing in the skin is the same as the active sensation of the finger pressing on the pins. According to research conducted by Lamotte [165], softness discrimination is the same in both situations. A natural feeling may also be affected if the temperature or the thermal conductance of the display is different from the desired environment, but this still needs a proper study.

To come to the actual design, some design choices present themselves. First of all, there are several modes of actuation possible. The skin can be indented orthogonally, or it can be stretched laterally, or both. Orthogonal indentation is the most obvious choice, as it can directly represent a pressure distribution or a shape on the finger. Hayward et al. [236], however, suggest lateral stimulation of the skin. They claim that lateral skin stretch alone can emulate a certain orthogonal sensation on the skin. A comparison of both approaches in the context of minimally invasive surgery shows that orthogonal indentation contains more information [240]. Combining both modes would result in a better performance, but would also increase the complexity of the display dramatically. It might be sufficient to move the entire display under the finger to get the proper feeling of sliding or lateral forces. Wiertlewski et al. [351] designed a low weight display for this purpose with a force of 0.6 N and a speed of 13 mm/s. Zhou et al. [360] mounted their tactile shape display with an xy-motor on a mouse. The tangential stimulus can be improved by restraining the finger with a fixed conical aperture above the display [88]. Caldwell et al. [41] used pneumatic muscle actuators to supply a shear force element by moving the entire display sideways.
If the tactile display is implemented on a complete haptic system with force feedback, this could provide a sensation of stretch. If the force feedback device provides resistance when the finger moves laterally, depending on how the finger is clamped, the skin of the fingerpad could automatically be stretched. The combination with a force feedback device has the additional advantage that only a relative shape or pressure map needs to be presented to the finger. Kinaesthetic feedback can take care of the spatial 'DC' signal. A reference position can be subtracted from all the pins in the display [154].
Another choice to be made is between force control and position control of the taxels [208]. This is a rather complex issue without a straightforward answer which depends on the actuation principle of the display and on the nature of the tactile sensor. The question is whether the finger detects pressure rather than shape, or the other way around. The goal of the tactile display is the implementation in a surgical tactile feedback system together with a tactile sensor. Most tactile

sensors are distributed pressure sensors and this is also the case for the tactile sensor designed for this application, as presented in Chapter 2. Presenting this pressure information with a force controlled display is more straightforward than with a shape controlled display, which would require a good model of the finger. Even a good model would introduce some errors. So even though Peine et al. [112] concluded that the shape is more important than pressure distribution in a tumour detecting task, shape control is not necessarily the best choice. This works best if the sensor has similar properties as the finger in order to deform the tissue in a similar way and have the desired pressure sensation.

If the spatial resolution of the tactile display is below the two point discrimination threshold of 0.9 mm (Section 1.2.2), it will feel as a smooth surface instead of separate pins. In case this tough requirement is not met, an elastic layer, acting as a low-pass filter is essential for a natural feeling [208]. The elastic layer also acts as anti-aliasing filter. A 3:2 thickness ratio of elastic layer thickness to sensor and display resolution reduces the energy of the sampling effects to undetectable levels [82].

3.1.2 Tactile Displays in Literature

Electromagnetic

Although they are generally cheap and easy to control, electromagnetic actuators do not scale down well. As a result, only a low power can be reached with a small, lightweight display. There is a trade-off between speed and force. Most systems have a low force and decent speed without transmission. This is because

$$F_{\text{em}} \sim AB^2, \tag{3.1}$$

with F_{em} a generalised electromagnetic force, A the surface, and B the magnetic induction. A large magnetic field density is required, which is hard to generate in a small volume [223].
Examples of electromagnetic actuators used in tactile displays are solenoids [83], servomotors [342] and voice coils [214] [239]. Wagner et al. [342] made a cheap, bulky display with RC servomotors and 6×6 pins, 2 mm stroke, 2 mm resolution and 7.5 Hz bandwidth. Drewing et al. [70] also use servomotors for a display with 4 pins which can move laterally in both horizontal directions. The resolution is 3 mm and the maximum lateral movement 2 mm.
More recently, smaller and lightweight, portable displays are developed. Sarakoglou et al. [270] constructed a 4×4 display in which the pins are controlled by nylon wires connected to a separate block with light electric motors and a spring to push them back. The display has a stroke of 2.5 mm, a resolution of 2 mm, a force of 1 N per taxel and a frequency range of 15 Hz. Ottermo et al. [230] [231] use very

small motors to drive a screw to move each pin up and down, trading in speed for force. They built a 4×8 display with a stroke of 3 mm, a force of 0.4–0.5 N and a resolution of 2.7 mm. The maximum frequency is only 0.7 Hz. A thin protective layer of silicone rubber is adhered to the top surface of the display to make discrete pins feel like a single continuous object. They connected it to a MIS grasper with a PPS TactArray tactile sensor with 15×4 elements.
Because at higher frequencies, the human skin is sensitive to lower forces, electromagnetism can be used for a vibrotactile display. An example of this is VITAL (VIbroTActiLe interface) [19]. It is actuated with 8×8 micro-coils, with a spatial resolution of 4 mm and a maximal force of 13 mN. The pin deflection is only 100 μm, while the bandwidth is 800 Hz. It is combined with thermal feedback to make a distinction between different materials like wood or glass. Kontarinis and Howe [153] used a display based on a modified loudspeaker. The vibration is measured with an accelerometer on the inside of the rubber skin of the slave fingertip and transferred to a single vibrating element. Fukuda et al. [85] developed an electromagnetic resonating tactile display. Tabli et al. [310] developed a 4×4 vibrotactile array. At the actuation frequency (250 Hz), the amplitude is 200 μm and the static force is 1.2 mN. Inaba and Fujita [116] designed a display that simulates touching objects by tightening a fabric strip against the fingertip with an electromotor. Streque et al. [305] attached a moving magnet to an elastomer membrane with a maximum elongation of 800% to construct a 4×4 tactile display of 20×20×7.4 mm^3. The force per taxel is 2.5 mN, the bandwidth 350 Hz and the spatial resolution 2 mm.
A less conventional display is the two-dimensional tactile slip display designed by Murphy et al. [213] [346]. A ball is positioned under the user's fingertip and is driven in both directions by electric motors with friction wheels. It allows users to use less force in a virtual paper manipulation task in combination with force feedback. Tsagarakis et al. [321] describe another two-dimensional tactile slip display.

Electrostatic – electrostrictive

Electrostatic actuators use Coulomb forces in the electric field E between two charged parallel plates. The size of this electrostatic force F_{es} is

$$F_{es} = \varepsilon_r \varepsilon_0 A E^2 = \varepsilon_r \varepsilon_0 A \frac{U^2}{d^2}, \tag{3.2}$$

with $\varepsilon_r \approx 1$–8 the relative permittivity or dielectric constant, $\varepsilon_0 = 8.8510^{-12}\,C^2/Nm^2$ the permittivity of vacuum, A the surface, d the distance between the plates and U the applied voltage. Very high voltages have to be applied and force and displacement remain low [129]. A polymeric elastic dielectric, sandwiched between compliant electrodes will contract perpendicular to the sheet when a voltage is applied, and expand in plane. Alternatively, electrostrictive polymers change shape

under the influence of an electric voltage, much like a piezoelectric crystal or an electrostatic actuator, but force and stroke are in between both [245]. A single 100-layer actuator is able to drive the maximum deflection of 0.5 mm at 1200 V [196]. This electro-active polymer (EAP) is electrostrictive. There is a lot of ongoing evolution and new developments on the field of electro-active polymers.
A very light tactile display is developed by Koo et al. [157]. It is based on membranes of electroactive polymers that buckle under high voltages. They realised a thin display with 4×5 elements. The taxels have a maximum displacement of 0.9 mm at 3 kV, and a force of 14 mN, while weighing only 2 g.
Carpi et al. [44] developed a single element electroactive polymer bubble tactile display to simulate blood pulses or tissue compliance. The display is a 20 mm diameter pad with a passive upper membrane for safety and an active lower membrane. There is a fluid between the two membranes to couple them. When the lower membrane is actuated, it expands and the upper membrane goes down as the pressure in the fluid decreases. The actuation voltage can be up to 8 kV, which means a special high voltage low power supply has to be used to limit the possible current. They made smaller 6 mm diameter bubbles for a multi element display [45]. The advantages are low specific weight, low cost and no noise. The bandwidth is 100 Hz.

Piezoelectric

The piezoelectric effect is the deformation of certain materials under the influence of an electric field E. The displacement Δl is very small, a few μm, but the force can be very large and the bandwidth very high. Because of the limited stroke, the displays use a large levering system, bimorphs or vibration. The effect is described by

$$\frac{\Delta l}{l} = \frac{\sigma}{E_{\mathrm{Y}}} + d_{\mathrm{p}} E, \tag{3.3}$$

with d_{p} the piezoelectric coefficient, E_{Y} the Young modulus and σ the mechanical stress [223].
To achieve larger displacements, multi-layer or bimorph actuators are used. A multi-layer actuator consists of about 100 piezo elements on top of each other. The advantages are large forces, fast response and relatively low activation voltage compared to bimorphs. Displacement is in the order of 10 μm, while bimorphs go up to a few 100 μm. A bimorph consists of two long piezo elements. When a Voltage is applied, one element shrinks and the other grows, which causes the bimorph to bend. Bimorphs typically have a slower response time and a lower force [215].
STReSS (Stimulator for Tactile Receptors by Skin Stretch) [236] is a piezoelectric tactile display developed at McGill university, following an earlier, more complex design [99]. It uses piezoceramic bimorphs to stretch the skin laterally. The resolution is 1 mm and the frequency range 700 Hz. The display uses an array

of one hundred laterally moving skin contactors designed to create a time-varying programmable strain field at the skin surface. The actuator movement is only 5% or 25 μm. These piezoceramic actuators can be operated over a large bandwidth and are relatively easy to form in a desired miniature structure. The next generation of this device [344] [345] is more robust, has a modular design, and reaches a deflection of 0.1 mm with maximised stimulation of the skin with a dual-pinned lever. The spatial resolution of the new device is 1.8×1.2 mm, with 6×10 teeth. The free movement at the tip is 0.1 mm and the blocked force 0.15 N, The bandwidth is about 250 Hz, it weighs only 60 g and the actuators follow the curvature of the fingertip.

Kyung et al. [163] also use piezoelectric bimorphs, but with a displacement larger than 1 mm and lower operating input voltage (60 V). The display has 8 bimorphs with each 6 pins moving together. Each bimorph can exert a force of 1 N, has 2 mm indentation and a frequency range up to 1 kHz. It combines normal with lateral movement. It was attached to a kinaesthetic feedback device and tested in virtual environment [142]. They also made a 5×6 display with 30 bimorphs with a resolution of 1.8 mm, 0.7 mm stroke and a frequency response up to 500 Hz [161]. Tests show a performance in the recognition of simple geometric shapes between 50% and 95%. Summers et al [308] built a 10×10 display with 1 mm resolution using bimorphs. The bandwidth is 20–400 Hz with an amplitude of 50 μm at 40 Hz and 6 μm at 320 Hz. It was designed and used for psychophysical experiments. Yet another display with bimorphs used three Braille cells converted to a 6×4 display with a resolution of 2 mm [360]. It is combined with an xy-motor capable of 7 N of force for lateral motion of the entire display under the finger.

Because of the low stroke and high frequency range, piezoelectricity is suited for vibrotactile displays, such as a bulky 5×10 taxel texture display by Ikei et al. [115] [114] with a spatial resolution of 2 mm. Van Doren et al. [328] designed a one-dimensional display with 88 plates 0.38 mm apart, a frequency range of 0–1000 Hz and a peak-to-peak of 11 μm.

Biet et al. [29] describe a display based on Lamb waves generated in a piezoelectric motor. It generates a variable shear force, resulting in a smooth or braking sensation. With lower frequencies, roughness can be simulated. Li et al. [176] excite different vibration modes of a plate with rib grooves to simulate different roughnesses.

Kim et al. [141] designed a Small and Lightweight Tactile display (SaLT) with 4×8 taxels. Unlike most piezoelectric displays it has a relatively large stroke because it uses piezoelectrically driven tiny ultrasonic linear actuators. The display is curved to the shape of the finger, which also allows for more space for the 4 mm diameter actuators. The spatial resolution is 1.5 mm, the bandwidth 20 Hz, the stroke 0.5 mm and the force 0.2 N.

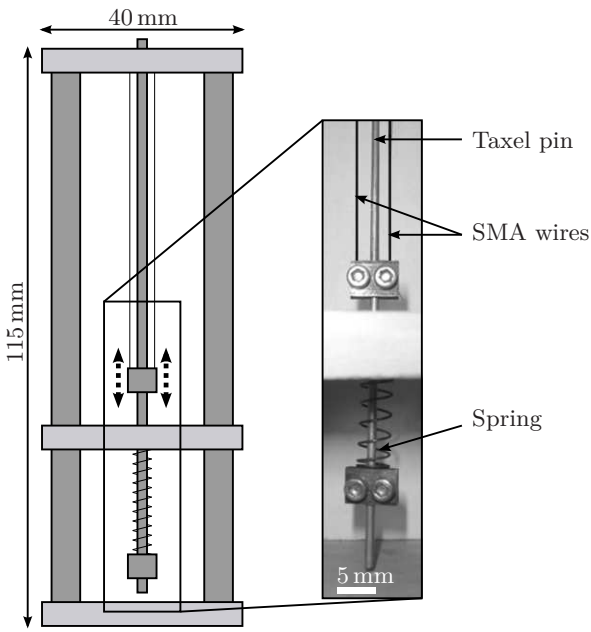

Figure 3.1: *One-pin prototype of an SMA based tactile display. Two SMA wires pull the pin upwards when an electric current flows through them to heat them. A spring pulls the pin down and offers pretension for the wires.*

Shape memory alloy

Shape memory alloys (SMA) are materials which change shape when heated, because of a phase transition. They "remember" a previous shape. Their most common shape is a wire, which can contract typically 2% for millions of times, but 4.5% strain is sometimes considered safe [349]. In most designs, the heat is produced by driving an electric current through the wire, which results in ohmic heating. To revert to the original shape, they need to cool down, leading to slow responsiveness.

SMAs are already used in several tactile displays [97] [112] [316] [349]. They are attractive because of their high power-to-volume, power-to-weight and force-to-weight ratios and their high intrinsic stiffness. Some disadvantages are their nonlinear behaviour, hysteresis, and directional asymmetry, but those can be overcome with appropriate control schemes. Another problem is the low efficiency and the resulting heat production. The maximum ideal efficiency of a typical SMA wire is 3.8% for a single acting actuator, and only 2.2% for an antagonistic actuator [319]. The efficiency of practical SMA actuators are even lower. A bistable SMA actuator accommodates this problem somewhat, but results in a binary display

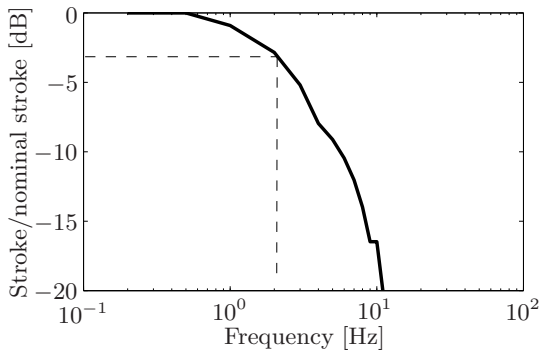

Figure 3.2: *Frequency response of an SMA pin with forced air cooling. 2 Hz is not sufficient for a tactile display.*

[334]. The actuation temperature is often above 50°C, which means the material should be sufficiently isolated from the fingertip to avoid burns. A last significant problem is the slow response time because the material has to cool down. For high frequencies, a high phase transition temperature is chosen, because the rate of cooling is linearly related to the temperature difference. Additional cooling can also improve the speed, but this also greatly increases the power usage.

A display by Howe et al. [112] [154] reaches almost 10 Hz with forced air cooling. It uses SMA wires of 30 mm long pulling at a lever, raising and lowering individual taxels to approximate the desired surface shape on the skin, with a maximum excursion of 3 mm. It has optical emitter-detector position sensors for each element. This display, with 4×6 elements (first 3×3) and a resolution of 2.1 mm was designed and tested for surgical applications. In a test a hard object, 4 mm in diameter, was located beneath 5 mm of foam with an error of less than 3 mm 95% of the time. Without tactile feedback, the mean error was 13 mm. With liquid cooling they reached a 40 Hz bandwidth in a display with 10 pins in a row [349] and 150 Hz can still be felt. They used a proportional controller with constant current feed-forward.

Nakatani et al. [219] built a large 3D form display with Coil-type SMA (C-SMA). It uses a 16×16 array of pin-rods with 30 mm stroke at 5 mm intervals. C-SMA is SMA material, shaped as a coil to create a very large strain, at the expense of force. It can be extended up to twice its original length, while producing a force of 0.4–0.6 N. The C-SMA is fan cooled. This low force (relative to the size of each pin), makes the display malleable. This property is proposed to be useful as a form of 3D CAD, in which modellers can sculpt directly by their own hands. It takes a long time to actuate every pin to present one shape (5–10 s). A faster linear programming method for actuating the pins is proposed.

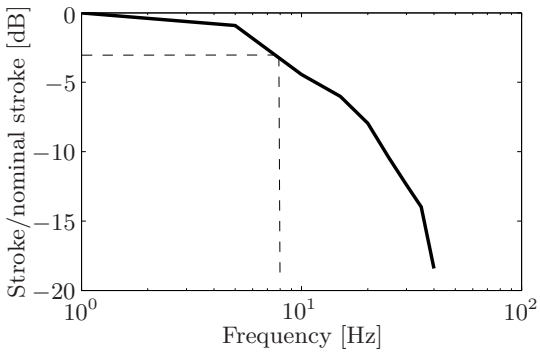

Figure 3.3: *Frequency response of an SMA pin with still water cooling. 8 Hz is relatively fast for an SMA, but still not sufficient for a tactile display. The power consumption rises to impractical levels.*

SMA based prototype For this work a one-pin prototype has been built and tested. It uses NiTiNol wires with a diameter of 80 µm. This material switches between a martensitic and an austenitic phase above ±50°C. In this initial prototype, the wires pull directly up, in the direction of pin movement. By using a lever or fixing the wires under an angle, the size of the display can be minimised. Figure 3.1 shows the configuration. To have a stroke of 2 mm with 3% strain, the wires need a length of 67 mm. Both wires are connected in series and their combined electrical resistance is 30–50 Ω. Since the wires can only pull, the pin is pushed downwards by a spring, which at the same time pretensions the wires. While the prototype is rather large for a single pin, its size does not increase with more pins and can even be decreased by fixing the wires in a triangular shape or using a lever. The stiffness of the taxel is about 4 N/mm. Due to the inherent high stiffness of the design, this is a shape controlled display.
The one-pin prototype is tested in different cooling conditions: still air, forced air and still water. The water has to be deionised, to avoid a short circuit. Neither force nor stroke were a problem and as expected both requirements were easily met. The bandwidth of the system is expected to be the critical aspect of this technology. The measurement of the bandwidth was the main purpose of this preliminary prototype. For still air, the cool down response time was found to be several seconds. For forced air and still water cooling, the frequency-response curves are given in Figures 3.2 and 3.3.
The bandwidth of about 2 Hz with forced air cooling increased to 8 Hz in still water. Apart from this, the issue of power consumption should also be considered. While the prototype consumes 1.5 W of electrical energy with forced air cooling, the power consumption increases to 10–20 W in still water. In a full-sized display with 50–100 pins, the generated heat per unit of volume would exceed that of a deep fryer.

An additional problem associated with the heat generation is the formation of gas bubbles around the wire. The lack of water cooling at these locations causes the exposed wire to break.

While SMA technology is promising, there are several problems that make it less suited for a compact tactile display. A significant problem is that of the limited bandwidth. Through the use of smart control methods this bandwidth could be increased to some extent. Further increases could be realised by implementing forced water cooling. The water flow would also reduce the problem of gas bubbles, as they would be washed away. However forced water cooling would make the whole system more bulky and increase the power consumption even more. An extra system to cool the water would be required. Another hurdle towards a full tactile display is the complexity of construction, and more specifically, the fixation of the wires, because the pretension in the wires has to be controlled and identical for all wires.

Active fluids

Several researchers have tried to make tactile displays with active fluids. Most are electrorheological (ERF) or magnetorheological (MRF) in nature, which means the viscosity of the fluid changes when an electric or a magnetic field is applied. Because it is only a viscosity change, and despite the misleading name "active" fluids, most of these displays are passive.
Klein et al. [40] [139] [152] made a system where a downward force of maximum 0.5 N/taxel is resisted by increasing the viscosity of an electrorheological fluid. Each taxel has a return spring to push the pin back up. The display of Taylor et al. [317] has no moving components and extra accessories. The electrorheological fluid is trapped between a flexible conductive rubber sheet and a 5×5 array of taxels with a resolution of 13 mm. A high voltage of up to 10 kV per 20 mA is required, and fabric is needed between the layers to prevent short circuit and to increase the force output. The fabric also smoothens the signal. They tried a similar configuration with MRFs instead of ERFs [179]. Voyles et al. [335] have developed an electrorheological sensor and 'inside-out' symmetric display. It suffers from all the disadvantages of MRFs: it is a passive system requiring a high voltage with no possibility to display edges and very rigid surfaces. It is shaped like a thimble around the finger, with the ERF between a hard outer shell and rubber inner shell.
Bicchi et al. [28] use magnetorheological fluids in their display. It has 4×4 elements with 45 mm resolution. The test persons have to insert a gloved hand in a box with fluid. It is a proof of concept and far from any practical application. They later presented a new and improved version of this Haptic Black Box (HBB II) [282]. It is very big and most of a gloved arm can be inserted.
MRFs and ERFs have a common problem of sedimentation: they degrade over time. Ferrofluids do not have this problem and might be an option for an active display,

but have not yet been used. To accomplish the necessary pressure difference of $0.5\,N/mm^2$ in a ferrofluid, the local difference in magnetic flux density has to be 10 T. This is the case for a fairly strong ferrofluid with a saturation magnetisation of 50 kA/m [66] [72]. It seems unlikely the requirements can be met in this kind of display. MRFs have a similar viscoelastic behaviour as biological tissue, ferrofluids do not.

There are also active displays using the properties of special fluids. One configuration uses electrolysis to increase or decrease the pressure of the resulting hydrogen and oxygen mixture inside a tactile display element [159]. Ionic conducting polymer gel film actuators pressing against the fingertip are used to present fine texture, such as in cloth [5] [155] [156]. Another example is a thermopneumatic tactile display, using a fluid with a low boiling point [333]. Each taxel has a closed reservoir filled with acetone. Heating the fluid boils it and actuates the taxel. The display has 4×4 taxels with 2.54 mm resolution and 0.7 mm stroke. Similar to other thermal actuators such as SMAs, the the cycle time of about 19 s is very long.

Pneumatic

Pneumatics have the advantage of a good power density and the possibility to use light and non-metal materials. Pneumatically actuated displays control the flow or pressure of air to drive pins [32] [41] [52] or inflate air chambers [146] [148] [210]. They are suited to combine with kinaesthetic feedback, because they have a very simple and light structure at the point of contact [144]. With lithography it is possible to miniaturise pneumatic cylinders down to a piston area of $0.15\,mm^2$, while still maintaining a stroke of 0.75 mm and a force of 0.1 N [36]. De Volder and Reynaerts [67] give an overview of pneumatic microactuators. However, nonlinear control of either pressure or flow, low power efficiency and the need for large valves are problems [49]. A disadvantage of this mechanical simplicity is that the length and diameter of the tubing clearly affects the time between the initial display of a stimulus and the actual tactile sensation of the user. In some situations this kind of latency may be simply unacceptable [143]. Proportional pneumatic valves tend to make a lot of noise, which can be disruptive for the concentration of the surgeon. Cohn et al. [52] made a display with 5×5 pneumatically-actuated pins, controlled by pulse-width modulated solenoid valves. Mounting on surgical instruments is difficult due to the large number of valves and tubes connected to its elements. Moy [208] [210] made a compliant tactile display with air chambers which allow ease of construction, low cost, no pin friction, no extraneous information from air leakage, and response linearity. It uses strain matching, has a 5–4–5 configuration with 2 mm resolution and 35–50 Hz bandwidth. However, the pneumatic valves make noise, and during experiments, the skin of the index finger gets numb. This is possibly caused by higher frequencies introduced by the opening and closing of the valves. The sensitivity can decrease after exposure of the skin to vibrations

[21] [183] (Section 1.2.3).
King et al. [146] [148] made a 3×2 element pneumatic display to mount on the da Vinci Surgical System. It is only 4 mm thick, weighs only 0.65 g and consists of 3 mm balloons with a 4.5 mm resolution at 8–10 Hz. An electropneumatic pressure regulator (SMC ITV0010-2MMS) controls the pressure. They studied the optimal balloon size by determining the number of pressure levels that can be easily discriminated. Five different pressure levels were selected with the highest at 100 kPa for all balloon sizes. The impact of spatial resolution was not taken into account and the 1.5 mm spacing between the balloons is necessary to avoid membrane disassociation. The maximum force is above 2 N and the stroke 1.5 mm. The compact displays, one on the thumb and one on the index finger, mounted on a da Vinci surgical system does not interfere in a peg transfer task [84]. The display is connected with a 3×2 piezoresistive tactile sensor mounted on a MIS grasper [145]. The sensor is based on a FlexiForce cell from Tekscan and has a spatial resolution of 2.375 mm and a hysteresis of 45%. This tactile feedback system led to a reduced grip force in a peg transfer task with rubber blocks, but not to an improvement of the speed [147].
A peculiar display is the CASR display developed by Bicchi et al. [27], based on their Contact Area Spread Rate hypothesis. This hypothesis states that stiffness can be simulated by adapting the rate at which the contact area of the display increases, and thus that softness can be discriminated using the display. Several experiments show that the performance is indeed better than with kinaesthetic feedback alone.
Makino and Shinoda [189] propose a suction based tactile display for the palm, with 5 mm resolution. The system uses the illusion that the human sense of touch cannot distinguish a compression by a pin like object from a suction pressure stimulation through a hole. How the amount of suction corresponds with the depth of indentation of a pin is not discussed. They can separately trigger SAI and FAI receptors by adding DC and 40 Hz signals; the deeper receptors are not stimulated.
Asamura et al. [9] designed an air pressure based display for psychophysical experiments. It has three elements, spaced 2.5 mm, with a small voice coil driven air pressure controller. The bandwidth is 300 Hz and the pressure 16.8 kPa.
The display of Caldwell et al. [41] has 4×4 elements, with a resolution of 3.5 mm. Pneumatic muscle actuators supply a shear force element by moving the entire display sideways. The total display weighs only 20 g and has a bandwidth of 11 Hz. A frequency signal of 20 Hz to 300 Hz is superimposed on the pressure signal by a solenoid valve. The stroke of the pins is 5 mm, with a maximum force of 3 N.
Another display makes use of air jets [143] [144]. The finger has to be pressed against tubes with an internal diameter of 1.5 mm, and these tubes are pressurised to produce a tactile sensation. This is essentially also a balloon actuator with the skin functioning as a membrane. If the skin is not pressed tightly enough, some air will escape, altering the sensation. It is currently unclear what the effect of an air jet is compared to a pin. The display has 5×5 elements with 3.2 mm resolution in one direction, and 2.4 mm in the other. It is a binary display and the pressure

is 100 kPa. The used valves are binary with a 20 ms latency. Three versions of the display were constructed [144]. One with 5×5 taxels with 1.0 and 1.8 mm spacing, one with 5×5 taxels with 2.4 and 3.2 mm spacing and one with 3×3 taxels with 4.5 and 5.3 mm spacing. Psychophysical experiments show that smaller jets result in better spatial performance. A simple virtual button pressing task shows that the combination of kinaesthetic and cutaneous cues is better than kinaesthetic cues only. This might be explained by a higher confidence level upon touching the buttons.

Acoustic

Iwamoto et al. [117] made a tactile display based on acoustic radiation pressure. The tactile sensation is produced with PZT-generated ultrasound through an ultrasound conducting gel. The sound has a frequency of 3 MHz which leads to a wave length of 0.5 mm. A focus of 1 mm is achieved and a scanning frequency of 1 kHz is possible. The force is very low, 6.4 mN, and can barely be felt. More recently they reached 20 mN [118]. A prototype in free space resulted in 3 mN force with a focus of 20 mm at 250 mm above the display [119].

Electrocutaneous

Instead off a straightforward display that indents the skin, a tactile sensation can be simulated by passing electric current through the skin [131] [227]. Kajimoto et al. [133] [134] designed an electrocutaneous display. Electrodes with an inner and an outer circle are placed on the skin. Anodic stimulation (current from the central to the outer electrode) elicit an acute vibratory sensation, while cathodic stimulation generates a vague pressure sensation [130] [256]. The static resolution of the display is 2–4 mm. The 4×4 electrodes are spaced 2 mm apart. It is not a natural sensation because only part of the mechanoreceptors are triggered: it gives a feeling of vibration, cold or even itchy. The sensation can be slightly improved by compensating for the variable impedance of the human skin [132]. Despite these efforts, the display feels uncomfortable and unnatural to some.

Another way to represent a tactile texture sensation is electrostatic tactile stimulation. When the finger touches and scans an insulated metal surface, the metal surface and the layer of conductive substance under the skin form a condenser. By applying cyclic voltage to the metal plate, an electrostatic attraction —and thus a friction force— is generated periodically, inducing a mechanical vibration on the moving finger [357]. Strong and Troxel [306] built a Braille display with this method with a resolution of 2.54 mm. The advantage is a simple structure that can be very thin. On the other hand, only texture can be displayed and it only works on dry skin [191]. When the finger is wet, a superficial water layer forms

a condenser together with the electrode. In this case, all of the electrostatic force acts on the water layer and not on the finger. Humidity can make the perception unstable [313]. This problem is solved with a very thin conductive slider [357]. Another problem is that when the taxels are made too small, the electrostatic force is too small to stimulate the finger [357]. A polyimide-on-silicon electrostatic fingertip tactile display creates an electrostatic attraction between the skin and electrode surface which presents a 'sticky' or 'buzzing' sensation [15]. A reason not to use electrostatic displays or electrocutaneous stimulation is the chance of electrochemical or thermal burns [208].

3.1.3 Braille Displays

Printed information in Braille is not abundant, so a display to make digital information available for blind people is very useful. Braille displays are related to tactile displays, but generally easier to build. The reason for that is that the requirements are lower: lower force, coarser spatial resolution, very low frequency and more available space for less elements. Another important difference is that Braille dots only have two states: up or down. The International Building Standard for Braille cells are a dot interval of 2.5 mm, a dot base diameter 1.5–1.6 mm and a dot height of 0.6–0.9 mm. The most frequently adopted technology for Braille displays are piezoelectric bimorphs. Nobels [223] gives a nice overview of Braille displays, and defines the requirements. The minimal force is 0.1 N and the minimal displacement 0.8 mm.
The binary operation allows for less actuators than there are dots. An example of this is developed by NIST [264]. A single actuator on an xy-table pushes the passive pins up. There are 71×51 elements with 2.54 mm in between. In a Braille mouse [223] four electromagnetic actuators push up the dots to generate 10 characters per second to glide under the finger. A problem is that blind people want to move their hands while reading, rather then passively experiencing the sensations.
Some of the first displays were Optacon and Optacon II (OPtical-to-TACtile CONversion). The Optacon has 144 vibrating pins (6×24) in a concave surface that fits the finger to represent the intensity pattern as a camera is manually scanned across a printed page [33] [303] [134]. It was produced by Telesensory Corp. in the 1960's and with some practice a reading speed of 10–100 words per minute [178] is possible, but there is a long learning curve. Some other displays are TVSS (Tactile Vision Substitution System) [11] and Kinotact (Kinaesthetic, optical and tactile display) [54]. Babbage sells Braille cells with sensors to detect the finger position and to take the reading speed into account.

Lee [172] presents a Braille display based on paraffin expanding when heated. It has a cycle time of 50 s, consuming 0.6 W per dot to reach a dot height of 0.6 mm, with a minimum of 0.3 W per dot. Silicone rubber is used to provide flexibility in volume change. Nakashige et al. [217] use low melting point metals. When the

metal melts, pins are pushed up or down with compressed air. It has 10×10 pins with 2 mm resolution. Matysek et al. [196] designed a single sell Braille display using electrostatic dielectric polymer actuators. The deflection is 0.5 mm and the actuation is active in the off position, when the pin disappears in the hole. The driving voltage is 1000 V. They want to use vibration because they only have one cell and static, passive touch is not very sensitive.

3.1.4 Comparison of Tactile Displays

Table 3.1 summarises the properties of different tactile displays found in literature. The table only contains displays which indent the finger orthogonally. Lateral skin stretch displays, electrocutaneous displays, or passive displays are not included because they are too different to compare. The remaining displays can mostly be divided into two categories. The first category comprises the shape or force displays. These can generally exert reasonably large forces of close to, or above 1 N combined with a large stroke in the order of magnitude of 1 mm. They are usually either slow or very bulky. Vibrotactile displays fill the second category. They are only capable of exerting very small forces and/or very small displacements, in the order of magnitude of millinewtons and micrometers, but their bandwidth is above 100 Hz and up to 1000 Hz. Often they only operate at one fixed frequency around 250 Hz, which is the frequency for which the human skin is most sensitive.
The comparison of the different displays requires some attention. The maximum force is often only reached at small displacements, while the maximum displacement is only valid in the absence of a load. This is especially the case for displays employing piezo bimorphs or pneumatic bubble actuators. For a pure force display, such as pneumatic cylinders, the force is independent of the position. For taxels of a very stiff display, on the contrary, the applied force has little influence on the position. Examples of this are most SMA displays and some electromagnetic displays with a large reduction ratio.

reference	principle	# elements	spatial resolution	stroke	force	bandwidth (frame rate)	MIS?
[19]	Electromagnetic	8×8	4 mm	0.1 mm	13 mN	800 Hz	
[85]	Electromagnetic	3×3	4.5 mm		0.23 mN	110 Hz	
[230]	Electromagnetic	4×8	2.7 mm	3 mm	0.5 N	0.7 Hz	yes
[270]	Electromagnetic	4×4	2 mm	2.5 mm	3 N	15 Hz	
[305]	Electromagnetic	4×4	2 mm		2.5 mN	350 Hz	
[310]	Electromagnetic	4×4		0.2 mm	1.2 mN	>250 Hz	
[342]	Electromagnetic	6×6	2 mm	2 mm	2 N	7.5 Hz	
[45]	Electrostatic	3–2–3	∼7 mm			100 Hz	
[157]	Electrostatic	4×5	3 mm	0.9 mm	14 mN	>100 Hz	
[115]	Piezoelectric	5×10	1.8 mm	0.05 mm	40 mN	>250 Hz	
[141]	Piezoelectric	4×8	1.5 mm	0.5 mm	0.2 N	20 Hz	
[161]	Piezoelectric	6×5	1.8 mm	0.7 mm	60 mN	1 kHz	
[308]	Piezoelectric	10×10	1 mm	0.04 mm		400 Hz	
[328]	Piezoelectric	1×88	0.38 mm	0.01 mm		1000 Hz	
[360]	Piezoelectric	6×4	2 mm				
[112]	SMA	4×6	2.1 mm	3 mm		10 Hz	yes
[219]	SMA	16×16	5 mm	30 mm	0.6 N	0.1 Hz	
[316]	SMA	8×8	3.6 mm	3.2 mm		<1 Hz	
[331]	SMA	8×8	2.6 mm	1.4 mm	0.32 N	1.5 Hz	
[349]	SMA	1×10	2 mm	3 mm	2 N	40 Hz	
[333]	Thermopneumatic	4×4	2.54 mm	0.7 mm	10 mN	0.05 Hz	
[41]	Pneumatic	4×4	3.5 mm	5 mm	3 N	11 Hz	
[145]	Pneumatic	2×3	4.5 mm	1.5 mm	>1 N	10 Hz	yes
[210]	Pneumatic	5×5	2 mm	0.7 mm		5 Hz	
[118]	acoustic	1 (moving)	∼1 mm		20 mN	1000 Hz	

Table 3.1: *Comparison of tactile displays*

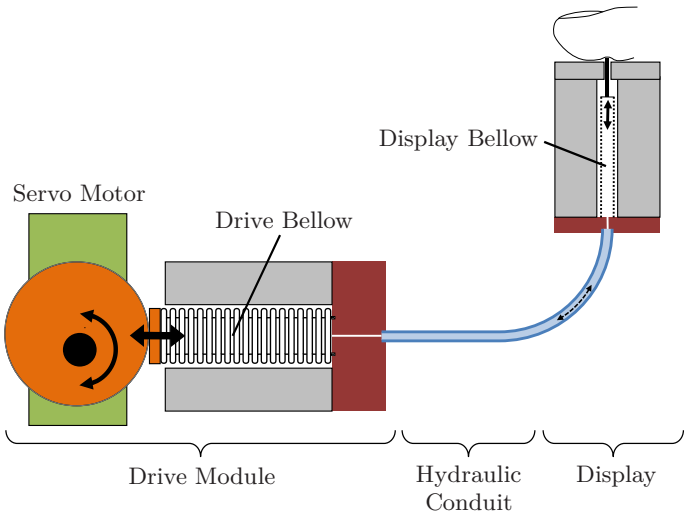

Figure 3.4: *Schematic representation of the closed hydraulic system. A servo motor, equipped with a camshaft, compresses the drive bellow. This bellow is a flexible reservoir of which the volume decreases on depression. Since the hydraulic system is closed and the hydraulic fluid is nearly incompressible, the volume in the display bellow has to increase. This in turn results in a taxel pin being pushed in the skin of the fingertip.*

3.2 Closed Hydraulic System

Hydraulics and pneumatics have the advantage that the power is generated at a distance. This results in a relatively high power-to-weight or power-to-volume ratio, especially in miniaturised systems. They are very well suited to combine with kinaesthetic feedback, because they have a very simple structure at the point of contact [144], and the use of light materials is possible. Potential problems include the difficult and nonlinear control of either pressure or flow, the low power efficiency and the need for large valves [49]. When a hydraulic cylinder decreases in size, sealing becomes a more challenging issue, because the friction in the seal only decreases linearly with size, while the actuation force decreases quadratically. The friction force thus gains relative importance.
Hydraulics and pneumatics have comparable characteristics, but hydraulics can potentially realise higher forces, bandwidth, and stiffness. Since hydraulic fluids in general are not compressible, the response time of a hydraulic system is much faster than that of a pneumatic system. The system described here is the first hydraulic tactile display reported.

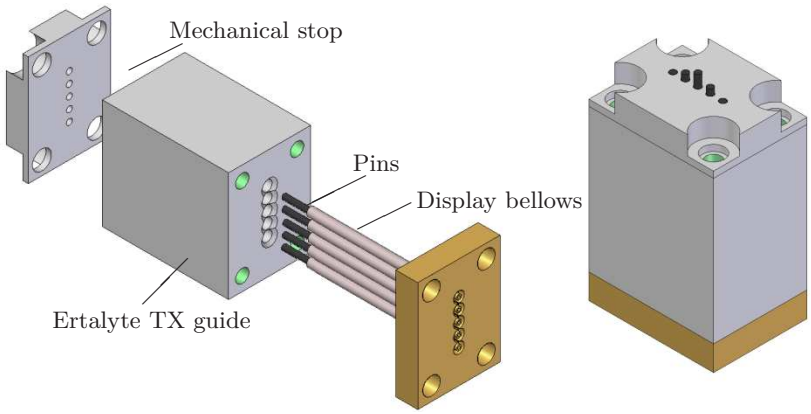

Figure 3.5: *CAD model of the display; left: exploded view; right: assembly*

The first tactile display is based on a closed microhydraulic system, driven by servo motors. The working principle is shown schematically in Figure 3.4. The hydraulic circuit is filled with degassed, deionised water. A servo motor, equipped with a camshaft, compresses the drive bellow. This bellow is a flexible reservoir of which the volume decreases on depression. Since the hydraulic system is closed and the hydraulic fluid is nearly incompressible, the volume in the display bellow has to increase. This in turn results in a taxel pin being pushed in the skin of the fingertip.
The entire setup consists of two functional parts, connected with a hydraulic conduit: the tactile display and the drive module. The bellows in the display each drive a pin up and down to provide a tactile sensation. The transmission ratio between camshaft and display depends on the diameters of the bellows and the properties of the conduit.

Display

The display itself consists of an array of small bellows in a guide block (Figure 3.5). The bellows have an outer diameter of 1.57 mm, sufficiently small for a spatial resolution of 2 mm. The length should be as small as possible, but depends on the maximum strain allowed to achieve a 2 mm stroke. The maximum stroke is 2.34 mm. A small pin is glued in the end of the bellow to close it and to serve as contact point with the finger.
The US company Servometer produced the nickel bellows by electrodeposition. Due to the required compliance, the walls are only 14.7 µm thin. The bellows are designed to allow a relatively large compression and extension without plastic deformation of the metal. Their stiffness is 148 N/m, with a 30% tolerance.

To prevent buckling of the weak bellows, they have to be guided. A low friction Ertalyte TX guide block provides the necessary support. Ertalyte TX is a polyethylene terephtalate (PET) compound incorporating a uniformly dispersed solid lubricant. The bellows reside in holes of 1.8 mm, 2 mm apart. To protect the bellows against overload, a mechanical stop is provided at the end. This stop is also the guide for the pins. Since the bellows are custom made and are produced with a lost mould method, they are rather expensive.

Drive module

The drive module provides the hydraulic pressure necessary to drive the taxel in the tactile display. Each taxel has its own drive module. Providing actuation from a distance makes it possible to use bigger and heavier actuators. The drive module consists of a servo motor, a camshaft and a drive bellow. The drive bellows have a similar guide as the display bellows. The chosen servo has an accuracy of less than one degree.
The camshaft transduces the rotational motion of the motor to the linear motion of the bellow. To easily manufacture an accurate camshaft, its shape is a simple eccentric cylinder. To have a reasonably linear angle-displacement relationship, the useful angle is smaller than 15°. The required stroke of the drive bellow depends on its diameter and the required volume change in the display bellow. When the volume losses in the elastic conduit are taken into account, this stroke is calculated to be 160 µm. The position x of the camshaft follows

$$r = \sqrt{x^2 + e^2 + 2er\cos\Theta}, \tag{3.4}$$

with e the eccentricity, $r = 16$ mm the radius of the shaft and Θ the angle of rotation. A desired change in the position of 160 µm in 15° leads to an eccentricity of 0.6 mm. To avoid friction and stick-slip effects, the chosen material is the low friction plastic Ertalyte TX.
A safety stop is fixed to the axis of the motor, so it cannot turn too far and increase the pressure of the system to a level that would damage the bellows.

Hydraulic conduit

The choice of the hydraulic conduit is not arbitrary. There are some conflicting requirements. On the one hand it has to be flexible, to allow free motion of the display. On the other hand, it has to be stiff to prevent a volume change under pressure. When the internal pressure rises, the volume of the conduit increases. Since water is incompressible and the hydraulic system is closed, each change in volume in the conduit is lost to the stroke of the display bellow. The diameter should be small to allow the easy connection of several conduits to the display.

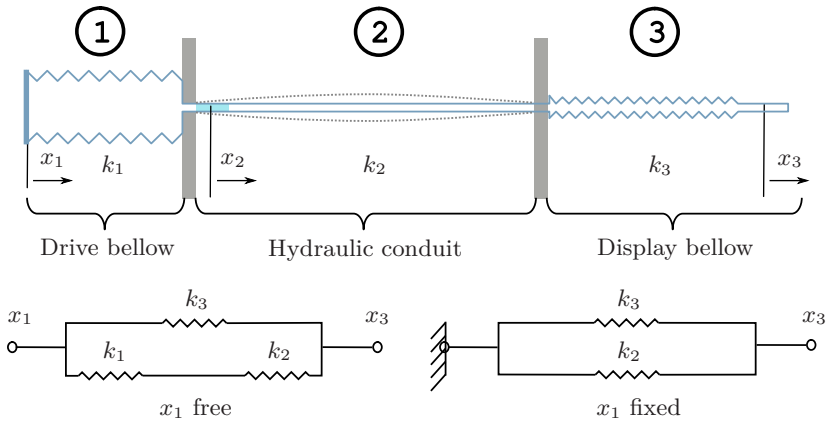

Figure 3.6: *Hydraulic circuit. While the fluid is nearly incompressible, the Teflon tubes can expand under pressure, which decreases the stiffness of the system.*

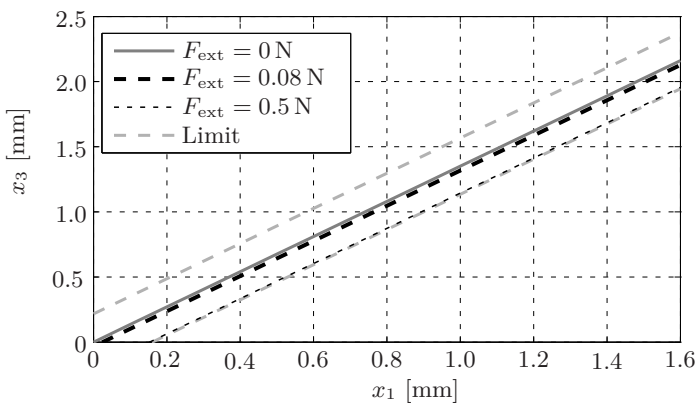

Figure 3.7: *Influence of an external force on the transmission ratio. For the hydraulic conduit used in the prototype, the accuracy of the displacement of the pin remains within the limit of 10%.*

Teflon tubes with a length of 200 mm, an outer diameter D_o of 1.5 mm and an inner diameter D_i of 0.85 mm are used. There is a small estimated loss in pressure of 0.02 bar at 20 Hz due to hydraulic resistance. The flow remains laminar.
To calculate the transmission ratio between drive bellow and display bellow, a scheme of the hydraulic circuit is given in Figure 3.6.

$$A_3 x_3 = A_1 x_1 - \Delta V_2, \tag{3.5}$$

where A_1 and A_3 are the cross sections of respectively the drive bellow and the display bellow, and ΔV_2 the volume change of the hydraulic conduit. This volume change, consists of three parts, a radial change $\Delta V_{2,\mathrm{r}}$, an axial change $\Delta V_{2,\mathrm{a}}$ and some boundary effects that are neglected.

$$\Delta V_{2,\mathrm{r}} = \frac{\pi L}{4}\left[\left(D_\mathrm{i} + \frac{D_\mathrm{i}^2 P}{E(D_\mathrm{o} - D_\mathrm{i})}\right)^2 - D_\mathrm{i}^2\right], \quad \text{and} \tag{3.6}$$

$$\Delta V_{2,\mathrm{a}} = \frac{\pi P L D_\mathrm{i}^3}{8E(D_\mathrm{o} - D_\mathrm{i})}, \tag{3.7}$$

where L is the length of the conduit, E its Young modulus and P the pressure inside the circuit. In an unloaded situation, this pressure originates from the spring force of the display bellow, or $P = F_3/A_3 = k_3 x_3/A_3$. The total volume loss becomes

$$\Delta V_2 = \Delta V_{2,\mathrm{r}} + \Delta V_{2,\mathrm{a}} + \Delta V_{2,\mathrm{boundary}} \tag{3.8}$$

$$\approx \frac{\pi L}{4}\left[\left(D_\mathrm{i} + \frac{D_\mathrm{i}^2 P}{E(D_\mathrm{o} - D_\mathrm{i})}\right)^2 - D_\mathrm{i}^2 + \frac{P D_\mathrm{i}^3}{2E(D_\mathrm{o} - D_\mathrm{i})}\right] \tag{3.9}$$

$$\approx \underbrace{\left(\frac{\pi L D_\mathrm{i}^4 k_3^2}{4A_3^2 E^2 (D_\mathrm{o} - D_\mathrm{i})^2}\right)}_{a} x_3^2 + \underbrace{\left(\frac{5\pi L k_3 D_\mathrm{i}^3}{8A_3 E(D_\mathrm{o} - D_\mathrm{i})}\right)}_{b} x_3, \tag{3.10}$$

which confirms that the conduit should be as stiff and as short as possible. The relation between x_1 and x_3 is

$$A_3 x_3 = A_1 x_1 - a x_3^2 + b x_3, \tag{3.11}$$

which results in

$$x_3 = \frac{b - A_3 + \sqrt{(A_3 - b)^2 + 4aA_1 x_1}}{2a}. \tag{3.12}$$

A Teflon tube with a length of 200 mm results in about 5% volume loss. An external force F_ext on the display, such as a finger pushing on it, will increase the pressure in the system, and thus the influence of the hydraulic conduit. An analogue calculation can be made, substituting $P = (k_3 x_3 + F_\mathrm{ext})/A_3$. The result is shown in Figure 3.7. For the hydraulic conduit used in the prototype, the accuracy of the displacement x_1 remains within the limit of 10%. Measuring the position of the display bellow or the pressure inside the hydraulic circuit would facilitate a closed loop control, but this would needlessly complicate the system.

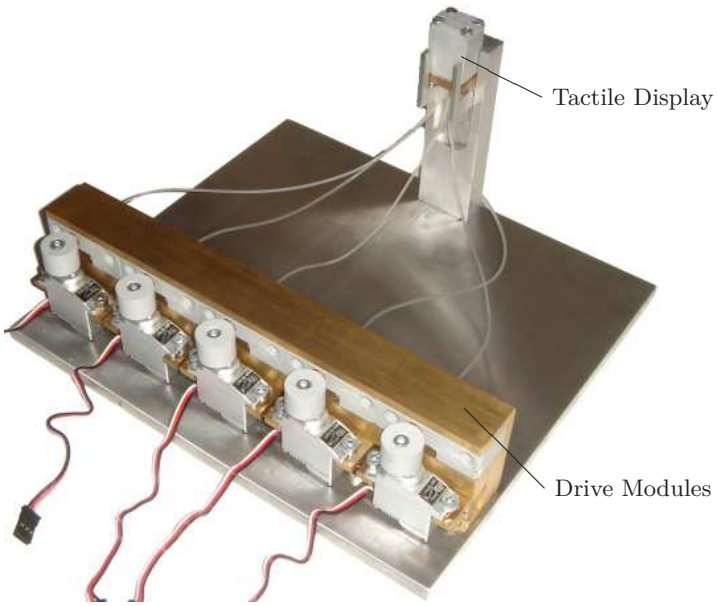

Figure 3.8: *Prototype of the closed hydraulic system. A prototype with five functional pins was constructed. The drive modules have to be reduced in size for a full display.*

Assembly

Assembling all components is a crucial step. It is very important that no air is left in the closed hydraulic system. That would greatly reduce the stiffness of the system and have a large influence on the transmission ratio. To prevent this, the components are filled with deionised water and put in a vacuum chamber to remove all air. This also removes the air that is dissolved in the water. Afterwards, the air-free components are assembled under water and the Teflon tubes clamped on their connection. The assembled system is then removed from the water and glued together.

3.2.1 Results and Discussion

A working prototype with five taxels was built (Figure 3.8). It allows large forces and has a good accuracy. The bandwidth is determined mainly by the bandwidth of the servo motor. This bandwidth is measured experimentally by steering the motors at the full desired amplitude of 15°. The result is a bandwidth of only 5.5 Hz, which is below the desired 30 Hz. A smaller amplitude would yield a

higher bandwidth, but there is a maximum bandwidth of 25 Hz, since the control frequency of the servo motor is 50 Hz.
In terms of stiffness, the system can be viewed as in Figure 3.6. k_3 equals 148 N/m and k_2 can be estimated from (3.5), with x_1 held constant and ΔV_2 force dependent, to be 834 N/m. The stiffness of the drive bellow has no influence, since it is held fixed against the camshaft. The resulting stiffness felt at the display is 982 N/m, which is the same order of magnitude as the stiffness of the skin.
The hydraulic tactile display compares well with other displays found in literature. As expected, force and stroke are very good, exceeding the requirements. The resolution of 2 mm is competitive but not yet sufficiently fine. Since this is a proof of concept, the number of taxels is low, but can easily be increased.
During construction, it became apparent that the display bellows were not robust enough with their wall thickness of only 14.7 µm. During the assembly and testing process, several bellows acquired a leak. Although the leak can be closed with glue, this is time consuming and decreases the performance of the display. Although possible, it proved difficult to get the microhydraulic circuit completely air free. A last problem was the price of the bellows, which would make a full-scale display with 54 taxels extremely expensive.
The servo motors also have to be replaced by a more robust alternative with a better performance. As mentioned above, their bandwidth is not sufficient. The best solution would be to replace the servo motors with another actuation principle altogether, such as a piezo-electric element or a solenoid.

3.2.2 Conclusion on the Closed Circuit Hydraulic Tactile Display

This section presents the first tactile display based on microhydraulics. The result is a powerful and compact display, with the actuation at a distance. It allows easy extension to more rows and columns without added complexity or size of the display. With a force of up to 4 N, a stroke of 2.34 mm and an accuracy within 10%, this principle meets most requirements. The spatial resolution of 2 mm is workable, but should preferably be a bit finer. The bandwidth is lacking due to the servo motors used. The principle of a closed hydraulic circuit, however, does not pose a real limit to the bandwidth.

3.3 Hydraulic Piezo Valve

To remove the problems associated with a closed circuit, such as the sensitivity to air bubbles and the requirement of no leakage, a novel prototype was designed, based on control by proportional valves. While the complexity of the display decreases, the main challenge moves to the design of a small high pressure proportional valve. An open hydraulic system naturally facilitates force control

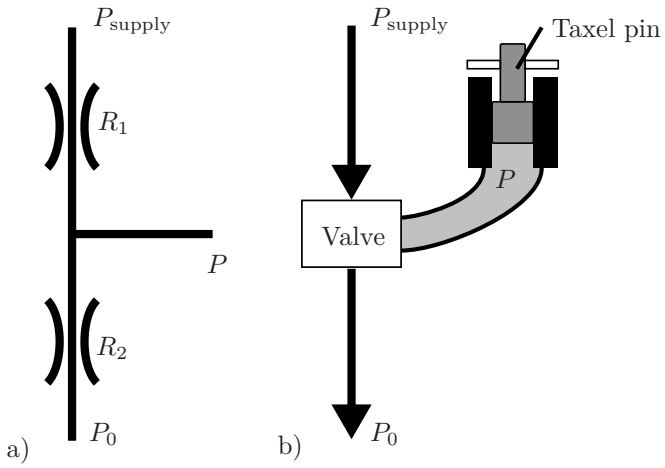

Figure 3.9: *Proportional valve with a pressure divider. a) Schematic principle. The output pressure P depends on the variable resistances R_1 and R_2. b) Working principle of a tactile display with a proportional valve. The output of the valve is connected to the tactile display, where the taxel pin is directly controlled by the pressure.*

of the taxels.
The real challenge is a miniaturised proportional valve to regulate each individual taxel. Pulse width modulation with a binary valve is a possible solution, but this can result in a high frequency vibration superimposed on the movement of the taxel. These higher frequencies can cause fatigue of the mechanoreceptors in the skin [21] [183], reducing the effectiveness of the display. Commercial valves driven by pulse width modulation also produce a lot of noise.
A full tactile display requires a series of proportional valves, one for every taxel. Commercially available proportional valves are either rather large, which makes them unsuited for a display that needs 50–100 valves, or only function at low pressure —too low to reach the necessary force. This means that a new proportional, high pressure, mass producible valve should be designed for this specific application. To get a reasonable force output on a taxel with a pin diameter of 1 mm, the pressure should be regulated between 0–7 bar. Pressures up to 13 bar would enable the rendering of forces of up to 1 N per taxel.
To control a pressure proportionally, a certain flow through the valve is required. Since the display itself consumes hardly any flow, the valve itself needs to provide it through a leakage channel. This leads to the design of a pressure divider (Figure 3.9a), where one or two hydraulic resistances R_1 and R_2 are controlled to change the functional pressure P. This pressure is branched towards the display

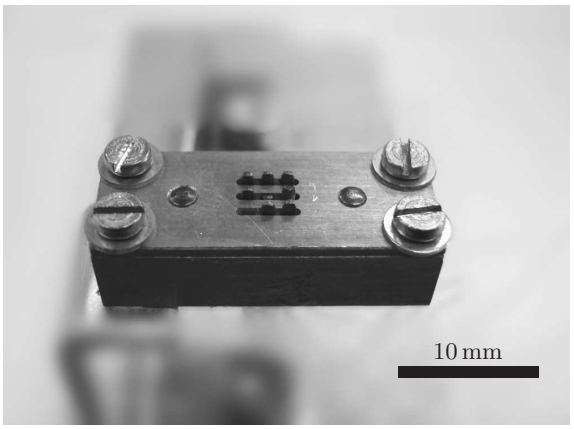

Figure 3.10: *Lightweight hydraulic tactile display. Steel pins can move in a bronze house. A small tolerance between pins and holes reduces leakage.*

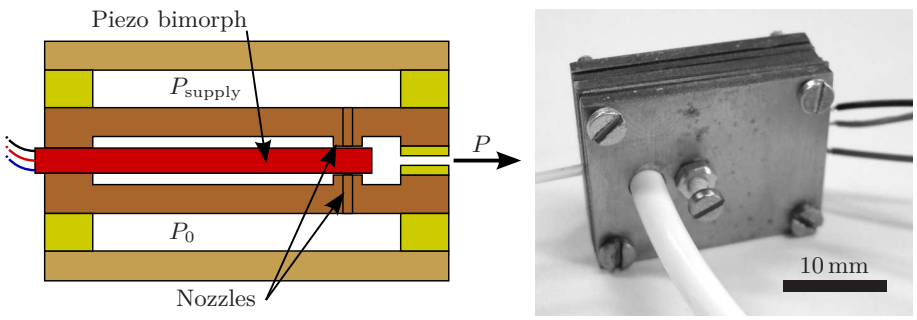

Figure 3.11: *Proportional valve based on a piezo bimorph. On the left is the schematic working principle of the valve. Two nozzles connect the supply pressure P_{supply} and the atmospheric pressure P_0 with the inner valve at pressure P. When the piezo bimorph moves up or down, one of the nozzles is opened, decreasing its hydraulic resistance, while the other closes, increasing its hydraulic resistance. On the right is a picture of the realised prototype. Because the piezo bimorph is not straight, the position of the nozzles has to be manually adjusted. This can be done with the screw in the middle.*

to control the pin (Figure 3.9b). To avoid that the leakage in the display affects the valve pressure, the flow through the valve has to be significantly larger than the flow to the display.

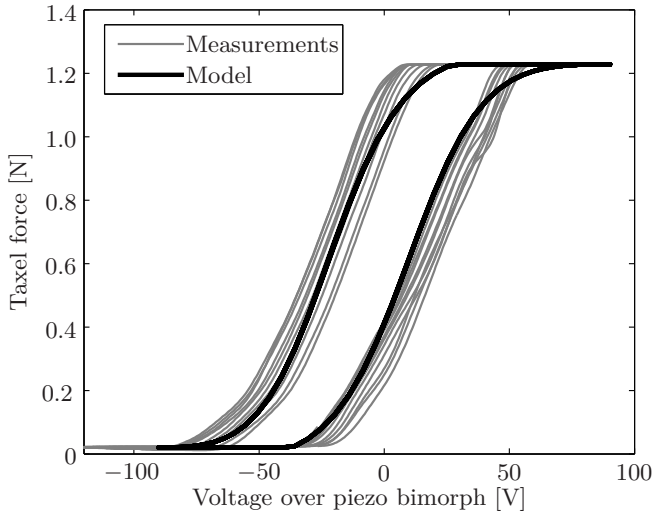

Figure 3.12: *Characteristics of a tactile display controlled by a piezo bimorph based proportional valve, compared with a model of the system. Both Coulomb friction of the pin and hysteresis of the bimorph are experimentally determined and implemented in the model.*

3.3.1 Experiments and Results

To test this principle, a working one-pin prototype was designed and built. The display is a simple brass prism with accurately reamed holes that offer a tight fit for the pins (Figure 3.10). Leakage is reduced by increasing the hydraulic resistance over the pins over a distance of 2 mm through the tight fit with 2–5 µm play. To avoid that the hydraulic liquid pushes the pins out of the holes, they are flattened and a plate with slits is fixed on top of the display. There is a small amount of Coulomb friction in the display, but the hydraulic oil offers some lubrication to reduce this problem. Since the pins are free to move in the holes, this design poses no immediate limitations on the stroke of the taxels. The display itself weighs only 15 g.

A first design uses a Noliac CMBP03 piezoelectric bimorph (Figure 3.11). These bimorphs have a working voltage of −100 to 100 V. On each side of the bimorph is a nozzle, one is the high pressure inlet, the other is the low pressure outlet. By bending the bimorph in one direction or the other, one of the nozzles is smothered, while the other is opened. Since the nozzles are small, the force on the bimorph remains sufficiently low and the valve is able to handle higher pressures. A large disadvantage of the design is that the bimorphs do not have a uniform thickness

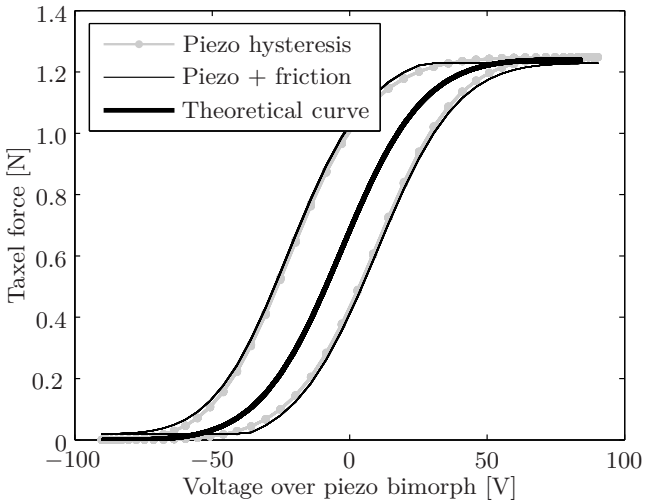

Figure 3.13: *Models of the tactile display characteristics with increasing complexity. The theoretical curve only includes the hydraulic model with the changing resistances of the nozzles. First the measured hysteresis of the piezo bimorph is added. Finally, Coulomb friction of the pin in the display is implemented.*

and they are not straight, while the gap between the nozzles and the bimorph has to be controlled between 0–80µm. This means that after assembly a tedious iterative correction has to be performed by adjusting the nozzles with an adjustment screw. Since the valve is sealed, this adjustment is performed blindly.
The valve was connected to the display and the system was tested with hydraulic oil at a maximum pressure of ±15 bar (Figure 3.12). The measurements show a good correlation with the theoretically predicted characteristics. The measured curve had to be moved on the voltage axis because of the uncertain shape and thickness of the piezo bimorph. The model used in Figure 3.12 is based on laminar flow. The Coulomb friction of the pins was measured independently to be 0.02 N and added to the model as a constant force in the opposite direction of motion. Viscous friction is not taken into account. The hysteresis of the piezo bimorph was also measured independently. It was not modelled, but numerically implemented in the model with the data of the measurement. Figure 3.13 shows models with increasing complexity to illustrate the impact of the different components.
The hydraulic model is based on a simple pressure divider with laminar flow through the resistors. The pressure drop over two parallel plates is then

$$\Delta P = \frac{Q}{12\mu a^3 bl}, \tag{3.13}$$

with Q the volume flow between the two plates, b the width of the plates perpendicular to the direction of flow, l the length of the plates along the flow, a the distance between the plates and μ the dynamic viscosity of the fluid. The hydraulic resistance R is the ratio of pressure drop over flow rate

$$R = \frac{\Delta P}{Q} = \frac{1}{12\mu a^3 bl}. \tag{3.14}$$

The pressure in the valve in the middle of the pressure divider is

$$P = P_0 + \frac{R_{\text{high}}}{R_{\text{high}} + R_{\text{low}}} \left(P_{\text{supply}} - P_0\right), \tag{3.15}$$

with R_{high} and R_{low} the hydraulic resistances of over respectively the high and the low pressure nozzle. Both nozzles have the same dimensions and are controlled antagonistically by the piezo bimorph. The nozzle resistance is approximated by (3.14) with $l = 0.5\,\text{mm}$, $b \approx 2\pi r_{\text{nozzle}} = 0.5\,\text{mm}$ and a varies between 0–40 µm. For the used hydraulic fluid, the maximal flow through the valve is $14.5\,\text{mm}^3/\text{s}$, while the maximal flow leakage at the taxel is only $5.7 \cdot 10^{-2}\,\text{mm}^3/\text{s}$ and is neglected in the model. These values allow to check the Reynolds number

$$R_{\text{e}} = \frac{\rho v a}{\mu} = \frac{\rho Q_{\max}}{b\mu} = 0.0014, \tag{3.16}$$

with ρ the density of the fluid and v the speed. The Reynolds number is significantly lower than 1000, guaranteeing that the flow is indeed laminar, as assumed in the model.
The maximum force measured was 1.2 N. Neither the piezo bimorph nor the hydraulic circuit poses a significant limit to the bandwidth. The full force range is reached up to 40 Hz which is the limit of the measurement system that was used. The maximum stroke in this design is 3 mm, but this could easily be increased by augmenting the length of the pin.

3.3.2 Conclusion on the Hydraulic Valve

The use of an open hydraulic circuit promised a simple, compact display with a very high force. This is realised with the aid of the proportional valve. The measurements showed that all quantitative requirements are met. The piezo bimorph in the valve, however, causes a considerable hysteresis, which has to be compensated for. Another problem lies in the repeatability of the shape of the bimorphs. There is a large variance on the thickness of these bimorphs, larger even than the desired working range. They also show a distinct curvature, aggravating the problem. Although a tedious, blind adjustment step can compensate, it is not feasible to repeat that for a large amount of valves.

3.4 Pneumatic Solenoid Valve

Similarly to hydraulics, pneumatics scale down comparatively well, but it does not have the same potential for high forces or speed. A big advantage of pneumatics is that pressurised air is often available, and leakage is usually not a big issue. This makes the design of the display even simpler, because it only requires a restriction seal, which can have low friction. While the concept is very promising, the design of a suitable valve is not straightforward. The valves have to regulate a pressure of 600 kPa proportionally. This section discusses the design of a simple valve that is actuated by a solenoid. Other pneumatic tactile displays in literature lack a miniaturised proportional valve [41] [52] [210].
The fact that the power is generated at a distance, results in an additional disadvantage for a pneumatic system. The length and diameter of the tubing clearly affects the time between the initial display of a stimulus and the actual tactile sensation of the user. In many situations this kind of latency will be simply unacceptable [143]. Furthermore, the large number of tubes necessary to control all the taxels makes mounting on a surgical instrument difficult [52].

3.4.1 Principle of Operation

Since tactile feedback requires a large amount of valves, they should be relatively small, simple, robust, easy to produce and to control, have a limited power consumption and be reasonably priced. These requirements suggest electromagnetic actuation, and more specifically a reluctance type actuator. Since the electromagnetic force does not scale down well, the operation force of the valve has to be limited.
Figure 3.14 shows the main principle of the valve, which is basically a pressure divider (Figure 3.9). Two variable hydraulic resistances regulate the output pressure. Since the tactile display consumes almost no air, the required flow for the pressure divider to work is generated by leaking air to the environment. If the airflow is too low, it will limit the bandwidth of the system. If it is too high, a tactile display with 100 valves would consume an excessive amount of pressurised air.
Accurate positioning of the piston is key to a proportional valve of this type. The proposed valve uses a reluctance actuator: a current through the coil causes a magnetic flux through the piston and the magnetic circuit, which pulls down the piston. In the absence of a permanent magnet or a large air gap, the problem can be solved analytically with high accuracy (Appendix A).
The spring translates this force to a position of the piston with micrometer precision. Two holes with a diameter of 100 µm act as pneumatic resistances; one is connected to a high pressure chamber (P_{supply}), the other to atmospheric pressure P_0. When the piston moves down, it opens up the upper hole, decreasing

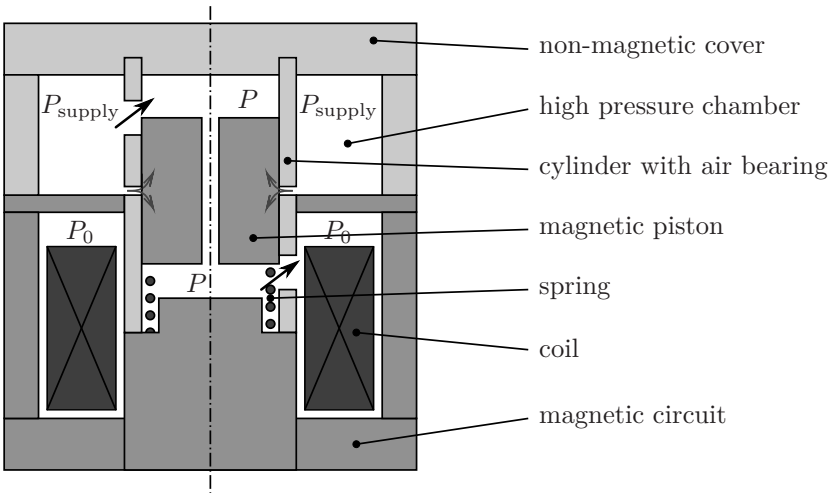

Figure 3.14: *Schematic drawing of the proportional valve. A current through the coil induces a magnetic reluctance force to pull the piston down the cylinder. The spring translates this force to a position of the piston with micrometer precision. Two holes with a diameter of 100 µm act as pneumatic resistances; one is connected to a high pressure chamber (P_{supply}), the other to atmospheric pressure P_0. When the piston moves down, it opens up the upper hole, decreasing its resistance, and closes the lower hole, increasing its resistance, thus increasing the regulated pressure P in the valve.*

its resistance, and closes the lower hole, increasing its resistance, thus increasing the regulated pressure P in the valve. While exact simulation is not feasible, the relation between piston position and valve pressure can be approximated with basic pneumatic equations.

Pneumatic circuit

The valve pressure P is regulated between the supply pressure P_{supply} (slit A) and the atmospheric pressure P_0 (slit B) via two variable slits in the valve cylinder. The movement of the piston changes the size of one or both slits. The Valve has an axisymmetric structure, except for the slits. The slits are symmetrical around the circumference of the valve to avoid disturbance forces. The valve design aims as much as possible at simplicity and an equilibrium of forces on the piston. For a small valve to work at high pressures, it is very important that the forces on the piston are reduced to a minimum. These forces are:

- **Gravity:** the weight of the piston pulls it down. If the spring is linear, and the mass of the piston is small, this gravity causes a small pretension in the spring that does not influence the behaviour of the valve.
- **Friction:** friction between the piston and the cylinder is hard to predict. The radial force on the piston is minimised by positioning the valve holes symmetrically around the circumference.
- **Pressure drop:** a difference in pressure between the top and the bottom of the piston results in an axial force. This pressure drop could be caused by the flow through the hole in the piston and the resulting conduit losses. Even for a small hole and exaggerated flows, this pressure drop is several orders of magnitude too low to ever become a problem.
- **Pressure distribution:** the incoming supply pressure does not drop to the valve pressure immediately, meaning a small region of the piston might still experience an increased pressure. Estimating this influence with any certainty is very difficult and it is determined experimentally to be indeed a problem. Adjusting the shape of the piston can solve it.

For the calculations, the air is assumed to be an ideal, compressible fluid. Two flow regimes can be present in the slits: subsonic flow ($M < 1$) and sonic flow ($M = 1$). Supersonic flow or a Mach number M bigger than 1 is not possible in the absence of a smooth convergent-divergent nozzle. The limit between both regimes is the critical pressure ratio for air of $P_{\text{low}}/P_{\text{high}} = r_{\text{C}} = 0.5283$. For two slits, this results in four possible situations, depending on the supply pressure. If the supply pressure is smaller than about 1.9 bar (atmospheric pressure divided by the critical pressure ratio), both slits will always have a subsonic flow regime.

1. P is close to P_{supply}. The regime is subsonic through slit A and sonic through slit B.
2. P is close to P_0. The regime is sonic through slit A and subsonic through slit B.
3. $P_{\text{supply}} > 3.6$ bar and $P_{\text{supply}} \cdot r_{\text{C}} > P > 1.9$ bar. The regime is sonic through both slits.
4. $P_{\text{supply}} < 3.6$ bar and $P_{\text{supply}} \cdot r_{\text{C}} < P < 1.9$ bar. The regime is subsonic through both slits.

In the following calculations, a supply pressure higher than $1/r_{\text{C}}^2$ =3.6 bar will be assumed. The mass flow through each slit $\dot{m}_{\text{A}}$ and $\dot{m}_{\text{B}}$ can be described in function of the effective area of the slit and the pressure drop over the slit.

$$\dot{m} = A_{\text{eff}} P_{\text{high}} \sqrt{\frac{2}{RT}} \Psi, \tag{3.17}$$

with A_{eff} the effective area of the slits, which is typically a little bit smaller than the real area, but difficult to estimate for a complex hole geometry. In the following calculations, the real area is used instead. P_{high} and P_{low} are the highest and the lowest pressures over the slit, T is the temperature in Kelvin, $R = 287.058\,\text{J/kg K}$ is the specific gas constant for dry air and the flow factor is

$$\Psi = \sqrt{\frac{\kappa}{\kappa - 1}\left(\left(\frac{P_{\text{low}}}{P_{\text{high}}}\right)^{\frac{2}{\kappa}} - \left(\frac{P_{\text{low}}}{P_{\text{high}}}\right)^{\frac{\kappa+1}{\kappa}}\right)} \tag{3.18}$$

for subsonic flow and

$$\Psi_{\text{C}} = \sqrt{\frac{\kappa}{\kappa + 1}}\left(\frac{2}{\kappa + 1}\right)^{\frac{1}{\kappa-1}} = 0.4842 \tag{3.19}$$

for sonic flow, independently of the pressure ratio and with $\kappa = 1.4$ the ratio of specific heats for air. If transient effects are neglected, the mass flow must be equal through both slits. This criterion leads to an expression of the valve pressure in function of the effective area of both slits. Since the fluid is compressible, the volume flow can be different. For the three regimes encountered during valve operation, the expressions for the ratio of the areas of the slits are

$$\left(\frac{A_{\text{B}}}{A_{\text{A}}}\right)_1 = \frac{P_{\text{supply}}\sqrt{\frac{\kappa}{\kappa-1}\left(\left(\frac{P}{P_{\text{supply}}}\right)^{\frac{2}{\kappa}} - \left(\frac{P}{P_{\text{supply}}}\right)^{\frac{\kappa+1}{\kappa}}\right)}}{P \cdot 0.4842}, \tag{3.20}$$

$$\left(\frac{A_{\text{B}}}{A_{\text{A}}}\right)_2 = \frac{P_{\text{supply}} \cdot 0.4842}{P\sqrt{\frac{\kappa}{\kappa-1}\left(\left(\frac{P_0}{P}\right)^{\frac{2}{\kappa}} - \left(\frac{P_0}{P}\right)^{\frac{\kappa+1}{\kappa}}\right)}}, \quad \text{and} \tag{3.21}$$

$$\left(\frac{A_{\text{B}}}{A_{\text{A}}}\right)_3 = \frac{P_{\text{supply}}}{P}. \tag{3.22}$$

$$\tag{3.23}$$

For each of these intervals, the slit area ratio can be written as a function of the piston position x. The total relation between piston position and pressure is found by combining the intervals of the three pressure regimes. This can be done for different valve designs:

1. slit A remains constant while slit B varies;
2. slit B remains constant while slit A varies;

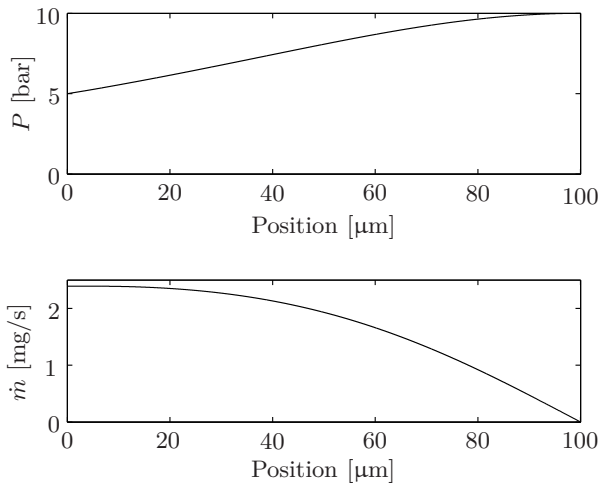

Figure 3.15: *Characteristics of a pressure divider with only slit B varying. Both slits are 20 µm wide. Slit B is 100 µm long and slit A 50 µm.*

3. slit A and B vary simultaneously, but antagonistically;
4. same as above, but one of both slits starts opening or closing before the other.

In the following calculations, the slits are 100 µm long and 20 µm wide. If a slit remains constant, it is only 50 µm long. The following paragraphs briefly discuss these designs, except for the last one. It spreads out the pressure change over a larger displacement of the piston without increasing the flow. Since this has no additional benefits, this last design is not discussed.

Slit A remains constant

$$\left(\frac{A_\mathrm{B}}{A_\mathrm{A}}\right) = \frac{1-x}{0.5}. \tag{3.24}$$

As Figure 3.15 shows, the useful range is at the end of the stroke, while low pressures cannot be reached, unless with a much larger slit B. The constant part at the beginning of the flow curve indicates the region where the flow through slit A is sonic and thus independent of the valve pressure.

Slit B remains constant

$$\left(\frac{A_\mathrm{B}}{A_\mathrm{A}}\right) = \frac{0.5}{x}. \tag{3.25}$$

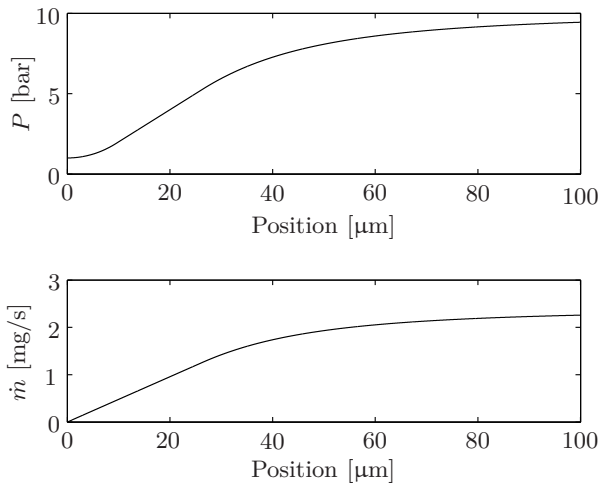

Figure 3.16: *Characteristics of a pressure divider with only slit A varying. Both slits are 20 µm wide. Slit B is 50 µm long and slit A 100 µm.*

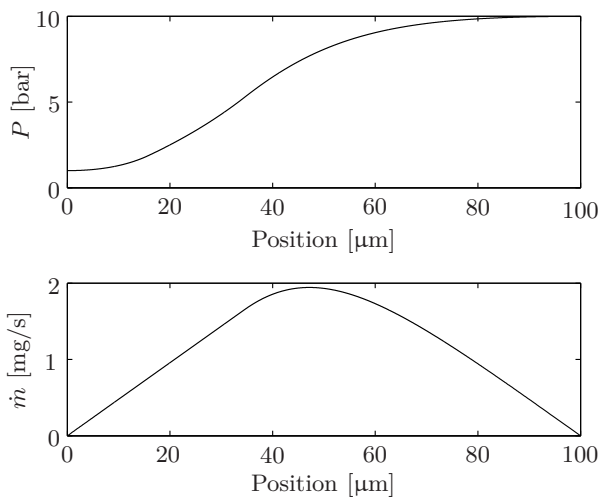

Figure 3.17: *Characteristics of a pressure divider with both slits varying. Both slits are 20 µm wide and 100 µm long.*

As Figure 3.16 shows, most of the useful range is at the beginning of the stroke, while the supply pressure cannot be reached. Most of the range is accessible. If in a particular valve design it is only feasible to vary one slit, it is best to keep slit B

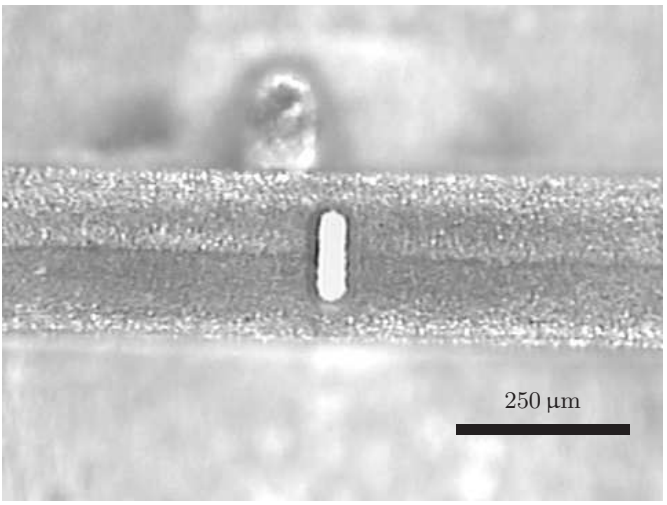

Figure 3.18: *Valve slit produced to test the manufacturing technology. The result measures about 130 µm by 35 µm. Smaller slits are possible, but there is a significant amount of deviation on the production process, which is poorly conditioned, and the results are not very repeatable.*

constant instead of slit A.

Both slits vary

$$\left(\frac{A_\mathrm{B}}{A_\mathrm{A}}\right) = \frac{1-x}{x}. \tag{3.26}$$

As Figure 3.17 shows, both high and low pressures can be reached in a more continuous manner. This is clearly advantageous, and if possible, a valve design where both slits vary is preferable.
The flow is of the order of magnitude of mg/s, which would be equivalent with $0.01\,\mathrm{Nm}^3/\mathrm{min}$ for a tactile display with 100 elements. For comparison, an economic foil bearing consumes $0.002\,\mathrm{Nm}^3/\mathrm{min}$, a regular air bearing around $0.05\,\mathrm{Nm}^3/\mathrm{min}$, and a pneumatic chisel 0.15–$0.7\,\mathrm{Nm}^3/\mathrm{min}$.

While it is possible to produce a slit of about the right dimensions by micro-EDM (Figure 3.18), there is a significant amount of deviation on the production process, which is poorly conditioned, and the results are not very repeatable. It is much easier to produce a round hole consistently. This will increase the flow, and

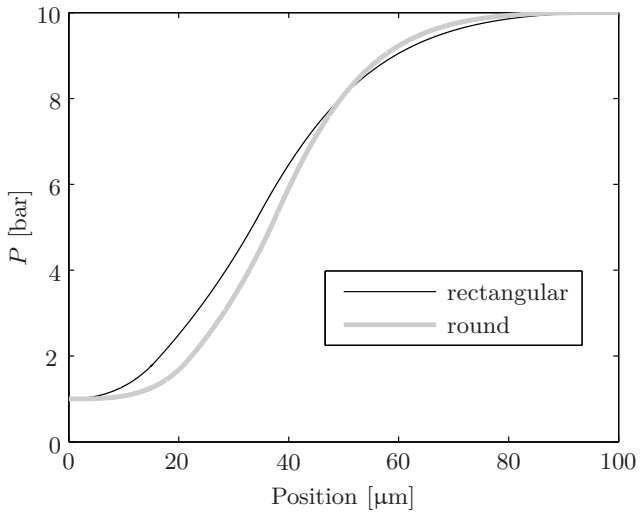

Figure 3.19: *Comparison of the valve characteristics with rectangular slits or with round slits. As could be expected, both curves intersect at a relative position of 0.5. The steepening og the round slit characteristic at both sides of that position is due to the fact that the average width of a larger opening will always be larger than that of a smaller opening.*

affect the valve characteristics somewhat. The slit area ratio changes to

$$\left(\frac{A_\mathrm{B}}{A_\mathrm{A}}\right) = \frac{\pi - \alpha + \sin\alpha\cos\alpha}{\alpha - \sin\alpha\cos\alpha}, \tag{3.27}$$

with

$$\alpha = \arccos\left(1 - \frac{x}{r}\right), \tag{3.28}$$

and r the radius of the holes. Figure 3.19 compares the position-pressure curve of a rectangular with a round hole. The curve is steeper, which is not desirable for a proportional valve, but the change is not dramatic and does not outweigh the advantage of the gained repeatability with a round hole.

Magnetic circuit

A solenoid actuator moves the piston to control the valve. This section calculates the magnetic reluctance force on the actuator. Figure 3.20 shows the structure of the actuator and names the relevant geometrical variables. The dark grey area

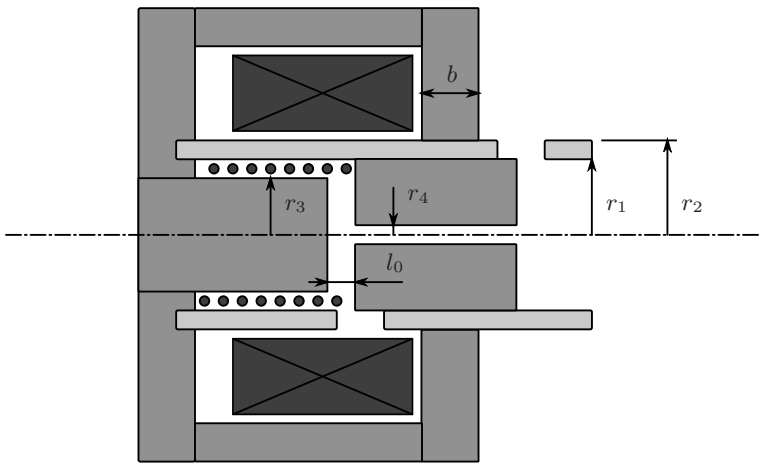

Figure 3.20: *Schematic representation of the magnetic circuit with the definition of the variables*

is soft magnetic steel which defines most of the magnetic circuit. The material used for circuit and piston is type 430F ferritic steel, which is corrosion resistant, magnetically soft and easy to machine. To augment its magnetic properties, i.e. reduce the magnetic hysteresis to a minimum, the steel is annealed for two hours at 800°C and cooled down at a rate of 50°C/hour [1].
In analogy with an electric circuit, a magnetic circuit can be described by Hopkinson's law

$$\Phi = \frac{NI}{\Re_{\mathrm{m}}}, \tag{3.29}$$

with Φ the magnetic flux, N the number of turns and I the current through the coil. The magnetic reluctance is

$$\Re_{\mathrm{m}} = \int_l \frac{dl}{\mu S}, \tag{3.30}$$

with S the area, l the length and μ the magnetic permeability. The total reluctance of the circuit is $\Re_{\mathrm{m}} = \Re_1 + \Re_2 + \Re_3$, where $\Re_1$ is the air gap reluctance between the piston and the core, $\Re_2$ is the air gap reluctance through the nonmagnetic copper tube, and $\Re_3$ the reluctance of the ferromagnetic material. Because the relative magnetic permeability of the annealed 430F is more than 1000, $\Re_3$ is neglected. Stray magnetic fields around corners and edges are small and are not taken into account either (Appendix A).

$$\Re_1 = \frac{l_0 - x}{\mu_0 \pi \left(r_3^2 - r_4^2\right)} \quad \text{and} \tag{3.31}$$

$$\Re_2 = \int_{r_1}^{r_2} \frac{dr}{\mu_0 2\pi r b} = \frac{1}{\mu_0 2\pi b} \ln\left(\frac{r_2}{r_1}\right). \tag{3.32}$$

$\mu_0 = 4\pi \cdot 10^{-7}\,\mathrm{Vs/Am}$ is the magnetic permeability of vacuum and b, r_1 and r_2 are defined by Figure 3.20. Since reluctance $\Re_2$ remains constant during operation of the actuator, it is easier to rewrite it as an equivalent air gap with the same area as $\Re_1$:

$$l_{\mathrm{eq}} = \frac{r_3^2 - r_4^2}{2b} \ln\left(\frac{r_2}{r_1}\right), \tag{3.33}$$

which makes

$$\Re_{\mathrm{m}} = \frac{l_0 + l_{\mathrm{eq}} - x}{\mu_0 \pi \left(r_3^2 - r_4^2\right)}. \tag{3.34}$$

Hopkinson's law now yields the magnetic flux Φ and, through $\Phi = BS$, the magnetic flux density B

$$B = \frac{NI}{\Re_{\mathrm{m}} S} = \frac{\mu_0 NI}{l_0 + l_{\mathrm{eq}} - x}. \tag{3.35}$$

The energy density w and the total magnetic energy E_{m} in the circuit are

$$w = \frac{B^2}{2\mu_0}, \quad \text{and} \tag{3.36}$$

$$E_{\mathrm{m}} = \int_V \frac{B^2}{2\mu_0} dV = \frac{\mu_0 \left(l_0 - x\right) S N^2 I^2}{2\left(l_0 + l_{\mathrm{eq}} - x\right)^2} + \frac{\mu_0 l_{\mathrm{eq}} S N^2 I^2}{2\left(l_0 + l_{\mathrm{eq}} - x\right)^2} = \frac{\mu_0 S N^2 I^2}{2\left(l_0 + l_{\mathrm{eq}} - x\right)}. \tag{3.37}$$

If now the position x of the piston decreases, there is an influx of electrical energy ΔE_{e}, part of which goes to an increase in magnetic energy ΔE_{m} and the rest goes to mechanical work W.

$$\Delta E_{\mathrm{e}} = \Delta E_{\mathrm{m}} + W \tag{3.38}$$

or, written as a derivative to the position:

$$\frac{dE_{\mathrm{e}}}{dx} = \frac{E_{\mathrm{m}}}{dx} + \frac{W}{dx}, \qquad \text{with} \qquad \frac{W}{dx} = F_{\mathrm{m}}. \tag{3.39}$$

First the input of electrical energy is calculated by

$$\Delta E_{\mathrm{e}} = \int_t UI dt, \tag{3.40}$$

with U the induced electrical potential difference according to Faraday's law

$$U = N\frac{d\Phi}{dt}. \tag{3.41}$$

This becomes

$$\Delta E_{\mathrm{e}} = \int_t N\frac{d\Phi}{dt} I dt = \int_\Phi NI d\Phi. \tag{3.42}$$

Calculating the derivative of the magnetic flux in this circuit

$$\Phi = \frac{\mu_0 SNI}{l_0 + l_{\mathrm{eq}} - x} \tag{3.43}$$

yields

$$d\Phi = \frac{\mu_0 SNI}{(l_0 + l_{\mathrm{eq}} - x)^2} dx. \tag{3.44}$$

Filling in (3.44) in (3.42) gives

$$\Delta E_{\mathrm{e}} = \int_x \frac{\mu_0 SN^2 I^2}{(l_0 + l_{\mathrm{eq}} - x)^2} dx \tag{3.45}$$

or the derivative to the position

$$\frac{dE_{\mathrm{e}}}{dx} = \frac{\mu_0 SN^2 I^2}{(l_0 + l_{\mathrm{eq}} - x)^2}. \tag{3.46}$$

The increase in magnetic energy is the derivative of (3.37)

$$\frac{E_{\mathrm{m}}}{dx} = \frac{\mu_0 SN^2 I^2}{2\,(l_0 + l_{\mathrm{eq}} - x)^2}. \tag{3.47}$$

Substituting (3.46) and (3.47) in (3.39) and rearranging, results in an expression for the reluctance force on the piston

$$F_{\mathrm{m}} = \frac{\mu_0 SN^2 I^2}{(l_0 + l_{\mathrm{eq}} - x)^2} - \frac{\mu_0 SN^2 I^2}{2\,(l_0 + l_{\mathrm{eq}} - x)^2} = \frac{\mu_0 SN^2 I^2}{2\,(l_0 + l_{\mathrm{eq}} - x)^2}. \tag{3.48}$$

Summarised, this means that half of the added energy is converted to magnetic energy and half goes to mechanical work. It is because μ_0 is constant, and thus the relation between B and the magnetic field strength H is linear, that this division is equal. An intuitive explanation about what happens physically is that the system wants to minimise the magnetic energy. It does that by replacing the air, which is a bad magnetic conductor, with the piston, a good magnetic conductor. The movement of the magnetised piston induces a positive voltage over the coil

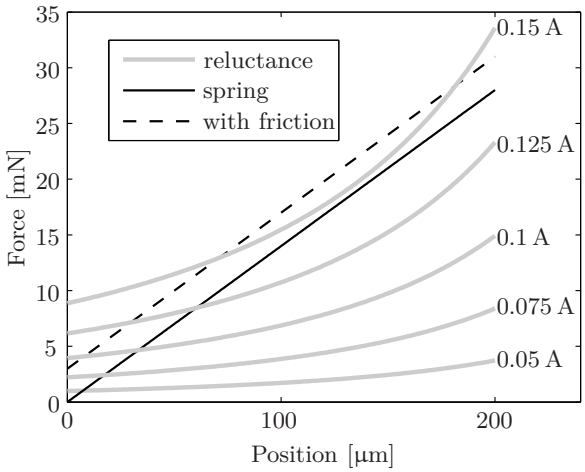

Figure 3.21: *Comparison between reluctance force and spring force to find the equilibrium position of the piston. For each current, there is a stable equilibrium point where both curves intersect, until the current becomes too high and the reluctance force exceeds the spring force everywhere. Even a small amount of friction has a strong influence on the equilibrium position and the maximum attainable stable position.*

and draws in electrical energy. The magnetic energy in the air gap has increased, because of the lower reluctance, but together with the energy input, it is minimised. To control the pressure of the valve, the position of the piston has to be regulated, while the reluctance actuator only regulates the force on the piston. The force can be transformed to a position by using a spring element. The piston will position itself at the point where the reluctance force is in equilibrium with the spring force.

The next sections discuss the interaction of the solenoid with a linear spring and with a nonlinear foil spring.

Linear spring

A linear spring is an element with a certain constant stiffness that reacts to a force according to Hook's law

$$F_\mathrm{s} = k\Delta l, \tag{3.49}$$

with k the spring constant or the stiffness, and Δl the change in length of the spring. Applied in the reluctance actuator, the spring constant determines at which

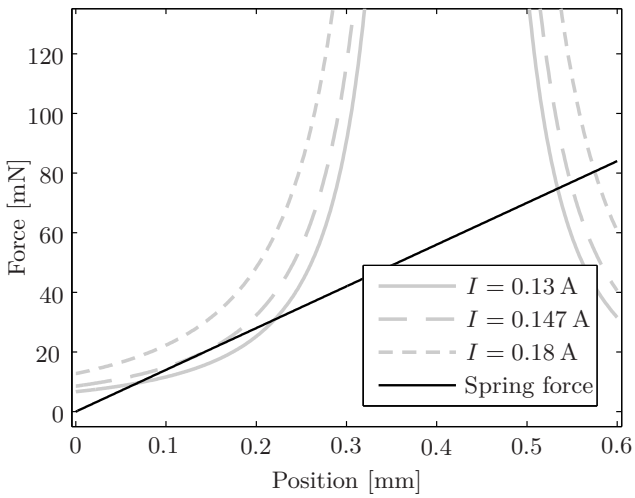

Figure 3.22: *Intersection points of the spring force with the reluctance force at several currents. The lowest curve has a stable and an unstable intersection point, the middle curve touches the spring force in a single point, and the upper curve does not intersect the spring force, which means there is no stable position. The third intersection point of each curve on the right has no physical meaning.*

point the piston is at an equilibrium. Figure 3.21 graphically shows where this equilibrium lies. For different values of the current, the reluctance force curve changes, while the curve of the spring force remains the same. The equilibrium point is the point where both curves intersect. It is clear from the graph that there is a problem when the current becomes too high: there is no longer an intersection point. The piston will jump towards the end of its stroke as if the spring is not there. This requires a closer look at this equilibrium point.
The relation between current and position is given by comparing spring force and magnetic force:

$$kx = \frac{\mu_0 S N^2 I^2}{2\left(l_0 + l_{\text{eq}} - x\right)^2}. \tag{3.50}$$

This can be simplified by substituting

$$K = \frac{\mu_0 S N^2 I^2}{2k}, \qquad \text{and} \qquad l_{\text{tot}} = l_{\text{eq}} + l_0 \tag{3.51}$$

to

$$x^3 - 2l_{\text{tot}}x^2 + l_{\text{tot}}^2 x - K = 0. \tag{3.52}$$

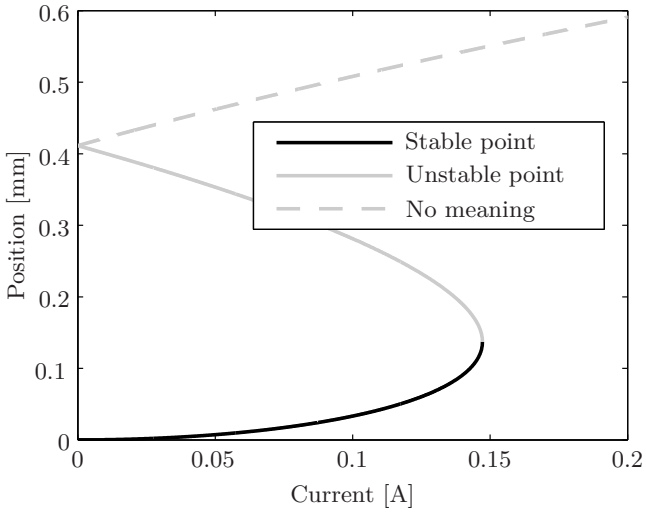

Figure 3.23: *Position-current characteristic of the reluctance actuator. All three mathematical intersection points are drawn.*

To find where the furthest equilibrium point is and thus where the two curves touch, a double root of (3.52) has to be found. A triple root is impossible for a non-zero current, as can be seen on Figure 3.22. There can either be three separate roots, a double and a single root, or a couple of imaginary roots and a single root. In all cases, this single root has no physical meaning.
The double root can be found by evolving

$$(a-x)^2(b-x)=0, \tag{3.53}$$

and comparing the coefficients with the equilibrium (3.52).

$$\left\{\begin{array}{rcl} 2a+b &=& 2l \\ a^2+2ab &=& l^2 \\ ba^2 &=& K \end{array}\right. \text{, which resolves to } \left\{\begin{array}{rcl} a_1 &=& l/3 \\ b_1 &=& 4l/3 \end{array}\right. \text{, or } \left\{\begin{array}{rcl} a_2 &=& l \\ b_2 &=& 0 \end{array}\right. ,$$

where the second solution is the trivial case where $I=0$. The first solution gives the position of the touching point, which occurs at

$$x=(l_0+l_{\mathrm{eq}})/3. \tag{3.54}$$

The conclusion is that the air gap l_0+l_{eq} has to be carefully determined to make sure that it is at least three times larger than the maximum desired stroke, so that x stays sufficiently below this threshold. Figure 3.23 shows all three solutions of (3.52). Only the bottom curve is useful, and spans only a third of the total air gap. It is also highly nonlinear, as is expected for a solenoid actuator.

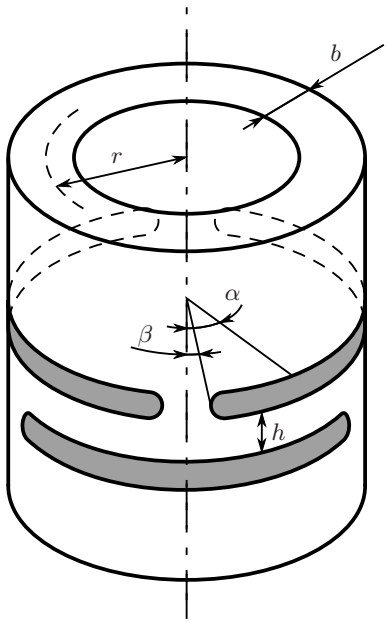

Figure 3.24: *Concertina spring (adapted from [158]). The design allows a relatively high dimensional accuracy of the rest length.*

Concertina spring The principle of concertina springs is shown in Figure 3.24. It is a linear spring that can be made more easily at small dimensions than a coil spring and of which the rest length can be controlled relatively accurately. It is produced by removing slits in a tube with quarter circle leaf springs as result. The stiffness of these springs is higher than for straight leaf springs of the same length, because there is a constrained torsional component. The boundary conditions are that at both ends, the slope and the twisting angle remains zero, while at one end the position is fixed. The formulas for position, derivative of position and twisting angle are:

$$\dot{y} = \left(\frac{\pi}{4} - \beta\right) \frac{Fr^2}{EI} \left(\sin\alpha + \frac{1 + \sin(2\beta)}{\cos(2\beta)} (\cos\alpha - 1)\right), \tag{3.55}$$

$$y = \left(\frac{\pi}{4} - \beta\right) \frac{Fr^3}{EI} \left(1 - \cos\alpha + \frac{1 + \sin(2\beta)}{\cos(2\beta)} (\sin\alpha - \alpha)\right), \quad \text{and} \tag{3.56}$$

$$\gamma = \frac{Fr^2}{GI_\mathrm{p}} \left(\left(\frac{\pi}{4} - \beta\right) \left(1 - \cos\alpha + \frac{1 + \sin(2\beta)}{\cos(2\beta)} \sin\alpha\right) - \alpha\right), \tag{3.57}$$

with r the average radius of the concertina spring, E the Young modulus, I the second moment of inertia of the beam, G the shear modulus, I_p the polar moment

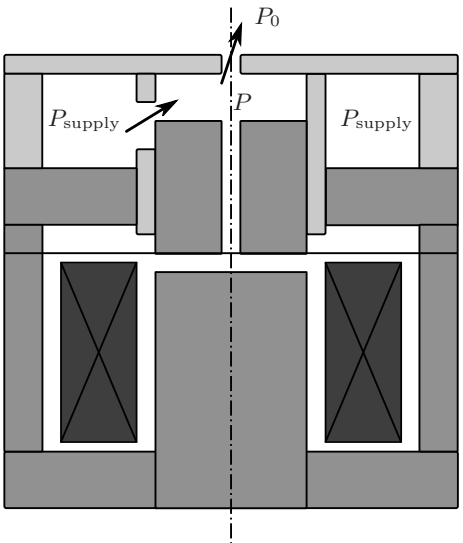

Figure 3.25: *Schematic concept of a valve with a foil spring. This concept uses a foil spring instead of a spiral spring or a concertina spring. The nonlinearity of the spring can be an advantage, because it extends the usable range of the piston. The foil spring needs a lot more space and thus increases the size of the valve and the size of the internal volume. Assembly is complicated.*

of inertia, α the angle around the centre of the spring and β the angle between the middle of the bar between the slits and the start of the slits. Because of the integration in polar coordinates, the variable of integration is $r \cdot d\alpha$, hence the extra r in (3.56). The stiffness is

$$k = \frac{Ebh^3}{24r^3} \frac{\cos(2\beta)}{\left(\frac{\pi}{4} - \beta\right)\left(\cos(2\beta) - \left(\frac{\pi}{4} - \beta\right)(1 + \sin(2\beta))\right)}, \tag{3.58}$$

which is about four times as stiff as for a straight leaf spring with the same dimensions due to the constraint torsional component. The stiffness of the combined spring is $4k/n$ where n is the number of springs in series and $n + 1$ is the number of consecutive slits.

Foil spring

An alternative to using a linear spring such as a coil spring is a foil spring or a membrane spring (Figure 3.25). The advantage is that it is easier to control the rest length than with a coil spring. Two foil springs in parallel could also guide the

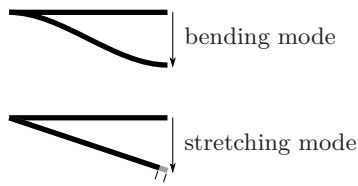

Figure 3.26: *Bending mode and stretching mode of foil spring. If the displacement is small compared to the thickness of the foil, the bending mode dominates and the spring behaves linearly. If the displacement is large compared to the thickness, the stretching mode dominates, resulting in nonlinear behaviour.*

piston, which could be advantageous with respect to friction between the piston and the cylinder. A downside is that the volume at valve pressure is higher, which results in a slower response of the valve. Other advantages become apparent as the equilibrium point is examined.

Foil spring stiffness The stiffness is calculated for one foil spring in a geometry of four rectangular foil springs in a cross around the piston. The foil springs have two components to their stiffness (Figure 3.26): one reacting to shear force (bending) and one reacting to normal force (stretching). Both occur, since the horizontal length of the beam remains constant while the vertical range changes. The bending force is

$$F_{\mathrm{s,b}} = \frac{Edb^3}{2l_{\mathrm{b}}^3}x, \tag{3.59}$$

with E the Young modulus, d the width, b the thickness, and l_{b} the length of the beam. The stretching force is

$$F_{\mathrm{s,s}} = Edb\,(\tan\alpha - \sin\alpha) \quad \text{with} \quad \alpha = \arctan\left(\frac{x}{l_{\mathrm{b}}}\right). \tag{3.60}$$

The Taylor expansions of sine, tangent and arctangent are

$$\sin x \approx x - \frac{x^3}{6} + \frac{x^5}{120} - ... \tag{3.61}$$

$$\tan x \approx x + \frac{x^3}{3} + \frac{2x^5}{15} + ... \tag{3.62}$$

$$\arctan x \approx x - \frac{x^3}{3} + \frac{x^5}{5} - ... \tag{3.63}$$

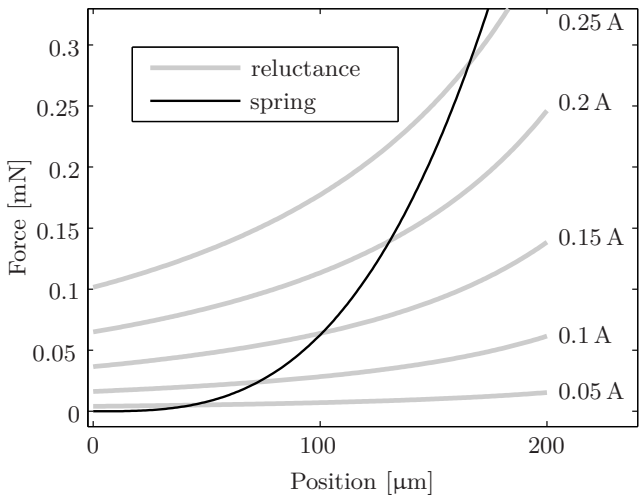

Figure 3.27: *Comparison between reluctance force and foil spring force to find the equilibrium position of the piston*

A very close approximation of this force can be given by

$$F_{\mathrm{s,s}} \approx \frac{Edb}{2l_{\mathrm{b}}^3} x^3. \tag{3.64}$$

The error for $x < 0.05 \cdot l_{\mathrm{b}}$ is smaller than 0.2%.
From (3.59) and (3.64) it is clear that for $x < b$, the bending mode is more important, while for $x > b$, the stretching mode is more important. In the valve, the stroke is in the range of 100 μm, while the thickness of the foil is less than 10 μm. At small displacements, bending forces are still relevant, but the offset caused by gravity on the piston already eliminates that region. Since the force originating from the bending mode will be 100 times lower than that of the stretching mode, the bending mode will be neglected. For symmetry, four rectangular foil beams are assumed around the piston.
A uniform membrane instead of separate beams yields a stretching force of

$$F_{\mathrm{s,s}} = \frac{2\pi Eb\,(r_2 - r_1)}{\ln\,(r_2/r_1)}\,(\tan\alpha - \sin\alpha) \approx \frac{\pi Eb}{\ln\,(r_2/r_1)\,(r_2 - r_1)^2} x^3, \tag{3.65}$$

with r_2 and r_1 the outer and inner radius of the membrane. It is the same order and thus has the same behaviour as the simple foil beams, and will not be discussed separately.
As with the linear spring, there are three possible situations for the intersection of

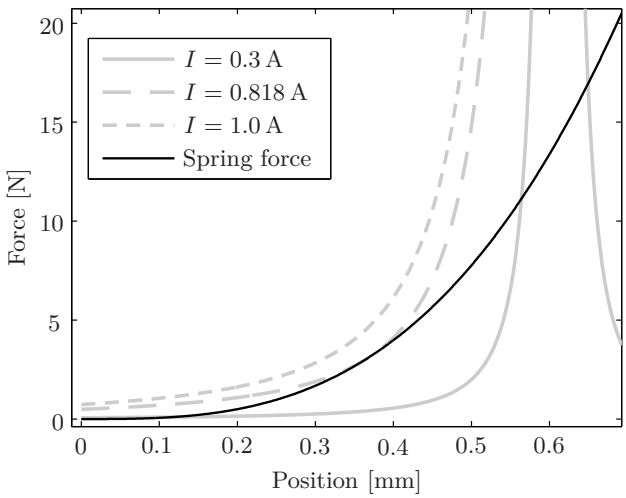

Figure 3.28: *Intersection points of the foil spring force with the reluctance force at several currents. If the current becomes too high, the reluctance force exceeds the spring force everywhere and there will be no equilibrium. The maximum attainable equilibrium is at a larger displacement as is the case for a linear spring.*

the spring force with the reluctance force (Figures 3.27 and 3.28). To check for the occurrence of the bifurcation point where the spring curve touches the magnetic curve, a similar procedure as above is followed. The equation is

$$\frac{Edb}{2l_{\mathrm{b}}^3}x^3 = \frac{\mu_0 S N^2 I^2}{2\left(l_0 + l_{\mathrm{eq}} - x\right)^2}. \tag{3.66}$$

This can be simplified by replacing

$$K = \frac{\mu_0 S N^2 I^2 l_{\mathrm{b}}^3}{Ebd}, \qquad \text{and} \qquad l_{\mathrm{tot}} = l_{\mathrm{eq}} + l_0 \tag{3.67}$$

to get

$$x^5 - 2l_{\mathrm{tot}}x^4 + l_{\mathrm{tot}}^2 x^3 - K = 0. \tag{3.68}$$

At the touching point, the derivative of both forces has to be equal, so the solution can be found by drawing the roots of the derivative of (3.68)

$$5x^4 - 8l_{\mathrm{tot}}x^3 + 3l_{\mathrm{tot}}^2 x^2 = 0, \qquad \text{or} \qquad \left(5x^2 - 8l_{\mathrm{tot}}x + 3l_{\mathrm{tot}}^2\right)x^2 = 0. \tag{3.69}$$

The trivial solutions are $x = 0$ and $x = l_{\mathrm{tot}}$. The touching point can be found at

$$x = \frac{3}{5}l_{\mathrm{tot}}. \tag{3.70}$$

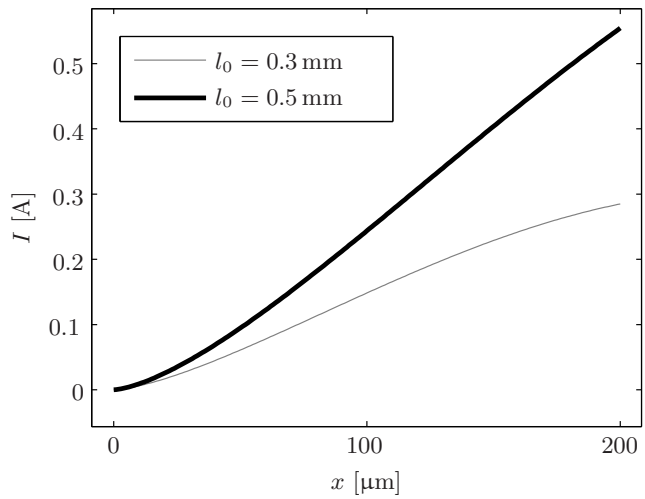

Figure 3.29: *Current-position characteristic of the piston with a foil spring. The behaviour in the desired range is surprisingly linear. The air gap can be decreased, while the range of the piston is still sufficiently large. This also increases the force of the actuator and its robustness against distortions.*

The design criterion becomes

$$x_{\max} < \frac{3}{5}\left(l_0 + l_{\mathrm{eq}}\right), \tag{3.71}$$

which means for the same required stroke of the piston, the air gap can be half as small as with a linear spring. As a result the actuator could be significantly smaller for the same force output, which is a clear advantage of the nonlinearity of the spring.
Another advantage becomes apparent by drawing the position in function of the current (Figure 3.29). While the analytical expressions or approximations thereof do not immediately indicate a linear behaviour, the characteristics are surprisingly linear compared to the actuator with a linear spring. If the air gap decreases, the behaviour becomes again somewhat less linear, but it is feasible to find a good trade-off between force and linearity around the position of the valve holes.
Because the spring is nonlinear, however, gravity does influence the behaviour. This influence is mainly present at very small forces, and causes a slight offset in the position, as well as a decrease in the useful range equal to this offset. Pretension in the foil due to the assembly process can be another source of deviation from the calculated behaviour. As long as this pretension is small, it can have a positive effect as it works opposite gravity and partially eliminates its

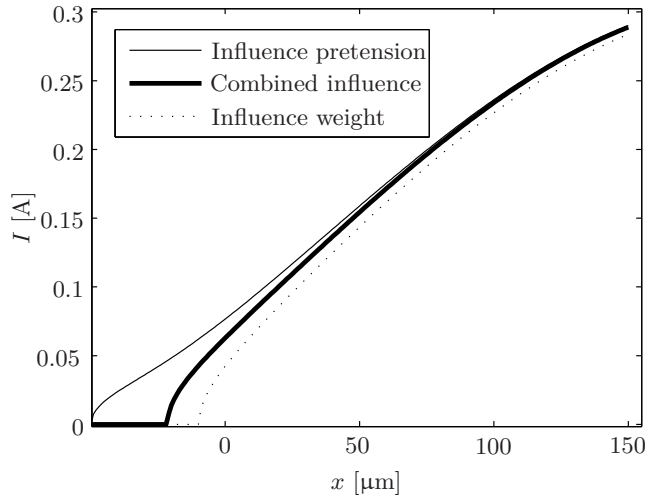

Figure 3.30: *Influence of piston weight and foil pretension on the current-position characteristic. Both effects mainly affect the initial displacement of the piston. A certain positive pretension is beneficial to decrease the total influence.*

influence (Figure 3.30). A "negative" pretension in the foil corresponds to slumping and has a similar effect as gravity. It should thus be avoided.
Something else that needs to be checked is the rotational stability. Due to the nonlinearity of the magnetic force, a slight rotation of the piston will result in a magnetic moment in the same direction, trying to turn it even further until it comes into contact with the sides of the cylinder. The foil springs cause a moment in the opposite direction to stabilise the piston. Gravity will add a negligible destabilising moment that is several orders of magnitude smaller than the others. The analytical expression of the magnetic moment can be approximated by

$$M_{\mathrm{m}} \approx -\frac{\mu_0 N^2 I^2 b D^3}{12 l_{\mathrm{e}}^3}\theta, \tag{3.72}$$

with l_{e} the variable air gap and D the diameter of the piston. A good approximation for small angles of the moment caused by the foil, based on numeric simulations is

$$M_{\mathrm{v}} \approx cst \cdot \frac{D}{12 l_{\mathrm{e}}^3 l_0^{3/2}}\theta. \tag{3.73}$$

The reason that this moment also depends on the air gap is that the geometry of the springs depends on the position of the piston. For small angles both moments have the same dependency on the position of the piston and both are linearly

related to the angle of rotation. For the dimensions of the valve, the slope for the returning moment of the foil is about an order of magnitude steeper than the slope of the magnetic moment, which means the horizontal position of the system is stable.

Practical considerations of the foil spring There are several constraining requirements for the spring: required stiffness, maximum stress in the material, price and availability. In case of a nonlinear spring, it is not really the stiffness which is a relevant, but rather a maximum displacement corresponding to a certain force. The required radius of the foil can be determined by taking the maximum stress into account. The ratio of maximum stress over the Young modulus of the material has to be as high as possible. Because of the high stiffness of steel, it needs a rather large foil. Even aluminium foil with a thickness of 5 μm needs to have a radius of 7 mm; the other dimensions are comparable to the valve designs in Section 3.4.2. Thinner foils are hard to find, very expensive and very fragile.
Apart from the relatively large required dimensions of the foils and the nonstandard material required, assembling the foil properly in the valve is not straightforward either, and several attempts have failed to provide a useful actuator. Despite its nice properties considering the behaviour, foil springs are not practical for use in a large array of valves.

Air bearing

Figure 3.21 also shows the effect of a small amount of friction between the piston and the cylinder. Not only does even a low level of friction result in hysteresis and a decreased resolution, it also moves the unstable position where the jump occurs to the left, decreasing the functional range of the piston. Therefore, it is desirable to eliminate friction entirely by including a miniature air bearing in the cylinder —pressurised air is obviously present anyway.
It might seem contradictory to include an air bearing in a pneumatic valve, but an analysis of the system shows that the influence on the valve function can be limited by a careful design of the bearing. To this end, the restrictor holes of the bearing are only 30 μm in diameter, and the play between piston and cylinder is 4 μm. This optimisation is performed with in-house finite element software. Including the bearing restrictors in the pneumatic equations show the influence of the additional air flow (Figure 3.31). There is a slight loss at the low pressure range, which starts a bit higher than 1 bar absolute pressure. Note that these simulations assume perfect production accuracy. In reality, as the following sections will show, this is not achievable. An additional problem at the high pressure end of the valve is anticipated: the flow through the bearing might become too low for it to work properly.
The analysis is performed for a minimum amount of four restrictors positioned

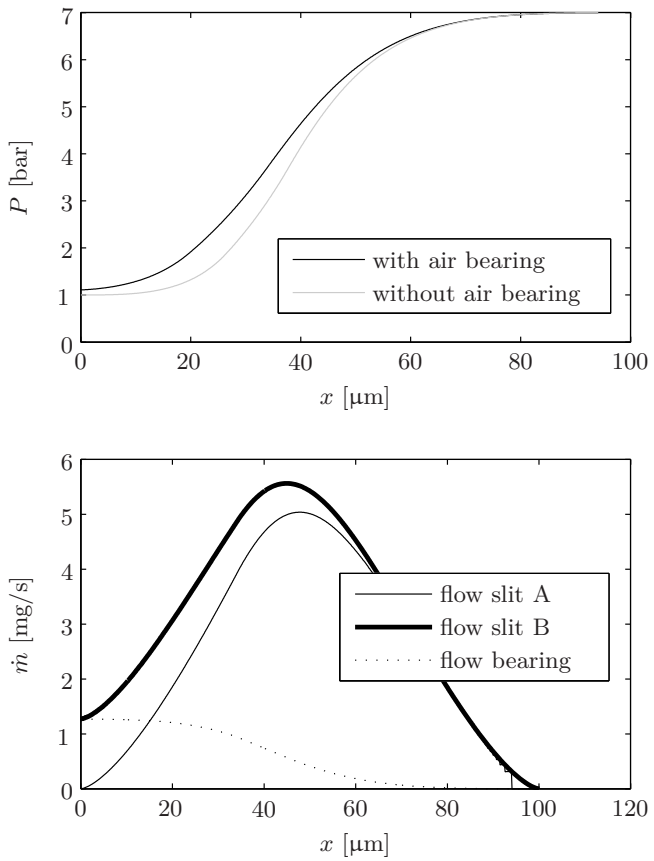

Figure 3.31: *Influence of the air bearing on the valve. Because the additional air flow introduced by the air bearing, the output pressure range of the valve decreases. The top graph shows the influence on the output pressure. The bottom graph shows the air flow through the holes of the bearing and the valve holes. The calculations for these curves were performed using an ideal configuration with only four bearing holes with a diameter of 30 µm.*

in a single row around the circumference of the cylinder. A design with two rows of six for a total of twelve restrictors offers a higher rotational stiffness but also increases the additional flow and thus the influence on the valve.

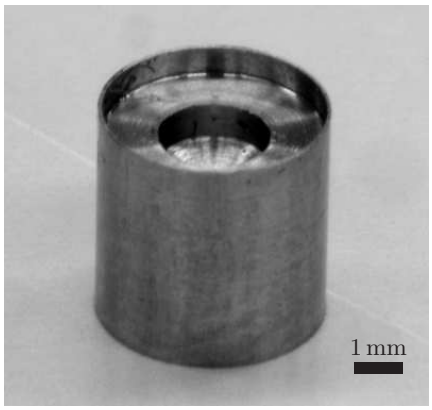

Figure 3.32: *Piston of the valve. The piston is made from annealed type 430F steel. It is machined on a Spinner precision lathe and polished by hand. The thin edge at the top has to avoid the influence of local high pressure at the inlet holes.*

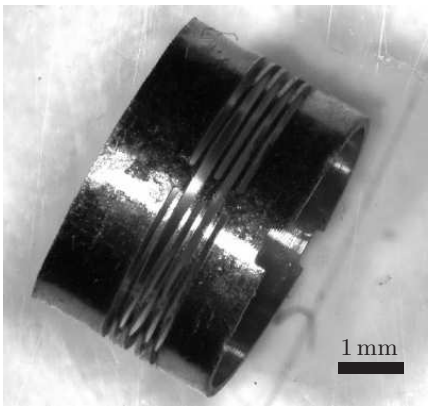

Figure 3.33: *Concertina spring. The spring is made from phosphor bronze, which has good elastic properties and is non-magnetic. The 100 µm slits are removed by micro-EDM.*

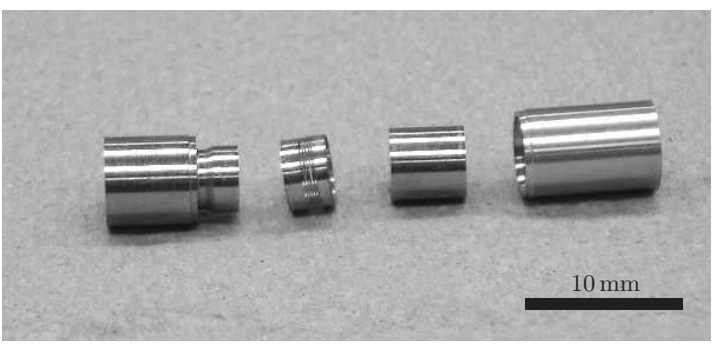

Figure 3.34: *The central parts of the valve; from left to right: magnetic core, concertina spring, piston and cylinder*

3.4.2 Prototypes and Results

All parts of the valve are specifically designed and manufactured. The magnetic circuit and piston are made of annealed type 430F ferritic steel, which is corrosion resistant, magnetically soft and easy to machine. The valve holes are 100 µm in diameter. To deal with inaccuracies during production and assembly, the stroke of

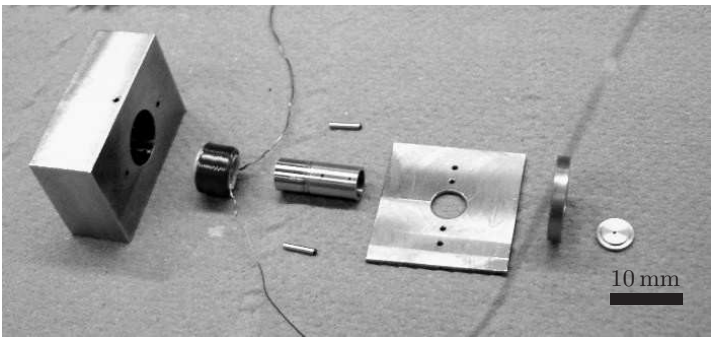

Figure 3.35: *The different parts of the display before assembly; from left to right: magnetic house, coil, assembled central valve and steel dowel pins, magnetic cover, non-magnetic high pressure chamber and cover of the cylinder with a hole to be connected with the tactile display*

the piston is designed to be 200 µm centred around the valve holes. The stroke of the concertina spring is an additional 50 µm to compensate for the gravity of the piston compressing it. The dimensions are based on a rather arbitrary choice of the piston diameter of 5 mm. The hole in the magnetic conduit is then chosen to be 6 mm, because it cannot be turned and has to be reamed. The air gap between the core and the piston is the same as the stroke to avoid the occurrence of an unstable jump even if the current becomes too high. The equivalent air gap can then be determined according to (3.54) to be two times the desired stroke plus a safety margin or 450 µm. This is equivalent to an inner diameter of the cylinder of 4.91 mm. The piston is a few micron smaller and has a thin edge at the top to reduce the effect of the high supply pressure (Figure 3.32).
The spring needs a specific stiffness of 0.25 N/mm and has to fit exactly into the provided space. A larger stiffness results in a stronger actuator, but which needs a higher current. The spring should not be magnetic, so it is made of phosphor bronze. The concertina structure (Figure 3.33) is manufactured by cutting slits in a tube with micro wire-EDM. The spring has small openings at the top to allow air to pass more easily and to avoid the spring-like behaviour of trapped air.
The cylinder and the cover are made from bronze, which is easy to machine, has good friction properties and is non-magnetic. The 100 µm holes of the valve and the 30 µm holes of the air bearing are drilled with a Sarix micro EDM machine to an accuracy of below 5 µm. In this prototype, an air bearing with twelve restrictor holes is provided to increase the robustness of the valve. Both the cylinder and the piston are produced on a precision lathe and polished to an R_a roughness of 0.1 µm. This yields a plateaued surface with a negatively skewed surface, meaning that it has grooves rather than peaks. The functional outer dimensions of the valve are $\varnothing 12 \times 15\,\mathrm{mm}^2$, while the prototype is larger for testing and manipulation purposes.

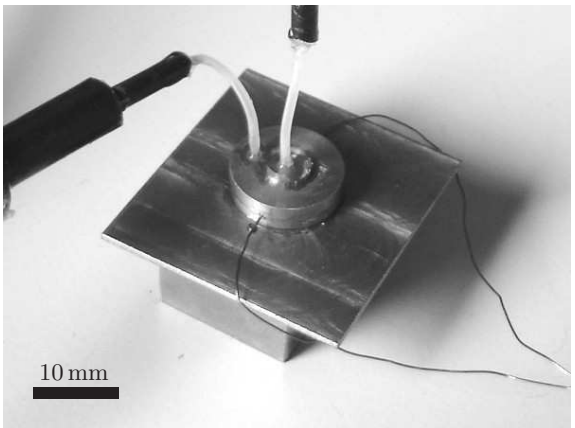

Figure 3.36: *The assembled valve prototype. The parts are connected and sealed with glue.*

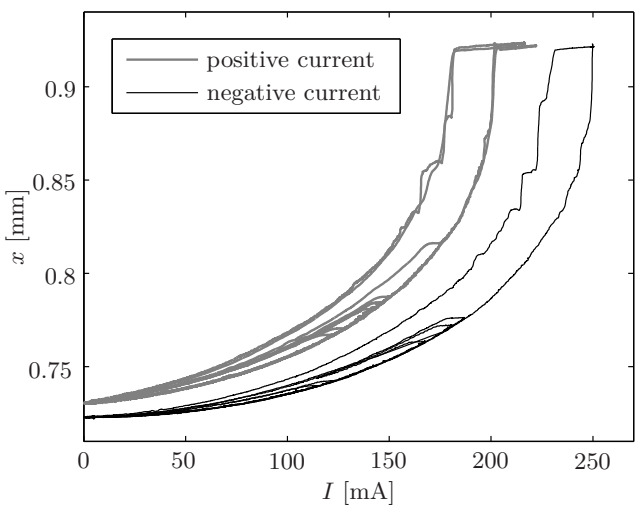

Figure 3.37: *Characteristic of the reluctance actuator with type 430F steel which is not annealed. The magnetic hysteresis is evident. The difference between positive and negative current is the result of a remanent field in the steel.*

The production of the other parts is less critical. The coil of the prototype has 119 windings and is handmade due to tight space restrictions. Figures 3.34 and 3.35 shows all the parts before assembly, while Figure 3.36 shows the assembled valve.

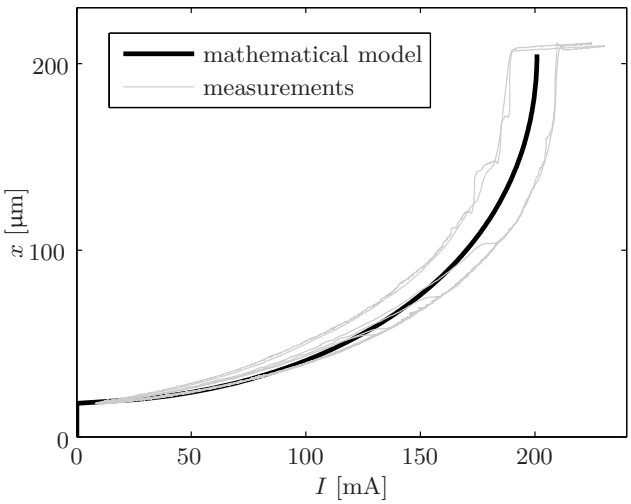

Figure 3.38: *Comparison of the actuator performance with the theoretical model. Magnetic hysteresis is not included in the model. Gravity on the piston and magnetisation of the steel is included.*

Reluctance actuator

Two prototypes are tested to verify the design of the valve. The main prototype is a complete valve as described above. Because it is difficult to test the actuator performance inside the closed valve, another prototype consists solely of the reluctance actuator and is built to evaluate the movement of the piston. Instead of a cylinder with valve holes and an air bearing, it has a simple ring to avoid that the piston moves sideways. While the behaviour follows the mathematical model nicely, there is some additional hysteresis because the Type 430F steel for this prototype is not annealed (Figure 3.37). The cause is the magnetisation of the material, which results in an additional, load dependent flux through the actuator. Both curves originate from the same actuator, but with the current reversed, indicating a significant remanent field in the material.
The second prototype reveals a close correlation with the analytically predicted behaviour. The predictions differ from the experimental results for two reasons: production accuracy and magnetisation of the material. The parts of the valve are produced on the limits of conventional production techniques, and some dimensions are difficult to measure with micrometer accuracy. Slight assembly errors and surface roughness are other sources of uncertainty. The annealed type 430F steel, while magnetically soft, still shows a slight magnetisation. On the one hand, this magnetisation results in some hysteresis; on the other hand, it causes a remanent

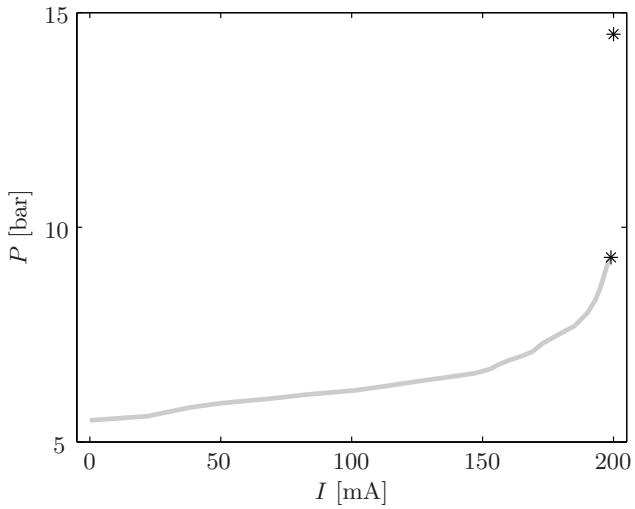

Figure 3.39: *Characteristics of the valve with a supply pressure of 14.5 bar. The asterisks on the right indicate the jump at the end of the stroke. The range is limited and the valve can only reach pressures between 5.5–9.5 bar.*

field which shifts the characteristics along the current axis.
Figure 3.38 shows the measurement results together with the theoretical model. It was possible to fit the model to the measurement data within the above described uncertainties by adding 30 µm to the equivalent air gap. Gravity working on the piston is also included in the model. The remanence of the magnetic circuit is modelled as an additional current of 8 mA through the coil. This remanence only shortens the flat part at the start of the current-position curve, with no influence on performance. The value of the remanence is not constant and increases as the air gap decreases, but because it is so small for Type 430F steel, this effect is not noticeable and thus not taken into account.

Finally, the full prototype is evaluated by connecting the output to a manometer. The supply pressure is varied between 1 bar and 15 bar above atmospheric pressure. There is no noticeable difference in performance depending on the supply pressure and the valve remains fully functional up to the highest pressure levels. The valve is perfectly proportional, and within the functional range all pressure levels can be reached easily. This leads to the conclusion that friction is absent and the air bearing is working properly.
Figure 3.39 shows the characteristics of the valve at a supply pressure of 14.5 bar above atmospheric pressure. The range is limited and the valve can only reach pressures between 5.5–9.5 bar. At the low pressure end, there are two reasons for

the limited range: the edges of the piston are not sharp enough and insufficiently cover the valve holes, and the air bearing is optimised for robustness and not to minimise its flow. The loss in range at the higher end is also partially due to the rounded edges of the piston and partially to the fact that the piston is not perfectly positioned and the theoretically predicted jump happens too soon. After this jump happens, both the current and the supply pressure have to be reset to get the piston from its stable position at the bottom of the valve. This is probably the result of the smooth finish of the core and the piston, which causes both flat surfaces to stick together under pressure.
These results show that the valve works and the experiments agree with the theory to within the uncertainty range. The design still needs to be optimised to create a proportional valve with full pressure range. The production of the prototype also learns that the design is not as simple and easy to produce as intended. The required accuracy and the additional holes for the air bearing require a tedious production process, and make the valve less suitable for mass production.

Construction of concertina spring It is difficult to find proper springs with the right dimensions and stiffness. Therefore, the springs have to be produced. The chosen production method is micro-EDM, though micro-milling might be viable as well.
To be able to control the height of the beams, the width of the EDM slit has to be measured. The slits are made with a wire as electrode. With constant sparking parameters, proper pretension of the wire electrode and a stable EDM process, the width of the slit stays constant to within 5–10 μm. It is also very important that the wire is as perfectly horizontal as possible. A slight slope causes a slight deviation of the height h of the springs which causes a large deviation to the stiffness (see (3.58)). Luckily, this deviation works in one way for half of the spring segments, and in the other way for the other half, in a symmetrical way. This means that the deviation on the total stiffness is somewhat reduced. Since the height of the springs will have to be smaller than 100 μm for the desired stiffness, it is easy to reach a large relative error.
A steel prototype with four slits was produced with the following parameters: an inner and outer diameter of $D_\mathrm{i} = 4\,\mathrm{mm}$ and $D_\mathrm{o} = 5\,\mathrm{mm}$, a distance between slits of $\beta D_\mathrm{o} = 0.5\,\mathrm{mm}$ and beams of $h = 0.1\,\mathrm{mm}$ high. With four slits, there are three springs in series. The calculated stiffness for the entire concertina spring is $4.85\,\mathrm{N/mm}$.
Due to inaccuracies during production, there are some deviations from those parameters. The most important one, the height of the beams, is lower, which has a large influence on the stiffness. The calculated stiffness for the spring based on the dimensional measurements of it is $3.50\,\mathrm{N/mm}$. To measure the stiffness, a probe attached to a double leaf spring system is lowered onto the concertina spring. The force is measured with a highly sensitive weighing device, and a Bentley induction distance sensor determines the deformation of the double leaf spring system. To

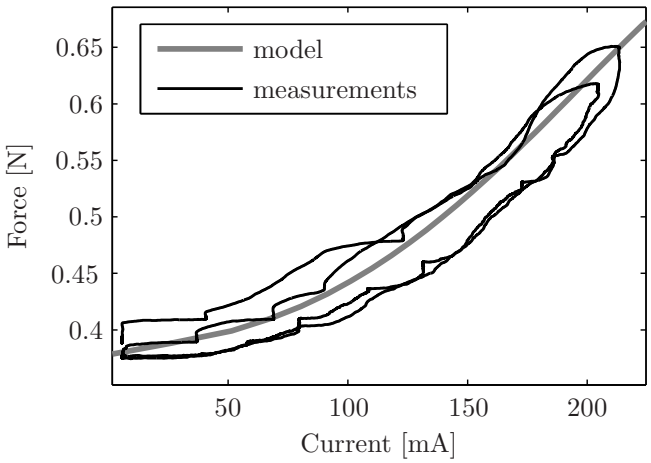

Figure 3.40: *The force on the taxel in function of the current through the valve. The supply pressure is 10 bar overpressure. The model includes the electromagnetic force of the solenoid, the remanent field of the steel, gravity and the pneumatic model presented earlier. Friction of the pin and magnetic hysteresis are not included.*

be able to measure the stiffness more accurately, first the stiffness of the system without the concertina spring is measured, then with the concertina spring. Then the stiffness to be measured can be easily derived from this.
The measured stiffness of the measurement system is 0.955 N/mm. The total stiffness of the spring in series with the system is 0.770 N/mm. This results in a stiffness of the spring of 3.981 N/mm.
For the actual valve prototype, phosphor bronze is used because of its excellent elastic properties. The spring has to fit in a very tight space. An outer and inner diameter of about 4.85 mm and 4.50 mm respectively gives it a little bit of play between the core and the cylinder. It has five slits and thus four sets of beams with a height of 100 µm. The total height of the spring is 3 mm. In an iterative process, the distance between the slits is adjusted to reach a stiffness of 0.243 N/mm, which is sufficiently close to the desired 0.25 N/mm.

3.4.3 Single Taxel Display

To test this principle, The same display as in Section 3.3 is used (Figure 3.10). Figure 3.40 shows the result of an experiment with a taxel connected to the valve, compared with a mathematical model. The model includes the electromagnetic

	Requirement	Closed hydraulic display	Open hydraulic display	Pneumatic display
Spatial resolution	1 mm	2 mm	1.5 mm	1.5 mm
# taxels	10×16	1×5	1	1
Frequency range	20–30 Hz	5 Hz	>40 Hz	
Force range	0.5 N	4 N	1.2 N	0.47 N
Stroke	2–3 mm	2.34 mm	3 mm	3 mm
Sensitivity	5–10 kPa	ok	ok	ok
Accuracy	10%	<10%	>10%	≪10%

Table 3.2: *Comparison of the characteristics of the different prototypes with the requirements*

force of the solenoid, the remanent field of the steel, gravity and the pneumatic model presented earlier. Friction of the pin and magnetic hysteresis are not included. Thanks to the air bearing, the piston of the valve experiences no friction. The model is adjusted slightly to take manufacturing and measurement errors into account, but within the limits of production accuracy.
These results demonstrate the concept, providing smooth operation at a high force. However, the valve is not yet fit for a final tactile display. The air bearing needs to be optimised to have a smaller flow and thus to allow for lower pressures to be reached, which is the main limitation of the current prototype. With an optimised valve, a very powerful and compact tactile display will be possible.

3.4.4 Conclusion on the Pneumatic Valve

This section describes a proof of concept for a light but powerful pneumatic tactile display. A valve was designed to control the air pressure proportionally and a prototype was built. While the prototype has a limited range and the proportional valve needs to be improved, the initial results are promising. With a standard pneumatic pressure of 6 bar, the force on a 1 mm diameter pin would be 0.47 N.

3.5 Conclusion

This chapter presents a number of concepts for a powerful, compact tactile display for robot assisted minimally invasive surgery. These concepts are implemented in several prototypes, each of which is evaluated. To partially overcome the requirement of a small, yet powerful actuator, actuation at a distance can offer a solution. Hydraulics is promising due to high power density, especially for smaller dimensions. A closed hydraulic system approaches the goal, but fails in robustness. An open hydraulic system is more robust and the developed display becomes actually very light and simple. An open pneumatic system with a reluctance actuated valve has similar characteristics. It has nearly no hysteresis compared to the piezoelectic valve in the hydraulic system, but the potential bandwidth is smaller. An additional advantage for a pneumatic tactile display is that a small amount of leakage is less of a problem.
Table 3.2 compares the different prototypes constructed in the context of this research. The principal focus was to produce a compact and lightweight, yet powerful tactile display. All prototypes are indeed small and light and easily reach a high force with a large stroke. In all cases the sensitivity is better than the measurements, while the accuracy of the open hydraulic system fails due to the large hysteresis of the piezo bimorph. In these initial prototypes, only a small number of taxels are implemented. A larger number of pins is not a real technological challenge, but the cost would be very high, especially for the bellows of the closed hydraulic display and the piezo bimorph of the open hydraulic display. The open hydraulic display suffers additionally from a very cumbersome manual adjustment after construction. The main problem for the production of a large array of pneumatic valves for the pneumatic display is the holes for the air bearing, which take a long time to drill.
This last technology is very promising. The challenge thereby lies in the construction of a miniature proportional valve to control the taxels.

Chapter 4

Integrated System

A tactile sensor or a tactile display on its own can already be very useful. The ultimate goal of this research, however, is a complete tactile feedback system. The display technologies developed for that purpose (see Chapter 3), while promising, require more research before they can be applied in a full tactile display. Especially the open pneumatic system has advantages, because of the simplicity and compactness of the display itself. The valve developed and described in Section 3.4 is small, makes almost no noise, consumes little power and has a high pressure resolution, but currently does not have a sufficiently large pressure range. To demonstrate the concept, a 'lite' version of the display is built with commercial valves, and connected with the finger shaped tactile sensor. This pneumatic tactile display is interfaced with the tactile sensor discussed in Chapter 2 to realise a tactile feedback system.

The connection between tactile sensor and tactile display can be very simple or very complex. Ideally, the tactile sensor approaches the properties of the human finger as closely as possible in terms of shape and compliance. That way, the pressure signal caught by the sensor can be sent to display without modifications. In soft tissue manipulation, the compliance of the sensor is less important, since the tissue itself complies to the finger or the sensor. For this proof of concept, the tactile sensor is relatively rigid, with a rubber layer of 1 mm. For hard object manipulation, it is possible to put a compliant material underneath the sensor, which increases compliance without affecting sensitivity.

To improve the mapping of the sensor signal to the fingertip, complex models of both sensor and finger are required. Such models have to be very accurate and robust against sensor noise to give a transparent system, yet they should be evaluated in real time. Alternatively, image processing techniques could enhance the tactile images, such as filtering —both in time and in space— or feature extraction. Apart from a simple convolution filter, these methods are not further

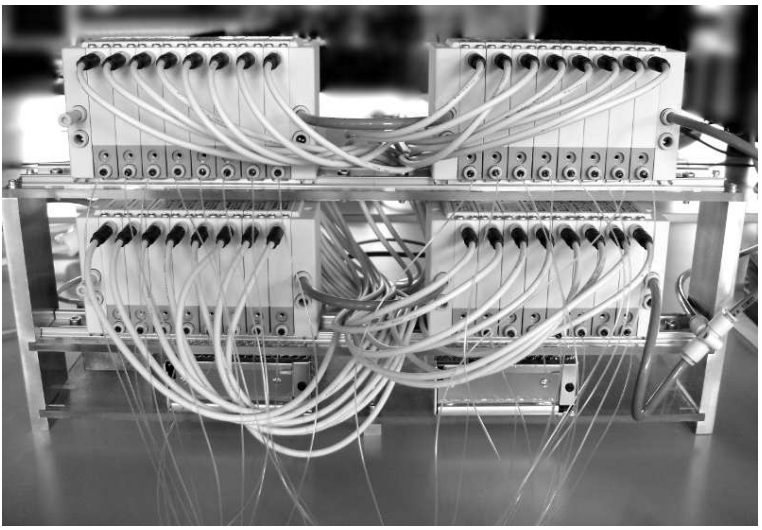

Figure 4.1: *Valve assembly of 32 valves of the proof of concept tactile display*

investigated.

First, Section 4.1 discusses the design and performance of the tactile display and its interfacing with the tactile sensor. The section concludes with some remarks on the implementation of the valve from Section 3.4 in a large valve array to replace the commercial valves. Section 4.2 describes an experiment to evaluate this tactile feedback system. Finally, Section 4.3 offers a conclusion.

4.1 Proof of Concept

The proof of concept tactile feedback system consists of a 16×16 taxel tactile sensor with a spatial resolution of 1 mm and an 8×4 tactile display with a spatial resolution of 2 mm that will be described below. Because of this discrepancy the sensor signal needs to be mapped on the limited number of taxels of the display. Since the sensor is wider than the display, and the sides of the sensor are less in contact with the palpated object, four columns on both sides of the sensor are discarded. The remaining 16×8 sensor image is down sampled by averaging squares of four taxels to one output signal, with an 8×4 tactile image as result. This image is rescaled to produce an output between −0.5–6 V, cropped to 0–6 V and sent to the display. The cropping reduces the impact of the memory effect in the sensor, caused by the rubber sticking to the electrodes after stimulation. Beyond that, the signal is not processed in this proof of concept.

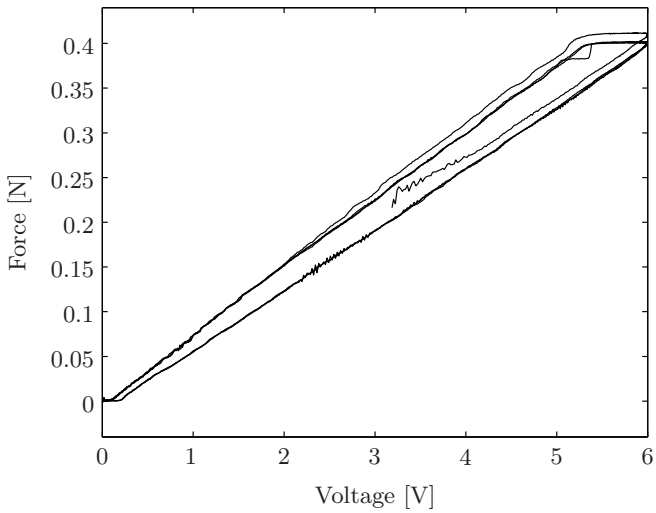

Figure 4.2: *Characteristic of a taxel in a bronze display. One of the valves is connected with a taxel pin in a bronze display. Friction is clearly visible.*

4.1.1 The Display

The display built for the proof of concept is a 'lite' version of the goal, which would meet all requirements. Because the valves developed in the previous chapter are not ready to be implemented in an array, 32 commercial valves ITV0050-3MN-Q from SMC Pneumatics control the pressure instead. These valves are relatively small and regulate the pressure proportionally in a range of 0–0.9 MPa, for a maximal supply pressure of 1.0 MPa. They do not require a flow and have a linearity within 1% and a hysteresis within 0.5%. Despite being relatively small, they still measures $82 \times 50 \times 15\,\text{mm}^3$ without connections. This results in a sizeable valve assembly, even for "only" 32 valves (Figure 4.1). The valves consume less than 3 W each, which is acceptable.

The display itself is very similar to the smaller display used in Sections 3.3 and 3.4. Besides a larger number of holes, the screws have sunken heads to not interfere with the tactile sensation. The most important difference is the material used. The friction between the pins and the holes of the bronze housing was still relatively large (Figure 4.2). This was measured by connecting a single taxel with a valve and measuring the deflection of a spring. Instead Ertalyte TX is used because of its much lower friction (Figure 4.3). It is important to use the grey 'XT' variant, because it is filled with lubricant. Ertalyte TX also has an excellent dimensional stability, which is important to establish a close fit between the pins and the holes. The same test setup showed that the valves reach full amplitude with a 90°

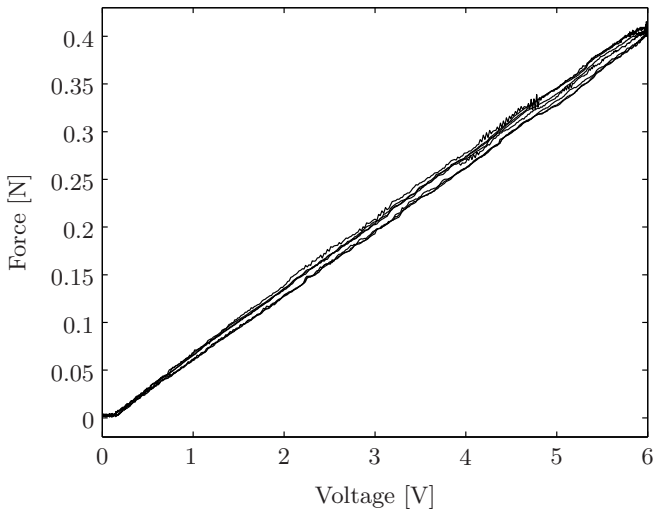

Figure 4.3: *Characteristic of a taxel in an Ertalyte TX display. One of the valves is connected with a taxel pin in an Ertalyte TX display. Ertalyte TX has outstanding friction properties.*

phase shift at 20 Hz. Above that, the output becomes erratic as the built-in control of the valves can no longer follow. With standard pressurised air at about 6 bar overpressure, the force on a single taxel is 0.47 N.
The pins are 1×6 hardened steel dowel pins with 4 mm ground flat to a thickness of 0.6 mm to fit through the 0.7 mm wide slits. The total display, including pins and nylon screws weighs 6 g and measures $17\times18\times6\,\mathrm{mm}^3$ and is thus well suited to be mounted on a haptic joystick without decreasing mobility (Figure 4.4). The display is connected with the valves by vinyl tubes with outer and inner diameters of respectively 0.99 mm and 0.58 mm. A tightly packed bundle of 32 tubes with a length of 100 mm has a stiffness of less than 5 N/m. The actual bundle of tubes is even less stiff and thus does not hinder movement at all.

The Labview card interfacing the system has only two analogue outputs, while it needs to control 32 valves. To accomplish that, four SMP08 sample-hold components are used. Each component has 8 outputs of which it keeps the voltage constant, and requires a three bit digital address. By using both analogue outputs and toggling two inhibition signals, four sample-hold outputs are refreshed every four time steps. The droop rate is only a few mV/s and the settling time is with less then 5 µs much faster than the response of the valve.

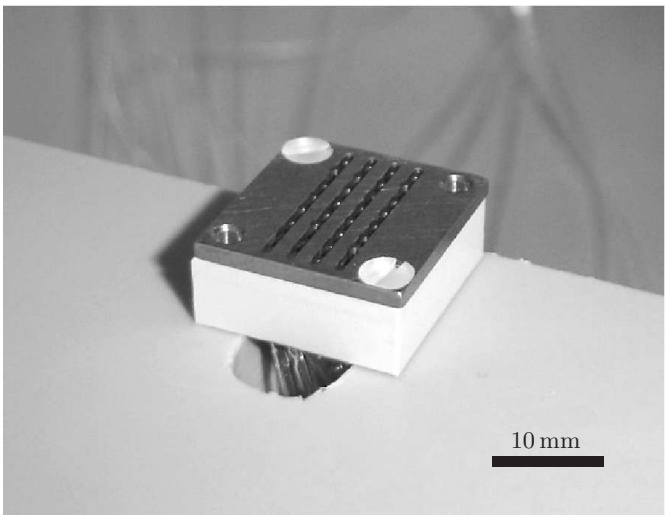

Figure 4.4: *The 8×4 proof of concept tactile display. The spatial resolution of the display is 2 mm. The display is largely made of the low friction Ertalyte TX and weighs only 6 g. Each pin is connected to one of 32 commercial proportional valves.*

4.1.2 Discussion

The tactile display works as well as could be expected. There are hardly any friction or nonlinear effects, and any signal below 10 Hz is transferred with virtually no deviation between atmospheric and maximum pressure. The valves are the limiting factor for the speed. The Labview program controlling the entire system runs at 100 Hz without error. As discussed earlier, the sensor and its readout electronics allow a frame rate of about 800 Hz. During normal palpation, the display will thus convey the image it gets from the sensor without a problem. Tapping, rubbing the sensor on a hard edge, pressing on the sensor with a small tool or similar signals can clearly be felt on the display.
The goal is to create a tactile feedback system for robot assisted minimally invasive surgery, where an important task is to find and discriminate hard balls in soft tissue. With the current proof of concept, a combination of factors makes this task nearly impossible. First of all, the kinaesthetic and tactile modalities are dissociated in the current system, which makes it harder to interpret the passive sensation on the finger. A second reason is high frequent noise on the sensor which is transmitted to the display and masks some information, together with a lack of repeatability and a strong memory effect. A last reason is the spatial resolution of the tactile display which is lower than the desired 1 mm. While a hard ball in a soft phantom can easily be discriminated visually on a 16×16 image with a spatial resolution of

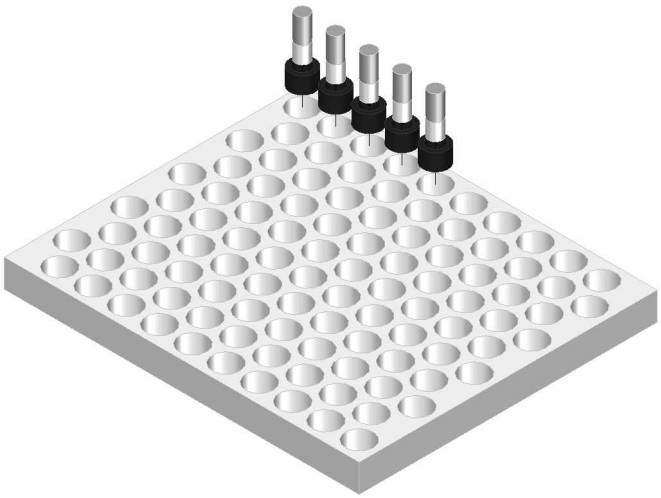

Figure 4.5: *A 3D view of how 100 valves can be built into an array of limited dimensions. The dark cylinders are the coils, and the lighter cylinders are the assembly of the valve cylinder with the core.*

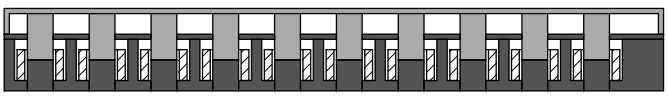

Figure 4.6: *Cross section of a schematic principle of an array of valves. The magnetic material is dark grey; the nonmagnetic material, including the cylinder, is light grey; the coils are hashed. One high pressure chamber suffices for all valves, reducing the overall complexity.*

1 mm (Section 2.3.4), it is nearly impossible when that same image is transformed to a 4×8 image with 2 mm resolution. More advanced image processing techniques might be able to enhance the signal, but with the risk of not transmitting the correct tactile information.

Apart from the speed, which is on the limit of the required bandwidth, the valves have a few other disadvantages. Because they are so large, an array of them would take up too much space to be positioned very close to the display, especially if it is mounted on a kinaesthetic feedback system. Longer tubes would mean a larger volume of air which has to travel over a larger distance, posing another limit to the bandwidth. A last significant problem is the loud noise the valves make, possibly disrupting the concentration of anyone working with the tactile display.

An improved version of the valve from Section 3.4 could solve these problems. It produces no discernible noise, because there is no mechanical contact between

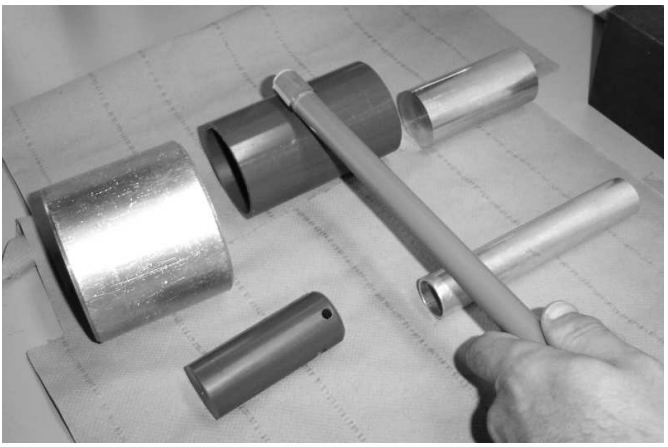

Figure 4.7: *Experimental setup to evaluate the integrated system. The experimenter manually rolls the tactile sensor over cylinders of different size. The test subject is positioned at the opposite side of a screen and has to say which cylinder is bigger.*

different moving parts and the air flow is limited. It is much smaller than the commercial valves, and its structure allows easy implementation of a large array. Figures 4.5 and 4.6 show how. The valves could fit into holes drilled in a $108\times128\times10\,\mathrm{mm}^3$ block of annealed type 430F steel, which serves as part of the magnetic circuit. The core, cylinder, spring and piston can be assembled as in a single valve. On top of this assembly, one plate with tightly fit holes for the cylinders closes off a single high pressure chamber for all valves, simplifying and reducing the combined system.

To avoid straining —or mixing up— the wires coming from the valves, they can be connected to a PCB which is fixed immediately on the bottom of the array. Sample-hold elements are again required to control the large number of valves. The voltage can easily be converted to a current, as the required power per valve is limited with less than 0.5 W.

Apart from improving the performance of the valve, the mass production possibilities will have to be studied as well. Currently, producing the holes of the air bearing for a single valve takes almost an entire day. The coils have to be wound automatically. The other components, although not trivial, are less time consuming to make.

4.2 Evaluation Experiment

Ideally a tactile display should be felt, but that is rather difficult through a paper dissertation. Neither can its performance be described merely by quantifying force, resolution or bandwidth. A tactile feedback system works in contact with a human, and perhaps even in cooperation, because the human sense of touch has an amazing power to extract information from the tactile data that is presented, especially if it is presented in a way that closely matches natural sensations.
The aim of the experiment is to show that the tactile feedback system allows to perform reasonably complex discrimination tasks. The task should neither be too easy nor too difficult. As discussed in the previous section, discriminating hard balls in soft tissue is too difficult for the current system.

4.2.1 Experiment Description

The selected experiment is a cylinder diameter discrimination task. The five cylinders have diameters of 90 mm, 63 mm, 41 mm, 31 mm and 25 mm. On one side of a screen, the experimenter manually operates the tactile sensor (Figure 4.7). He presses it against the cylinders and rolls it backward and forward. He tries to control the force and speed of this manipulation to be as constant as possible across the experiments. He visually checks the sensor performance on the computer monitor. The test subject sits on the other side of the screen and puts the index finger of his principal hand on the tactile display. He cannot see the experimenter, the cylinders or the monitor. The tactile display is covered with a 0.5 mm thick rubber sheet to smoothen the feeling, without decreasing the spatial resolution.
At the start of the experiment, the test subject can familiarise himself with the display. While a sine wave moves over the display with an amplitude and speed that is comparable to the signal of the actual experiment, the test subject has to find the pressure he has to apply with his finger on the display to get the best feeling. During the next step, the test subject is familiarised with the sensation of the cylinders. The experimenter first rolls over the largest and the smaller cylinder, and then rolls over each of the cylinders in order, mentioning which cylinder it is. During the actual experiment, the experimenter rolls the sensor over two cylinders, and the test subject says which one he thinks is the largest in a forced choice procedure. This means the subject has to nominate a cylinder, even if no difference is felt. The test subject can ask to feel the cylinders as often as he wishes. The experimenter gives no feedback about the correctness to avoid a learning effect.
The entire experiment consists of 40 couples of cylinders, with each of the 10 possible combinations repeated four times, with two of each four starting with the smallest and the other two starting with the largest. These 40 couples are randomised in four separate sequences. The test subject was allowed to take a

break halfway the experiment if he so desired. Five test subjects performed the test. They are all male engineers between 22 and 27 years old.

4.2.2 Results and Discussion

The tests took between 37 and 48 minutes, excluding the break if there was one. The sine wave was very clearly felt by all test subjects, as was the backward and forward movement of the cylinder under the sensor. Discriminating the different diameters was perceived as very hard. The number of correct responses by the five test subjects in the order that the experiments where performed are 32, 29, 29, 25 and 24. The first three are significantly better than random guesses, with $p < 0.01$, while the last two are not. Degradation of the sensor signal over the course of the experiments might partially explain this, and was also noticed visually by the experimenter on the computer monitor. One column in the sensor signal almost completely failed near the end. During the course of the experiments three taxels in the display failed because of a rupture in the connection of the tube, but this probably did not significantly affect performance. One of the two test subjects with the worst results repeatedly noted that he felt very little, the other needed a longer break because of fatigue in hand and finger.

The discrimination results of all couples of cylinders are summarised in Table 4.1. Every couple is tested a total of 20 times, 10 with either of the cylinders first. The third column shows the chance of getting the respective result or higher if the subject was merely guessing. The ability to discriminate them was not significantly better than guessing for all couples, but the fact that the result is higher than 10 for all couples is. For the total of $n = 200$ discrimination tests, there where 139 correct answers. With a large number of trials n, this binomial distribution can be approximated by a normal distribution with mean $\mu = 100$ and standard deviation $\sigma = \sqrt{np(1-p)} = 7$ with $p = 0.5$ the chance of a correct answer in case the subject is guessing. The chance that a result of 139 on 200 is achieved by guessing is smaller than $5 \cdot 10^{-7}$. This demonstrates that the test subjects were able to discriminate between the diameters of the cylinders with only the tactile feedback provided by the system.

There is no meaningful relation between the results and the difference in diameter of the cylinders. The reason could be that the differences for this test are all above the discrimination threshold, but the sensor performance masked the signal due to the noise and the memory effect. The fact that the experimenter controlled the applied force and the speed of the sensor manually also introduces a variability which can affect the results. It should be noted that the tactile sensor is designed for soft tissue palpation and is less compliant than the human fingertip. This difference also results in a different sensation from actually feeling the cylinders. Most of the fingertip comes into contact with the cylinder because it conforms to the surface, while the sensor feels the cylinder only in part of its area, which gives the feeling of a much smaller object. Figure 4.8 shows examples of the output of

couple	# correct	$p(\geqslant \#$ correct$)$
1/2	11	0.41
1/3	13	0.13
1/4	16	0.0059
1/5	15	0.021
2/3	14	0.058
2/4	12	0.25
2/5	12	0.25
3/4	15	0.021
3/5	14	0.058
4/5	17	0.0013

Table 4.1: *Results of the cylinder diameter discrimination task per couple. There is no meaningful relation between the results and the difference in diameter of the cylinders.*

the sensor which was sent to the display for the five different cylinders.
This experiment also shows the amazing ability of the human sense of touch to extract information from noisy and incomplete data. A direct tactile feedback system profits from the experience and training of the human nervous system, while a system that presents the tactile data through another modality looses this advantage.

4.3 Conclusion

A proof of concept was built with the tactile sensor that was developed and a 'lite' version of a full pneumatic tactile display, controlled by pneumatic valves. The display shows very little friction and easily follows any control signals up to 10 Hz. With a miniaturised, less noisy valve, this concept is very promising to meet all design requirements. The performance of the tactile feedback system is evaluated. The evaluation experiment shows that it facilitates relatively complex discrimination tasks. It does not, however, allow easy detection of a hard ball in soft tissue, which is due to both the sensor performance and the limited spatial resolution of the display.
The experience with this proof of concept strongly indicates that the properties of the human sense of touch should not be neglected. Dissociating the tactile and the kinaesthetic sense is less intuitive and therefore requires more concentration. This pneumatic tactile display can easily be mounted on a mobile interface, since it is

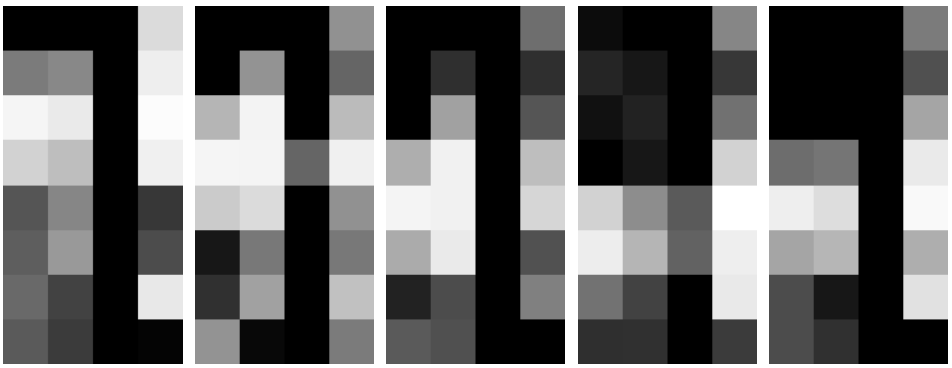

Figure 4.8: *The signal of the tactile sensor sent to the display while manipulating cylinders of different diameters. Five static images are shown, one for each cylinder diameter. The axis of the cylinder is horizontal. Visually, it is very hard to distinguish the different diameters through the sensor noise. One of the columns of the sensor is malfunctioning.*

small, very lightweight and the bundle of tubes offer nearly no resistance. Care should also be taken when processing the tactile information before sending it to the display. As the experiment to evaluate the system shows, the human tactile sense has an amazing ability to recover information from noisy data, which might be compromised if the data is processed.

Chapter 5

General Conclusion

Tactile feedback and, more specifically, intuitive, transparent tactile shape feedback remains a big technological challenge. This dissertation describes the different components necessary for, and the progress towards, a functional tactile feedback system that meets the requirements based on the human psychophysics of touch. The properties of these components, a tactile sensor and a tactile display, are summarised in Table 5.1. The elastoresistive tactile sensor meets these requirements in theory, but in practice still suffers from hysteresis, noise and drift which cloak the useful signal. These disadvantages especially manifest themselves when the tactile image is downsampled to the resolution of the proof of concept display.

The different display technologies mostly reach the requirements, but currently they all still have shortcomings preventing their application in a full tactile display. The technology used in the proof of concept tactile display easily allows for a resolution of 1 mm and a larger number of taxels, thereby passing all the quantitative requirements, while it is at the same time very compact and light. It suffers from the large commercial valves used in its design. They take up too much space, especially if their number would be quadrupled, and they make too much noise. This last requirement is prohibitive in an operating room, where the surgeon needs to concentrate and some information is transferred via auditory channels.

Section 5.1 lists the main contributions of this work. The last section proposes several possible improvements and paths for future research following up the work reported in this dissertation.

	Goal	Sensor	Closed hydraulic display	Open hydraulic display	Open pneumatic display	Proof of concept
Spatial resolution	1 mm	1 mm	2 mm	1.5 mm	1.5 mm	2 mm
# taxels	10×16	16×16	1×5	1	1	4×8
Frequency range	20–30 Hz	78 Hz	5 Hz	>40 Hz		20 Hz
Force range	0.5 N	∼1 N	4 N	1.2 N	0.47 N	0.47 N
Stroke	2–3 mm	N/A	2.34 mm	3 mm	3 mm	3 mm
Sensitivity	5–10 kPa	<4 kPa	ok	ok	ok	ok
Accuracy	10%	∼10%	<10%	>10%	≪10%	≪10%

Table 5.1: *Comparison of the characteristics of the tactile sensor and the different tactile displays with the requirements*

5.1 Contributions

- The requirements for a tactile feedback system are evaluated and redefined. The requirements found in literature are not always consistent or linked with the human sense of touch. Research about the human tactile acuity is studied, both in and out of the context of tactile feedback or MIS.
- An extensive literature survey is offered on both tactile sensors and tactile displays. From this, general design guidelines are distilled to aid future sensor and display design.
- The principle of elastoresistance is studied in detail. The fact that only the contact resistance between the rubber and the electrodes plays a role is confirmed.
- An existing elastoresistive sensor is adapted for the right pressure range, the resolution is slightly improved and it is made flexible. The readout electronics are optimised to increase the bandwidth significantly and to allow smaller resistances to be measured accurately. It is adjustable to a wide range of elastoresistive sensors.
- The first hydraulic tactile displays are realised. They have a high force and a large stroke. The closed hydraulic system has the potential for a large bandwidth and does not need a proportional valve, but the spatial resolution

is too large and the taxels are not robust. The open hydraulic system does have a large bandwidth and no immediate limit on the resolution or the stroke, but it has a large hysteresis, the valve is difficult and expensive to produce in large numbers, and leakage at the display should be avoided.

- A miniature proportional pneumatic valve is developed to be simple, and easy to miniaturise. It does not need expensive exotic materials, but the construction is, because of the required air bearing, not as straightforward as desired. It has no immediate limitation on the stroke or the resolution, it produces no noise, has a high theoretical bandwidth and leakage of a small amount of air is no problem. The range of the output pressure of the prototype, however, is not yet sufficient.
- A proof of concept of the pneumatic tactile display is built with commercial valves. It meets most requirements and is an improvement in comparison with the state of the art in tactile displays. The size and noise of the commercial valves is the main problem.

5.2 Future Work

Tactile sensor

The first and most direct improvement for the tactile sensor would be its connection with the electronics. In the current sensor, tedious soldering very near to the sensor surface is necessary, which subjects the sensor surface to undesired deformations and tensions. It is also possible that the heat from the soldering process somehow influences the electrode surface, which in turn can influence the behaviour of the contact resistance with the conductive rubber. A simple solution is printing the connecting wires immediately on the flexible PCB (Figure 5.1). Since the outer sides of the sensor are not used, they are omitted, reducing the number of taxels to 10×16. Additionally, but not shown in the figure, the outside of the flexible print can immediately be covered with a grounded electrode while the wires are printed on the inside.

The elastoresistive tactile sensor has been adapted for the right sensitivity range, optimised for speed and made flexible. Otherwise it is no better or worse than previous elastoresistive tactile sensors. The work reported in this dissertation does provide more insight into the working principle. A simple experiment could confirm a direct link between the effective contact surface, depending on the roughness of both the electrodes and the conductive rubber. To perform this experiment, a sheet of conductive rubber could be laid on the hypotenuse of a right angled triangular prism. If light shines on one of the remaining sides, it is reflected by total internal

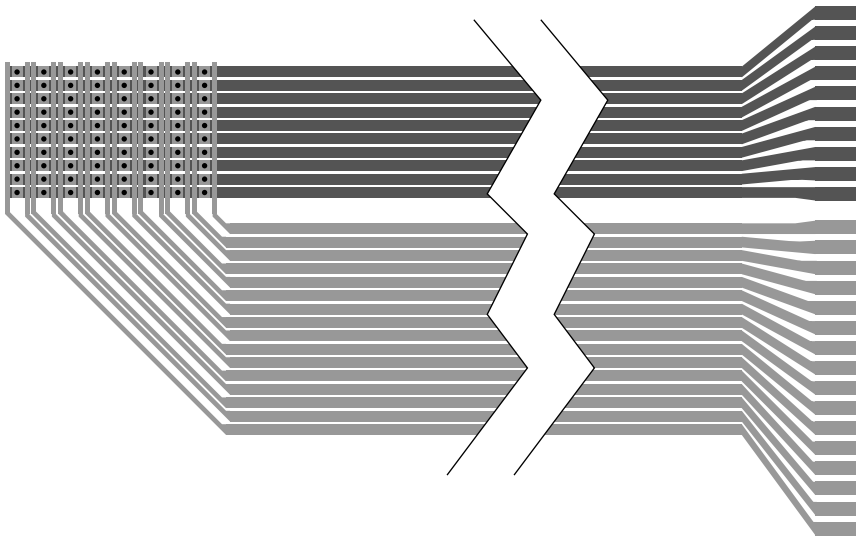

Figure 5.1: *Improved layout of the flexible PCB. Printing the wires on the flexible PCB allows easier construction of the sensor without affecting the sensor area.*

reflection. This total internal reflection is broken when the rubber comes into contact with the glass. Observing the reflection with an optical microscope while pressure is applied to the rubber sheet yields a direct link between pressure and contact surface. This could provide interesting insights towards the behaviour of the contact surface and the contact resistance between conductive rubber and electrodes.
Furthermore the effect of different materials, surface finish, and coating should be investigated to find a more optimal combination. Ideally, the adhesion between electrode and conductive rubber should be minimised to minimise hysteresis.

Section 2.2.1 hints at another possible research path. In most conductive rubbers, the conductive contents exceeds the percolation threshold, because their original purpose requires them to conduct electricity well. A rubber with a content very close to the percolation threshold could yield a different behaviour and show very strong elastoresistance in the bulk material itself, rather than only in the contact surface. If the rubber is chemically fixed to the electrodes with for example a conductive glue, the surface effects could be eliminated entirely. However, it is not guaranteed that this would yield a superior sensor, since the signal still depends on the deformation of a nonlinear, viscoelastic material.

As long as the sensor uses some kind of piezoresistive approach, the readout electronics can be reused without modifications. The acquisition software needs

at most some minor adjustments.

Tactile display

The future work for the tactile display is evident and has been hinted at several times in this work. The pneumatic principle works very well and the display itself needs very little adjustment. Using smaller pins and putting them closer together is all it takes to make a full tactile display with the required number of elements. This is no problem with the present technology.
The real challenge remains the proportional valves. Commercially available valves are too large and produce too much noise. Furthermore, their bandwidth is on the limit, although it could be sufficient. The pneumatic valve designed in Section 3.4 is a good start, since it is small, has no internal friction, is able to handle high pressures and works nearly noiseless. The air bearing and production process need to be optimised to increase the range of the output pressure and to allow for easy manufacturing of a large array of valves. Section 4.1.2 shows what this array could look like.

Integrated system

The signal processing of the tactile image between the sensor and the display offers some possibilities to enhance the signal. First of all, the sensor signal could be improved by filtering out noise or implementing drift compensation. Secondly, image processing techniques could be used to extract features. Desired features could be enhanced, while undesired features could be removed. This becomes less useful if the sensor and display improve to match the resolution of the human skin. If possible, improving the hardware is a better solution than trying to fix the shortcomings.

The existing proof of concept setup can be used to acquire useful information about the application and the requirements. Currently, there is still a significant uncertainty about the necessary bandwidth, force or resolution. Comparative experiments with the tactile display are feasible, limiting the bandwidth, the maximum force or the force resolution to study their effect on certain discrimination tasks.

Appendix A

Magnetic Modelling

An analytical model has significant advantages over numerical models. An analytical model shows behaviour and relationships which can remain hidden in an equivalent numerical model. Moreover, optimising a design with a numerical model can be very time consuming, while an analytical model often only requires a simple calculation.
Both analytical and numerical models make simplifications of the real world to make the calculations manageable. Before using a model, its validity should be verified for the specific application. The goal of this appendix is to check the applicability of analytical models in the calculation of magnetic circuits. Three separate cases are studied, all of them ferromagnetic circuits with a moveable piston and a small air gap. The first has a coil around the core, the second has a permanent magnet in the core, and the last has both a coil and a permanent magnet (Figure A.1). The numerical model is an axisymmetrical finite element model calculated in Comsol and processed in Matlab. The finite element model is assumed to be accurate with a small mesh and a large volume of air surrounding the magnetic circuit.

In analogy with an electric circuit, a magnetic circuit can be described by Hopkinson's law

$$\Phi = \frac{\Theta}{\Re_{\mathrm{m}}}, \tag{A.1}$$

with Φ the magnetic flux through the circuit, equivalent with an electrical current, Θ the magnetomotive force, equivalent with an electrical voltage, and $\Re_{\mathrm{m}}$ the magnetic reluctance, equivalent with an electrical resistance. Per unit of area, this

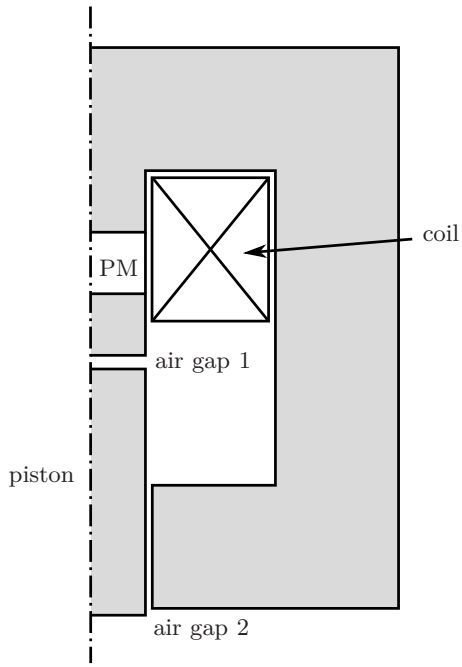

Figure A.1: *Axisymmetrical model of a magnetic circuit with a coil and a permanent magnet (PM)*

becomes

$$B = \frac{\Theta}{S\Re_{\mathrm{m}}}, \tag{A.2}$$

with B the magnetic induction or magnetic flux density and S the cross section. The force on the piston can be described by the Maxwell stress

$$\sigma_{\mathrm{m}} = \frac{B^2}{2\mu_0}, \tag{A.3}$$

with μ_0 the permeability of vacuum. Usually, the reluctance of the air gap is much higher than the reluctance of the ferromagnetic material. Neglecting this last reluctance, assuming a homogeneous magnetic field and rewriting the reluctance of the second air gap yields

$$F_{\mathrm{m}} = \frac{\mu_0 S \Theta^2}{2(l_0 + l_{\mathrm{eq}} - x)^2}. \tag{A.4}$$

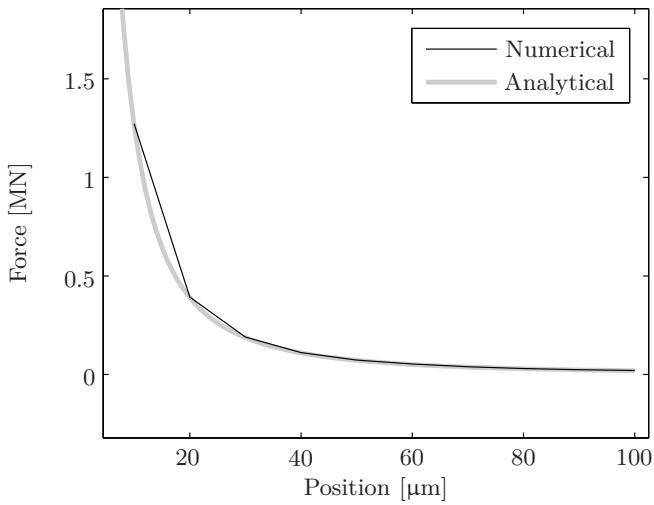

Figure A.2: *Comparison between analytical and numerical models with only a coil. The models match nearly perfectly, which means that the analytical model is valid in this situation.*

Coil only

The calculation of the magnetomotive force produced by a coil is straightforward, since a coil is equivalent to a pure voltage source.

$$\Theta = NI, \tag{A.5}$$

with N the number of windings of the coil and I the current through it. The force on the piston is

$$F_{\mathrm{m}} = \frac{\mu_0 S N^2 I^2}{2(l_0 + l_{\mathrm{eq}} - x)^2}. \tag{A.6}$$

Figure A.2 compares this result with the numerical finite element model. The match is nearly perfect. There are hardly any stray field lines.

Permanent magnet only

A permanent magnet is equivalent to neither a current nor a voltage source. Its magnetic flux density is described by

$$B_{\mathrm{PM}} = \mu_0(M + H_{\mathrm{PM}}), \tag{A.7}$$

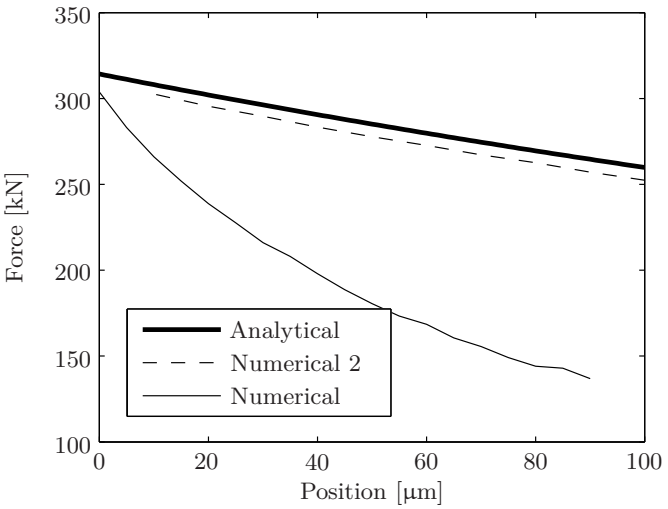

Figure A.3: *Comparison between analytical and numerical models with only a permanent magnet. Numerical 2 denotes an artificial situation where the air is made very diamagnetic to force the magnetic field into the circuit. The analytical model is not valid in this situation. Because the permanent magnet introduces a large air gap, a large part of the magnetic flux lines do not stay inside the magnetic circuit.*

where M is the magnetisation of the material of the permanent magnet and H_{PM} the magnetic field inside the permanent magnet, which is negative in the absence of other magnets or coils. This appendix only considers rare earth magnets such as SmCo or NeFeB, which have a linear behaviour, unlike for example AlNiCo or martensitic steel. The magnet is equivalent to a voltage source with a resistance in series. If the load increases —a larger air gap— the magnetic field increases and the flux decreases. In the magnetic model this can be modelled as a magnetomotive force

$$\Theta = M l_{PM}, \tag{A.8}$$

with l_{PM} the length of the magnet, and an air gap of l_{PM} in series. This reflects the fact that the local relative permeability of the magnet is about 1, which means it is effectively a large air gap. The force on the piston is

$$F_{\mathrm{m}} = \frac{\mu_0 S M^2 l_{PM}^2}{2(l_0 + l_{\mathrm{eq}} + l_{PM} - x)^2}. \tag{A.9}$$

Figure A.3 compares this result with the numerical finite element model. As the air gap increases, the error becomes very large, even up to 100%. The large additional

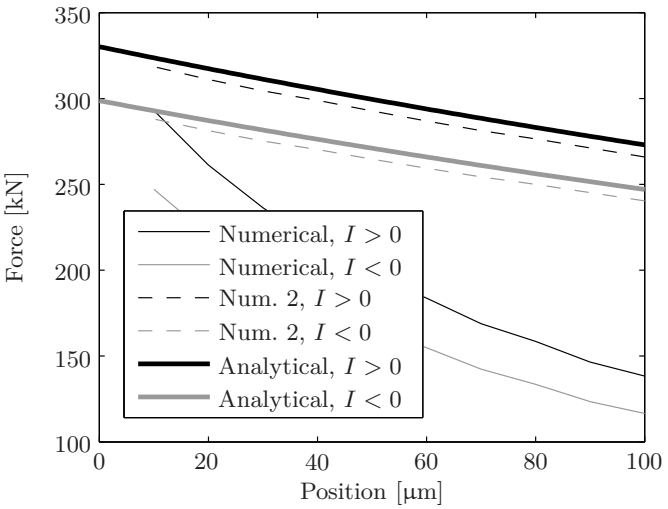

Figure A.4: *Comparison between analytical and numerical models with a coil and a permanent magnet. Num. 2 denotes an artificial situation where the air is made very diamagnetic to force the magnetic field into the circuit. The analytical model is not valid in this situation. Because the permanent magnet introduces a large air gap, a large part of the magnetic flux lines do not stay inside the magnetic circuit.*

air gap introduced by the magnet causes a significant amount of stray field lines. Because these field lines no longer pass through the piston, the force decreases with respect to the analytical model, which assumes that all field lines go through the magnetic circuit and the piston. The result is still in the same order of magnitude. To check whether stray field lines are indeed the main source of this difference, a second numerical model is evaluated. In this model, the magnetic susceptibility of the air is set to -1, making it perfectly diamagnetic. In reality, this is only possible inside superconductors. This forces all magnetic field lines through the magnetic circuit and the piston, as is assumed by the analytical model. The result only has a small error (Figure A.3), which confirms the above.

Coil and permanent magnet

For completeness, a coil and a permanent magnet are combined in the third model. The magnetomotive force becomes

$$\Theta = NI + Ml_{PM}, \tag{A.10}$$

and the force on the piston

$$F_{\mathrm{m}} = \frac{\mu_0 S(NI + Ml_{PM})^2}{2(l_0 + l_{\mathrm{eq}} + l_{PM} - x)^2}. \tag{A.11}$$

Figure A.4 compares this result with the numerical finite element model. As could be expected, the same conclusions as with only the permanent magnet can be drawn. Note, however, that both analytical and numerical model stop being valid when the magnetic field produced by the coil becomes larger than the coercive field of the permanent magnet, which can cause the magnet to demagnetise.

Bibliography

[1] Carpenter technical datasheet, Carpenter stainless type 430F solenoid quality, 2004.

[2] Minimally invasive surgery and the challenges in medical training. *GMV News*, (36):4–7, 2007.

[3] PCR Technical. How to use analog type pressure-conductive rubber CSA. Technical report, 2002.

[4] P. Adl, Z.A. Memon, D.J. Mapps, and R.T. Rakowski. Serpentine magnetoresistive elements for tactile sensor applications. *IEEE Transactions on Magnetics*, 26(5):2047–2049, 1990.

[5] K. Akazawa, M. Konyo, S. Tadokoro, and T. Takamori. Softness display for touch feel using high polymer gel actuators. In *Proceedings of the Virtual Reality Society of Japan Annual Conference*, volume 8, pages 221–224, 2003.

[6] R. Allen. Tactile sensor tucks a 256-point array into a robot's palm. *Electronic Design*, 33(11):45–46, 1985.

[7] J. Andersson and A. Lundberg. Multimodal machines makes military move – a visiotactile artefact for augmented soldier communication. Technical Report 2004:42, IT University of Göteborg, 2004.

[8] N. Asamura, T. Shinohara, Y. Toyo, N. Koshida, and H. Shinoda. Necessary spatial resolution for realistic tactile feeling display. In *Proceedings of the IEEE International Conference on Robotics and Automation*, volume 2, pages 1851–1856, 2001.

[9] N. Asamura, N. Yokoyama, and H. Shinoda. Selectively stimulating skin receptors for tactile display. *IEEE Computer Graphics and Applications*, 18(6):32–37, 1998.

[10] M. Ayyildiz, B. Guclu, M.Z. Yildiz, and C. Bastogan. A novel tactile sensor for detecting lumps in breast tissue. In *Proceedings of Eurohaptics*, volume 1, pages 367–372, 2010.

[11] P. Bach-y-Rita. *Brain Mechanisms in Sensory Substitution*. Academic Press, 1972.

[12] G.H. Ballantyne. Robotic surgery, telerobotic surgery, telepresence, and telementoring – review of early clinical results. *Surgical Endoscopy*, 16(10):1389–1402, 2002.

[13] C. Bao and H. Van Brussel. A sensory controlled gripper system. *Robotics and Autonomous Systems*, 6(3):283–295, 1990.

[14] D.J. Beebe, D.D. Denton, R.G. Radwin, and J.G. Webster. A silicon-based tactile sensor for finger-mounted applications. *IEEE Transactions on Biomedical Engineering*, 45(2):151–159, 1998.

[15] D.J. Beebe, C.M. Hymel, K.A. Kaczmarek, and M.E. Tyler. A polyimide-on-silicon electrostatic fingertip tactile display. In *Proceedings of the 1995 IEEE Conference of the Engineering in Medicine and Biology Society*, volume 2, pages 1545–1546, 1995.

[16] M. Beedie. Tactile sensor hits high-resolution mark of robotic vision systems. *Electronic Design*, 33(3):69–70, 1985.

[17] S. Begej. Planar and finger-shaped optical tactile sensors for robotic applications. *IEEE Journal of Robotics and Automation*, 4:472–484, 1988.

[18] W.A. Bemelman, J. Ringers, D.W. Meijer, C.W.M. de Wit, and J.J.G. Bannenberg. Laparoscopic-assisted colectomy with the dexterity pneumo sleeve. *Diseases of the Colon and Rectum*, 39(10):S59–S61, 1996.

[19] M. Benali Khoudja and M. Hafez. VITAL: a vibrotactile interface with thermal feedback. In *Journée Scientifique Internationale IRCICA*, 2004.

[20] M. Benali Khoudja, M. Hafez, J.M. Alexandre, and A. Kheddar. Tactile interfaces: a state-of-the-art survey. In *Proceedings of the 35th International Symposium on Robotics*, pages 721–726, 2004.

[21] S.J. Bensmaïa, Y.Y. Leung, S.S. Hsiao, and K.O. Johnson. Vibratory adaptation of cutaneous mechanoreceptive afferents. *Journal of Neurophysiology*, 94:3023–3036, 2005.

[22] W.M. Bergmann Tiest and A.M.L. Kappers. Cues for haptic perception of compliance. *IEEE Transactions on Haptics*, 2(4):189–199, 2009.

[23] D.T. Beruto, M. Capurro, and G. Marro. Piezoresistance behavior of silicone-graphite composites in the proximity of the electric percolation threshold. *Sensors and Actuators A*, 117:301–308, 2005.

[24] S. Bhat, J.G. Webster, W.J. Tompkins, and J.J. Wertsch. Piezoelectric sensor for foot pressure measurement. In *Proceedings of the 1989 Conference of the IEEE Engineering in Medicine and Biology Society*, pages 1435–1436, 1989.

[25] O.S. Bholat, R.S. Haluck, W.B. Murray, P.J. Gorman, and T.M. Krummel. Tactile feedback is present during minimally invasive surgery. *Journal of the American College of Surgeons*, 189(4):349–355, 1999.

[26] A. Bicchi and P. Dario. Intrinsic tactile sensing for artificial hands. In *Proceedings of the International Symposium on Robotics Research*, pages 83–90, 1988.

[27] A. Bicchi, E.P. Scilingo, and D. De Rossi. Haptic discrimination of softness in teleoperation: the role of the contact area spread rate. *IEEE Transactions on Robotics and Automation*, 16(5):496–504, 2000.

[28] A. Bicchi, E.P. Scilingo, N. Sgambelluri, and D. De Rossi. Haptic interfaces based on magnetorheological fluids. In *Proceedings of Eurohaptics*, pages 6–11, 2002.

[29] M. Biet, F. Giraud, and B. Semail. New tactile devices using piezoelectric actuators. In *Proceedings of Actuator 2006*, pages 989–992, 2006.

[30] I. Birznieks, P. Jenmalm, R.S. Johansson, and A.W. Goodwin. Encoding of direction of fingertip forces by human tactile afferents. *Journal of Neuroscience*, 21:8222–8237, 2001.

[31] I. Birznieks, P. Jenmalm, R.S. Johansson, and A.W. Goodwin. Responses in human tactile afferents to fingertip forces with tangential force components in distal and proximal directions. *Acta Universitatis Latviensis*, 631:7–23, 2001.

[32] J.C. Bliss. A relatively high-resolution reading aid for the blind. *IEEE Transactions on Man-Machine Systems*, 10:1–9, 1969.

[33] J.C. Bliss, M.H. Catcher, C.H. Rogers, and R.P. Shepard. Optical-to-tactile image conversion for the blind. *IEEE Transactions on Man-Machine Systems*, 11(1):58–65, 1970.

[34] D.H. Boehm, M.B. Arnold, C. Detter, and H. Reichenspurner. Incorporating robotics into an open-heart program. *Surgical Clinics of North America*, 83(6):1369–1380, 2003.

[35] S. Bolanowski, G. Gescheider, R. Verrillo, and C. Checkosky. Four channels mediate the mechanical aspects of touch. *The Journal of the Acoustical Society of America*, 84(4):1680–1694, 1988.

[36] W. Bracke, P. Merken, R. Puers, and C. Van Hoof. On the optimization of ultra low power front-end interfaces for capacitive sensors. *Sensors and Actuators A*, 117:273–285, 2005.

[37] S.A. Brewster and A.A. King. The design and evaluation of a vibrotactile progress bar. In *Proceedings of World Haptics Conference 2005*, pages 499–500, 2005.

[38] S.R. Broadbent and J.M. Hammersley. Percolation processes I. *Mathematical Proceedings of the Cambridge Philosophical Society*, 53(3):629–641, 1957.

[39] L.M. Brown, S.A. Brewster, and H.C. Purchase. A first investigation into the effectiveness of tactons. In *Proceedings of World Haptics Conference 2005*, pages 167–176, 2005.

[40] H. Böse, G.J. Monkman, H. Freimuth, D. Klein, H. Ermert, M. Baumann, S. Egersdörfer, and O.T. Bruhns. ER fluid based haptic system for virtual reality. In *Proceedings of the 8th International Conference on New Actuators*, pages 351–354, 2002.

[41] D.G. Caldwell, N. Tsagarakis, and C. Giesler. An integrated tactile/shear feedback array for stimulation of finger mechanoreceptor. In *Proceedings of the IEEE International Conference on Robotics and Automation*, volume 1, pages 287–292, 1999.

[42] M. Calis and M.P.Y. Desmulliez. Haptic sensing technologies for a novel design methodology in micro/nanotechnology. *Nanotechnology Perceptions*, 1:89–97, 2005.

[43] A. Cameron, R. Daniel, and H. Durrant-Whyte. Touch and motion. In *Proceedings of the IEEE International Conference on Robotics and Automation*, volume 2, pages 1062–1067, 1988.

[44] F. Carpi, G. Frediani, and D. De Rossi. Electroactive elastomeric haptic displays of organ motility and tissue compliance for medical training and surgical force feedback. *IEEE Transactions on Biomedical Engineering*, 56(9):2327–2330, 2009.

[45] F. Carpi, G. Frediani, and D. De Rossi. Bubble-like dielectric elastomer actuator with hydrostatic coupling for tactile displays. In *Proceedings of Actuator 2010*, pages 884–887, 2010.

[46] R. Carta, P. Jourand, B. Hermans, J. Thoné, D. Brosteaux, T. Vervust, F. Bossuyt, F. Axisa, J. Vanfleteren, and R. Puers. Design and implementation of advanced systems in a flexible-stretchable technology for biomedical applications. *Sensors and Actuators A*, 156(1):79–87, 2009.

[47] R. Carter, F.W. Poon, D. Hemingway, J.A. McKillop, T.G. Cooke, C.S. McArdle, and R. Pickard. A prospective study of six methods for detection of hepatic colorectal metastases. *Annals of the Royal College of Surgeons of England*, 78:27–30, 1996.

[48] X. Chen, S. Yang, M. Hasegawa, K. Kawabe, and S. Motojima. Tactile microsensor elements prepared from arrayed superelastic carbon microcoils. *Applied Physics Letters*, 87(5):054101/1–054101/3, 2005.

[49] K.H. Chiang. *Limits of microvalve design*. PhD thesis, UC Berkeley, 2000.

[50] H. Chigusa, Y. Makino, and H. Shinoda. Large area sensor skin based on two-dimensional signal transmission technology. In *Proceedings of World Haptics Conference 2007*, pages 151–156, 2007.

[51] W.R. Chitwood. Endoscopic robotic coronary surgery – is this reality or fantasy. *Journal of Thoracic and Cardiovascular Surgery*, 118(1):1–3, 1999.

[52] M.B. Cohn, M. Lam, and R.S. Fearing. Tactile feedback for teleoperation. In *Proceedings of Telemanipulator Technology*, volume 1833, pages 240–254, 1992.

[53] P. Coiffet. *Robot Technology 2: Interaction with the environment*, chapter Interactions involving physical contact between robot and environment: tactile detection, pages 75–89. 1983.

[54] J.C. Craig. Pictorial and abstract cutaneous displays. *Cutaneous Communication Systems and Devices*, pages 78–83, 1973.

[55] Z. Cui, M. Ogawa, S. Kono, K. Matsunaga, and K. Shidoji. Effects of tactile feedback on simulated telesurgery work in network delay environment. In *Proceedings of the Virtual Reality Society of Japan Annual Conference*, volume 9, pages 575–578, 2004.

[56] M.R. Cutkosky, J.M. Jourdain, and P.K. Wright. Skin materials for robotic fingers. In *Proceedings of the IEEE International Conference on Robotics and Automation*, volume 4, pages 1649–1654, 1987.

[57] R.S. Dahiya, G. Metta, M. Valle, and G. Sandini. Tactile sensing – from humans to humanoids. *IEEE Transactions on Robotics*, 26(1):1–20, 2010.

[58] J. Dargahi, S. Payandeh, and M. Parameswaran. A micromachined piezoelectric teeth-like laparoscopic tactile sensor: theory, fabrication and experiments. In *Proceedings of the IEEE International Conference on Robotics and Automation*, volume 1, pages 299–304, 1999.

[59] P. Dario and G. Buttazzo. An anthropomorphic robot finger for investigating artificial tactile perception. *International Journal of Robotics Research*, 6(3):25–48, 1987.

[60] P. Dario and D. De Rossi. Tactile sensors and the gripping challenge. *IEEE Spectrum*, pages 46–52, 1985.

[61] P. Dario, D. De Rossi, C. Domenici, and R. Francesconi. Ferroelectric polymer tactile sensors with anthropomorphic features. In *Proceedings of the IEEE International Conference on Robotics and Automation*, pages 332–340, 1984.

[62] D. De Bruyker, A. Cozma, and R. Puers. A combined piezoresistive/capacitive pressure sensor with self-test function based on thermal actuation. *Sensors and Actuators A*, 66:70–75, 1998.

[63] G. De Gersem. *Kinaesthetic feedback and enhanced sensitivity in robotic endoscopic telesurgery*. PhD thesis, K.U.Leuven, 2005.

[64] G. De Gersem, H. Van Brussel, and F. Tendick. Reliable and enhanced stiffness perception in soft-tissue telemanipulation. *International Journal of Robotics Research*, 24(10):805–822, 2005.

[65] D. De Rossi, F. Carpi, and E.P. Scilingo. Polymer based interfaces as bioinspired 'smart skins'. *Advances in Colloid and Interface Science*, 116:165–178, 2005.

[66] M. De Volder, P. Goethals, S. Eeckhoudt, J. Peirs, and D. Reynaerts. A ferrofluid seal technology for hydraulic microactuators. In *Proceedings of Actuator 2006*, pages 693–696, 2006.

[67] M. De Volder and D. Reynaerts. Pneumatic and hydraulic microactuators: a review. *Journal of Micromechanics and Microengineering*, 20(4):043001, 2010.

[68] L. Demonie and R. Verbrugghe. Ontwikkeling van een tactiel krachtplatform ter identificatie van onderdelen. Master's thesis, K.U.Leuven, 1987.

[69] P.D. Dimitropoulos, D.P. Karampatzakis, G.D. Panagopoulos, and G.I. Stamoulis. A low-power/low-noise readout circuit for integrated capacitive sensors. *IEEE Sensors Journal*, 6(3):755–769, 2006.

[70] K. Drewing, M. Fritschi, R. Zopf, M.O. Ernst, and M. Buss. First evaluation of a novel tactile display exerting shear force via lateral displacement. *ACM Transactions on Applied Perception*, 2(2):118–131, 2005.

[71] T. du Moncel. *Le téléphone, le microphone et le phonographe*. Hachette, 1878.

[72] S. Eeckhoudt and P. Goethals. Ontwikkeling van een ferrofluïdische afdichting voor een lineaire, hydraulische microactuator. Master's thesis, K.U.Leuven, 2005.

[73] F. Eghtedari and C. Morgan. A novel tactile sensor for robot applications. *Robotica*, 7(4):289–295, 1989.

[74] R.E. Ellis, S.R. Ganeshan, and S.J. Lederman. A tactile sensor based on thin-plate deformation. *Robotica*, 12:343–351, 1994.

[75] M.E.H. Eltaib and J.R. Hewit. Tactile sensing technology for minimal acces surgery – a review. *Mechatronics*, 13:1163–1177, 2003.

[76] J. Engel, J. Chen, and L. Chang. Development of polyimide flexible tactile sensor skin. *Journal of Micromechanics and Microengineering*, 13:359–366, 2003.

[77] J. Engel, J. Chen, Z. Fan, and C. Liu. Polymer micromachined multimodal tactile sensors. *Sensors and Actuators A*, 117:50–61, 2005.

[78] H.A. Ernst. MH-1, a computer-operated mechanical hand. In *Proceedings of the Spring Joint Computer Conference*, pages 39–51, 1962.

[79] N. Famaey and J. Vander Sloten. Soft tissue modelling for applications in virtual surgery and surgical robotics. *Computer Methods in Biomechanics and Biomedical Engineering*, 11(4):351–366, 2008.

[80] F. Farhat, F. Depuydt, F. Van Praet, J. Coddens, and H. Vanermen. Hybrid cardiac revascularization using a totally closed-chest robotic technology and a percutaneous transluminal coronary dilatation. *The Heart Surgery Forum*, 3(2):119–122, 2000.

[81] R.S. Fearing. Tactile sensing mechanisms. *International Journal of Robotics Research*, 9(3):3–23, 1990.

[82] R.S. Fearing, G. Moy, and E. Tan. Some basic issues in teletaction. In *Proceedings of the IEEE International Conference on Robotics and Automation*, volume 4, pages 3093–3099, 1997.

[83] H. Fischer, B. Neisius, and R. Trapp. Tactile feedback for endoscopic surgery. *Interactive Technology and New Paradigm for Healthcare*, pages 114–117, 1995.

[84] M.L. Franco, D.-H. King, M.O. Culjat, E. Lewis, J.W. Bisley, E.C. Holmes, W.S. Grundfest, and E.P. Dutson. An integrated pneumatic tactile feedback actuator array for robotic surgery. *The International Journal of Medical Robotics and Computer Assisted Surgery*, 5:13–19, 2009.

[85] T. Fukuda, H. Morita, and F. Arai. Micro resonator using electromagnetic actuator for tactile display. In *Proceedings of the International Symposium on Micromechatronics and Human Science*, pages 143–148, 1997.

[86] A. Gallace, H.Z. Tan, and C. Spence. Tactile change detection. In *Proceedings of World Haptics Conference 2005*, pages 12–16, 2005.

[87] F.A. Geldard and C.E. Sherrick. The cutaneous "rabbit": a perceptual illusion. *Science*, 178(4057):178–179, 1972.

[88] B.T. Gleeson and W.R. Provancher. Embedding tactile feedback into handheld devices: an aperture-based restraint for the finger or tumb. In *Proceedings of Eurohaptics*, volume 2, pages 297–302, 2010.

[89] A. Grahn and L. Astle. Robotic ultrasonic force sensor array. In *Proceedings of the Robots 8 Conference*, volume 2, pages 21.1–21.18, 1984.

[90] A. Grahn and L. Astle. Tactile sensor, US Patent Nr. 4,964,302, 1990.

[91] B.L. Gray and R.S. Fearing. A surface-micromachined microtactile sensor array. In *Proceedings of the IEEE International Conference on Robotics and Automation*, volume 1, pages 1–6, 1996.

[92] J.A. Greenwood and J.B.P. Williamson. Contact of nominally flat surfaces. *Proceedings of the Royal Society of London, Series A, Mathematical and Physical Sciences*, 295(1442):300–319, 1966.

[93] D. Göger, K. Weiß, C. Burghart, and H. Wörn. Sensitive skin for a humanoid robot. In *Proceedings of Human-Centered Robotic Systems*, 2006.

[94] J.M. Hammersley. Percolation processes II. *Mathematical Proceedings of the Cambridge Philosophical Society*, 53(3):642–645, 1957.

[95] H.Y. Han and S. Kawamura. Analysis of stiffness of human fingertip and comparison with artificial fingers. In *Proceedings of the IEEE International Conference on Systems, Man, and Cybernetics*, pages 800–805, 1999.

[96] L.D. Harmon. Automated tactile sensing. *International Journal of Robotics Research*, 2(1):3–32, 1982.

[97] C.J. Hasser and M.W. Daniels. Tactile feedback with adaptive controller for a force-reflecting haptic display. In *Proceedings of the 15th Southern Biomedical Engineering Conference*, pages 526–533, 1996.

[98] V. Hayward. A brief taxonomy of tactile illusions and demonstrations that can be done in a hardware store. *Brain Research Bulletin*, 75(6):742–752, 2008.

[99] V. Hayward and J.M. Cruz-Hernández. Tactile display device using distributed lateral skin stretch. In *Proceedings of the Symposium on Haptic Interfaces for Virtual Environments and Teleoperator Systems*, pages 1309–1314, 2000.

[100] V. Hayward and K.E. MacLean. Do it yourself haptics: part I. *IEEE Robotics & Automation Magazine*, 14(4):88–104, 2007.

[101] G. Hellard and R.A. Russel. A robust, sensitive and economical tactile sensor for a robotic manipulator. In *Proceedings of the 2002 Australasian Conference on Robotics and Automation*, pages 100–104, 2002.

[102] M. Helsel, J.N. Zemel, and V. Dominko. An impedance tomographic tactile sensor. *Sensors and Actuators*, 14(1):93–98, 1988.

[103] J.S. Heo, J.H. Chung, and J.J. Lee. Tactile sensor arrays using fiber Bragg grating sensors. *Sensors and Actuators A*, 126:312–327, 2006.

[104] J.W. Hill and A.J. Sword. Manipulation based on sensor-directed control: an integrated end effector and touch sensing system. In *Annual Human Factors Society Convention*, 1973.

[105] W.D. Hillis. A high-resolution imaging touch sensor. *International Journal of Robotics Research*, 1(2):33–44, 1982.

[106] M. Hollins, S.J. Bensmaïa, and E.A. Roy. Vibrotaction and texture perception. *Behavioural Brain Research*, 135:51–56, 2002.

[107] E. Holweg. Tactiele sensoren. *Mikroniek*, 37(1):6–14, 1997.

[108] T. Homma, S. Ino, H. Kuroki, T. Izumi, T. Tanabe, and T. Ifukube. Transmitted information using a fingerpad-sized tactile display. In *Proceedings of the Virtual Reality Society of Japan Annual Conference*, volume 8, pages 229–232, 2003.

[109] R.D. Howe. Tactile sensing and control of robotic manipulation. *Advanced Robotics*, 8(3):245–261, 1994.

[110] R.D. Howe and M.R. Cutkosky. Dynamic tactile sensing – perception of fine surface-features with stress rate sensing. *IEEE Transactions on Robotics and Automation*, 9(2):140–151, 1993.

[111] R.D. Howe and D.A. Kontarinis. Task performance with a dextrous teleoperated hand system. In *Proceedings of SPIE, Telemanipulator Technology*, volume 1833, pages 199–207, 1992.

[112] R.D. Howe, W.J. Peine, D.A. Kontarinis, and J.S. Son. Remote palpation technology for surgical applications. *IEEE Engineering in Medicine and Biology Magazine*, 14(3):318–323, 1995.

[113] E.S. Hwang, J.H. Seo, and Y.J. Kim. A polymer-based flexible tactile sensor for both normal and shear load detections and its application for robotics. *Journal of Microelectromechanical Systems*, 16(3):556–563, 2007.

[114] Y. Ikei, K. Wakamatsu, and S. Fukuda. Texture presentation by vibratory tactile display – image based presentation of a tactile texture. In *Proceedings of the Virtual Reality Annual International Symposium*, pages 199–205, 1997.

[115] Y. Ikei, M. Yamada, and S. Fukuda. A new design of haptic texture display —texture display2— and its preliminary evaluation. In *Proceedings of the IEEE Virtual Reality 2001 Conference*, pages 21–22, 2001.

[116] G. Inaba and K. Fujita. A pseudo-force-feedback device by fingertip tightening for multi-finger object manipulation. In *Proceedings of Eurohaptics*, pages 475–478, 2006.

[117] T. Iwamoto, D. Akaho, and H. Shinoda. High resolution tactile display using acoustic radiation pressure. In *Proceedings of SICE*, pages 1239–1244, 2004.

[118] T. Iwamoto and H. Shinoda. Ultrasound tactile display for stress field reproduction – examination of non-vibratory tactile apparent movement. In *Proceedings of World Haptics Conference 2005*, pages 220–228, 2005.

[119] T. Iwamoto, M. Tatezono, and H. Shinoda. Non-contact method for producing tactile sensation using airborne ultrasound. In *Proceedings of Eurohaptics*, pages 504–513, 2008.

[120] D.T. Jenstrom and C.L. Chen. A fiber optic microbend tactile sensor array. *Sensors and Actuators*, 20(3):239–248, 1989.

[121] A.R. Jiménez, A.S. Soembagijo, D. Reynaerts, H. Van Brussel, R. Ceres, and J.L. Pons. Featureless classification of tactile contacts in a gripper using neural networks. *Sensors and Actuators A*, 62:488–491, 1997.

[122] R.S. Johansson and R.H. LaMotte. Tactile detection thresholds for a single asperity on an otherwise smooth surface. *Somatosensory Research*, 1(1):21–31, 1983.

[123] R.S. Johansson, U. Landström, and R. Lundström. Responses of mechanoreceptive afferent units in the glabrous skin of the human hand to sinusoidal skin displacements. *Brain Research*, 244:17–25, 1982.

[124] R.S. Johansson and Å.B. Vallbo. Tactile sensibility in the human hand: relative and absolute densities of four types of mechanoreceptive units in glabrous skin. *Journal of Physiology*, 286:283–300, 1979.

[125] R.S. Johansson and Å.B. Vallbo. Tactile sensory coding in the glabrous skin of the human hand. *Trends in Neurosciences*, 6(1):27–32, 1983.

[126] R.S. Johansson and G. Westling. Roles of glabrous skin receptors and sensorimotor memory in automatic control of precision grip when lifting rougher or more slippery objects. *Experimental Brain Research*, 56:550–564, 1984.

[127] K.O. Johnson and J.R. Phillips. Tactile and spatial resolution I: two point discrimination, gap detection, grating resolution, and letter recognition. *Journal of Neurophysiology*, 46(6):1177–1191, 1981.

[128] Y.J. Jung, S. Kar, S. Talapatra, C. Soldano, G. Viswanathan, X. Li, Z. Yao, F.S. Ou, A. Avadhanula, R. Vajtai, S. Curran, O. Nalamasu, and P.M. Ajayan. Aligned carbon nanotube-polymer hybrid architectures for diverse flexible electronic applications. *Nano Letters*, 6(3):413–418, 2006.

[129] M. Jungmann and H.F. Schlaak. Miniaturised electrostatic tactile display with high structural compliance. In *Proceedings of Eurohaptics*, pages 12–17, 2002.

[130] K.A. Kaczmarek, M.E. Tyler, and P.Bach-y-Rita. Electrotactile haptic display on the fingertips: preliminary results. In *Proceedings of the 16th International Conference of the IEEE Engineering in Medicine and Biology Society*, pages 940–941, 1994.

[131] K.A. Kaczmarek, J.G. Webster, P. Bach-y-Rita, and W.J. Tompkins. Electrotactile and vibrotactile displays for sensory substitution systems. *IEEE Transactions on Biomedical Engineering*, 38(1):1–16, 1991.

[132] H. Kajimoto. Electro-tactile display with real-time impedance feedback. In *Proceedings of Eurohaptics*, pages 285–291, 2010.

[133] H. Kajimoto, M. Inami, N. Kawakami, and S. Tachi. SmartTouch: electric skin to touch the untouchable. *IEEE Transactions on Computer Graphics and Applications*, Jan-Feb:36–43, 2004.

[134] H. Kajimoto, N. Kawakami, T. Maeda, and S. Tachi. Electro-tactile display with force feedback. In *Proceedings of the World Multiconference on Systemics, Cybernetics and Informatics*, pages 95–99, 2001.

[135] P. Kammermeier, M. Buss, and G. Schmidt. A systems theoretical model for human perception in multimodal presence systems. *IEEE/ASME Transactions on Mechatronics*, 6(3):234–243, 2001.

[136] T. Katsuno, X. Chen, S. Yang, and S. Motojima. Observation and analysis of percolation behavior in carbon microcoils/silicone-rubber composite sheets. *Applied Physics Letters*, 88(23):232115-1–232115-3, 2006.

[137] K. Kawahata, M. Yoneda, and I. Igarashi. Tactile image detection using a 1k-element silicon pressure sensor array. *Sensors and Actuators A*, 22:239–248, 1990.

[138] O. Kerpa, K. Weiß, and H. Wörn. Development of a flexible tactile sensor system for a humanoid robot. In *Proceedings of the IEEE/RSJ International Conference on Intelligent Robots and Systems*, volume 1, pages 1–6, 2003.

[139] W. Khaled, S. Reichling, O.T. Bruhns, H. Böse, M. Baumann, G.J. Monkman, S. Egersdörfer, D. Klein, A. Tunayar, H. Freimuth, A. Lorenz, A. Pessavento, and H. Ermert. Palpation imaging using a haptic system for virtual reality applications in medicine. In *Proceedings of the 12th Annual Medicine Meets Virtual Reality Conference*, pages 147–153, 2004.

[140] B.E. Kilbride, J.N. Coleman, J. Fraysse, P. Fournet, M. Cadek, A. Drury, S. Hutzler, S. Roth, and W.J. Blau. Experimental observation of scaling laws for alternating current and direct current conductivity in polymer-carbon nanotube composite thin films. *Journal of Applied Physics*, 92(7):4024–4030, 2002.

[141] S.-C. Kim, C.-H. Kim, G.-H. Yang, T.-H. Yang, B.-K. Han, S.-C. Kang, and D.S. Kwon. Small and lightweight tactile display(SaLT) and its application. In *Proceedings of World Haptics Conference 2009*, 2009.

[142] S.-Y. Kim, K.U. Kyung, and J. Park. Real-time area-based haptic rendering and the augmented tactile display device for a palpation simulator. *Advanced Robotics*, 21(9):961–981, 2007.

[143] Y. Kim, I. Oakley, and J. Ryu. Combining point force haptic and pneumatic tactile displays. In *Proceedings of Eurohaptics*, pages 309–316, 2006.

[144] Y. Kim, I. Oakley, and J. Ryu. Human perception of pneumatic tactile cues. *Advanced Robotics*, 22:807–828, 2008.

[145] C.H. King, M.O. Culjat, M.L. Franco, J.W. Bisley, G.P. Carman, E.P. Dutson, and W.S. Grundfest. A multielement tactile feedback system for robot-assisted minimally invasive surgery. *IEEE Transactions on Haptics*, 2(1):52–56, 2009.

[146] C.H. King, M.O. Culjat, M.L. Franco, J.W. Bisley, E. Dutson, and W.S. Grundfest. Optimization of a pneumatic balloon tactile display for robot-assisted surgery based on human perception. *IEEE Transactions on Biomedical Engineering*, 55(11):2593–2600, 2008.

[147] C.H. King, M.O. Culjat, M.L. Franco, C.E. Lewis, E.P. Dutson, W.S. Grundfest, and J.W. Bisley. Tactile feedback induces reduced grasping force in robot-assisted surgery. *IEEE Transactions on Haptics*, 2(2):103–110, 2009.

[148] C.H. King, M.L. Franco, M.O. Culjat, A.T. Higa, J.W. Bisley, E. Dutson, and W.S. Grundfest. Fabrication and characterization of a balloon actuator array for haptic feedback in robotic surgery. *Journal of Medical Devices*, 2:041006–1–041006–7, 2008.

[149] A. Kis, F. Kovács, and P. Szolgay. 3D tactile sensor array processed by CNN-UM: a fast method for detecting and identifying slippage and twisting

motion. *International Journal of Circuit Theory and Applications*, 34:517–531, 2006.

[150] A. Kis, F. Kovács, and P. Szolgay. Grasp planning based on fingertip contact forces and torques. In *Proceedings of Eurohaptics*, pages 455–458, 2006.

[151] M. Kitagawa, D. Dokko, A.M. Okamura, and D.D. Yuh. Effect of sensory substitution on suture-manipulation forces for robotic surgical systems. *The Journal of Thoracic and Cardiovascular Surgery*, 129(1):151–158, 2005.

[152] D. Klein, H. Freimuth, G.J. Monkman, S. Egersdörfer, A. Meier, and H. Böse. Electrorheological tactel elements. *Mechatronics*, 15:883–897, 2005.

[153] D.A. Kontarinis and R.D. Howe. Tactile display of vibratory information in teleoperation and virtual environments. *Presence – Teleoperators and Virtual Environments*, 4(4):387–402, 1995.

[154] D.A. Kontarinis, J.S. Son, W.J. Peine, and R.D. Howe. A tactile shape sensing and display system for teleoperated manipulation. In *Proceedings of the IEEE International Conference on Robotics and Automation*, volume 1, pages 641–646, 1995.

[155] M. Konyo, T. Maeno, A. Yoshida, and S. Tadokoro. Roughness sense display representing temporal frequency changes of tactile information in response to hand movements. In *Proceedings of World Haptics Conference 2005*, pages 609–610, 2005.

[156] M. Konyo, S. Tadokoro, and T. Takamori. Artificial tactile feel display using soft gel actuators. In *Proceedings of the IEEE International Conference of Robotics and Automation*, volume 4, pages 3416–3421, 2000.

[157] I.M. Koo, K. Jung, J.C. Koo, J.D. Nam, Y.K. Lee, and H.R. Choi. Development of soft-actuator-based wearable tactile display. *IEEE Transactions on Robotics*, 24(3):549–558, 2008.

[158] M.P. Koster. *Constructieprincipes voor het nauwekeurig bewegen en positioneren*. Twente University Press, 1998.

[159] R. Kowalik and I. Postawka. The concept of a full screen tactile display (FSTD) driven by electrochemical reactions. In *Proceedings of the 4th International Conference on Computers for Handicapped Persons*, pages 455–460, 1994.

[160] G.M. Krishna and K. Rajanna. Tactile sensor based on piezoelectric resonance. *IEEE Sensors Journal*, 4(5):691–697, 2004.

[161] K.U. Kyung, M. Ahn, D.S. Kwon, and M.A. Srinivasan. A compact broadband tactile display and its effectiveness in the display of tactile form. In *Proceedings of World Haptics Conference 2005*, pages 600–601, 2005.

[162] K.U. Kyung, M. Ahn, D.S. Kwon, and M.A. Srinivasan. Perceptual and biomechanical frequency response of human skin: implication for design of tactile displays. In *Proceedings of World Haptics Conference 2005*, pages 96–101, 2005.

[163] K.U. Kyung, S.W. Son, D.S. Kwon, and M.S. Kim. Design of an integrated tactile display system. In *Proceedings of the IEEE International Conference on Robotics and Automation*, pages 776–781, 2004.

[164] S.P. Lacour, C. Tsay, and S. Wagner. An elastically stretchable TFT circuit. *IEEE Electron Device Letters*, 25(12):792–794, 2004.

[165] R.H. LaMotte. Softness discrimination with a tool. *Journal of Neurophysiology*, 83:1777–1786, 2000.

[166] R.H. LaMotte and M.A. Srinivasan. Tactile discrimination of shape: responses of slowly adapting mechanoreceptive afferents to a step stroked across the monkey fingerpad. *Journal of Neuroscience*, 7(6):1655–1697, 1987.

[167] A.R. Lanfranco, A.E. Castellanos, J.P. Desai, and W.C. Meyers. Robotic surgery – a current perspective. *Annals of Surgery*, 239(1):14–21, 2004.

[168] L. Lanotte, G. Ausanio, C. Hison, V. Iannotti, C. Luponio, and C.Jr. Luponio. State of the art and development trends of novel nanostructured elastomagnetic composites. *Journal of Optoelectronics and Advanced Materials*, 6(2):523–532, 2004.

[169] H.E. Larcombe. Carbon fiber tactile sensors. In *Proceedings of the 1st International Conference on Robot Vision and Sensory Control*, pages 273–277, 1981.

[170] S.J. Lederman. *Encyclopedia of human biology*, chapter Skin and touch, pages 51–63. 1991.

[171] S.J. Lederman and R.A. Browse. The physiology and psychophysics of touch. In *Proceedings of the NATO Advanced Research Workshop on Sensors and Sensory Systems for Advanced Robots*, volume F43, pages 71–91, 1988.

[172] J.S. Lee and S. Lucyszyn. A micromachined refreshable Braille cell. *Journal of Microelectromechanical Systems*, 14(4):673–682, 2005.

[173] M.H. Lee and H.R. Nicholls. Tactile sensing for mechatronics – a state of the art survey. *Mechatronics*, 9:1–31, 1999.

[174] S. Lee. Proprioception: how and why? `http://serendip.brynmawr.edu/exchange/node/1699`, 2002.

[175] V. Levesque and V. Hayward. Experimental evidence of lateral skin strain during tactile exploration. In *Proceedings of Eurohaptics*, pages 261–275, 2003.

[176] C. Li, H. Yao, J. Xu, Y. Zhang, and B. Kuang. A plate tuning fork shaped tactile display using elastic waves. In *Proceedings of the Symposium on Haptic Interfaces for Virtual Environments and Teleoperator Systems*, pages 375–376, 2008.

[177] K.B. Lim and Y.S. Chong. Low cost tactile gripper using silicone rubber sensor array. *Robotica*, 6:23–30, 1988.

[178] J.G. Linvill and J.C. Bliss. A direct translation reading aid for the blind. In *Proceedings of the Institute of Electrical and Electronics Engineers*, volume 54, pages 40–51, 1966.

[179] Y. Liu, R.I. Davidson, P.M. Taylor, J.D. Ngu, and J.M.C. Zarraga. Single cell magnetorheological fluid based tactile display. *Displays*, 26:29–35, 2005.

[180] J.M. Loomis. An investigation of tactile hyperacuity. *Sensory Processes*, 3(289):302, 1979.

[181] J.M. Loomis and S.J. Lederman. *Handbook of human perception and performance*, chapter Tactual perception, pages 1–41. 1986.

[182] M. Lu, D. Lee, T. Yeom, and T. Cui. Micro tactile sensors with a suspended and oriented single walled carbon nanotube beam embeded in PDMS elastomer. In *Proceedings of Transducers*, pages 457–460, 2009.

[183] R. Lundström and R.S. Johansson. Acute impairment of the sensitivity of skin mechanoreceptive units caused by vibration exposure of the hand. *Ergonomics*, 29:687–698, 1986.

[184] R.C. Luo, F. Wang, and Y.X. Liu. A piezoelectric film sensor for robotic end-effectors. In *Proceedings of SPIE, Intelligent Robots and Computer Vision*, volume 521, pages 264–270, 1984.

[185] M. MacFarlane, J. Rosen, B. Hannaford, C. Pellegrini, and M. Sinanan. Force-feedback grasper helps restore sense of touch in minimally invasive surgery. *Journal of Gastrointestinal Surgery*, 3(3):278–285, 1999.

[186] K.E. MacLean and V. Hayward. Do it yourself haptics: part II. *IEEE Robotics & Automation Magazine*, 15(1):104–119, 2008.

[187] H. Maekawa, K. Tanie, K. Komoriya, M. Kaneko, C. Horiguchi, and T. Sugawara. Development of a finger-shaped tactile sensor and its evaluation by active touch. In *Proceedings of the IEEE International Conference on Robotics and Automation*, pages 1327–1334, 1992.

[188] V. Maheshwari and R.F. Saraf. High-resolution thin-film device to sense texture by touch. *Science*, 312:1501–1504, 2006.

[189] Y. Makino and H. Shinoda. Selective stimulation to superficial mechanoreceptors by temporal control of suction pressure. In *Proceedings of World Haptics Conference 2005*, pages 229–234, 2005.

[190] J. Mallin. A simple sense of touch for robotic fingers. *Robotics age*, 24–27 1989.

[191] E. Mallinckrodt, A.L. Hughes, and J.W. Sleator. Perception by the skin of electrically induced vibrations. *Science*, 118:277–278, 1953.

[192] J. Marescaux, J. Leroy, M. Gagner, F. Rubino, D. Mutter, M. Vix, S.E. Butner, and M.K. Smith. Transatlantic robot-assisted telesurgery. *Nature*, 413(6854):379–380, 2001.

[193] J. Marescaux, M.K. Smith, D. Fölscher, F. Jamali, B. Malassagne, and J. Leroy. Telerobotic laparoscopic cholecystectomy: initial clinical experience with 25 patients. *Annals of Surgery*, 234(1):1–7, 2001.

[194] M. Matsumoto and Y. Miyata. Complex permittivity based on equivalent circuit model for polymer/metal composite. *IEEE Transactions on Dielectrics and Electrical Insulation*, 6(1):27–34, 1999.

[195] M. Matsumoto and Y. Miyata. Polymer absorbers containing magnetic particles: effect of polymer permittivity on wave absorption in the quasi-microwave band. *Journal of Applied Physics*, 91(12):9635–9637, 2002.

[196] M. Matysek, P. Lotz, and H.F. Schlaak. Braille display with dielectric polymer actuator. In *Proceedings of Actuator 2006*, pages 997–1000, 2006.

[197] F. McGlone and D. Reilly. The cutaneous sensory system. *Neuroscience and Biobehavioral Reviews*, 34(2):148–159, 2010.

[198] R.B. McIntosh, P.E. Mauger, and S.R. Patterson. Capacitive transducers with curved electrodes. *IEEE Sensors Journal*, 6(1):125–138, 2006.

[199] D.S. McLachlan and M.B. Heaney. Complex AC conductivity of a carbon black composite as a function of frequency, composition, and temperature. *Physical Review B*, 60(18):12746–12751, 1999.

[200] W.S. McMath, S.K. Yeung, and E.M. Petriu. Tactile sensing for space robotics. In *Proceedings of the Instrumentation and Measurement Technology Conference*, pages 128–131, 1989.

[201] A.P. Miller, W.J. Peine, J.S. Son, and Z.T. Hammoud. Tactile imaging system for localizing lung nodules during video assisted thoracoscopic surgery. In *Proceedings of the IEEE International Conference on Robotics and Automation*, pages 2996–3001, 2007.

[202] S. Misra and A.M. Okamura. Environment parameter estimation during bilateral telemanipulation. In *Proceedings of the Symposium on Haptic Interfaces for Virtual Environments and Teleoperator Systems*, pages 301–307, 2006.

[203] J. Missinne, G. Van Steenberge, B. Van Hoe, K. Van Coillie, T. Van Gijseghem, P. Dubruel, J. Vanfleteren, and P. Van Daele. An array waveguide sensor for artificial optical skins. In *Proceedings of SPIE*, volume 7221, pages 722105-1–722105-9, 2009.

[204] G.J. Monkman, S. Egersdörfer, A. Meier, H. Böse, M. Baumann, H. Ermert, W. Khaled, and H. Freimuth. Technologies for haptic displays in teleoperation. *Industrial Robot*, 30(6):525–530, 2003.

[205] K. Moorthy, Y. Munz, A. Dosis, J.D. Hernandez, S. Martin, F. Bello, T. Rockall, and A. Darzi. Dexterity enhancement with robotic surgery. *Surgical Endoscopy*, 18(5):790–795, 2004.

[206] D.H. Mott. An experimental very-high-resolution tactile sensor array. *Robot Sensors*, 2:179–188, 1986.

[207] F.W. Mott and C.S. Sherrington. Experiments upon the influence of sensory nerves upon movement and nutrition of the limbs. preliminary communication. *Proceedings of the Royal Society of London*, 57:481–488, 1895.

[208] G. Moy. *Bidigital teletaction system design and performance*. PhD thesis, University of California, 2002.

[209] G. Moy, U. Singh, E. Tan, and R.S. Fearing. Human psychophysics for teletaction system design. *Haptics-e*, 1(3), 2000.

[210] G. Moy, P.S. Wellman, and R.S. Fearing. A compliant tactile display for teletaction. In *Proceedings of the IEEE International Conference on Robotics and Automation*, volume 4, pages 3409–3415, 2000.

[211] T. Mukai. Development of soft areal tactile sensors for symbiotic robots using semiconductor pressure sensors. In *Proceedings of the IEEE International Conference on Robotics and Biomemetics*, pages 96–100, 2004.

[212] Y. Munz, K. Moorthy, A. Dosis, J.D. Hernandez, S. Bann, F. Bello, S. Martin, A. Darzi, and T. Rockall. The benefits of stereoscopic vision in robotic-assisted performance on bench models. *Surgical Endoscopy*, 18(4):611–616, 2004.

[213] T.E. Murphy, R.J. Webster, and A.M. Okamura. Design and performance of a two-dimensional tactile slip display. In *Proceedings of EuroHaptics*, pages 130–137, 2004.

[214] A.M. Murray, R.L. Klatzky, and P.K. Khosla. Enhancing subjective sensitivity to vibrotactile stimuli. In *Proceedings of the ASME Dynamic Systems and Control Division*, pages 157–162, 1998.

[215] M. Märtens and H. Waller. Vibration control of a mechanical structure with piezoelectric actuators – a comparison of bimorph and stack actuators. In *Proceedings of Actuator 1998*, pages 269–272, 1998.

[216] K. Nakamura, S. Toda, and M. Yamanouchi. A two-dimensional optical fibre microphone array with matrix-style data readout. *Measurement Science and Technology*, 12:859–864, 2001.

[217] M. Nakashige, K. Hirota, and M. Hirose. High resolution tactile display. In *Proceedings of the Virtual Reality Society of Japan Annual Conference*, volume 8, pages 253–254, 2003.

[218] M. Nakatani, R.D. Howe, and S. Tachi. The fishbone tactile illusion. In *Proceedings of Eurohaptics*, pages 69–73, 2006.

[219] M. Nakatani, H. Kajimoto, K. Vlack, D. Sekiguchi, N. Kawakami, and S. Tachi. Control method for a 3D shape display with coil-type shape memory alloy. In *Proceedings of the IEEE International Conference on Robotics and Automation*, pages 1344–1349, 2005.

[220] T. Nasilowski, T. Martynkien, G. Statkiewicz, M. Szpulak, J. Olszewski, G. Golojuch, W. Urbanczyk, J. Wojcik, P. Mergo, M. Makara, F. Berghmans, and H. Thienpont. Temperature and pressure sensitivities of the highly birefringent photonic crystal fiber with core assymmetry. *Applied Physics B: Lasers and Optics*, 81(2-3):325–331, 2005.

[221] T.J. Nelson, R.B. van Dover, S. Jin, S. Hackwood, and G. Beni. Shear-sensitive magnetoresistive robotic tactile sensor. *IEEE Transactions on Magnetics*, 22(5):394–396, 1986.

[222] C. Nies, R. Leppek, H. Sitter, H.J. Klotter, J. Riera, K.J. Klose, W.B. Schwerk, and M. Rothmund. Prospective evaluation of different diagnostic techniques for the detection of liver metastases at the time of primary resection of colorectal carcinoma. *European Journal of Surgery*, 162:811–816, 1996.

[223] T. Nobels. *Ontwerp en realisatie van een Braillecomputermuis*. PhD thesis, K.U.Leuven, 2005.

[224] A. Nomura, I. Abiko, I. Shibata, T. Watanabe, and K. Nihei. Two-dimensional tactile sensor using optical method. *IEEE Transactions on Components, Hybrids and Manufacturing Technology*, 8(2):264–268, 1985.

[225] Y. Ohmura, Y. Kuniyoshi, and A. Nagakubo. Conformable and scalable tactile sensor skin for curved surfaces. In *Proceedings of the IEEE International Conference on Robotics and Automation*, pages 1348–1353, 2006.

[226] A.M. Okamura. Methods for haptic feedback in teleoperated robot-assisted surgery. *Industrial Robot*, 31(6):499–508, 2004.

[227] N.P. Ostrom, K.A. Kaczmarek, and D.J. Beebe. A microfabricated electrocutaneous tactile display. In *Proceedings of the First Joint BMES/EMBS Conference*, volume 2, page 838, 1999.

[228] H. Osumi, N. Ishii, K. Takahashi, K. Umeda, and G. Kinoshita. Optimal grasping for a parallel two-fingered hand with compliant tactile sensors. In *Proceedings of the IEEE/RSJ International Conference on Intelligent Robots and Systems*, pages 799–804, 1999.

[229] D.M. Ota. Laparoscopic colectomy for cancer: a favorable opinion. *Annals of Surgical Oncology*, 2(1):3–5, 1995.

[230] M.V. Ottermo, Ø. Stavdahl, and T.A. Johansen. Electromechanical design of a miniature tactile shape display for minimally invasive surgery. In *Proceedings of World Haptics Conference 2005*, pages 561–562, 2005.

[231] M.V. Ottermo, Ø. Stavdahl, and T.A. Johansen. Design and performance of a prototype tactile shape display for minimally invasive surgery. *Haptics-e*, 4(4), 2008.

[232] J.N. Palasagaram and R. Ramadoss. MEMS-capacitive pressure sensor fabricated using printed-circuit-processing techniques. *IEEE Sensors Journal*, 6(6):1374–1375, 2006.

[233] H. Park and J. Lee. Adaptive impedance control of a haptic interface. *Mechatronics*, 14:237–253, 2004.

[234] M. Paré, C. Behets, and O. Cornu. Paucity of presumptive ruffini corpuscles in the index finger pad of humans. *The Journal of Comparative Neurology*, 456(3):260–266, 2003.

[235] J. Pasquero. Survey on communication through touch. Technical Report TR-CIM 06.04, Center for Intelligent Machines, McGill University, 2006.

[236] J. Pasquero and V. Hayward. STReSS: a practical tactile display system with one millimeter spatial resolution and 700 Hz refresh rate. In *Proceedings of Eurohaptics*, pages 94–110, 2003.

[237] P. Patel-Predd. Sensitive synthetic skin in the works for prosthetic arms. *IEEE Spectrum*, 2008.

[238] D.T.V. Pawluk, J.S. Son, P.S. Wellman, W.J. Peine, and R.D. Howe. A distributed pressure sensor for biomechanical measurements. *ASME Journal of Biomechanical Engineering*, 102(2):302–305, 1998.

[239] D.T.V. Pawluk, C.P. van Buskirk, J.H. Killebrew, S.S. Hsiao, and K.O. Johnson. Control and pattern specification for a high density tactile array. In *Proceedings of the ASME Dynamic Systems and Control Division*, pages 97–102, 1998.

[240] K. Peeters, M. Sette, P. Goethals, J. Vander Sloten, and H. Van Brussel. Design considerations for lateral skin stretch and perpendicular indentation displays to be used in minimally invasive surgery. In *Proceedings of Eurohaptics*, pages 325–330, 2008.

[241] W.J. Peine and R.D. Howe. Do humans sense finger deformation or distributed pressure to detect lumps in soft tissue. In *Proceedings of the ASME Dynamic Systems and Control Division*, volume 64, pages 273–278, 1998.

[242] W.J. Peine, J.S. Son, and R.D. Howe. A palpation system for artery localization in laparoscopic surgery. In *Proceedings of the First International Symposium on Medical Robotics and Computer Assisted Surgery*, pages 250–253, 1994.

[243] W.J. Peine, P.S. Wellman, and R.D. Howe. Temporal bandwidth requirements for tactile shape displays. In *Proceedings of the Symposium on Haptic Interfaces for Virtual Environments and Teleoperator Systems*, pages 107–113, 1997.

[244] J. Peirs, J. Clijnen, D. Reynaerts, H. Van Brussel, P. Herijgers, B. Corteville, and S. Boone. A micro optical force sensor for force feedback during minimally invasive robotic surgery. *Sensors and Actuators A*, 115:447–455, 2004.

[245] R.E. Pelrine, R. Kornbluh, and J.P. Joseph. Electrostriction of polymer dielectrics with compliant electrodes as a means of actuation. *Sensors and Actuators A*, 64(1):77–85, 1998.

[246] J.R. Phillips and K.O. Johnson. Tactile spatial resolution III: a continuum mechanics model of skin predicting mechanoreceptor responses to bars, edges and gratings. *Journal of Neurophysiology*, 46(6):1204–1225, 1981.

[247] C. Pramanik and H. Saha. Piezoresistive pressure sensing by porous silicon membrane. *IEEE Sensors Journal*, 6(2):301–308, 2006.

[248] D. Prattichizzo, C. Pacchierotti, S. Cenci, K. Minamizawa, and G. Rosati. Using a fingertip tactile device to substitute kinesthetic feedback in haptic interaction. In *Proceedings of Eurohaptics*, volume 1, pages 125–130, 2010.

[249] P. Puangmali, K. Althoefer, L.D. Seneviratne, D. Murphy, and P. Dasgupta. State-of-the-art in force and tactile sensing for minimally invasive surgery. *IEEE Sensors Journal*, 8(4):371–381, 2008.

[250] J.A. Purbrick. A force transducer employing conductive silicone rubber. In *Proceedings of the 1st International Conference on Robot Vision and Sensory Controls*, pages 73–80, 1981.

[251] V.L. Pushparaj, L. Ci, S. Sreekala, A. Kumar, S. Kesapragada, D. Gall, O. Nalamasu, and A.M. Pulickel. Effects of compressive strains on electrical conductivities of a macroscale carbon nanotube block. *Applied Physics Letters*, 91(153116), 2007.

[252] M.A. Qasaimeh, S. Sokhanvar, J. Dargahi, and M. Kahrizi. PVDF-based microfabricated tactile sensor for minimally invasive surgery. *Journal of Micromechanical Systems*, 18(1):195–207, 2009.

[253] M.H. Raibert and J.E. Tanner. Design and implementation of a VLSI tactile sensing computer. *International Journal of Robotics Research*, 1(3):3–17, 1982.

[254] M. Ramezanifard, S. Sokhanvar, J. Dargahi, W.F. Xie, and M. Packirisamy. Graphical reproduction of tactile information of embedded lumps for MIS applications. In *Proceedings of the Symposium on Haptic Interfaces for Virtual Environments and Teleoperator Systems*, pages 247–252, 2008.

[255] J. Rassweiler, J. Binder, and T. Frede. Robotic and telesurgery: will they change our future? *Current Opinion in Urology*, 11:309–320, 2001.

[256] F. Rattay. *Electrical nerve stimulation*. Springer-Verlag, 1990.

[257] T.S. Ravikumar, S. Buenaventura, R.R. Salem, and B. D'Andrea. Intraoperative ultrasonography of liver: detection of occult liver tumors and treatment by cryosurgery. *Cancer Detection and Prevention*, 18(2):131–138, 1994.

[258] J. Rebman and K.A. Morris. A tactile sensor with electrooptical transduction. In *Proceedings of the 3rd International Conference on Robot Vision and Sensory Controls*, pages 210–216, 1983.

[259] C.M. Reed. The implications of the Tadoma method of speechreading for spoken language processing. In *Proceedings of the 4th International Conference on Spoken Language Processing*, volume 3, pages 1489–1492, 1996.

[260] H. Reichenspurner, R.J. Damiano, M. Mack, D.H. Boehm, H. Gulbins, C. Detter, B. Meiser, R. Ellgass, and B. Reichart. Use of the voice-controlled and computer-assisted surgical system Zeus for endoscopic coronary artery

bypass grafting. *Journal of Thoracic and Cardiovascular Surgery*, 118(1):11–16, 1999.

[261] D. Reynaerts. *Control methods and actuation technology for whole-hand dexterous manipulation*. PhD thesis, K.U.Leuven, 1995.

[262] M.J. Riezenman. Haptics takes hold. *The Institute*, 32(1):6, 2008.

[263] J.W. Roach, P.K. Paripati, and M. Wade. Model-based object recognition using a large-field passive tactile sensor. *IEEE Transactions on Systems, Man and Cybernetics*, 19(4):846–853, 1989.

[264] J. Roberts. NIST refreshable tactile graphic display: a new low-cost technology. In *Proceedings of the Technology and Persons with Disabilities Conference*, 2004.

[265] B.E. Robertson and A.J. Walkden. Tactile sensor system for robotics. In *Proceedings of the 3rd International Conference on Robot Vision and Sensory Controls*, pages 572–577, 1983.

[266] F. Robicsek. Robotic cardiac surgery: time told! *Journal of Thoracic and Cardiovascular Surgery*, 135(2):343–246, 2008.

[267] J. Rosen and B. Hannaford. Doc at a distance. *IEEE Spectrum*, 43(10):34–39, 2006.

[268] R.A. Russel. A tactile sensory skin for measuring surface contours. In *Proceedings of the IEEE Region 10 Conference, Tencon*, pages 262–266, 1992.

[269] J.P. Ruurda and I.A.M.J. Broeders. Feasibility of robot assisted laparoscopic cholecystectomy. In *Proceedings of CARS*, pages 159–164, 2001.

[270] I. Sarakoglou, N. Tsagarakis, and D.G. Caldwell. A portable fingertip tactile feedback array – transmission system reliability and modelling. In *Proceedings of World Haptics Conference 2005*, pages 547–548, 2005.

[271] S.S. Sastry, M.B. Cohn, and F. Tendick. Milli-robotics for remote, minimally invasive surgery. *Robotic and Autonomous Systems*, 21:305–316, 1997.

[272] H.R. Schiffman. *Sensation and Perception*, chapter The skin, body and chemical senses, pages 70–96. 1995.

[273] P.A. Schmidt, E. Maël, and R.P. Würtz. A sensor for dynamic tactile information with applications in human-robot interaction and object exploration. *Robotics and Autonomous Systems*, 54:1005–1014, 2006.

[274] J.L. Schneiter and T.B. Sheridan. An optical tactile sensor for manipulators. *Computer Integrated Manufacturing*, 1(1):65–72, 1984.

[275] J.S. Schoenwald, A.W. Thiele, and D.E. Gjellum. A novel fiber optic tactile array sensor. In *Proceedings of the IEEE International Conference on Robotics and Automation*, pages 1792–1797, 1987.

[276] S. Schostek, M.O. Schurr, and G.F. Buess. Review on aspects of artificial tactile feedback in laparoscopic surgery. *Medical Engineering & Physics*, 31:887–898, 2009.

[277] M. Schuenemann and H. Widmann. Tactile actuators for tactile feedback systems. In *Proceedings of the 6th International Conference on New Actuators*, pages 333–336, 1998.

[278] K. Sett and C. Vipulanandan. Modeling and verification of the behavior of piezoresistive material under uniaxial loading. *ASCE Journal of Engineering Mechanics*, In review, 2007.

[279] M.M. Sette, J. Camino, J. D'Hooge, H. Van Brussel, and J. Vander Sloten. Comparing optimization algorithms for the Young's modulus reconstruction in ultrasound elastography. In *Proceedings of the IEEE International Ultrasonics Symposium*, page 445, 2007.

[280] M.M. Sette, J. D'Hooge, S. Langeland, P. Goethals, H. Van Brussel, and J. Vander Sloten. Tactile feedback in minimally invasive procedures using an elastography-based method. *International Journal of Computer Assisted Radiology and Surgery*, 2(Suppl. 1):S504, 2007.

[281] M.M. Sette, P. Goethals, J. D'Hooge, H. Van Brussel, and J. Vander Sloten. Algorithms for ultrasound elastography: a survey. *Journal of Computer Methods in Biomechanics and Biomedical Engineering*, accepted for publication, 2010.

[282] N. Sgambelluri, E.P. Scilingo, A. Bicchi, R. Rizzo, and M. Raugi. Advanced modelling and preliminary psychophysical experiments for a free-hand haptic device. In *Proceedings of the 2006 IEEE/RSJ International Conference on Intelligent Robots and Systems*, pages 1558–1563, 2006.

[283] C.E. Sherrick and R. Cholewiak. *Handbook of Perception and Human Performance – Sensory Processes and Perception*, chapter Cutaneous sensitivity, pages 12–30. 1986.

[284] C.E. Sherrick and J.C. Craig. *Tactual Perception: A Sourcebook*, chapter The Psychophysics of Touch, pages 55–81. 1982.

[285] K.B. Shimoga. Finger force and touch feedback issues in dextrous telemanipulation. In *Proceedings of the 4th Annual Conference on Intelligent Robotic Systems for Space Exploration*, pages 159–178, 1992.

[286] K.B. Shimoga and A.A. Goldenberg. Soft materials for robotic fingers. In *Proceedings of the IEEE International Conference on Robotics and Automation*, volume 2, pages 1300–1305, 1992.

[287] M. Shimojo. Spatial filtering characteristic of elastic cover for tactile sensor. In *Proceedings of the IEEE International Conference on Robotics and Automation*, volume 1, pages 287–292, 1994.

[288] M. Shimojo, M. Ishikawa, and K. Kanaya. A flexible high resolution tactile imager with video signal output. In *Proceedings of the IEEE International Conference on Robotics and Automation*, volume 1, pages 384–391, 1991.

[289] M. Shimojo, A. Namiki, M. Ishikawa, R. Makino, and K. Mabuchi. A tactile sensor sheet using pressure conductive rubber with electrical-wires stitched method. *IEEE Sensors Journal*, 4(5):589–596, 2004.

[290] M.H. Shiu. A surgeon's look at the treatment of cancer. *Annals of The College of Surgeons Hong Kong*, 7:B7–B17, 2003.

[291] D. Siegel, S. Drucker, and I. Garabieta. Performance analysis of a tactile sensor. In *Proceedings of the IEEE International Conference on Robotics and Automation*, volume 4, pages 1493–1499, 1987.

[292] D. Siegel, I. Garabieta, and J.M. Hollerbach. An integrated tactile and thermal sensor. In *Proceedings of IEEE International Conference on Robotics and Automation*, pages 1286–1291, 1986.

[293] C.S. Smith. Piezoresistance effect in germanium and silicon. *Physical Review*, 94(1):42–49, 1954.

[294] K. Smolders. Tracking control of continuous-time nonlinear systems: a model-based iterative learning approach. PhD thesis, K.U.Leuven, 2007.

[295] A.S. Soembagijo. Application of neural networks to derive manipulation force vectors from tactile sensing images. Master's thesis, K.U.Leuven, 1992.

[296] T. Someya, Y. Kato, T. Sekitani, S. Iba, Y. Noguchi, Y. Murase, H. Kawaguchi, and T. Sakurai. Conformable, flexible, large-area networks of pressure and thermal sensors with organic transistor active matrixes. *PNAS*, 102(35):12321–12325, 2005.

[297] T. Someya, T. Sekitani, S. Iba, Y. Kato, H. Kawaguchi, and T. Sakurai. A large-area, flexible pressure sensor matrix with organic field-effect transistors for artificial skin applications. *PNAS*, 101(27):9966–9970, 2004.

[298] R. Souchon, L. Soualmi, M. Bertrand, J.Y. Chapelon, F. Kallel, and J. Ophir. Ultrasonic elastography using sector scan imaging and a radial compression. *Ultrasonics*, 40:867–871, 2002.

[299] T.H. Speeter. Tactile sensing system for robotic manipulation. Technical report, 1988.

[300] M.A. Srinivasan. Surface deflection of primate fingertip under line load. *Journal of Biomechanics*, 22(4):343–349, 1989.

[301] M.A. Srinivasan and R.H. LaMotte. Tactual discrimination of softness. *Journal of Neurophysiology*, 73(1):88–101, 1995.

[302] D. Stauffer and A. Aharony. *Introduction to percolation theory*. Taylor and Francis, 1994.

[303] D.K. Stein. The Optacon: past, present and future. `http://nfb.org/legacy/bm/bm98/bm980506.htm`, 1998.

[304] D. Stern. Revival of an extinct species. *MST News*, (3):13, 2006.

[305] J. Streque, A. Talbi, P. Pernod, and V. Preobrazhensky. Control strategies and performance of a magnetically actuated tactile micro-actuator array. In *Proceedings of Eurohaptics*, volume 2, pages 385–391, 2010.

[306] R.M. Strong and D.E. Troxel. An electrotactile display. *IEEE Transactions on Man-Machine Systems*, 11(1):72–79, 1970.

[307] S. Sugiyama, H. Kawaguchi, T. Someya, T. Sekitani, and T. Sakurai. Cut-and-paste customization of organic fet integrated circuit and its application to electronic artificial skin. *IEEE Journal of Solid-State Circuits*, 40(1):177–185, 2005.

[308] I.R. Summers and C.M. Chanter. A broadband tactile array on the fingertip. *Journal of the Acoustical Society of America*, 112(5):2118–2126, 2002.

[309] S. Takenawa. A magnetic type tactile sensor using a two-dimensional array of inductors. In *Proceedings of IEEE International Conference on Robotics and Automation*, pages 3295–3300, 2009.

[310] A. Talbi, O. Ducloux, N. Tiercelin, Y. Deblock, P. Pernod, and V. Preobrazhensky. Vibrotactile using micromachined electromagnetic actuators array. In *Proceedings of Actuator 2006*, pages 120–123, 2006.

[311] H.Z. Tan and A. Pentland. Tactual displays for wearable computing. *Personal Technologies*, 1:225–230, 1997.

[312] H.Z. Tan, M.A. Srinivasan, B. Ebermann, and B. Cheng. Human factors for the design of force-reflecting haptic interfaces. *Dynamic Systems and Control*, 55(1):353–359, 1994.

[313] H. Tang and D.J. Beebe. A microfabricated electrostatic haptic display for persons with visual impairments. *IEEE Transactions on Rehabilitation Engineering*, 6(3):241–248, 1998.

[314] M. Taya. *Electronic Composites*. Cambridge University Press, 2005.

[315] M. Taya, W.J. Kim, and K. Ono. Piezoresistivity of a short fiber/elastomer matrix composite. *Mechanics of Materials*, 28:53–59, 1998.

[316] P.M. Taylor, A. Moser, and A. Creed. A sixty-four element tactile display using shape memory alloy wires. *Displays*, 18(3):163–168, 1998.

[317] P.M. Taylor, D.M. Pollet, A. Hosseini-Sianaki, and C.J. Varley. Advances in an electrorheological fluid based tactile array. *Displays*, 18(3):135–141, 1998.

[318] J. Tegin and J. Wikander. Tactile sensing in intelligent robotic manipulation – a review. *Industrial Robot*, 32(1):64–70, 2005.

[319] M.A. Thrasher, A.R. Shahin, P.H. Meckl, and J.D. Jones. Efficiency analysis of shape memory alloy actuators. *Smart Materials and Structures*, 3:226–234, 1994.

[320] D.J.F. Toal, C. Flanagan, W.B. Lyons, S. Nolan, and E. Lewis. Proximal object and hazard detection for autonomous underwater vehicle with optical fibre sensors. *Robotics and Autonomous Systems*, 53:214–229, 2005.

[321] N. Tsagarakis, T. Horne, and D.G. Caldwell. Slip aestheasis: a portable 2D slip/skin stretch display for the fingertip. In *Proceedings of World Haptics Conference 2005*, pages 214–219, 2005.

[322] M. Umemori, J. Sugawara, M. Kawauchi, and H. Mitani. A pressure-distribution sensor (PDS) for evaluation of lip functions. *American Journal of Orthodontics and Dental Orthopedics*, 109(5):473–480, 1996.

[323] Å.B. Vallbo. Sensations evoked from the glabrous skin of the human hand by electrical stimulation of unitary mechanosensitive afferents. *Brain Research*, 215:359–363, 1981.

[324] Å.B. Vallbo and R.S. Johansson. Properties of cutaneous mechanoreceptors in the human hand related to touch sensation. *Human Neurobiology*, 3:3–14, 1984.

[325] R.B. Van Boven and K.O. Johnson. The limit of tactile spatial resolution in humans: grating orientation discrimination at the lip, tongue and finger. *Neurology*, 44:2361–2366, 1994.

[326] H. Van Brussel and H. Belien. A high resolution tactile sensor for part recognition. In *Proceedings of RoViSeC6*, pages 49–60, 1986.

[327] D.J. van den Heever, K. Schreve, and C. Scheffer. Tactile sensing using force sensing resistors and a super-resolution algorithm. *IEEE Sensors Journal*, 9(1):29–35, 2009.

[328] C.L. Van Doren, D.G. Pelli, and R.T. Verrilo. A device for measuring tactile spatiotemporal sensitivity. *Journal of the Acoustical Society of America*, 81(6):1906–1916, 1987.

[329] J.B.F. van Erp, K.U. Kyung, S. Kassner, J. Carter, S. Brewster, G. Weber, and I. Andrew. Setting the standards for haptic and tactile interactions: ISO's work. In *Proceedings of Eurohaptics*, volume 2, pages 353–358, 2010.

[330] B. Van Hoe, D. Lamon, E. Bosmans, G. Van Steenberge, J. Missinne, P. Goethals, P. Krassimir, D. Reynaerts, J. Vanfleteren, and P. Van Daele. Embedded high resolution sensor based on optical feedback in a vertical cavity surface emitting laser. In *Proceedings of SPIE, Smart Sensor Phenomena, Technology, Networks, and Systems*, volume 7648, 76480N, 2010.

[331] R. Velázquez, E. Pissaloux, M. Hafez, and J. Szewczyk. A low-cost highly-portable tactile display based on shape memory alloy micro-actuators. In *Proceedings of the IEEE Symposium on Virtual Environments, Human-Computer Interfaces and Measurement Systems*, pages 121–126, 2005.

[332] E. Verrijssen and E. Taeymans. Kunsthuid voor robotvingers. Master's thesis, K.U.Leuven, 1984.

[333] F. Vidal-Verdú and R. Navas-González. Thermopneumatic actuator for tactile displays. In *Proceedings of SPIE*, volume 5836, pages 484–492, 2005.

[334] R. Vitushinsky, S. Schmitz, and A. Ludwig. Bistable thin-film shape memory actuators for applications in tactile displays. *Journal of Microelectromechanical Systems*, 18(1):186–194, 2009.

[335] R.M. Voyles, G. Fedder, and P.K. Khosla. Design of a modular tactile sensor and actuator based on an electrorheological gel. In *Proceedings of the IEEE International Conference on Robotics and Automation*, pages 13–17, 1996.

[336] R.M. Voyles, J.D. Morrow, and P.K. Khosla. Shape from motion approach to rapid and precise force/torque sensor calibration. In *Proceedings of the ASME Dynamic Systems and Control Division*, pages 67–73, 1995.

[337] J.M. Vranish. Magnetoresistive skin for robots. *Robot Sensors*, 2:99–111, 1986.

[338] G. Vásárhelyi and B. Fodor. Enhancing tactile capabilities with elastic hemispheres. In *Proceedings of Eurohaptics*, pages 491–494, 2006.

[339] G. Vásárhelyi, M. ÃĄdám, ÃĽ. Vázsonyi, Z. Vízváry, A. Kis, I. Bársony, and C. Dücsõ. Characterization of an integrable single-crystalline 3-D tactile sensor. *IEEE Sensors Journal*, 6(4):928–934, 2006.

[340] K. Wada, T. Shibata, T. Musha, and S. Kimura. Evaluation of neuropsychological effects of interaction with seal robots on demented patients. In *Proceedings of Eurohaptics*, pages 427–432, 2006.

[341] C.R. Wagner and R.D. Howe. Force feedback benefit depends on experience in multiple degree of freedom robotic surgery task. *IEEE Transactions on Robotics*, 23(6):1235–1240, 2007.

[342] C.R. Wagner, S.J. Lederman, and R.D. Howe. Design and performance of a tactile display using RC servomotors. *Haptics-e*, 3(4), 2004.

[343] C.R. Wagner, N. Stylopoulos, P.G. Jackson, and R.D. Howe. The benefit of force feedback in surgery: examination of blunt dissection. *Presence – Teleoperators and Virtual Environments*, 16(3):252–262, 2007.

[344] Q. Wang and V. Hayward. Compact, portable, modular, high-performance, distributed tactile display device based on lateral skin deformation. In *Proceedings of the Symposium on Haptic Interfaces for Virtual Environments and Teleoperator Systems*, pages 67–72, 2006.

[345] Q. Wang and V. Hayward. Biomechanically optimized distributed tactile transducer based on lateral skin deformation. *International Journal of Robotics Research*, 29(4):323–335, 2010.

[346] R.J. Webster, T.E. Murphy, L.N. Verner, and A.M. Okamura. A novel two-dimensional tactile slip display: design, kinematics and perceptual experiment. *ACM Transactions on Applied Perception*, 2(2):150–165, 2005.

[347] K. Weiß and H. Wörn. The working principle of resistive tactile sensor cells. In *Proceedings of the IEEE International Conference on Mechatronics & Automation*, pages 471–476, 2005.

[348] P.S. Wellman, R.D. Howe, N. Dewagan, M.A. Cundari, E.P. Dalton, and K.A. Kern. Tactile imaging: a method for documenting breast masses. In *Proceedings of the First Joint BMES/EMBS Conference*, page 1131, 1999.

[349] P.S. Wellman, W.J. Peine, G. Favalora, and R.D. Howe. Mechanical design and control of a high-bandwidth shape memory alloy tactile display. *Experimental Robotics V*, 232:56–66, 1998.

[350] E.P. Westebring – van der Putten, R.H.M. Goossens, J.J. Jakimowicz, and J. Dankelman. Haptics in minimally invasive surgery – a review. *Minimally Invasive Therapy and Allied Technologies*, 17(1):3–16, 2008.

[351] M. Wiertlewski, J. Lozada, E. Pissaloux, and V. Hayward. Tactile interface for stimulation of fingertip via lateral traction. In *Proceedings of Actuator 2010*, pages 520–523, 2010.

[352] B. Willaert, P. Goethals, D. Reynaerts, H. Van Brussel, and E. Vander Poorten. *Advances in Haptics*, chapter Transparent and shaped stiffness reflection for telesurgery, pages 259–282. 2010.

[353] M.R. Wolffenbuttel. *Surface micromachined capacitive tactile image sensor*. PhD thesis, Technische Universiteit Delft, 1994.

[354] J. Wu. Introduction to percolation theory. `http://www.people.fas.harvard.edu/~wu2/paper1/paper1.html`, 1997.

[355] H. Wörn, C. Burghart, K. Weiß, and D. Göger. *Human Haptic Perception – Basics and Applications*, chapter Haptic perception in human robotic systems, pages 427–436. 2008.

[356] W. Xu and M.G. Allen. Fabrication of patterned carbon nanotube (CNT) / elastomer bilayer material and its utilization as force sensors. In *Proceedings of Transducers*, pages 2242–2245, 2009.

[357] A. Yamamoto, S. Nagasawa, H. Yamamoto, and T. Higuchi. Electrostatic tactile display with thin film slider and its application to tactile telepresentation systems. *IEEE Transactions on Visualization and Computer Graphics*, 12(2):168–177, 2006.

[358] X. Yang, Z.Y. Zhou, F.Z. Zheng, M. Zhang, J. Zhang, and Y.G. Yao. A high sensitivity single-walled carbon-nanotube-array-based strain sensor for weighing. In *Proceedings of Transducers*, pages 1493–1496, 2009.

[359] F. Zee, E.G.M. Holweg, W. Jongkind, and G. Honderd. Shear force measurement using a rubber based tactile matrix sensor. In *Proceedings of ICAR*, pages 733–738, 1997.

[360] Y. Zhou, M. Ohka, and T. Miyaoka. A tactile display presenting pressure distribution and slippage force. In *Proceedings of the Symposium on Haptic Interfaces for Virtual Environments and Teleoperator Systems*, pages 281–285, 2008.

List of Publications

P. Goethals, M. Sette, H. Van Brussel, and D. Reynaerts. Towards the design of powerful and compact tactile displays. In *Proceedings of Actuator*, pages 524–527, 2010.

P. Goethals, H. Van Brussel, and D. Reynaerts. A miniature proportional pneumatic valve for a tactile display. In *Proceedings of Actuator*, pages 793–796, 2010.

M.M. Sette, P. Goethals, J. D'Hooge, H. Van Brussel, and J. Vander Sloten. Algorithms for ultrasound elastography: a survey. *Journal of Computer Methods in Biomechanics and Biomedical Engineering*, accepted for publication, 2010.

B. Van Hoe, D. Lamon, E. Bosman, G. Van Steenberge, J. Missinne, P. Goethals, P. Krassimir, D. Reynaerts, J. Vanfleteren, and P. Van Daele. Embedded high resolution sensor based on optical feedback in a vertical cavity surface emitting laser. In *Proceedings of SPIE*, 76480N, 2010.

B. Willaert, P. Goethals, D. Reynaerts, H. Van Brussel, and E. Vander Poorten. *Advances in Haptics*, chapter Transparent and shaped stiffness reflection for telesurgery, pages 259–282, 2010.

P. Goethals, M. Sette, D. Reynaerts, and H. Van Brussel. Flexible elastoresistive tactile sensor for minimally invasive surgery. In *Flex Stretch Electronics*, 2009.

P. Goethals, H. Lintermans, M. Sette, D. Reynaerts, and H. Van Brussel. Powerful compact tactile display with microhydraulic actuators. In *Proceedings of Eurohaptics*, pages 447–457, 2008.

P. Goethals, M. Sette, D. Reynaerts, and H. Van Brussel. Flexible elastoresistive tactile sensor for minimally invasive surgery. In *Proceedings of Eurohaptics*, pages 573–579, 2008.

P. Goethals, D. Reynaerts, and H. Van Brussel. Tactile feedback in surgery – an introduction. *Haptic Rendering Workshop – Eurohaptics*, 2008.

K. Peeters, M. Sette, P. Goethals, J. Vander Sloten, and H. Van Brussel. Design considerations for lateral skin stretch and perpendicular indentation displays to be used in minimally invasive surgery. In *Proceedings of Eurohaptics*, pages 325–330, 2008.

P. Goethals, G. De Gersem, M. Sette, D. Reynaerts, and H. Van Brussel. Accurate Haptic Teleoperation on Soft Tissues through Slave Friction Compensation by Impedance Reflection. In *Proceedings of World Haptics Conference 2007*, pages 458–463, 2007.

P. Goethals, B. Willaert, M. Sette, D. Reynaerts, and H. Van Brussel. Tactile sensing technology for robot assisted minimally invasive surgery. *Journal of Biomechanics*, 40(S2) page S647, 2007.

M.M. Sette, J. D'Hooge, S. Langeland, P. Goethals, H. Van Brussel, and J. Vander Sloten. Tactile feedback in minimally invasive procedures using an elastography-based method. *International Journal of Computer Assisted Radiology and Surgery*, 2(Suppl. 1):S504, 2007.

M. Sette, J. D'Hooge, S. Langeland, P. Goethals, H. Van Brussel, and J. Vander Sloten. Tactile feedback in minimally invasive procedures using an elastography-based method. In *Proceedings of CARS*, 2007.

M. De Volder, P. Goethals, S. Eeckhoudt, J. Peirs, and D. Reynaerts. A ferrofluid seal technology for hydraulic microactuators. In *Proceedings of Actuator 2006*, pages 693–696, 2006.

M. De Volder, P. Goethals, S. Eeckhoudt, and D. Reynaerts. A ferrofluid seal technology for hydraulic microactuators. In *Proceedings of the AMS Workshop*, 2006.

P. Goethals. *Eten om nooit te vergeten*, chapter Fruitlasagne, page 93, 2006. available online: `https://sites.google.com/site/fruitlasagne/home`

M. Sette, P. Goethals, J. Vander Sloten, and H. Van Brussel. *Minimally Invasive Therapies & Novel Embedded Technology Systems*, chapter Tactile sense in minimally invasive surgery, pages 159–171, 2006.

P. Goethals, H. Van Brussel, D. Reynaerts, M. Nuttin, and J. Vander Sloten. Tactile feedback for robot assisted endoscopy. In *Proceedings of the AMS Workshop*, 2005.

Arenberg Doctoraatsschool Wetenschap & Technologie
Faculteit Ingenieurswetenschappen
Departement Werktuigkunde
Afdeling Productietechnieken, Machinebouw en Automatisering (PMA)
Celestijnenlaan 300B
B-3001 Heverlee